The influence of topography and model grid resolution on extreme weather forecasts over South Africa

By

Thizwilondi Robert Maisha

Submitted in partial fulfilment of the requirements for the degree

Masters of Science (Meteorology)

In the Faculty of Natural and Agricultural Sciences

University of Pretoria©

Pretoria

February 2014

UNIVERSITEIT VAN PRETORIA
UNIVERSITY OF PRETORIA
YUNIBESITHI YA PRETORIA

DECLARATION OF ORIGINALITY

This is to certify that the work is entirely my own and not of any other person, unless explicitly acknowledged (including citation of published and unpublished sources). The work has not previously been submitted in any form to the University of Pretoria or to any other institution for assessment or for any other purpose.

Signed _____

Date _____

The influence of topography and model grid resolution on extreme weather forecasts over South Africa

Student: *Thizwilondi Robert Maisha*

Supervisor: *Prof George Djolov*

Co-supervisor: *Dr Thando Ndarana*

Department: *Department of Geography, Geo-Informatics and Meteorology*

Faculty: *Faculty of Natural and Agricultural Sciences*

University: *University of Pretoria*

Degree: *Masters of Science*

SUMMARY

The topography of South Africa (SA) shows complex variations and is one the main factors that determine the daily weather patterns and climate characteristics. It affects for example temperature, winds and rainfall (intensity and distribution). Mesoscale numerical weather prediction (NWP) models are used to simulate atmospheric motions with high horizontal grid resolution using appropriate cumulus parameterisation schemes. They also allow users to investigate the effects of topography and surface heating on the development of convective systems.

The Weather Research and Forecasting (WRF) model was applied over the complex terrain of SA to simulate extreme weather events and evaluate the influence of topography and grid resolution on the accuracy of weather simulations. This includes heavy precipitation event that lead to floods over Limpopo region of SA which was caused by the tropical depression Dando for the period 16 -18 January 2012; the heat wave events over Limpopo region for the period 22-26 October 2011 and also over Cape region for the period 15-18 January 2012. The Grell-Devenyi Ensemble (GDE) cumulus parameterization scheme was applied. The WRF model was run at a horizontal resolution of 9 km with 3 km nests, one over Limpopo and another over Cape region respectively. A total of 210 South African Weather Service (SAWS) synoptic stations data were used to verify the model, with 37 stations located over Limpopo and 88 over Cape region.

The WRF model simulations are able to capture the spatial and temporal distribution of the heat wave over Limpopo and Cape regions respectively. The model verification with observational data showed that the performance statistics are in the expected range. The experiments without topography give unrealistic verification scores. The increase of model grid resolution from 9 to 3 km improved the spatial and temporal distribution and performance statistics. The above findings are in general similar for the two heat wave events, although the influence of topography over Cape region is not too pronounced. This can be attributed to different topographic variations over the Cape region as compared to the Limpopo region.

The WRF model captured well the spatial and temporal distribution of rainfall patterns; verification statistics shows over-prediction of its intensity in simulation with topography. The simulation without topography shows unrealistic space and intensity of rain distribution. An increase in model grid resolution from 9 to 3 km shows improved spatial and temporal distribution of rainfall. The importance of high grid resolution and the use of non-hydrostatic equations are confirmed by the analysis of the vertical velocity distribution and moisture fluxes.

The overall findings proved that topography plays a major role to weather and climate over SA. The high grid resolution allows for a better topography representation and capturing convective activities by the use of nonhydrostatic approximations. Therefore the WRF model proved to be useful forecasting tool for weather and climate simulations and can be used for operational weather forecasting over South Africa.

Keywords: topography of SA, mesoscale models, numerical weather prediction, cumulus parameterization, high grid resolution

AKNOWLEDGEMENTS

I would like to acknowledge and thank the following people for their assistance

- Prof. George Djolov - Supervisor for all the support, motivation, and research articles
- Dr. Thando Ndarana - Co-supervisor for all the support, motivation and research articles
- Prof. Hannes Rautenbach – Head of Department GGM for all the support and motivation
- UP Faculty of Natural Science - for granting me the study leave so that I could finish my studies
- Dr. Patricia Smit - UP Department of Research and Innovation Support –for providing funding for my replacement lecturer during my studies
- Mr. Human Buirski - Colleague for all the IT support
- Dr. J.Venkata Ratnam and Dr. Satyaban B. Ratna-collaborator at JAMSTEC for all the technical expertise and support
- JICA, JAMSTEC and Mr. George Sakurai – for providing the Kaminari super computer and for funding my trip to Japan
- SAWS team-(Librarians, NWP, and forecasting) - for providing study materials, observations data, guidance in script writing and insight on synoptic analysis)
- UP Librarians team - for continued support with downloading of research materials
- WRF help - WRF team for all the WRF installation support and advise
- Dr. Liesl Dyson - Colleague for all the question, support, scripting and motivation
- Mr. Philemon Tsela - for motivation and assistance with document setup
- Pastor Mashudu Mufamadi - for all the prayers during my tribulations times

  “For with God nothing is impossible”- Luke 1:37

PREVIOUS PUBLICATIONS BY THE AUTHOR

1. **Evaluation of WRF as a meteorological forecasting tool over the complex terrain of South Africa:**

   Maisha, R., Djolov, G., and Ndarana, T.

   Proceedings of 29th Annual Conference of South African Society for Atmospheric Sciences, ISBN 978-0-620-56626-1, 25-27 September, 2013, Durban, (south Africa), pg., 114-117

TABLE OF CONTENTS

LIST OF SYMBOLS

D or d	distance
L	horizontal length scale
r or a	radius of the earth, r=6374 000 m
ϕ	latitude
λ	longitude
Σ	summation
$\sqrt{}$	Square root
u	horizontal velocity (east-west direction) component
v	horizontal velocity (south-north direction) component
dw	rate of change of vertical velocity with time
dt	rate of change of time
dw/dt	rate of change of vertical velocity with time
F	Froude number
N	Brunt-Väisälä frequency
h	orogen-scale topographic relief
Ω	Angular speed of rotation of the earth in radians per second
ρ	density of the earth in kilogram per meter cube
g	gravitational acceleration in meters per second squared
dx	rate of change in the x-direction
dy	rate of change in the y-direction
dz	rate of change in the z-direction
dp/dz	rate of change of pressure in the z-direction (vertical)
dT/dt	rate of change of temperature with time
dT/dx	rate of change of temperature in the x-direction
dT/dy	rate of change of temperature in the y-direction

LIST OF ABBREVIATIONS

ARC	Agricultural Research Council
ARPS	Advanced Regional Prediction System
BMJ	Betts-Miller-Janjic Scheme
Bias	Mean Error
BL	Boundary Layer
CAPE	Convective Available Potential Energy
C-CAM	Conformal-Cubic Atmospheric Model
CSI	Critical Success Index
CSIR	Council for Scientific and Industrial Research
CSIRO	Australia's Council for Scientific and Industrial Research
DEM	Digital Elevation Model
DGGM	Department of Geography, Geo-Informatics and Meteorology
DJF	December-January-February
ENSO	El Niño Southern Oscillation
FAR	False Alarm Ration
FORTRAN	Formula Translation
GDE	Grell-Devenyi Ensemble scheme
GFS	Global Forecast System
GCM	Global Circulation Model
GrADS	Grid Analysis and Display System
hPa	Hectopascal
IC	Initial Conditions
IPCC	Intergovernmental Panel on Climate Change
ITCZ	Intertropical Convergence Zone
JAMSTEC	Japan Agency for Marine-Earth Science and Technology
JICA	Japan International Cooperation Agency
KF	Kain-Fritsch scheme
KZN	Kwazulu-Natal
LAM	Limited Area Model
LBC	Lateral Boundary Conditions
MAE	Mean Average Error
MSE	Mean Square Error

MCS	Mesoscale Convective System
MM5	Mesoscale Model version 5
MMM	Mesoscale and Microscale Meteorology
MSL	Mean Sea Level
MODIS	Moderate Resolution Imaging Spectroradiometer
NCEP	National Centers for Environmental Prediction
NCAR	National Center for Atmospheric Research
NMS	National Meteorological Service
NOAA	National Oceanic and Atmospheric Administration
NWP	Numerical Weather Prediction
PBL	Planetary Boundary Layer
POD	Probability of Detection
PC	Percentage Correct
PCC	Pearson Correlation Coefficient
RCM	Regional Climate Model
RH	Relative Humidity
RK-3	Runge-Kutta 3 numerical scheme
RMSE	Root Mean Square Error
RRTM	Rapid Radiative Transfer Model
SA	South Africa
SAST	South African Standard Time
SAWS	South African Weather Service
SICZ	South Indian Convergence Zone
Soutpansberg	Salt Pan Mountains
SST	Sea Surface Temperature
TTT	Tropical Temperate Trough
UCAR	University Cooperation for Atmospheric Research
UP	University of Pretoria
UTC	Universal Coordinated Time
WMO	World Meteorological Organization
WRF	Weather Research and Forecasting Model
WRF (V3.4a)	Weather Research and Forecasting Model Version 3.4a
WRF-ARW	Advanced Research WRF
2-D	2 Dimensional

LIST OF FIGURES

LIST OF TABLES

APPENDIX A

CHAPTER 1

NUMERICAL WEATHER PREDICTION

This chapter introduces the research area which is the relationship between topography and meteorological variables. It then highlights different aspects of modelling from global to regional models. Scaling method is discussed as it defines the non-hydrostatic modelling approach. The temperature advection equation is also emphasized. The initial and boundary conditions, physical and cumulus parameterization schemes and also the model errors are also discussed. Although the main focus of this study is topography, the influence of grid resolution is also highlighted. Lastly, the problem statement, the aims and objectives of research and the study outline are elaborated.

1.1 Introduction

The complexity of terrain affects the atmospheric flow dynamics and is one of the major challenges faced by meteorological science. It is widely accepted that topography has a significant, varied and complex influence on the dynamics of different scales of atmospheric flows. The description of some of the major effects of topography on the flow dynamics and thermodynamics includes: (a) orographic precipitation and air mass transportation (Schulze, 1997; Riphagen *et al*., 2001; Mass *et al*., 2002; Singleton and Reason, 2005; Potgieter, 2006; Blamey and Reason, 2009; Galewsky, 2009; Van Schalkwyk, 2011); (b) temperature distribution and (c) wind flow (Jimenez and Dudhia, 2011). Wind flow generally includes the known facts like flow separation, blocking, gravity wave, gravity wave breaking and wave drag.

The complex terrain features also determines the daily weather patterns, climate characteristics and anticipated climate change, air pollution transport (Gross *et.al.,* 1987; McQueen *et al*., 1995; Smith, 2004), diffusion potential, cloud formation, rainfall intensity and distribution (Tennant and Van Heerden, 1994), extreme minimum and maximum temperature occurrence (Giorgi, 1990; Smith, 2004).

The topographic features that affect the atmospheric air flow dynamics includes the effect of terrain on winds (Jimenez and Dudhia, 2011), thermal effect of hills and slopes on local circulations, mechanisms resulting in upslope and downslope winds, airflow

acceleration through mountain gaps, mountain drag and wave momentum fluxes. These features also affect the general circulations (Smith, 2004). Most of the mesoscale circulations are created by the interactions between synoptic scale flow and mesoscale terrain; and are however forced by topography (Riphagen *et al*., 2001) and surface contrast (Bonnardot and Cautenet, 2009). Therefore mesoscale predictability is controlled by large scale, longer-lived synoptic scale predictability (Mass *et al*., 2002).

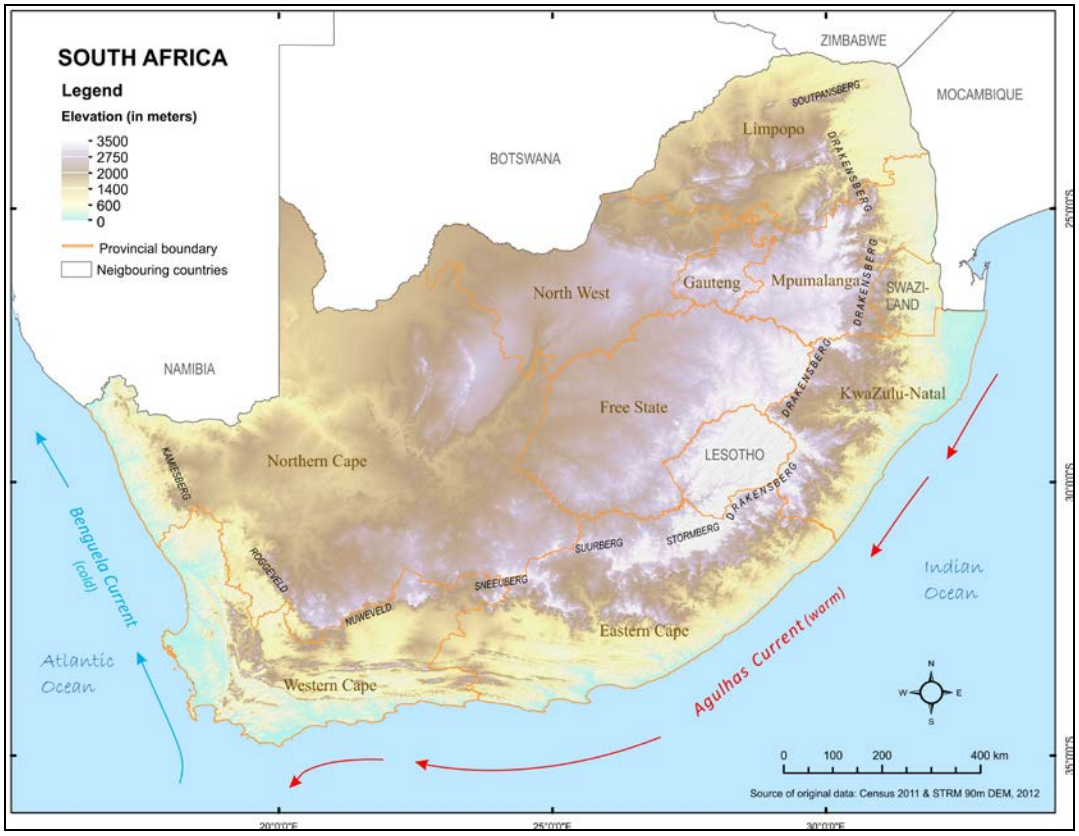

Figure 1.1: The topographic map of South Africa with its nine provinces, its mountains and the surrounding countries, the major oceans and their currents. Topography is depicted in meters and both the cold Benguela and warm Agulhas currents are depicted by arrows (created from Digital Elevation Model (DEM) by Mrs I. Booysen, from the Department of Geography, Geo-Informatics and Meteorology, Unit for Geo-Informatics and Mapping).

On both macroscale and mesoscale, topography acts as a barrier to the rain-bearing air-masses, *i.e.* in Western Cape province of South Africa (SA) during winter months (June, July and August: JJA) (see map of SA in Figure 1.1). Topography can also force moist air to rise as a result of lifting (Schulze, 1997; Riphagen *et al*., 2001; Potgieter, 2006; Blamey and Reason, 2009; Galewsky, 2009; Kruger *et al*., 2010), with the windward

slopes experiencing more rainfall, more rain days and more rainfall per rain days, *i.e.* Drakensberg Mountains during summer months (December, January and February: (DJF)). High altitudes that are associated with steep topographic gradients also result in an increase in both thunderstorms and lightning activities (Schulze, 1997).

In areas of complex terrain, one finds various types of vegetation. Therefore the amount, type, and the conditions of vegetation cover and the canopy provided by plants to the surface have a direct influence on heat exchange between the surface and the atmosphere above it. It therefore also affects weather and climate. An increase in vegetation covers result in an increase of relative and specific humidity, equivalent potential temperature, retention of moisture, minimum temperature and leads to an increase in the formation of clouds, which enhances upward motion and precipitation (McPherson, 2007). However, such an increase in vegetation covers result in a decrease of surface winds, runoff and erosion, Bowen ratio and maximum temperature (Bonnardot and Cautenet, 2009).

1.1.1 Global and mesoscale numerical weather prediction models

Global circulation models (GCM's) can used to produce forecast on different time scales, ranging from climate to seasonal modelling (Giorgi, 1990; Caldwell *et al*., 2009; Mbedzi, 2010). For climate modelling, variables like temperature, rainfall, wind, humidity and cloudiness are simulated for present climate, and predicted for future changes in climate (Watterson, 1993). For seasonal forecasts, global sea surface temperature (SST), cloud depth and upper zonal winds have been used as predictors (Reason *et al.*, 2006). However, due to their lower grid resolution, GCM's cannot be used for numerical weather prediction (NWP) (Caldwell *et al*., 2009; Mbedzi, 2010; Cretat *et al*., 2012) since they are unable to capture some important mesoscale and represent local sub-grid scale features (Giorgi, 1990; Ratnam *et al*., 2011) including hills, valleys and they over-estimate rainfall (Galanis *et al*., 2006; Reason *et al.*, 2006; Libonati *et al*., 2008; Mbedzi, 2010). One of the challenges faced by GCM's models is that low grid resolution does not adequately define the mesoscale precipitation features associated with topographic barriers (Mass *et al.*, 2002). In order to solve this problem, regional climate models (RCM) are used together with dynamical downscaling techniques (Kgatuke *et al*., 2008; Caldwell *et al*., 2009; Ratna *et al*., 2013) instead of GCM's (Cretat *et al*., 2012).

These regional or limited area models (LAM) are used operationally in different meteorological centres around the globe including South Africa for NWP purposes (Giorgi and Bi, 2000; Riphagen *et al*., 2001; Landman, 2012), as they can address both diurnal cycles and rainfall frequency. These models are also used for climate studies (Giorgi and Bi, 2000). In SA, the South African Weather Service (SAWS) provides operational weather forecasts to the southern Africa community at large. For research purpose, regional models like the Weather Research and Forecasting (WRF) model is applied at University of Pretoria (UP) and the Conformal-Cubic Atmospheric model (C-CAM) at the Council for Scientific and Industrial Research (CSIR) (Landman, 2012).

Regional models are also applied for mesoscale modelling, for meteorological events with a scale of order 100x100x5 km; with a horizontal grid resolution of at least 12 km or less. These mesoscale models are able to capture atmospheric motions like eddies, small plumes, and cumulus clouds (Markowski and Richardson, 2010). These regional model forecasts are also able to reproduce cyclone motions although such cyclones are weaker than observations, but more realistic as compared to vortices produced by the GCM's (Giorgi, 1990; Reason *et al.*, 2006; Mbedzi, 2010).

Mesoscale atmospheric modelling has also been encouraged by the advancement in computer resources (Mass *et al*., 2002; Potgieter, 2006; Schulze, 2007; Landman, 2012); are capable of running weather forecast at very high grid resolution of at least a single digit (Reason *et al.*, 2006). From the global and local perspective, the availability of global forecast system (GFS) re-analysis data also contributed to the growth of research in the field of atmospheric modelling and climate analysis. These improvements also affect research capabilities in SA. Research studies have shown that regional models add value to a forecast since they have more skills than GCM's (Reason *et al.*, 2006; Cretat *et al*., 2012; Landman, 2012). In order to capture mesoscale events, these models have been setup to use the non-hydrostatic approach.

1.1.2 The non-hydrostatic modelling approach

The advancement of computers has encouraged modellers to apply non-hydrostatic approach for NWP forecasting to replace the traditionally used hydrostatic momentum

approximation. The non-hydrostatic approximation has been derived from the vertical momentum equation (eq. 1.1)

$$\frac{dw}{dt} - 2\Omega u\cos\Phi - (\frac{u^2+v^2}{a}) = -\frac{1}{\rho}\frac{\partial p}{\partial z} - g \qquad \textbf{(1.1)}$$

$$\frac{\partial p}{\partial z} = -\rho g \qquad \textbf{(1.2)}$$

For hydrostatic approximation, equation (1.2) is used where vertical velocity (w), Coriolis parameter ($2\Omega\cos\Phi$) and horizontal velocity terms u and v are ignored. This result in hydrostatic balance between pressure gradient term $-\partial p/\rho\partial z$ and the gravitational acceleration term g (Holton, 2004; Markowski and Richardson, 2010). The hydrostatic approximation is applied mostly for large scale synoptic scale circulation and can therefore be considered a traditional method for climate and weather simulations. In non-hydrostatic approximation all the terms in equation (1.1) are included in the application. The non-hydrostatic models are able to capture mesoscale events with a length scale up to 20 km and vertical scale up to 10 km. These events include turbulence and also thunderstorms which have vertical velocity up to 10 m/s (Markowski and Richardson, 2010). The non-hydrostatic models include vertical acceleration term dw/dt since vertical motion is of significance during updrafts and thunderstorm formations (Holton, 2004; Markowski and Richardson, 2010). Following Holton, (2004) and also Markowski and Richardson, (2010), meso-gamma scale has a horizontal scale of 20 km and dw/dt term is used when modelling thunderstorms motion. Applying scale analysis (Holton, 2004; Markowski and Richardson, 2010), vertical velocity has an order $O(w) \approx VD/L$, with V a characteristic horizontal velocity scale, D being the depth (height) scale and L the horizontal length scale. In this instance, V is approximately 10 m/s, D is 10 km, and L is approximately 20 km. Therefore vertical velocity is of order $O(w) \approx 10 ms^{-1}$ and cannot be ignored. Likewise, the vertical acceleration is of order $O(dw/dt) \approx UW/L$, where U is also a characteristic horizontal velocity scale of magnitude $10\,ms^{-1}$. Therefore vertical acceleration is of order $O(dw/dt) \approx 10^{-2} ms^{-2}$ and therefore cannot be ignored.

1.1.3 The temperature advection equation

The temperature advection equation (1.3) assists modellers in understating the behaviour of temperature and can be derived as follows:

$$\frac{\partial T}{\partial t} = -u\frac{\partial T}{\partial x} - v\frac{\partial T}{\partial y} \qquad \textbf{(1.3)}$$

where $\partial T / \partial t$ is the rate of change of temperature with time, u and v are both meridional and zonal wind speed, $\partial T / \partial x$ is the rate of change of temperature in the x-direction and $\partial T / \partial y$ is the rate of change of temperature in the y-direction (Markowski and Richardson, 2010).

Since NWP models are deterministic in nature; the concept that the future state of the atmosphere depends on the current state and its evolution is governed by the deterministic equations of motion is applied. However, the atmosphere is itself nonlinear/chaotic in nature and this limits the predictability of weather, which is also controlled by the nature of the initial state and lateral boundary conditions of the atmosphere (Potgieter, 2006; Cheng and Steenburgh, 2007; Schulze, 2007; Cretat *et al*., 2012; Landman, 2012).

1.1.4 Initial and boundary conditions

NWP models uses initial and boundary conditions (Giorgi and Bi, 2000; Potgieter, 2006) to integrate forward in time the equations of motion (Schulze, 2007). The initial and boundary conditions are provided by different GCM's models (Giorgi, 1990; Watterson, 1993; Giorgi and Bi, 2000; Cheng and Steenburgh, 2007; Schulze, 2007; Mbedzi, 2010; Ratnam *et al*., 2011). These GCM model fields are dynamically downscaled to high grid resolutions before they are used by mesoscale models (Kgatuke *et al*., 2008; Caldwell *et al*., 2009 and Ratnam *et al*., 2011). The objective of this exercise is to produce very fine resolution forecasts that have more skill than GCM's (Reason *et al.*, 2006). Therefore accurate NWP forecasts will depends on accurate description of the initial state of atmosphere (Giorgi and Bi, 2000; Galanis *et al.*, 2006; Potgieter, 2006; Schulze, 2007; Landman, 2012).

Although it is well known that the improvement in computer resources led to an improvement in NWP models (Mass *et al*., 2002; Potgieter, 2006; Caldwell *et al*., 2009), the meteorological community is still faced with a challenge when predicting the intensity, spatial and temporal resolution of precipitation accurately (Schulze, 1997). This is because computer resources lead to limitations in spatial resolution which can partially resolve convection explicitly. Such a limitation has resulted in modellers developing cumulus parameterization schemes (Grell and Devenyi, 2002; Gilliland and Rowe, 2009).

1.1.5 Physical and cumulus parameterization schemes

Regional models add value to forecasts although their forecasts skill depends on the choice of cumulus parameterisation schemes (Reason *et al.,* 2006; Cretat *et al*., 2012; Landman, 2012). Therefore accurate predictability of precipitation requires a thorough knowledge and application of atmospheric moisture dataset. It is also a challenge to predict rainfall within tropics where precipitation originates from convective activities including the SA summer rainfall region (Schulze, 1997; Tyson and Preston-Whyte, 2000; Blamey and Reason, 2009; Cretat and Pohl, 2011; Cretat *et al*., 2011; Ratnam *et al*., 2011; Cretat *et al*., 2012; Landman, 2012).

NWP models use physical and cumulus parameterization schemes to effectively simulates the effects of convection (Grell and Devenyi, 2002; Gilliland and Rowe, 2009), atmospheric instability and the vertical distribution of momentum, heat and moisture in the atmosphere (Engelbrecht *et al.,* 2007; Landman, 2012) to produce rainfall forecasts. These physical parameterization schemes represent atmospheric processes including dynamics and the microphysics within the clouds (Schulze, 2007; Gilliland and Rowe, 2009). Convection schemes can be used to exploit the understanding of physics and dynamics of convective clouds in order to express the interaction between large scale flow and convective clouds (Grell and Devenyi, 2002).

Cumulus parameterizations are very important for summertime convection (Cretat and Pohl, 2011; Cretat *et al.,* 2012) since during summer convection is represented less accurately than during cold season events. The dominant large-scale dynamics forcing are well modelled during cold seasons than during warm season's strong thermal forcing. The prediction of summer convective activities and rainfall may vary due to different

timing and location of initial convection which is determined by the chosen cumulus parameterization scheme (Gilliland and Rowe, 2009).

The main objective of using convective parameterization schemes in atmospheric models is to generate rainfall, and this depends on the availability of moisture and also the instability in the atmosphere (Ratna *et al*., 2013). These convection schemes used are also subjected to model uncertainty and are statistical in nature and lead to uncertainty in model predictions (Engelbrecht *et al.*, 2007; Mbedzi, 2010; Landman, 2012). The uncertainty and assumptions made by cumulus parameterization schemes result in incorrect temporal and spatial distribution of precipitation (Gilliland and Rowe, 2009; Mbedzi, 2010; Cretat *et al*., 2012; Landman, 2012; Vigaud *et al*., 2012). Therefore it is required that there must be enough moisture and vertical motions for precipitation to occur. When applying cumulus parameterization schemes, it is of importance to decide on the scheme to use depending on the type of convection system likely to develop. Users also need to have an understanding of how such a scheme will handle the type of environment, depending on whether it is moist or dry (Gilliland and Rowe, 2009).

Model physical parameterization scheme contributes significantly to the model forecasts error (Blamey and Reason, 2009; Caldwell *et al*., 2009) including temperatures (Homleid, 1995). When applying numerical model, the simulation of turbulence and cloud physics parameterization is very complex and has an element of uncertainty (Cretat *et al*., 2011). In mesoscale model application (Jandieri, *et al.*, 2011) parameterization algorithms can be very complex to apply in curvilinear coordinates system and results in additional work. Cumulus parameterization schemes limit the capabilities of NWP models since they require simplifications for computational purpose. They are also unable to realistically resolve very small scale weather features since they are limited by physical processes that need to be parameterized (Galanis and Anadranistakis, 2002; Galanis *et al.*, 2006; Cretat *et al*., 2012).

Cumulus parameterization schemes are also beneficial when running NWP models in an environment where major synoptic forcing are weak as they are required to represent sub-grid scale convection and precipitation. Most of the current cumulus parameterization schemes are designed for models with grid resolution between 32 and 48 km and not for finer scale grid used in mesoscale models including the WRF model which is designed to

run at grid spacing between 1 and 10 km. However, some models are designed to run at grid resolution less than 4 km and do not require cumulus parameterization since it is assumed that these models resolve some mesoscale processes explicitly. For these models, cumulus parameterization schemes may not work properly and may result in model misrepresentation of convection (Gilliland and Rowe, 2009). By trying to simplify the physical schemes, this may also result in internal model errors and uncertainties within the forecasts (Blamey and Reason, 2009; Landman, 2012). In order to solve the issues with NWP models, models must be tested, validated and model inter-comparison must be continued in order to identify errors (Klemp and Skamarock, 2004).

As much as physical and cumulus parameterization schemes are necessary, NWP models including the WRF model which is operated at a grid resolution less than 10 km (Gilliland and Rowe, 2009) also required the use of high grid resolution topography to match the model grid points in order to reduce these model errors (McQueen et *al*., 1995).

1.1.6 Higher grid resolution numerical weather prediction

During the 1950's, there has been improvement in computing power which has led to an increase in model horizontal grid resolution for operational purpose for the national meteorological service (NMS) (Mass *et al*., 2002; Schulze, 2007; Landman, 2012). Since then there has been an increasing trend in NWP modellers switching to high grid resolution modelling of less than 10 km, this was complemented by improvements in vertical resolution.

An increase in model grid resolution was motivated by the fact that when atmospheric forcing are weak, only high grid resolution observations produce detailed initialization needed to run atmospheric models (Mass *et al*., 2002; Schulze, 2007; Bonnardot and Cautenet, 2009). Higher grid resolution mesoscale models are capable of investigating the effects of topography (Bonnardot and Cautenet, 2009) and surface heating on the development of convective systems. In this instance, higher grid resolution topography is used to match the model's chosen grid points (McQueen et *al*., 1995). In either operational NWP or research purpose; higher grid resolution regional models can be used together with nests over a specific area of interest (Giorgi, 1990; Giorgi and Bi, 2000;

Landman, 2012). This technique was found to produce high resolution forecasts with superior quality and add value to forecasts (Schulze, 2007; Landman, 2012).

Higher grid resolution mesoscale models improve the representation of both the model physics and dynamics (Riphagen *et al.*, 2001). High grid resolution models can produce better results than lower grid resolution (Bonnardot and Cautenet, 2009) ensembles because ensembles use statistical averaging techniques (Landman, 2012). Higher grid resolution mesoscale models also improve the model output and predictability of small spatial scale events (Mass *et al*., 2002; Cretat *et al*., 2011). Evaluations of forecasts have shown that increasing the model horizontal resolutions produce better defined and more realistic meteorological structures (Riphagen *et al*., 2001; Mass *et al.*, 2002; Galanis *et al*., 2006; Skamarock and Klemp, 2008; Bonnardot and Cautenet, 2009).

The forecast accuracy, when measured objectively over an extended period of time increases as grid resolution increases to a value below 10 km (Mass *et al.*, 2002; Landman, 2012). However, higher grid resolution forecasts require the use of more computer resources (Mass *et al.*, 2002; Caldwell *et al*., 2009; Landman, 2012; Ratna *et al*., 2013). Other research studies show that deterministic short-term forecasts are more useful for convective events (Mass *et al.*, 2002). The objectively evaluated forecasts show significant benefits in increasing the model grid resolutions (Riphagen *et al*., 2001; Schulze, 2007) especially in regions where topographic flows or diurnal circulations are important (Mass *et al*., 2002).

Different meteorological centres use numerical models at various resolutions; *i.e.* National Centres for Environmental Prediction (NCEP) have used Mesoscale Model (MM5) at 12 km horizontal resolution. However its successor, the WRF model was implemented to use a horizontal resolution between 1 and 10 km. The MyCast prediction services at Digital Cyclone Incorporated make use of Penn State/National Center for Atmospheric Research (NCAR) MM5 with a horizontal resolution of 6 km (Mass *et al.*, 2002).

Various meteorological modellers have been experimenting with such high horizontal grid resolution models. The value of high grid resolution numerical forecasts varies according to application and need for users. This includes simulation of winds,

temperatures and rainfall (McQueen, *et al.*, 1995; Mass *et al.*, 2002; Bonnardot and Cautenet, 2008 and also Gilliland and Rowe 2009). When regional models are applied at high horizontal and vertical grid resolutions, they are able to capture mesoscale and small scale features which are topographically induced (Giorgi, 1990, Tennant and Van Heerden, 1994).

McQueen *et al*., (1995) have found that a 25 km horizontal grid combined with a high vertical resolution produce realistic meteorological structure. The authors also found that there is a great predictability and slower error growth at high grid resolution. This was attributed to the fact that LBC can significantly reduce error growth in local area models (LAM) since large scale information constantly sweeps through the inflow boundaries (Mass *et al*., 2002).

A study of convective systems with nonhydrostatic model, the Advanced Regional Prediction System (ARPS) model with grid spacing of +/- 4 km shows that a model is able to reproduce the observed structural evolution of a range of mesoscale convective systems (MCS). A grid resolution less than 5 km produce realistic convective evolution, and simulations start showing meso-cyclogenesis when grid spacing was less than 1.5 km. At 36 km the model could not simulate convergence features, at a grid resolution of 4 km, the model was able to simulate the convergence zone, and reproduced fine scale mesoscale features (Mass *et al*., 2002). Mass *et al*., (2002), also shows that wind speed error improves as resolution increases, whereby at 12 km, bias was less than at 36 km. However, when resolution was increased to 4 km, winds were marginally improved. This was attributed to sub-grid scale drag parameterization that was used for lower resolution model domain over complex terrain, which was not applied at higher grid resolution.

Gilliland and Rowe (2009) found that in idealized simulations, a 4 km grid resolution WRF model is capable of simulating or resolving main features super-cell and simulates the environment in a similar way as a 2 km model grid resolution without cumulus parameterization schemes.

High grid resolution mesoscale forecasts can increase the skill of human forecasters. As an educational tool, mesoscale model output helps human forecasters with complex evolution of 3-D mesoscale structures and how they are modulated or controlled by

synoptic scale flow. The value of using high grid resolution can be achieved when forecasting near substantial mesoscale terrain, in areas where there is a dense observational network or when synoptic flow is slow varying (Mass *et al.*, 2002).

1.1.7 Errors associated with numerical weather prediction models

Numerical models have been found to exhibit systematic errors (Persson, 2003, Libonati *et al*., 2008) especially when forecasting near-surface variables like temperatures (Cheng and Steenburgh, 2007) and wind speed (Mass *et al*., 2002; Jimenez and Dudhia, 2011). Firstly, model errors are due to inaccuracies in initialization data (Cheng and Steenburgh, 2007; Schulze, 2007). Secondly model errors are also due to the model formulations (physics and dynamics) (Galanis and Anadranistakis, 2002; Cheng and Steenburgh, 2007; Libonati *et al*., 2008; Blamey and Reason, 2009). Lastly model errors are also due to the model's inability to successfully handle sub-grid scale phenomena especially when interpolating to areas which are not close to model grid points (Homleid, 1995; Galanis and Anadranistakis, 2002; Galanis *et al.*, 2006, Cheng and Steenburgh, 2007, Libonati *et al*., 2008, Louka *et al*., 2008).

One of the challenges facing numerical modellers is that even though they can increase the model grid resolution, bias will still exist. This is due to differences in model elevation and observations sites (Cheng and Steenburgh, 2007, Libonati *et al.,* 2008). A height difference larger than 100 m between model and real topography result in large systematic bias in surface temperature forecasts (Homleid, 1995). The model horizontal grid resolution associated with smoothing of topography and landscape characteristics leads to weaker representation of local effects of airflow (Galanis *et al.,* 2006; Louka *et al.,* 2008). Therefore deterministic models produce accurate forecasts for a few days and then the accuracy deteriorates with time (Landman, 2012).

According to Mass *et al.,* (2002), in real-time MM5 objective forecasts, there is minimal forecasts improvements as grid spacing decreases from 12 to 4 km, therefore timing and position error increases as resolution increases. At higher grid resolution the structures are more realistic, the existence of timing errors results in lower objective values as resolution increases. The objective values depend on quantity and density of observational network. When data density is insufficient, important mesoscale structures

can be missed or poorly represented in analysis, resulting in no difference between verifications for lower grid resolution domains and higher grid resolution. However, there may also be less dense observational networks in mountainous areas and foothills. Therefore small scale structures observed at 12 km may not be observed at 4 km resolution.

The complexity of topography and local effects are not easily resolved by the numerical models and such a misrepresentation of model surface variables can result in conditional bias on forecasts (Homleid, 1995; Persson, 2003; Galanis *et al*., 2006; Cheng and Steenburgh, 2007; Libonati *et al.,* 2008, Louka *et al*., 2008; Jimenez and Dudhia, 2011). It is therefore important to initialise the model simulations with topography data at grid resolution corresponding to the model grid resolution in order to avoid smoothening of model topography (McQueen et *al*., 1995).

1.1.8 Atmospheric modelling at the University of Pretoria

The University of Pretoria (UP) has been active in the field of NWP for a while focussing on seasonal and long-time scales (Potgieter, 2006; Engelbrecht *et al.*, 2007), where previously a global model, a Conformal-Cubic Atmospheric model (C-CAM) from Australia's Council for Scientific and industrial Research (CSIRO) has been used. This model employed a variable stretched grid to allow for fine grid resolution simulations over a particular region of interest within the globe. The C-CAM model applies a hydrostatic dynamical core with a split semi-Lagrangian integration scheme in a terrain-following coordinate equation set at high computational efficiency and accuracy (Potgieter, 2006; Reason *et al.,* 2006; Landman, 2012).

Currently the University has acquired one of most world-wide used mesoscale model, the WRF model (Klemp and Skamarock, 2004; Skamarock and Klemp, 2008; Wang *et al.,* 2010). The WRF model has been installed on a super-compute named the Kaminari which was donated by Japan Agency for Marine-Earth Science and Technology (JAMSTEC). Most of the technical support was provided by JAMSTEC and Japan International Cooperation Agency (JICA) scientists. The relationship between UP and JICA/JAMSTEC also facilitates collaborations and enhances research capabilities. As

WRF is used operationally around the globe, new implementations are incorporated depending on needs as soon as they are communicated from the developers.

1.2 Problem statement

SA has varied and complex terrain features, including mountains and valleys which affect the weather within the country (see Figure 1.1 for the topographic map of SA). Extreme weather conditions like rainfall that result in floods and heat waves that result in extreme high temperatures are enhanced by the orientation and complexity of topography (Giorgi, 1990; Lyon, 2009; Barriopedro *et al.*, 2011; Ratna *et al.*, 2013). These two extreme events lead to catastrophe to human lives and also destruction to infrastructure.

A few research and modelling studies have been done to determine the influence of topography and resolution on the daily weather forecasts over SA. More research focused on the use of regional models to predict daily weather using ensemble forecasts and also seasonal forecasts and climate studies. This has been encouraged by the fact that single deterministic forecasts are subjected to criticism since they have been found to capture synoptic scale events and fail to capture mesoscale events including topographic induced systems. Ensemble forecasts are probabilistic in nature and believed to show good skill (Landman, 2012). Therefore in depth study of how topography influences daily weather pattern will be beneficial to the meteorology, agro-meteorology and farming community at large.

A lot of modelling studies are applied at a horizontal resolution lower than 20 km and daily operational weather forecast models are applied at a horizontal resolution lower than 10 km. However, in order to capture most of the mesoscale events, there is a need to apply very high horizontal grid resolution mesoscale models (Gross *et al.*, 1987; Marengo *et al.*, 1997; Pezza and Ambrizzi, 2005; Emmanouil, *et al.*, 2006; Muller and Berri, 2007; Skamarock and Klemp, 2008). These mesoscale models are able to achieve this task without much limitations since computer resources have reached an advanced stage (Mass *et al.*, 2002; Potgieter, 2006; Skamarock and Klemp, 2008) and the dynamical equations applied (non-hydrostatic approximations) are suitable to simulate and describe the atmospheric flow including topographic features (Gross *et al.*, 1987; Markowski and Richardson, 2010).

NWP forecasts for temperatures, rainfall and winds are very important for daily activities for farming, aviation industries and general public usage (Emmanouil *et al.*, 2006; Cheng and Steenburgh, 2007) and also to farmers during growing seasons, but also for planning during extreme (wet and dry) seasons (Lutgens and Tarbuck, 2010). The introduction of a mesoscale model, like the WRF model (Klemp and Skamarock, 2004; Skamarock and Klemp, 2008; Wang *et al.*, 2010) as a forecast guidance tool can benefit the community at large. This model will be able to solve the challenges mentioned above. Although the WRF model uses cumulus parameterization schemes like Grell-Devenyi ensemble scheme (Grell and Devenyi, 2002); these schemes have been developed in such a way that they effectively simulates the effects of convection accurately.

In order to achieve these tasks, large meteorological centres including NCEP-NCAR and ECMWF are available to support small centres with data used to run NWP models (Reason *et al.*, 2006). They supply research community and weather forecasting centres with observational and analyses dataset from the global forecasting system (GFS) models. These global model output can be downloaded and used to run weather prediction models at both regional and mesoscale resolutions (Giorgi, 1990).

1.3 Study aim and objectives

This study aim to apply the WRF model to achieve the following three interrelated goals:

- *To evaluate the capability of the WRF model as a NWP model to predict extreme weather events including heavy precipitation and heat wave events over SA*

The first aim will be achieved by running the WRF model at a horizontal grid resolution of 9 km with topography to simulate heavy precipitation and heat wave events over SA and compare the model output with station observations. For this runs, WRF simulated variables including rainfall, temperature, wind speed and relative humidity are compared to SAWS observations.

- *To evaluate the influence of topography on extreme weather events over SA*

The second aim will be achieved by running WRF model at a horizontal grid resolution of 9 km without topography to simulate heavy precipitation and heat wave events over SA and compare the model output without topography together with WRF simulations with topography and also station observations to determine if there have been any

changes between the two simulations. The above mentioned WRF variables are compared with station observations.

- *To evaluate the influence of grid resolution on simulations of extreme weather events over SA*

The last aim will be achieved by running WRF model at a horizontal grid resolution of 9 km (with topography) with a 3 km nest over Limpopo and Cape regions to simulate heavy precipitation event and heat wave events over SA and compare the model output at both 9 and 3 km with station observations to determine how an increased resolution affects the model output. It should be noted that the Limpopo region is considered to include the whole Limpopo province, parts of Mpumalanga, Northwest and Gauteng provinces, while Cape region includes stations located over Northern Cape, Western Cape and western parts of Eastern Cape respectively.

1.4 Study outline

The report is organised as follows: Chapter 2 introduces the topography of SA, which is the area of study. The chapter discuss the influence of complex terrain on rainfall, temperatures and winds over SA. Chapter 3 discusses the data, methods used, design of experiments, the WRF model as a NWP tool and its setup over SA domain, the WRF physics schemes and dynamics, case studies and techniques applied and verification methods together with the student's t-test statistics applied in order to verify simulations against observations. Chapter 4 and 5 discuss the results, with chapter 4 focusing on 9 km simulations with and without topography, whereas chapter 5 compares the results at 9 and 3 km grid resolutions. There are three case studies. The first case study is for a heat wave over Limpopo region for the period 22-26 October 2011. The second case study is for heavy precipitation event that resulted in floods which was caused by tropical depression Dando over Limpopo region for the period 16-18 January 2012 and the third case study is for a heat wave over Cape region for the period 15-18 January 2012. For all the case studies, the WRF model simulations are performed with and without topography and the results are compared with SAWS observations. Chapter 6 summarise the research findings, draw conclusions, assessing the scientific contribution of the study and make recommendations.

CHAPTER 2

THE INFLUENCES OF TOPOGRAPHY ON WEATHER OF SOUTH AFRICA

This chapter discusses the role that topography of South Africa has on meteorological variables including rainfall, temperature and winds. Initially, the study area (SA), together with its topography is introduced. It then discusses how topography has an influence on the weather of SA. Most attention is given to the relationship between topography, rainfall, temperature and winds. Knowledge of the role of topography on numerical weather forecasting improves the forecaster's skill, especially when issuing forecasts in areas of high topography. It also improves the meteorologist, agro-meteorologists and climatologists' knowledge and understanding of atmospheric dynamics over mountainous areas.

2.1 The topography of South Africa

South Africa (SA) has a varied terrain and is located in the southern parts of the African continent between (22^0S-35^0S; 16^0E-34^0E). The country is bounded on its western side by the cold Benguela current on the Atlantic Ocean and on the eastern side by the warm Agulhas current on the Indian Ocean (Blamey and Reason, 2009); see Figure 1.1 for detailed map of SA. The country has narrow coastal areas with low altitudes, which widens along the north-eastern coast of KwaZulu-Natal (KZN) Province, with an extension towards the "lowveld" which includes Mpumalanga and Limpopo Provinces (Mason, 1996; Schulze, 1997) and also incorporating the "flat" of the Western Cape Province. From the coastline, there is a steep rise in topography over the plateau from a level of 1-1.2 km towards the escarpment. The escarpment rises to a height of at least 3 km above sea level (Van Schalkwyk, 2011). The escarpment stretches from 20^oE-31^oE and between 200-300 km inland from the south and the east coasts. The peak of the escarpment is located over the Drakensberg mountains areas of KZN Province and Lesotho and constitutes the Maluti Mountains of Lesotho. A vast interior plateau to the inland of the escarpment drops gently from 1.5 km over the east to 1 km to the western side of the country (Schulze, 1997; Singleton and Reason, 2005; Blamey and Reason, 2009). The interior plateau occupies at least two thirds of the country (Tennant and Van Heerden, 1994). Then there is variability in altitudes, including irregular folded

mountains in Western and Eastern Cape Provinces, KZN and also Swaziland. This area descends abruptly into the coastlines (Bruyere, 1997; Schulze, 1997; Potgieter, 2006; Van Schalkwyk, 2011; Esau *et al*., 2012).

2.2 The weather of South Africa

2.2.1 Atmospheric circulation over South Africa

SA is situated within the subtropics, and its weather pattern is dominated by the high pressure belt which results in semi-arid conditions (Potgieter, 2006; Mason and Jury, 1997; Ratna *et al*., 2013). The country is therefore mostly dominated by anti-cyclonic flow (Landman, 2012). This results in a generally sunny skies and moderate temperatures at the surface. The country also receives insufficient rainfall which affects agricultural production (Bruyere, 1997; Hargraves and Jury, 1997).

The country's weather is also influenced by the circulation pattern due to both tropical and mid-latitudes system (Potgieter, 2006; Cretat *et al*., 2011; Cretat *et al*., 2012, Vigaud *et al*., 2012; Ratna *et al*., 2013) that also affects southern Africa and the surrounding oceans. A deviation in the mean circulation pattern may result in a variety of weather. This includes heat wave conditions and extreme rainfall. These extreme weather events can either be localized or may extend over large regions for months or years (Harrison, 1988; Potgieter, 2006).

The passage of cold front over the area from the west to the east coast over the Atlantic Ocean result in a high pressure system that ridges in behind it (Esau *et al*., 2012) and an advection of cold and dry air over the country. This is followed by subsidence behind a cold front and also dry adiabatic warming by subsiding air and absorption of solar radiation at the surface under clear skies. This system is responsible for raising surface temperatures to above normal temperatures (Taljaard, 1995; Potgieter, 2006). The detailed study on the weather pattern of South Africa has been described in Taljaard (1994, 1995) and also Tyson and Preston-Whyte (2000).

2.2.2 Temperature distribution and heat waves

Temperature has a direct effect on life, as it affects activities and processes including human comfort, energy supply, heat and cooling, crop and animal response (Schulze,

1997). Due to its location and topographical orientation, SA is also affected by the occurrence of extreme weather events including heat waves and drought during summer months. These two extreme events lead to socioeconomic and environmental impacts (Bruyere, 1997; Cassou *et al*., 2005). This is a period when most rainfall is expected, and such a dry summer season may lead to drought. The joint occurrence of drought and heat waves exuberate related impact in farming and agriculture (Lyon, 2009). Since the economy of SA is boosted by agricultural production (Ratna *et al*., 2013), a large amount of grains are lost in rain-fed agricultural region, a shortage of rainfall during drought season result in crop losses, livestock and human mortality and also stress to regional water supplies (Schulze, 1997; Robinson, 2000; Lyon, 2009; Barriopedro *et al*., 2011).

During heat wave episodes, daily maximum temperatures usually rise to values over 40^{o}C and minimum temperatures above 26^{o}C for a period of at least two consecutive days (Robinson, 2000). The high level of discomfort is experienced as soon as temperature values are higher than 35^{o}C and average relative humidity more than 25%. However, this criterion is considered subjective since heat waves are rare per decade (Robinson, 2000).

According to Lengoasa (1988), during summer months, when the presence of a high pressure system is located over the north-eastern parts of the country and a low pressure system over the south-west and south coast of the country, it result in westerly air flow over the western parts of the country. When this air moves eastwards, it is modified by surface heating and turbulent mixing of warm air near the ground. At the same time subsiding air due to anti-cyclonic motion produce dynamic warming of air mass as a result of adiabatic heating, especially in coastal areas which are affected by berg winds. Onshore flow of cool air across the west coast produce negative temperature anomalies, and when this air reaches the east coast it will be warmer and result in above normal temperatures by at least 4^{o}C. The presence of the high pressure system over the east coast will result in north-easterly air flow towards the western interior of the country. On the equator ward side, the airflow is easterly, which is continuously modified due to upper air and surface warming. By the time this air reaches the west coast, the temperature will be above normal by at least 1^{o}C.

A study by Bonnardot and Cautenet (2009) have shown that during high temperatures over Western Cape region, a high pressure system is located over the western interior and

a coastal low along the west coast. The system results in offshore flow (berg winds) ahead of the surface trough, and an onshore flow of dry air (Potgieter, 2006) behind the trough. As the trough moves eastwards, strong northerly winds impose high temperatures between 37^{o}C and 38^{o}C and relative humidity of at least 30%. Such conditions result in very high temperatures and dry weather.

Barriopedro *et al*., (2011) has also associated heat waves with specific atmospheric circulation patterns represented by a semi-stationary height anomaly at 500 hPa that dynamically produce subsidence, clear skies, light winds and warmer air advection and also prolonged heat conditions at the surface.

2.3 The influence of topography on weather variables

2.3.1 The influence of topography on rainfall

Orographic precipitation, synoptic scale systems and different air masses result in different types of weather patterns (Taljaard, 1996; Schulze, 1997). This pose a challenge to the field of meteorology since such a study involves the knowledge of both air flow dynamics and cloud physics. Knowledge gained from the study of mountain meteorology is very vital as it impacts water resources, flood and the role that mountains plays in the formation of deserts and also inter-ocean water transport. A study of mountain meteorology also address issues regarding topographic lifting (Schulze, 1997; Landman, 2012), and the importance of environmental parameters such as temperature, aerosol content and latent heat fluxes influence on air flow dynamics (Watterson, 1993). Such a study also addresses issues on whether the existing mesoscale or simpler models capture essential elements of orographic precipitation (Schulze, 1997; Smith, 2004).

Over the summer rainfall region of SA, mostly the eastern escarpment region including Limpopo region receives orographic precipitation due to slopes (Tennant and Van Heerden, 1994; Mason, 1996; Bruyere, 1997; Schulze, 1997; Riphagen *et al*., 2001; Potgieter, 2006; Cretat *et al*., 2012; Landman, 2012). This region covers a large proportion of agriculturally productive land of SA, receives on average the annual rainfall of approximately 1000 mm (Schulze, 1997; Dyson, 2008); with most rainfall occurring during summer months especially over the northern and central interior of the country

(Mason, 1996; Ratnam *et al*., 2011; Cretat *et al*., 2012; Landman, 2012; Ratna *et al*., 2013).

Most of the summer rainfall over the country result from deep convection embedded within rain bearing systems such as inter-tropical convergence zone (ITCZ), south Indian convergence zone (SICZ), easterly waves and tropical storms (Cretat *et al*., 2012). However over the western parts, including Western Cape Province most of the rainfall is received during winter months (Van Schalkwyk, 2011; Landman, 2012). Some areas over the southern Cape and coast receive rainfall throughout the year (Schulze, 1997; Landman, 2012).

Vertically propagating gravity waves consisting of updrafts and downdrafts develop over topography and produce orographic clouds and enhances precipitation. This was found to contribute 80% of total precipitation at high elevation. Orographic clouds can act as a feeder condensate for orographic enhancement of precipitation in large scale weather systems (Galewsky, 2009).

Topographically induced mesoscale circulations often result from the interaction of synoptic scale flow with fixed complex terrain (Bonnardot and Cautenet, 2009), and thus result in mesoscale predictability being controlled by synoptic scale predictability (Mass *et al*., 2002). During weak synoptic scale systems, convective clouds develop in mountainous areas. This is triggered by local topography circulations resulting from differential heating of surface, sufficient moisture and instability (Potgieter, 2006).

Higher grid resolution mesoscale models have been used to investigate the effects of topography and surface heating on the development of convective systems (Bonnardot and Cautenet, 2009). This is due to the fact that convective events are mostly caused by the steepness of topography. The interaction between airflow and topography determines the preferred area of cloud and precipitation development; whereas the steepness of topographic gradients controls the intensity of the storm (Bruyere, 1997; Singleton and Reason, 2005). In flat areas, surface heating affects the development of convection (Blamey and Reason, 2009). In this instance surface heating controls the time of initial development and the duration of the storm. It has also been found that most convective

activities occurs during the late afternoon, *i.e.* between 15h00 and 16h00 South African Standard Time (SAST) (Esau *et al.*, 2012).

Tennant and Van Heerden (1994) found that model simulations of precipitation with topography indicate that mountains are responsible for large amount of orographic precipitation, *i.e.* in Eastern Cape. However, when topography is removed from the simulations, little or no rain was simulated. This occurs when the south Atlantic high pressure system begins to ridge into the south of the country, advecting moist maritime air onto the east coast (Esau *et al.*, 2012). In simulation without topography, a strong upper-air divergence resulted in no surface convergence and uplift development. This was found to result in weaker surface pressure system and upper-air cut-off low moving eastward rapidly (Tennant and Van Heerden, 1994).

An experiment was performed by Singleton and Reason (2005) on rainfall over SA using the 5th generation, Pennsylvania State University-National Centers for Atmospheric Research (NCAR) regional MM5 model. Simulations were performed with and without topography. Over the continent, there were differences in simulation, with a meso-beta scale low extending further west of the country in simulation without topography whereas it was located to the east of the country in simulation with topography. This result indicates the importance of the Drakensberg over the eastern parts of SA which was responsible for maintaining the position of the trough over the east coast of SA.

Blamey and Reason (2009) found that topography of the eastern parts of SA triggers the formation of MCS and also the evolution of cut-off lows. This is attributed to a fact that topography promotes uplift of moist air, and when topography was removed, there was reduction of uplift by 75%. The removal or smoothening of topography reduces uplift and then resulting in less precipitation. It was therefore suggested that topography was responsible for directing winds than to influence its magnitude. The removal of topography also leads to weaker low level moisture convergence over the region. When topography was removed, a high pressure system between 800-700 hPa was missing. This high pressure system was responsible for increasing the onshore moisture advection into the coastal areas to enhance precipitation in simulation with topography. The absence of the high pressure system resulted in reduced rainfall. From this experiment it was suggested that the eastern escarpment enhanced the storm (Hargraves and Jury,

1997), and that without topography synoptic scale forcing were not capable of producing significant precipitation.

Ratna *et al.*, (2013) confirmed in their studies that WRF simulations show high wet bias near the Drakensberg Mountains due to strong topography that triggers convection. An abundance of low level moisture and the presence of a low pressure system result in topography triggering convective clouds due to moisture convergence zone (Potgieter, 2006; Ratna *et al*., 2013). Fog bearing winds (warm moist maritime air) from the Indian Ocean moves over the eastern escarpment rises against the elevated terrain (steep mountains) and result in stratocumulus clouds (Van Schalkwyk, 2011). Wind speed and moisture content of fog increase with height, and areas with high elevation of at least 1km *i.e.* Soutpansberg (Salt Pan Mountains) receives more water from fog. The problem of water shortages and the frequent occurrence of fog in this drought prone area have led to an initiative to harvest fog water to alleviate water shortage to some of the rural communities over the province (Olivier and Rautenbach, 2002; Dyson, 2008).

2.3.2 The influence of topography on temperatures

Higher altitudes generally result in lowered temperatures, even though the temperature lapse rate varies with region and season. Changes in altitudes during cooler months result in cold air drainage in valleys. This occurs during night-time and often results in an increase in frost occurrence (Schulze, 1997; Libonati *et al*., 2008). Temperature can also be influenced by the amount of total monthly rainfall and latitudes, whereby temperature decreases as latitudes increases towards the poles (Schulze, 1997). An increase in altitude which can also be linked to reduced atmospheric pressure can be a direct factor in enhancing solar radiation. Such an increase in altitude results in increased rate of vaporisation under clear sky conditions. The opposite is the case under cloud cover where evaporation is reduced (Schulze, 1997).

Topographic slopes and orientation determines daily temperatures (Cretat *et al*., 2012). On a microscale, changes in altitudes affect solar radiation and temperature distribution, and this depends on the orientation of landscape (Esau *et al*., 2012). The north facing slopes receive more incoming solar radiation and are warmer than the south facing slopes which receive less radiation and are therefore cooler (Schulze, 1997). The east facing

slope are normally warmer than western facing slope, due to that the east facing slope experience long sunny hours than the west facing slopes. In general, the west facing slopes also cool faster with altitude as compared to the warmer east-facing slopes resulting in lapse rate very close to adiabatic (Schulze, 1997; Smith, 2004).

The presence of mountains results in temperature lapse rates which usually show a decrease of temperature with height, whereas positive temperature lapse rates are connected with the intersection of an elevated atmospheric inversion with the sloping terrain. These lapse rates also vary with latitudes, region, season (Schulze, 1997) and the availability of cooler mountain conditions reduces extreme heat and humidity. Maritime air masses and moderate diurnal temperatures (Van Schalkwyk, 2011) prevent excessively high temperatures in summer and extreme low temperatures in winter (Bonnardot and Cautenet, 2009). Changes in altitudes can cause cooler months under atmospheric stability to result in cold air drainage in valley during night time, resulting in frost occurrence (Schulze, 1997).

Lyon (2009) has shown that the anomalously westerly low level flow across a very cool south-east Atlantic Ocean into the western and southern parts of SA was consistent with some probability of heat waves during drought. The analysis of 850 hPa reanalysis winds data over St. Lucia bay (KZN) shows a north-westerly downslope flow. Likewise further analysis of coastal stations indicates that steep topography and adiabatic ascent in the form of berg winds are important for the development of heat waves at coastal stations due to local topography and ocean effects. It is also known that daily maximum temperatures are also affected by variations in cloud cover, proximity to large water bodies, prevailing wind direction and thermal advection.

2.3.3 The influence of topography on winds

The origin of all local winds is due to the discontinuity in the energy balance fields. The discontinuities occur in various places, *i.e.,* across the shorelines of lakes and seas, between sloping surfaces and the air beyond those surfaces, and also between mountains and valleys. Therefore a clear distinction between local and regional winds is required when considering land and sea breezes and topographically induced winds occurring over

slopes and valleys (Tyson and Preston-Whyte, 2000; Bonnardot and Cautenet, 2009; Markowski and Richardson, 2010).

In orographic mesoscale phenomena, winds are generated by heating and cooling of slope terrain (Tyson and Preston-Whyte, 2000) or differences in diurnal temperature ranges within valleys as compared to the surrounding plains (Mass *et al*., 2002; Bonnardot and Cautenet, 2009). The driving force for the valley winds is buoyancy, which is generated by warming (cooling) of the layer of air adjacent to the slope (Tyson and Preston-Whyte, 2000; Markowski and Richardson, 2010).

During cold air outbreaks in mountainous areas, mountains act as a barrier, where cold events are accompanied by the meridional elongated pressure ridge (high) and a strong low-level ageostrophic winds that blows parallel the mountains (Marengo *et al.*, 1997). A pronounced tendency of air flow around hills (Smith, 2004) is due to a stable stratified layer of air at the lowest layer of atmosphere. This occurs as a result of drainage flow from the slopes which oppose the geostrophic wind flow pattern (Gross *et al.*, 1987). The occurrence of strong winds, moderate static stability over a low mountains result in a flow where an air parcel can easily flow over a mountain. The presence of weak winds, strong static stability and high mountains result in low-level airflow which stagnates or run parallel to the terrain contours. The stagnated air fills the valleys and upslope regions and winds aloft still hit the exposed mountain peaks, causing gravity waves aloft (Stull, 1988; Taljaard, 1996; Smith, 2004; Galewsky, 2009; Markowski and Richardson, 2010; Jandieri *et al.*, 2011).

During the day, a horizontal buoyancy gradient exists between air in contact with the heated or cooled slope surface and the air at same altitude far away from the surface that is relatively unaffected by the heating or cooling of the surface. The heating of mountain slopes during the day result in upslope (slope or anabatic) winds and the night-time radiative cooling of mountain slopes generates downslope (valley or katabatic) wind (Tyson and Preston-Whyte, 2000; Pielke Sr, 2002; Bonnardot and Cautenet, 2009; Markowski and Richardson, 2010). During the day, thermal stratification is neutral or unstable in the lowest layers, resulting in winds flowing over the obstacle or a steep slope (Smith, 2004). The nonhydrostatic mesoscale models (Pielke Sr, 2002) are able to simulate the velocity and also the turbulent kinetic energy fields. The hydrostatic models

cannot be applied for this simulation since the horizontal length of the flow is very short to apply in a hydrostatic dynamical core (Gross *et al.*, 1987).

The ambient air flow is superimposed on thermally induced circulations, and these results in a complex flow pattern. At night cold air currents develop, which are a characteristic of a river valleys and depressions. This occurs when gradient wind caused by prevailing synoptic system (Tyson and Preston-Whyte, 2000) does not dominate the flow (Taljaard, 1996) and result in stagnation (Stull, 1988). This process starts after sunset and continues throughout the night, when calm air in contact with the ground rapidly cools down in the absence of clouds (Schulze, 1997; Emmanouil *et al.*, 2006). A layer of dense air starts to move down the slopes (katabatic drainage) and collects in valleys (Markowski and Richardson, 2010) under the influence of gravity. The temperature difference in the same horizontal level creates a pressure gradient which causes this air to move down the slopes, with a speed of about 1 m/s at a height of 1 m and is a result of colder air adjacent to the ground (Gross *et al.*, 1987).

In numerical modelling, the application of terrain following coordinates system causes problems when subjected to a weak flow. For instance when wind cannot flow over a mountain and a motion has to go around the slope. Likewise numerical diffusion and pressure gradient errors along the coordinate surface degrade the model accuracy (Jandieri, *et al.*, 2011). Application of Froude number ($F = Nh/u$), where F is the Froude number, N is the Brunt-Väisälä frequency and h is the orogen-scale topographic relief, indicates that in a 2-D topography, when F is very small the terrain is considered to be hydro-dynamically low and air can flow directly over topography without any deflection. However, when F is very large, topography is considered hydro-dynamically high and winds are blocked by terrain and therefore cannot flow directly over the terrain which results in a more complex flow regime (Galewsky, 2009).

CHAPTER 3

DATA AND METHODOLOGY

In the current chapter, all the dataset used and the methodology applied to simulate the atmospheric motion case studies and also to verify the WRF model output are discussed. The chapter also gives a brief description of the SAWS synoptic station data used to verify the WRF model output. It also includes information on the SAWS daily weather bulletins used as reference to explain the surface synoptic pattern of the events that took place and compare with the WRF model output. The chapter also describes the WRF model setup in details. It also discusses the model input data used during model setup including topography. The GFS input data; both initial and boundary conditions are also discussed. The physics, including the cumulus parameterization schemes and dynamics are also discussed. The last part describes the statistics used and the formulae applied for verification process. The studies focus on (i) heat wave for the period 22-26 October 2011; (ii) heavy precipitation event that resulted in floods for the period 15-19 January 2012 and also (iii) heat wave during the same period 15-19 January 2012. A heat wave is described as an event whereby a station recorded maximum temperature higher than the climate's daily average maximum temperature over the province for such a particular month. However for heavy precipitation event that resulted in floods, the SAWS observed and WRF simulated rainfall median values has been compared with the average rainfall median values for January as applied in Schulze (1997) climatological record (see Figure A.7).

3.1 Data used

3.1.1 The Weather Research and Forecast model

The WRF model was developed by the National Center for Atmospheric Research (NCAR) (Ratna *et al.,* 2013) and maintained by the Mesoscale and Microscale Meteorology (MMM) division of UCAR (Wang *et al.,* 2010). The WRF model is a nonhydrostatic mesoscale NWP model, fully compressible and has terrain following sigma coordinates (Ratna *et al.,* 2013); with grid staggering options as it provides a better representation of gravity waves. These staggering grids admit the possibility of null modes, which assume that there is no decoupling of odd and even grid point pressure values. Grid staggering also allows for discretization of pressure gradient and divergence

terms across a single grid interval without applying any averaging (Skamarock and Klemp, 2008). The purpose of the WRF model is to provide meteorologists and atmospheric scientists with a tool that can be used for both daily operational weather prediction, support research work on climate studies and also air pollution.

3.1.2 Weather Research and Forecast model verifications

The South African Weather Service (SAWS) weather stations surface synoptic data are used to verify the WRF model meteorological simulations. On average, a total of the country's 210 synoptic stations with complete daily surface dataset for the period of study were acquired. Of this dataset an average of 37 stations are located over Limpopo and 88 over Cape regions respectively. It should be noted that the Limpopo region is considered to include stations over the whole Limpopo province, parts of Mpumalanga, Northwest and Gauteng provinces, while Cape region includes stations over Northern Cape, Western Cape and western parts of Eastern Cape Province respectively. The surface observations dataset includes maximum and minimum temperature, rainfall, relative humidity and wind speed. The WRF model's 24 hourly simulations are evaluated during each case study. Rainfall's 24 hourly total is calculated from 06h00 on the day of interest to 06h00 the following day. However, for temperatures, wind speed and relative humidity, 24 hourly data is calculated from 00h00 on the day of interest to 00h00 the following day. These dataset has been subjected to quality control, where invalid or erroneous data is removed before verification process. A missing data is assigned a value of -999.0 for that variable at that particular station. Formula Translation (FORTRAN) programs were written to read SAWS station dataset into a format compatible with Grid Analysis and Display System (GrADS) program, to read model data, to interpolate model data to SAWS stations and to perform verifications. As a reference for synoptic patterns, SAWS daily weather bulletin maps have been acquired for the duration of study. They provide guidance on mean sea level pressure, rainfall, maximum and minimum temperatures and winds.

3.1.3 National Centre for Environmental Prediction global forecasting system data

The National Oceanic and Atmospheric Administration (NOAA), National Centers for Environmental Prediction (NCEP) research archived dataset is used to initialize and provide boundary conditions to the WRF model. The data are made available by the University Cooperation for Atmospheric Research (UCAR) as grib-2 NCEP research archived dataset with a horizontal resolution of (1^{o}x1^{o}) and available every 6 hours at 00, 06, 12 and 18 universal coordinated time (UTC). In this study, the WRF model was initialized using the 00h00 UTC dataset. The dataset is made available for download at UCAR research archive website (NCEP, 2000).

3.2 Methodology

3.2.1 Numerical experiment design

The WRF model has been setup to use the Eulerian integration time step method. The model has been configured to simulate meteorological events on a real mode for research case studies. The WRF model is set-up to perform simulations over southern Africa domain at horizontal grid resolution of 9 km (11^{0}S-38^{0}S; 11^{0}E-51^{0}E) with 451 grid points in the east-west and 337 grid points in the south-north direction and 29 vertical sigma levels (Figure 3.1 b). For higher grid resolution simulations, the WRF model has been nested with a 3 km domain over Limpopo region, (22^{0}S-26^{0}S; 26^{0}E-32^{0}E) with 211 grid points in the east-west and 151 grid points in the south-north direction (Figure 3.1 d). This setup applies for both the October 2011 and January 2012 case studies. The 9 km resolution has also been nested with a 3 km domain over the Cape region, (26^{0}S-35^{0}S; 16^{0}E-26^{0}E) with 336 grid points in the east-west and 381 grid points in the south-north direction (Figure 3.1 f). This setup applies for the January 2012 case study. In Figure 3.1, the top panels show the real or digital elevation model (DEM) topography map of SA at 0.25x0.25 grid resolution (Figure 3.1a) and the WRF 9 km model domain with topography over South Africa (Figure 3.1b). The middle panels show both the WRF 9 km (Figure 3.1c) and the WRF 3 km (Figure 3.1d) model domain over Limpopo region.

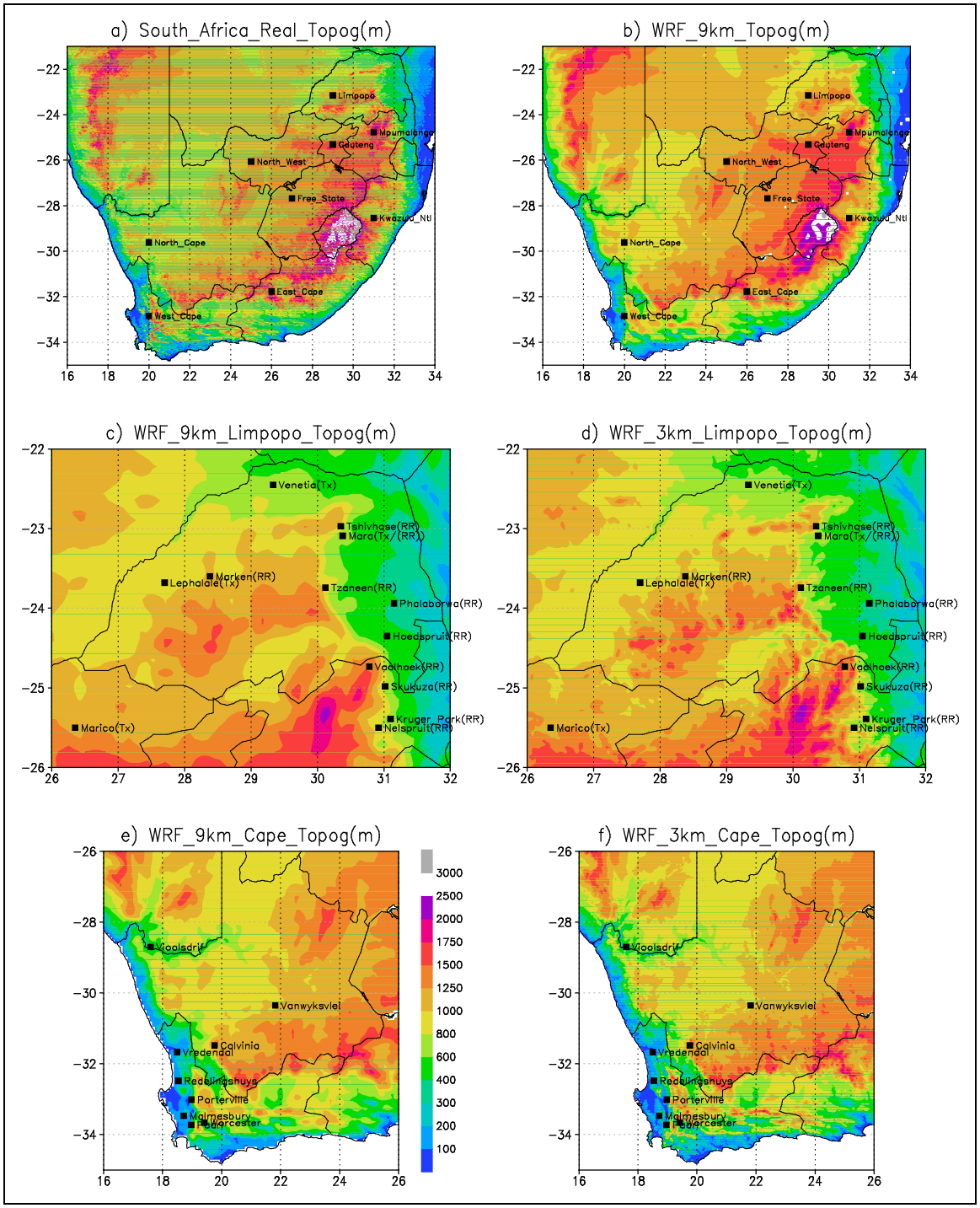

Figure 3.1: SA real topography map (DEM) (a); WRF 9 km domain over South Africa (b) WRF 9 km domain over Limpopo region (c) WRF 3 km domain over Limpopo region (d) WRF 9 km domain over Cape region (e) and WRF 3 km domain over Cape region. The WRF model topography is depicted in meters. Also depicted are some of the stations used for verifications

The bottom panels show both the WRF 9 km (Figure 3.1e) and the WRF 3 km (Figure 3.1f) model domain over Cape region respectively. This WRF model setup uses the

Mercator map projection, as it is more suitable for sub-tropics with a predominant west to east extent. This projection also helps reduce distortions of the area covered by the model grid points and avoids unnecessary restriction of the model time steps (Wang *et al.*, 2010). The WRF setup includes a one way nesting approach, where the nests can only receive initial and boundary conditions from the parent domain and do not provide feedback to the parent domain (Giorgi, 1990; Tesche and Tremback, 2002; Kgatuke *et al*., 2008, Mbedzi, 2010; Boulard *et al*., 2012). However, depending on the objective of the study, some researchers apply a two way nesting techniques, *e.g*., Ratna *et al*., (2013). Data assimilation schemes and smoothing options are not applied for this model setup (Wang *et al.*, 2010).

The WRF model is installed with a data pre-processing component for the advanced research WRF (ARW) dynamical core. The GFS table is applied to match GFS initialization dataset. This table includes variables like, temperature, winds, relative humidity, pressure (surface and sea-level), soil moisture and temperature at different levels below the ground, sea ice, land-see-interface, skin temperature, snow, and soil and land-use threshold (Wang *et al.*, 2010). The 9 km domain uses 2 arc-minute (equivalent of 3 km) and the 3 km domain uses 30 arc-second (equivalent of 1km) topographical data for the simulations (McQueen et *al*., 1995). The WRF model setup includes four levels of soil moisture and temperature below the ground. The model runs use multiple processors in order to process large domain dataset in a short period of time while reducing computer time (Wang *et al.*, 2010)

3.2.2 The WRF model initialization and boundary conditions

The WRF model is initialized with the NCEP grib2 format dataset. A default four-point data interpolation method was applied for the terrestrial data. The WRF-ARW model setup contains executable that automatically creates initial and boundary conditions for both the parent domain and the nest before it performs model simulations. During the initialization stage, the model interpolates meteorological data in the vertical coordinates. The current WRF model setup of 9 km grid resolution applies an integration time step of $6x\,dx$, which is equal to 54 seconds, whereby dx is in kilometers as recommended in the model setup manual. The model is setup to perform forward numerical integration up to

96 hours during January's heavy precipitation event and 48 hours during October heat wave event, using a Runge-Kutta 3 time integration scheme (Wang *et al.*, 2010).

3.2.3 The WRF model physical parameterization schemes

The WRF model is applied with a full range of physical parameterization schemes for land-use, PBL, atmospheric and surface radiation, cloud microphysics and cumulus convection. A simple and efficient WRF single moment 3-class microphysics scheme has been applied. For long wave radiation; a rapid radiative transfer model (RRTM) scheme was applied. For short-wave radiation, a Dudhia scheme was also applied. WRF applies MM5 similarity surface layer physics scheme. The PBL scheme applied is the Yonsei University scheme. Heat and moisture fluxes from the surface are also prescribe in the model setup. The soil temperature surface physics has been activated. Cloud effects are taken into account with a scheme compatible to the long wave and short wave radiation schemes (Wang *et al.*, 2010). The chosen physical packages has also been used in different studies including Cretat *et al*., (2011); Ratnam *et al*., (2011) and also recently by Ratna *et al*., (2013).

3.2.4 WRF cumulus parameterization schemes

For cumulus parameterization, a Grell-Devenyi Ensemble (GDE) scheme has been selected. The scheme applies ensemble data assimilation techniques to find the best value to feedback to larger scale model. It also applies statistical techniques to find the most probable solutions (Grell and Devenyi, 2002; Ratna *et al*., 2013). During convection, the cumulus parameterization schemes play a major role in producing precipitation (Cretat and Pohl, 2011). This is attributed to the fact that GDE scheme is able to detect the development of convection. The dynamic controls, *i.e*. moisture convergence within the GDE scheme triggers convection. The weakness of GDE scheme is that it triggers convection very early and that the scheme may result in a development of broad area of convection that is not representative of the actual isolated nature of convective cells. However, the GDE scheme is on overall able to represent the general area and the intensity of precipitation (Gilliland and Rowe, 2009). The GDE scheme was found to reproduce South African rainfall (Cretat and Pohl, 2011; Ratnam *et al*., 2011; Ratna *et al*., 2013).

3.2.5 WRF dynamical schemes

The WRF model uses different numerical solvers for dynamic equations with a focus on Eulerian split-explicit versions of a set of basic equations and numerical techniques. The WRF model is setup to use a Runge-Kutta 3 time-split integration technique as it efficiently integrate a fully compressible nonhydrostatic equation of motion (Skamarock and Klemp, 2008) with time-split small steps for acoustic and gravity wave modes. The model was setup to use a 2nd to 6th order advection schemes in both horizontal and vertical (Wang *et al.,* 2010). The WRF model includes two diffusion parameters, (i) diffusion option which selects how derivatives used in the diffusion processes are calculated and (ii) K-option; which selects how the K coefficients are calculated. For the applied model version, *i.e.* WRF (V3.4a), the vertical diffusion is linked to the surface fluxes. A simple diffusion scheme is applied with gradients taken along the coordinate's surface. The model physics included a PBL scheme for vertical diffusion, resulting in the selection of a 2 dimensional (2-D) deformation K-option for the horizontal deformation. The WRF model also has a 6th order horizontal diffusion scheme which acts as a selective short wave numerical noise filter (Wang *et al.,* 2010). The model also applies an artificial energy sink to avoid re-tuning of sub-grid turbulence parameterization in order to achieve a realistic energy spectrum at smaller scales (Klemp and Skamarock, 2004).

3.3 Model verification statistics

In order to evaluate the performance of the WRF model, the output from the simulations is verified objectively using World Meteorological Organization (WMO), verification methods as stipulated in Gordon and Shaykewich (2000). This is performed in order to test for the accuracy and reliability of the model output.

3.3.1 The WRF model runs

The WRF model experiments are setup to simulate weather at both 9 and 3 km resolution, respectively with and without topography. For the first objective verifications, the model results for the 9 km experiments are compared objectively to SAWS surface synoptic maps to determine if the model is able to capture the synoptic events as described in section 4.1 and 4.2 respectively. The variables evaluated include pressure and winds at the surface or 1000 hPa. Likewise, synoptic evolution at different pressure levels is analyzed to determine how the synoptic scale systems influenced these extreme weather

events. The variables analyzed include geopotential heights, horizontal winds, and vertical velocity and moisture fluxes at pressure levels 850, 700 and 500 hPa respectively.

For the second objective verification, the model simulations are interpolated to the SAWS station locations. The haversine formula (3.1) is used to calculate the distances between the model grid point and the observation station for the total of four model grid points surrounding each SAWS weather station. Thereafter, a weighted average value is computed using formula (3.2), whereby more weight is allocated to the grid point closest to the station. This technique has also been used by Mass *et al*., (2002) and also Jimenez and Dudhia (2011). It is assumed that the technique works well as there is a good agreement between model time step and times of observations (06h00 UTC) and also heights (2 m for temperatures and 10 m for winds). The technique faces challenge in mountainous areas, including SA where there are fewer or no synoptic stations (Mass *et al*., 2002). Thereafter comparison with surface observations is done to (i) evaluate the capability of the WRF model using the GDE scheme to simulate extreme weather events, (ii) to evaluate the role of topography on both extreme weather events, (iii) to evaluate the role of different grid resolutions on extreme weather events simulations. The built in functions within the WRF model post-processing programs calculated most of the atmospheric variables used as output. This includes rainfall, temperature, wind speed and relative humidity.

$$d = 2r\left[\sqrt{\sin^2\left(\frac{\Phi_2-\Phi_1}{2}\right)+\cos(\Phi_1)\cos(\Phi_2)\sin^2\left(\frac{\lambda_2-\lambda_1}{2}\right)}\right] \quad \textbf{(3.1)}$$

$$T\max(station) = \frac{\sum_{k=1}^{n} w(n)T\max(n)}{\sum_{k=1}^{n} w(n)};\ w(n) = \frac{1}{d_i^{\,2}} \quad \textbf{(3.2)}$$

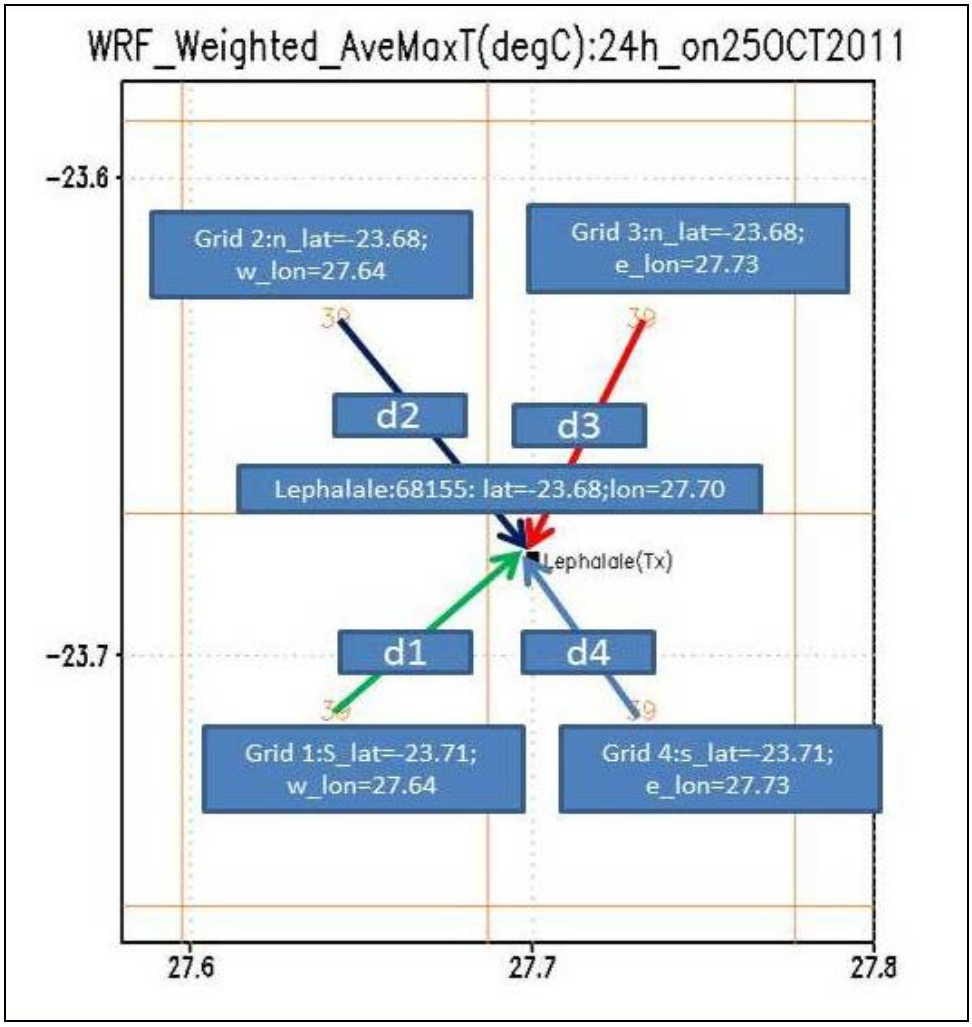

Figure 3.2: The WRF 9 km grid points over Limpopo station (Lephalale) illustrating the weighted average method to interpolate model grid values to SAWS synop station. The grid point that is closest to the station is allocated more weight whereas the grid point that is furthest from the station is allocated less weight.

where d is the distance between the synop station and the model grid point, r is the radius of the earth, $r = 6374000m$, Φ_1 latitude where the synop station is located; Φ_2 latitude at the model grid point; similarly $\Phi_2 - \Phi_1$ is the difference between the two latitudes (one latitude for the synop station and another for the grid point, λ_1 longitude where the synop station is located; λ_2 longitude at the model grid point; $\lambda_2 - \lambda_1$ is the difference between the two longitudes (one longitude for the synop station and another for the grid point; $w(n)$ is the weight assigned to the particular grid point with respect to the observation station and $1/d_1^2$ is the square of the distance between the observation

station and the model grid point. Lastly the term $T\max(n)$ is the model simulated maximum temperature at each grid point whereas $T\max(station)$ is the weighted maximum temperature for that particular station. Similarly, equation (3.2) has also been applied to minimum temperature, rainfall, maximum wind speed and maximum relative humidity.

3.3.2 Verification statistics

(a) Temperature, wind speed and relative humidity verifications

If N is the sample number of forecasts or observations, f is the model simulation and o is the observations, then the following formulae apply. Bias (3.3) measures the average difference between the model simulation and observations. The mean absolute error (MAE) formula (3.4) is an accuracy measure; it measures the absolute difference between the model simulation and observations. The mean square error (MSE) formula (3.5) measures the square of the average difference between the model simulation and observations. The root mean square error (RMSE) formula (3.6) measures the square root of the MSE (Gordon, and Shaykewich, 2000; Tesche and Tremback, 2002).

$$Bias = \frac{1}{N}\sum_{i=1}^{N}(f_i - o_i) \qquad \textbf{(3.3)}$$

$$MAE = \frac{1}{N}\sum_{i=1}^{N}(|f_i - o_i|) \qquad \textbf{(3.4)}$$

$$MSE = \frac{1}{N}\sum_{i=1}^{N}(|f_i - o_i|)^2 \qquad \textbf{(3.5)}$$

$$RMSE = \sqrt{MSE} = \sqrt{\frac{1}{N}\sum_{i=1}^{N}(f_i - o_i)^2} \qquad \textbf{(3.6)}$$

$$r_{f,O} = \frac{\sum_{i=1}^{N}(f_i - \bar{f})(o_i - \bar{o})}{\sqrt{\sum_{i=1}^{N}(f_i - \bar{f})^2}\sqrt{\sum_{i=1}^{N}(o_i - \bar{o})^2}} \qquad \textbf{(3.7)}$$

The Pearson correlation coefficient (CORR) formula (3.7) measures the strength of the relationship between the model simulation and observations, whereby $r_{fO} \in [-1,1]$. A CORR of +1 indicates a perfect positive linear relationship; a value of 0 indicates no linear relationship; and -1 indicates a perfect negative linear relationship between the

model simulation and observations. The statistical techniques are applied to test for model reliability and accuracy includes bias (3.3), RMSE formula (3.6) and CORR formula (3.7) for all continuous variables, *i.e*. temperatures, maximum wind speed and maximum relative humidity. Accuracy is a measure of how close the model simulation is to the observations. Also reliability of the model simulation is tested, whereby the average bias of the model simulation is compared to average bias of the observation. From this statistic, a bias value of "0" indicates a perfect score (Gordon and Shaykewich, 2000). It should be noted that all the scores are calculated over a period of 24 hours stating from 00h00 UTC on the day of the forecast to 00h 00UTC the following day.

(b) Rainfall verifications

For rainfall thresholds, the statistics includes bias (eq. 3.8), probability of detection (*POD*) formula (3.9) and Pearson correlation coefficient (CORR). These statistical values are derived and calculated using table (3.1) and formulae (3.8-3.9) below. Please note that bias is calculated differently for rainfall (formula 3.8) as compared to temperature, wind speed and relative humidity (3.3).

Let A = number of correct rainfall forecast when rainfall was observed, B=number of correct rainfall forecast when rainfall was not observed, C= number of no rainfall forecast when rainfall was observed and D= number of no rainfall forecast when rainfall was not observed. Bias formula (3.8) is a measure of reliability, and is a ratio of the number of times an event was forecast divide by the number of times the event was observed. This value is always positive; a reliable and perfect forecast has a bias value of "1". Probability of detection (POD) is a measure of accuracy, it measures the proportion of times that the event occurred and also correctly forecasted. The following scores, percentage correct (PC), POD, false alarm ration (FAR) and critical success index (CSI) are considered a measure of accuracy. POD and the last two scores are considered good measures for rare events like heavy precipitation (Gordon and Shaykewich, 2000; Tesche and Tremback, 2002). The rainfall median is considered to be the numerical value obtained after sorting data from the lowest to highest value. The median is then considered the middle value and it separates data into lower and upper half. However it depends on whether data is even or odd, whereby for odd numbers, the median is the

middle value. However, for even numbers there is no median and therefore the median is considered the average of the two middle values. It should be noted that all the scores were calculated over a period of 24 hours stating from 06h00 UTC on the day of the forecast to 06h00 UTC the following day.

Table 3.1: Table of rainfall verification statistics adapted from Gordon and Shaykewich, (2000)

		Forecast	
		Yes	No
Observed	Yes	A	B
	No	C	D

$$Bias = \frac{(A+B)}{(A+C)} \quad \textbf{(3.8)}$$

$$POD = \frac{(A)}{(A+C)} \quad \textbf{(3.9)}$$

(c) T-test significance statistic

In order to test for the significance of the strength of the relationship between observation and the model simulations, a two tailed student-test formula (3.10) is applied to maximum temperature and rainfall, where t statistic is defined by:

$$t = \frac{(\bar{f} - \bar{o})}{S_{fO}\sqrt{\frac{2}{n}}} \quad \textbf{(3.10)}$$

Where S_{fO} is the standard deviation of both the forecast and the observation, and n is the sample size, $\bar{f}$ is the average value of forecast and $\bar{o}$ is the average value of observation. In this instance it is assumed that the sample size of the forecast and the observations is equal. The standard deviation S_{fO} is defined by:

$$S_{fO} = \sqrt{(\tfrac{1}{2}(S_f{}^2 + S_O{}^2)} \quad \textbf{(3.11)}$$

The standard deviation of the forecast S_f is defined by equation (3.12) and the standard deviation of the observations S_O is defined by equation (3.13)

$$S_f = \sqrt{\frac{\sum_{i=1}^{N} (f_i - \bar{f})^2}{n-1}} \quad \textbf{(3.12)}$$

$$S_o = \sqrt{\frac{\sum_{i=1}^{N} (O_i - \bar{O})^2}{n-1}} \quad \textbf{(3.13)}$$

In this instanced the degree of freedom, df is defined by the equation (3.14)

$$df = 2n - 2 \quad \textbf{(3.14)}$$

For hypothesis testing using student's t-test applied in all objectives; the null hypothesis H_O (eq. 3.15) states that there is no difference between the mean for the WRF simulation and the mean for the observation, therefore assuming equal variance. The alternative hypothesis H_1 (eq. 3.16) state that mean of the simulation is different from the mean for the observation. This test implies a two sided hypothesis using a 95% confidence level. If H_O is true, the null hypothesis is accepted and on the table of results, significant difference is indicated by "FALSE", whereas if H_1 is true, the table will indicate significant difference as "TRUE". All the t-test scores are tabulated in the results section in chapter 4 and 5.

$$H_O : \bar{f}_{forecast} - \bar{O}_{Obs} = 0 \quad \textbf{(3.15)}$$

$$H_1 : \bar{f}_{forecast} - \bar{O}_{Obs} \neq 0 \quad \textbf{(3.16)}$$

3.4 Limitation to the methodology of the study

It is understood that most modelers including Ratna *et al.*, (2013) included a two way nesting approach in their studies in order to improve the model output for both the parent domain and the nest. However, in this study, only one way nesting is applied for simplicity and in order to determine the contribution of nesting on the higher grid resolution output. Secondly, the model setup allows one to describe the integration time step for the parent domain, and not for the nest. As a consequence of this, the model

adjusts the time step for the nest by satisfying the Courant-Friedrichs-Lewy (CFL) condition automatically. Another limitation involves the application of cumulus parameterization scheme at 3 km grid resolution. This was not applied as it is assumed that the model is able to explicitly resolve cumulus clouds at a grid resolution less than 4 km. Lastly, due to the uneven distribution of observation stations over the country, some areas have less dense network than others, *e.g.* there are less stations over the Limpopo region as compared to Cape region. Therefore resampling technique is not applied. Instead, a four point weighted averaging technique is applied in order to allocate more weight to a model grid point value that is found closer to the observation station.

CHAPTER 4

THE WRF MODEL SIMULATION OF EXTREME WEATHER EVENTS AND THE ROLE OF TOPOGRAPHY

This chapter discuss the WRF model simulations for the case studies performed over the SA domain. The purpose is to test for the stated aims and objectives which are: (i) to evaluate the capability of the WRF model as an NWP tool to predict extreme weather events over SA, and (ii) to evaluate the influence of the WRF model topography on extreme weather events. The case studies analysed includes: (a) the heat wave over the Limpopo region of SA from 22 to 26 October 2011 and (b) the heavy rainfall associated with tropical depression Dando over the Limpopo region of SA from 16 to 18 January 2012 and (c) the heat wave over the Cape region from 15 to 18 January 2012.

It should be noted that the Limpopo region is considered to include the whole Limpopo province, parts of Mpumalanga, Northwest and Gauteng provinces (22^0S-26^0S; 26^0E-32^0E). This is also considered as the north-eastern parts of SA or the summer rainfall region of SA. The Cape region is defined as Northern, Western Cape provinces and western parts of Eastern Cape Province (26^0S-35^0S; 16^0E-26^0E). Firstly synoptic scale analysis is done to compare the WRF model simulations of sea level pressure and winds with SAWS surface weather maps to determine if the model was able to reproduce the synoptic scale systems. Secondly, statistical analysis is done with the WRF model grid simulations interpolated to the nearest stations using weighted averages method and verification scores computed as a measure of the model's reliability and accuracy (Gordon and Shaykewich, 2000). The variables investigated include maximum and minimum temperatures, rainfall, maximum wind speed, maximum relative humidity, and vertical velocity.

The South African Weather Service applies the following convention with regards to observation recording. For rainfall analysis, a 24 hours rainfall is recorded as the accumulated rainfall over the station from 06h00 UTC on the day of simulation to 06h00 UTC the following day, whereas for *i.e.* maximum temperatures, a 24 hours temperature is calculated as the recorded maximum temperatures at the station from 00h00 UTC on the day of simulation to 00h00 UTC the following day.

4.1 Heat wave episode 22-26 October 2011

4.1.1 Synoptic description with topography

(a) Mean sea level pressure and winds

From the 22nd to 26 October 2011, most of the northern parts of SA experienced a heat wave that resulted in very high temperatures. Maximum temperatures rose to above 40°C in areas around Limpopo, Northwest and Mpumalanga provinces. Figure 4.1 shows the SAWS weather map (SAWS, 2011) for the period 23 to 26 October 2011, whereas Figure 4.2 shows the WRF 9 km mean sea level (MSL) synoptic scale circulations over southern Africa for the same period at 12h00 UTC. It should be noted that the resolution of the two images varies, the resolution of the SAWS synoptic map is lower that the model resolution, which is at a resolution of 9 km and that the SAWS map was plotted by hand.

The SAWS synoptic map (Figure 4.1) shows two low pressure systems over the subcontinent; the first was located within the tropics (15°S-20°S; 25°E-35°E). This pressure system was very intense and has a central pressure of 996 hPa. The 1000 hPa isobar was located on the border of Limpopo province and Zimbabwe. This low pressure system resulted in northerly to north-westerly winds over the northern parts of the country including Limpopo region. The WRF model simulation with topography (Figure 4.2) also captured the spatial distribution of this low pressure system (especially on the 25th and 26th October; Figure 4.2 bottom panels). The WRF model simulated the low pressure system over the tropics with a central pressure 1004 hPa, which was 8 hPa weaker than the one on the SAWS synoptic map. The WRF model simulation shows that the winds associated with the low pressure system were weak and north-easterly. The WRF model did not capture the wind direction very well.

The SAWS synoptic map shows the second low pressure system located over the central parts of the country (25°S-30°S, 25°E-30°E). This area includes the higher topography areas along the escarpment of Free State, Gauteng, Mpumalanga and KZN Provinces of SA and also Lesotho. The second low pressure system has a central pressure of 1000 hPa and was weaker than the low pressure system over the tropics by at least 4 hPa. The second low pressure system resulted in westerly winds over the western and central parts of the country and also south-easterly over the eastern parts of Limpopo region. The

WRF model captured the second low pressure system over central parts of the country, but shows a central pressure of 1004 hPa, which was also 4 hPa higher than on the low pressure system on SAWS synoptic map. The WRF model simulation shows south-westerly winds over the central parts of the country, as compared to westerly on SAWS synoptic map. The WRF model simulated easterly winds over the eastern half of Limpopo region towards the Indian Ocean as compared to south-easterlies on the SAWS synoptic map. In this instance the WRF model captured wind speed very well but not the wind direction.

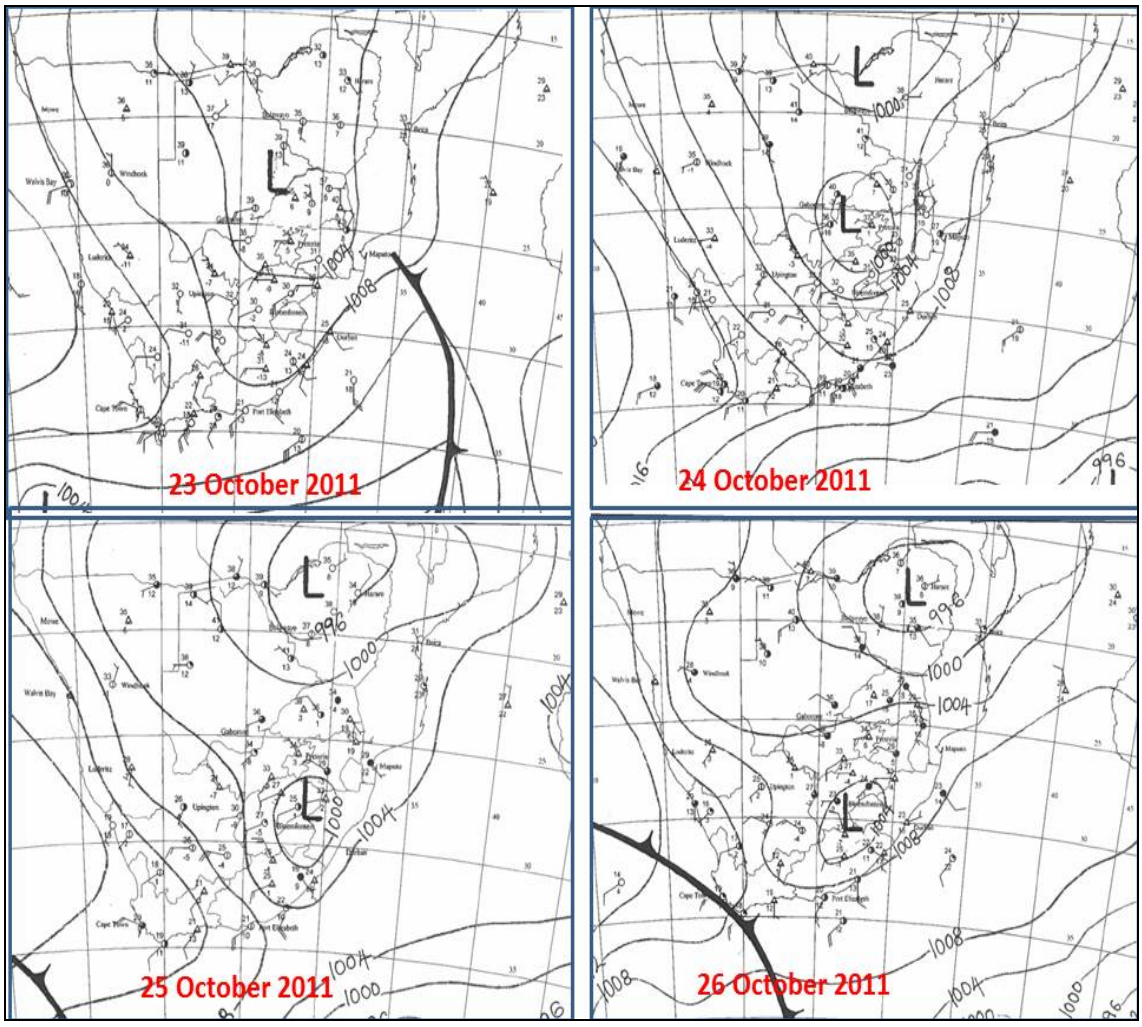

Figure 4.1: SAWS synoptic map at 12h00 UTC (adapted from SAWS, 2011) with mean sea level pressure in hPa (contours) and surface winds (barbs in knots) for the period 23-26 October 2011. Figure is labelled as follows: top left (23 October); top right (24 October), bottom left (25 October) and bottom right (26 October).

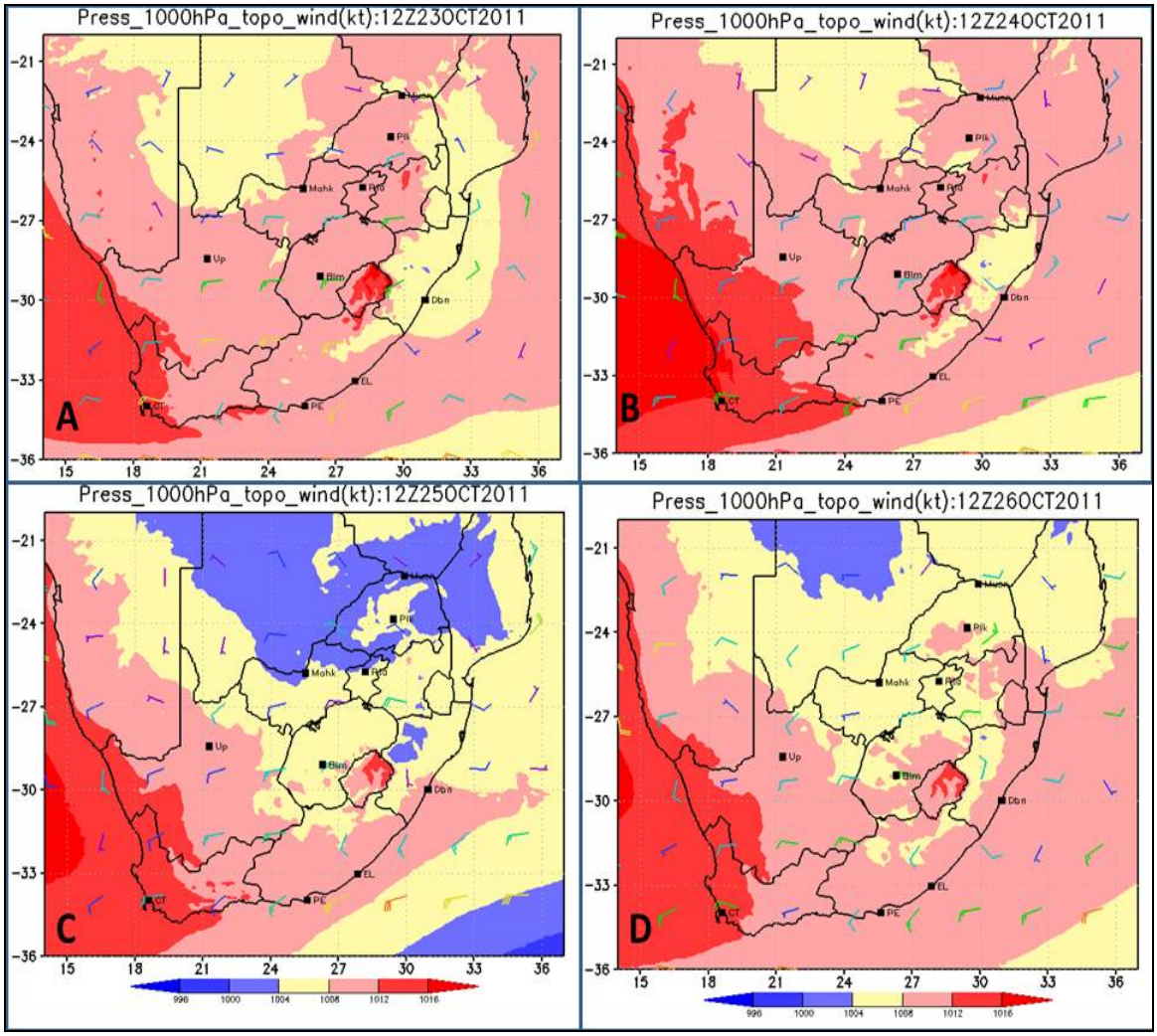

Figure 4.2: WRF 9 km simulated synoptic map at 12h00 UTC with mean sea level pressure in hPa (contours), and surface winds (barbs in knots) simulation for the period 23-26 October 2011. Figure is labelled as follows: top left (23 October); top right (24 October), bottom left (25 October) and bottom right (26 October).

SAWS synoptic map shows a ridging high pressure system into the country from the west coast; over the border between Western and Northern Cape provinces at 15^{o}E (only a ridge line is indicated). This high pressure system has a 1008 hPa isobar over Northern Cape Province, and has less influence on weather over Limpopo region. The WRF model simulation also captured the ridging high pressure system and placed the 1008 hPa isobar correctly. The WRF model simulated westerly winds over the central parts of the country and was in agreement with the SAWS synoptic map.

The low pressure system over the tropics resulted in advection of both warm and dry tropical air towards Limpopo region. Such an advection resulted in surface heating and

turbulent mixing of warm surface air. Likewise subsidence due to an upper air high pressure system over Limpopo region resulted in dynamic warming due to adiabatic heating, and together with advection contributed to the heat wave and very hot conditions over northern parts of the country including Limpopo region. The low pressure system over the central parts of the country resulted on the advection of dry and cooler air from the central interior towards Limpopo region, however, this low pressure system shows less impact on weather over Limpopo since it was weaker and the winds associated with it were also weaker.

(b) Moisture fluxes and vertical velocity at different vertical levels

The WRF model simulation at 1000 hPa shows neither surface moisture flux convergence nor divergence over the land, but along the surrounding oceans (Figure 4.3a). Similarly, there was neither a region of updrafts nor downdrafts over the land (Figure 4.4a). This was due the fact that most parts of SA have topography at levels higher than 1000 hPa. However, over the Indian Ocean, the WRF model shows more divergence (Figure 4.3a) and also downdrafts (Figure 4.4a) over the Mozambique Channel due to a low pressure system over the Indian Ocean.

At 850 hPa, the WRF model simulation with topography shows a high pressure system over northern parts of the country with its centre over Zimbabwe and Limpopo region. This high pressure system was not visible at 1000 hPa due to that Limpopo region has topography at an altitude higher than 1000 hPa. It resulted in northerly to north-westerly winds over Limpopo region, with dry tropical air advected over Limpopo region and enhanced moisture flux divergence (Figure 4.3c). Due to the anti-cyclonic circulation from the high pressure system, there were very little updrafts over Limpopo region (Figure 4.4c).

At 700 hPa, the WRF model simulation with topography (Figure 4.3b) also shows a high pressure system over the northern parts of the country, including Limpopo region and Zimbabwe. The winds were mostly north-westerly at this level, and there was a reduction in the amount of moisture flux divergence as compared to 850 hPa (Figure 4.3b). Similarly, updrafts were enhanced over the western half of Limpopo region and reduced over the eastern parts of Limpopo region. This was due to north-westerly winds advecting

moist tropical air from the tropical region including Angola towards Limpopo region (Figure 4.4b).

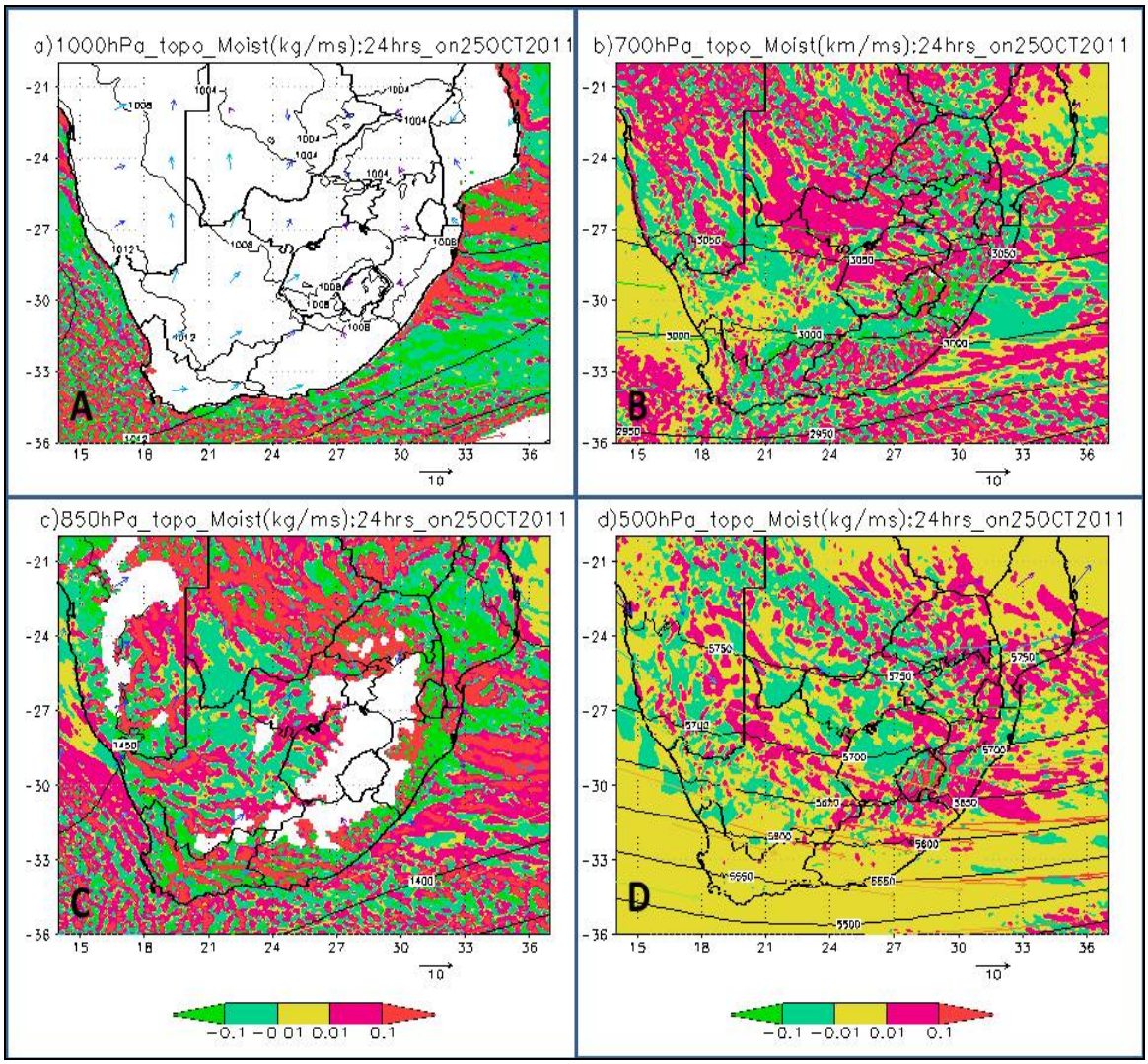

Figure 4.3: The WRF model simulation of 1000 hPa (top left), 850 hPa (bottom left), 700 hPa (top right) and 500 hPa (bottom right) geopotential height levels (isobars in contour), moisture flux in $kgm^{-1}s^{-1}$(shadings) and horizontal winds (vector on ms^{-1}) simulation as on 25 October 2011. The yellow colour on the image, interval (-00.1to 0.01) indicates transition area, whereas white colour indicates that topography is higher than the plotted geopotential heights.

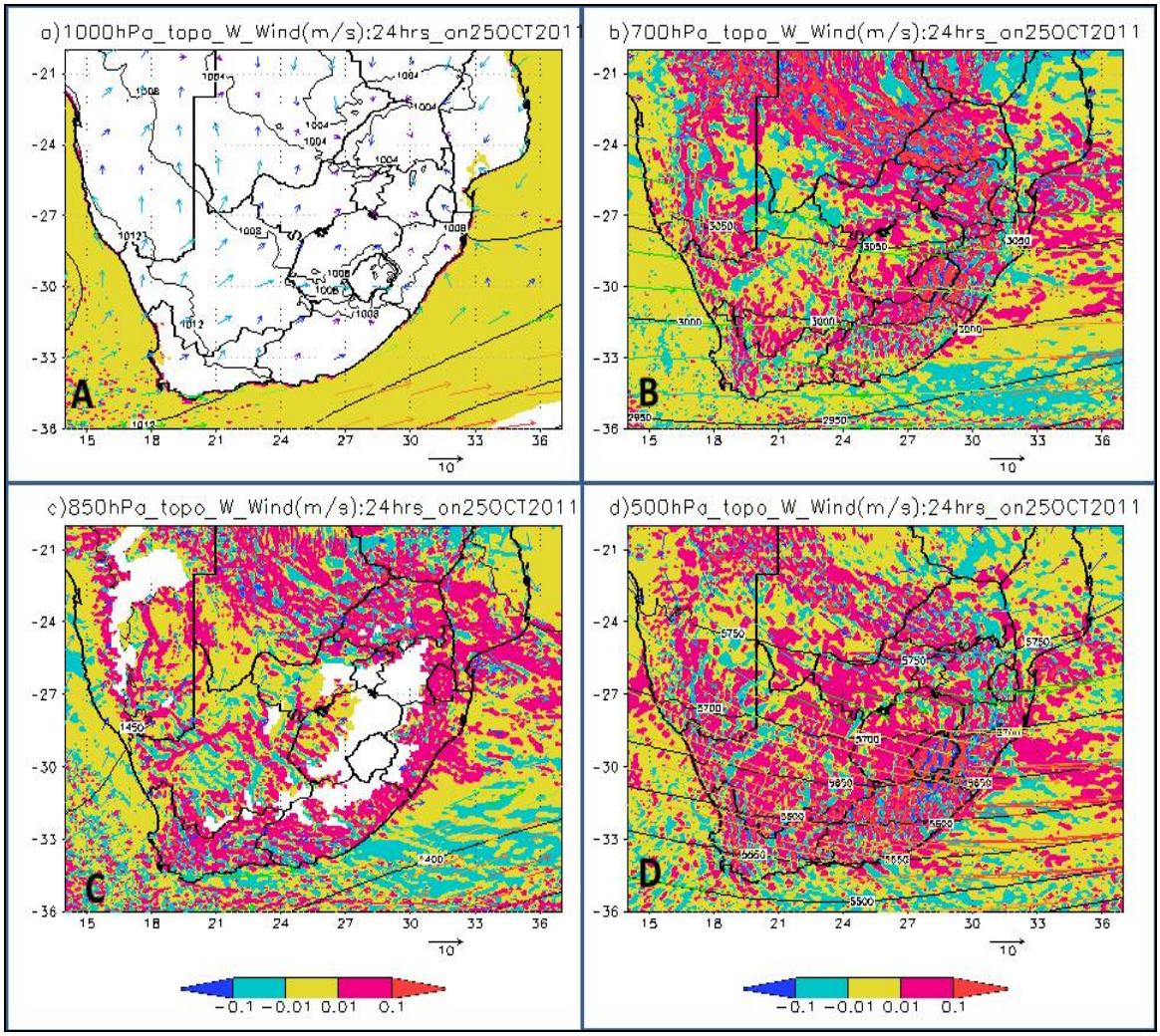

Figure 4.4: The WRF model simulation of 1000 hPa (top left), 850 hPa (bottom left), 700 hPa (top right) and 500 hPa (bottom right) geopotential height levels (isobars are in contours), vertical velocity in ms^{-1} (shaded) and horizontal winds (vector in ms^{-1}) simulation as on 25 October 2011. The yellow colour on the image, interval (-00.1to 0.01) indicates transition area, whereas white colour indicates that topography is higher than the plotted geopotential heights.

At 500 hPa, the WRF model simulation also shows a high pressure system over the northern parts of Limpopo region. It resulted in westerly winds over the region. The north-eastern parts of the country including Limpopo region shows moisture flux convergence, whereas the western half shows moisture flux divergence (Figure 4.3d). Simulation of vertical velocity indicates weakening updrafts at this level due to an upper air high pressures system. The upper air high pressure system enhanced subsidence that contributed to the heat wave and therefore very high temperatures over Limpopo region (Figure 4.4d).

From this simulation it can be deduced that the presence of topography has an impact on the location of both the high and the low pressure system, and also their intensities. Topography also has an impact on the strength of both horizontal and vertical winds as well as moisture flux distribution.

(c) Maximum temperature simulation

Figure 4.5 shows the WRF 9 km simulations of maximum temperature with and without topography for the period 23 to 25 October 2011. The WRF model simulation with (Figure 4.5a and c) shows a west to east temperature isotherms with higher temperatures over the lower topography areas to the west and lower temperatures over the higher topography areas to the east over Limpopo region. The winds were north-easterly to easterly on 23 and 24 October, and were responsible for advection of dry air from the tropics and east coast towards Limpopo region of South Africa. This could be attributed to the location of the escarpment as a result of the orientation of the Soutpansberg (see Figure 1.1) which is located over most of the central parts of Limpopo province. Its orientation shows lower topography areas to the west, north and the eastern parts of Limpopo, with higher topography to the south. The presence of the escarpment along the Soutpansberg and Drakensberg resulted in easterly winds flowing over Limpopo river valley (on the border of Limpopo province and Zimbabwe towards the Botswana. The escarpment also prevented dry and hot air from penetrating into the interior of the country and therefore this resulted in hot and dry air circulating over northern parts of Limpopo region (Figure 4.5a and c).

The WRF model simulation also shows north-south maximum temperature isotherms over the country as well as Limpopo region with higher temperatures to the north and lower temperatures to the south (especially on the 25 October). Northerlies were responsible for the advection of dry tropical air towards northern parts of Limpopo, whereas southerlies advected dry mid-latitudes air towards Limpopo region.

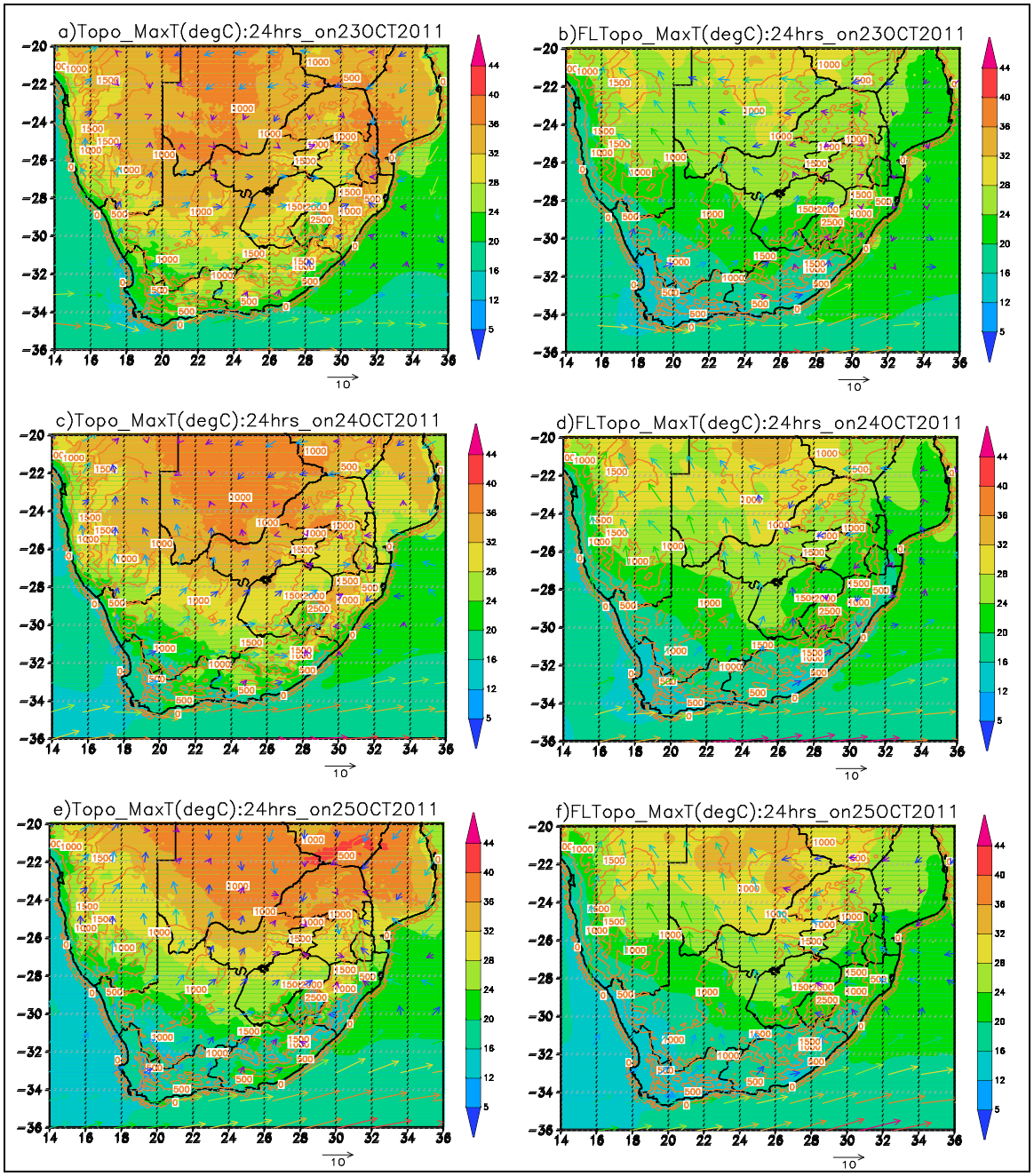

Figure 4.5: The WRF 9 km maximum temperature (in degree Celsius) simulation with and without topography for the period 23-25 October 2011. Temperature is shaded; the model topography is in meters (contoured) and horizontal winds (vectors in ms^{-1}). A 24 hours temperature is calculated as the recorded maximum temperatures at the station from 00h00 UTC on the day of simulation to 00h00 UTC the following day. The image is labelled as follows: top left (23 October, simulation with topography); top right (23 October, simulation without topography); middle left (24 October, simulation with topography); middle right (24 October, simulation without topography); bottom left (25 October, simulation with topography) and bottom right (25 October, simulation without topography).

However, the presence of the higher topography along the Soutpansberg and could have prevented dry tropical air from mixing with subtropical air over Limpopo region. The upper air high pressure system resulted in subsidence. The combination of both subsidence and dry advection resulted in higher temperatures located over Limpopo valley (Figure 4.5e). These temperatures were however lower than observed by up to 4^{o}C (shown in Figure 4.6 and 4.7). However, on the 26 October (not shown), there was north-ward shift from higher tropical temperatures to moderate mid-latitude temperatures over the country, marking the dissipation of the heat wave episode.

From this analysis, it was shown that the presence of the low pressure system over the tropics together with northerly winds resulted in advection of hot tropical air towards Limpopo valley. This hot and dry air experienced surface heating and turbulent mixing as it moves down the towards Limpopo valley. The low pressure system over the subtropics together with southerlies advected cold subtropical air from the interior of the country towards Limpopo region. Likewise this air also experienced surface heating and turbulent mixing as it moves down the escarpment towards Limpopo valley. The high pressure system at 500 hPa over Limpopo region resulted in adiabatic warming due to subsidence and therefore enhanced the heat wave leading to high surface temperatures over Limpopo region. This type of synoptic circulation has been confirmed in a study involving berg winds over the west coast by Lengoasa (1988) and also Mason and Jury (1997).

4.1.2 Synoptic description without topography

(a) Mean sea level pressure and winds

At 1000 hPa, the WRF model simulations show that a low pressure system over the tropics (Zimbabwe) has migrated further north. A ridging high pressure system from the western parts of the country also strengthened and moved further east into the land. There was a weakening of south-westerly and westerly winds over the interior of the country. A low pressure system that was located over the interior of the country (escarpment area) in simulation with topography dissipated (Figure A.1). As a result, Limpopo region was dominated by weak low pressure system.

(b) Moisture fluxes at different levels and vertical velocity

At 1000 hPa, the WRF model simulation without topography shows weakened moisture flux divergence and downdrafts over the interior of the country including Limpopo region (Figure A.2). Simulation with topography shows neither moisture fluxes nor vertical velocity over the land due to higher inland topography at this level. This could be attributed to the absence of topography which was responsible for producing semi-stationary systems in simulation with topography.

At 850 hPa, the WRF model simulated a high pressure system covering most of the southern parts subcontinent, including the Limpopo region. This high pressure system was however stronger than in simulation with topography and was associated with a north-east to south-west oriented ridge line. As a result of the high pressure system, winds were north-westerly over the northern parts of the country and changed direction to westerly over the east coast (Figure A.2). Due to the anti-cyclonic motion of a high pressure system, enhanced moisture flux divergence and weaker downdrafts were simulated over Limpopo region (Figure A.3). It could be deduced that the removal of topography resulted in a weak low pressure system Limpopo region. This also resulted in increased downdrafts and subsidence over the country (Figure A.3).

At 700 hPa, the high pressure system covered the northern parts of the country and Botswana. It resulted in weaker north-westerly over Limpopo region. There was enhanced moisture flux divergence with weaker updrafts over the northern parts of the country including Limpopo region (Figure A.2).

At 500 hPa, the high pressure system over the northern parts of the country strengthened and covered most parts of the tropics including Limpopo region. This high pressure system was stronger than for simulation with topography. The high pressure system resulted in a north-south elongated ridge line towards the low pressure system over the south coast of the country. Winds were north-westerly to the west of the ridge over Limpopo region (Figure A.1). The amount of moisture flux divergence (Figure A.2) and downdrafts were nearly similar to simulation with topography over the entire Limpopo region (Figure A.3).

(c) Maximum temperature simulation

Figure 4.5 (right panels) also shows the WRF 9 km simulations of maximum temperatures without topography. From this model simulations (Figure 4.5 b, d and e), very high temperatures simulated by the WRF model with topography were reduced, whereas lower temperatures increased over the country. Both the north-south temperature isotherms over the country and Limpopo region were also reduced. These simulations show the removal of topography removed the impact of surface heating and turbulent mixing. When wind flows down topography, wind speed increases resulting in higher temperatures in lower topography areas. The removal of topography resulted in constant wind speed and reduced the effect of surface heating, but subsidence remains similar, resulting in mild temperatures over Limpopo region and the entire country.

From the analysis of the WRF model simulation without topography, a high pressure system at 500 hPa located over the northern parts of Limpopo region was responsible for dynamic warming due to adiabatic heating during subsidence. The absence of topography reduced surface heating thus reduced the impact of heat wave. The southerlies also have more influence on temperatures than the northerlies in simulation without topography.

4.1.3 Statistical analysis: simulation with and without topography (heat wave 22-26 October 2011)

In this section the WRF model output for maximum and minimum temperatures, wind speed as well as relative humidity over Limpopo region of SA is discussed. The statistical values are compared at 9 km for both the model simulations with and without topography. Verification statistics include bias, root mean square error (RMSE), and Pearson correlation coefficient (CORR).

a) Maximum temperature

The WRF 9 km simulation of maximum temperature with and without topography together with statistics over Limpopo region is shown in Figure 4.6. The WRF model simulation with topography has under-predicted maximum temperatures over the region.

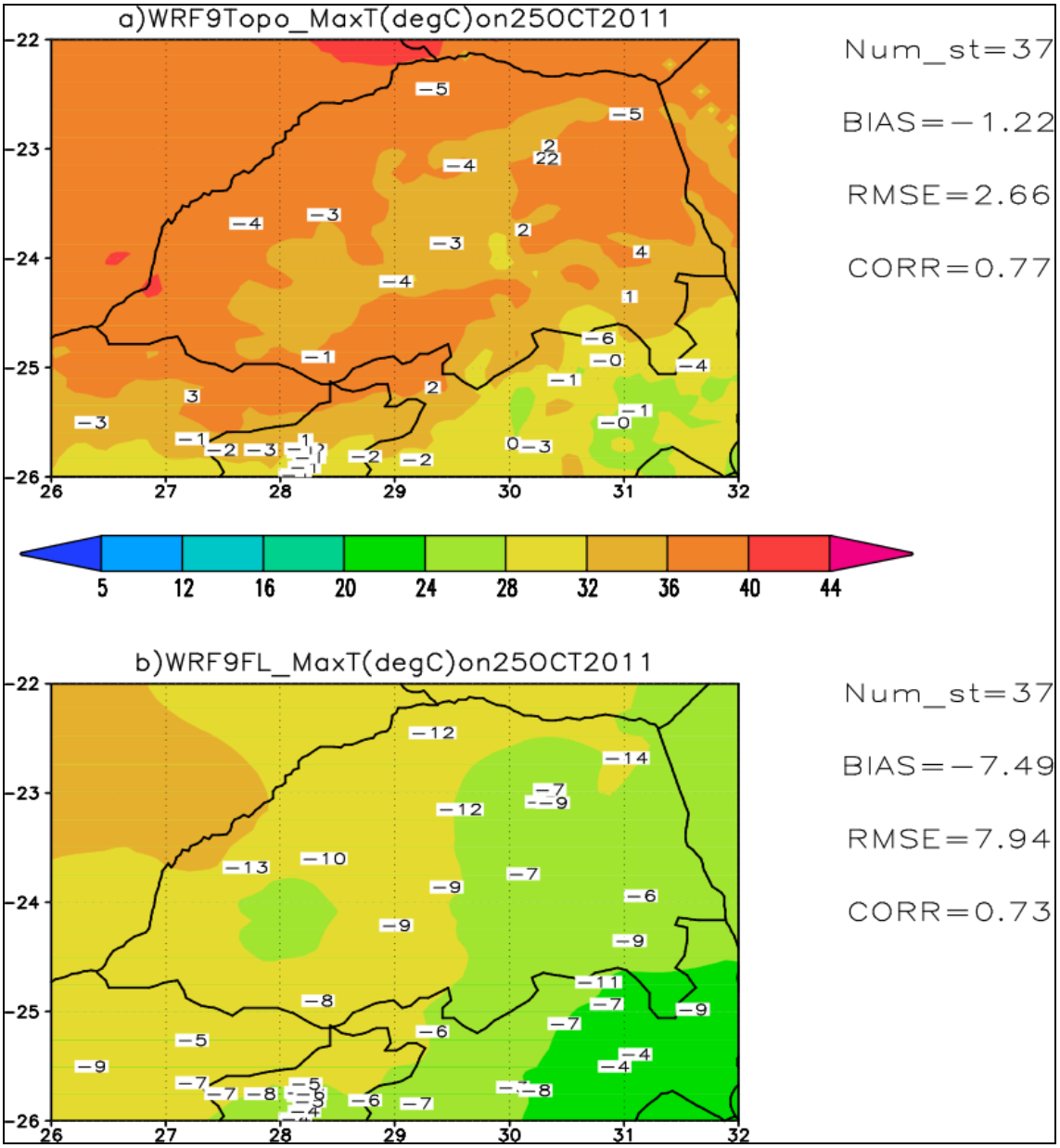

Figure 4.6: WRF 9 km with topography and without topography simulated maximum temperature (in degree Celsius) with statistics over Limpopo region on 25October 2011. Bias values at each observation station are indicated as numbers and the model simulated temperatures are in shadings.

However, some stations show a close agreement between the WRF model simulations and observations (Figure 4.6a). When topography was removed, very high and low maximum temperatures were reduced over the entire Limpopo region and temperatures were much lower than simulation with topography and also the observed. This could be attributed to reduced surface heating and reduced mixing of different air mass in the

absence of topography, resulting in lower temperatures over Limpopo region and the entire country (Figure 4.6b).

In Figure 4.7, verification statistics of maximum temperatures over the entire country and Limpopo region is depicted. For simulation with topography, bias values (top) were negative and consistent for the entire simulation period over the entire country and Limpopo region. The RMSE values (middle) show the spread of bias which were on average less than 4^{o}C. The CORR values (bottom) were positive and show strong linear relationship between the WRF model simulations and observed maximum temperatures over the country and Limpopo region. This result indicates that the WRF model simulation with topography is capable of simulating SA maximum temperatures, and that topography plays an important role in temperature distribution.

When topography was removed, it is shown that bias values (top) and RMSE values (middle) were increased. This result indicates that the model simulations lose reliability and accuracy. The CORR values (bottom) remained positive and were also reduced. The CORR values were reduced by almost half over Limpopo region, and were negative 23 October. This value was inconsistent with other days and is difficult to explain (Figure 4.7).

For both simulations, bias values were negative and larger than +/- 0.5^{o}C and the RMSE values were also larger than 2^{o}C used as an MM5 model benchmark applied in Tesche and Tremback (2002). It can therefore be deduced that simulation with topography yield reliable, accurate and realistic results than simulation without topography and that topography is important in temperature distribution although caution should be taken in areas of higher topography. Topographic heights and orientation also plays important role as indicated in temperature distribution map (see also Figure 4.5).

	22-Oct-11	23-Oct-11	24-Oct-11	25-Oct-11	26-Oct-11	Average
MaxT_9KM_SA_Topo	-3.73	-2.45	-3.55	-2.74	-3.06	-3.11
MaxT_9KM_Limp_Topo	-4.05	-3.90	-3.68	-1.22	-3.19	-3.21
MaxT_9KM_SA_FLTopo	-9.51	-8.80	-8.78	-5.86	-5.37	-7.66
MaxT_9KM_Limp_FLTopo	-8.73	-11.14	-9.89	-7.49	-3.76	-8.20

	22-Oct-11	23-Oct-11	24-Oct-11	25-Oct-11	26-Oct-11	Average
MaxT_9KM_SA_Topo	4.15	3.35	4.01	3.53	3.8	3.77
MaxT_9KM_Limp_Topo	4.31	4.11	4.19	2.66	4.13	3.88
MaxT_9KM_SA_FLTopo	10.14	9.43	9.31	6.69	6.52	8.42
MaxT_9KM_Limp_FLTopo	9.11	11.63	10.24	7.94	5.84	8.95

	22-Oct-11	23-Oct-11	24-Oct-11	25-Oct-11	26-Oct-11	Average
MaxT_9KM_SA_Topo	0.93	0.92	0.96	0.95	0.92	0.94
MaxT_9KM_Limp_Topo	0.82	0.93	0.81	0.77	0.89	0.84
MaxT_9KM_SA_FLTopo	0.69	0.81	0.91	0.86	0.76	0.81
MaxT_9KM_Limp_FLTopo	0.19	-0.12	0.66	0.73	0.62	0.42

Figure 4.7: WRF 9 km with topography and without topography simulated for maximum temperatures (in degree Celsius) with statistics over SA and Limpopo region for the period 22-26 October 2011

Table 4.1 show the number of stations that recorded very high temperatures for a period of three successive days over the Limpopo region. The station observed maximum temperatures are much higher than the average daily maximum temperatures as tabulated in Schulze (1997) climate record for October. The table also shows the model simulated maximum temperature at 9 km with and without topography. These results confirm that although the model simulated temperatures with topography were lower than observations by at least 4^{o}C, results were realistic and the removal of topography yield unreliable results.

Table 4.1: Station observed and the WRF model simulated maximum temperatures (in degree Celsius) over Limpopo region during heat wave for the period 23-25 October 2011.

Maximum temperatures(> 38 degree celsius) 9 km topography versus flat topography											
			on 23 October 2011			on 24 October 2011			on 25October 2011		
no	Station name	stid	Obs	wrf_topo	wrf_fltopo	Obs	wrf_topo	wrf_fltopo	Obs	wrf_topo	wrf_fltopo
1	Lephalale(lat:-23.68; lon:27.7)	68155	40.00	35.31	26.09	41.50	36.80	28.03	42.60	39.00	29.84
2	Mara(lat:-23.15; lon: 29.57)	68176	38.20	33.10	24.64	38.20	33.51	27.29	39.90	36.21	27.88
3	Marico(lat:-25.5; lon: 26.35)	68248	39.40	34.41	26.97	41.30	35.70	27.58	38.20	34.74	29.01
4	Venetia (lat:-22.45; lon:29.33)	68172	40.20	34.99	27.05	38.60	34.13	29.29	42.70	37.54	30.45
		Averag	39.45	34.45	26.19	39.90	35.04	28.05	40.85	36.87	29.30
		BIAS		-5.00	-13.26		-4.86	-11.85		-3.98	-11.56

In table 4.2, the student t-test indicates that over the period of four days, there was significant difference between the mean of the WRF model simulation and the observations. This result applies for both WRF simulations with topography and also without topography over the entire country and also Limpopo. However, t-statistic also shows that this difference were small in simulation with topography and large in simulation without topography. The only difference noticed was for WRF 9 km results over Limpopo region on 25 October in simulation with topography, which indicated agreement between the model simulation and observations. However this result was difficult to draw any conclusion from it. Therefore from this statistic, it can be deduced that there was a significant difference between the mean of the WRF model simulation and observations.

Table 4.2: Students t-test for maximum temperatures at 9 km grid resolution over SA and Limpopo region for the period 22-26 October 2011 for both simulation with topography (a and c), and also for simulations without topography (b and d). A 95% confidence level was applied, and "TRUE" indicates that there is significant difference between the mean of observation and the mean for the WRF simulation, whereas "FALSE" indicate that there was no significant difference between the mean of observation and the mean for the WRF simulation.

	a) MaxT_9KM_SA_Topo					
Date	22_Oct_2011	23_Oct_2011	24_Oct_2011	25_Oct_201	26_Oct_201	Average
T_test	-8.0576	-4.3102	-5.6409	-4.1395	-5.6066	-5.5510
df	404.00	406.00	406.00	406.00	406.00	405.60
T_crit95%	1.9659	1.9658	1.9658	1.9658	1.9658	1.9658
significant difference	TRUE	TRUE	TRUE	TRUE	TRUE	TRUE

	b) MaxT_9KM_SA_FLTopo					
Date	22_Oct_2011	23_Oct_2011	24_Oct_2011	25_Oct_201	26_Oct_201	Average
T_test	-22.4957	-17.4656	-16.3008	-10.3482	-10.2158	-15.3652
df	404.00	406.00	406.00	406.00	406.00	405.60
T_crit95%	1.9659	1.9658	1.9658	1.9658	1.9658	1.9658
significant difference	TRUE	TRUE	TRUE	TRUE	TRUE	TRUE

	c) MaxT_9KM_Limp_Topo					
Date	22_Oct_2011	23_Oct_2011	24_Oct_2011	25_Oct_201	26_Oct_201	Average
T_test	-7.6762	-5.8578	-5.2454	-1.4095	-3.0339	-4.6446
df	70.00	68.00	70.00	70.00	70.00	69.60
T_crit95%	1.9944	1.9955	1.9944	1.9944	1.9944	1.9946
significant difference	TRUE	TRUE	TRUE	FALSE	TRUE	TRUE

	d) MaxT_9KM_Limp_FLTopo					
Date	22_Oct_2011	23_Oct_2011	24_Oct_2011	25_Oct_201	26_Oct_201	Average
T_test	-18.7749	-20.0662	-15.8507	-10.5301	-4.0305	-13.8505
df	70.00	68.00	70.00	70.00	70.00	69.60
T_crit95%	1.9944	1.9955	1.9944	1.9944	1.9944	1.9946
significant difference	TRUE	TRUE	TRUE	TRUE	TRUE	TRUE

b) Minimum temperature

Figure 4.8 shows the WRF model simulation verification statistics of minimum temperature over the country and Limpopo region at 9 km grid resolution with and without topography. Bias values (top) were consistently positive and higher over the country and also Limpopo region.

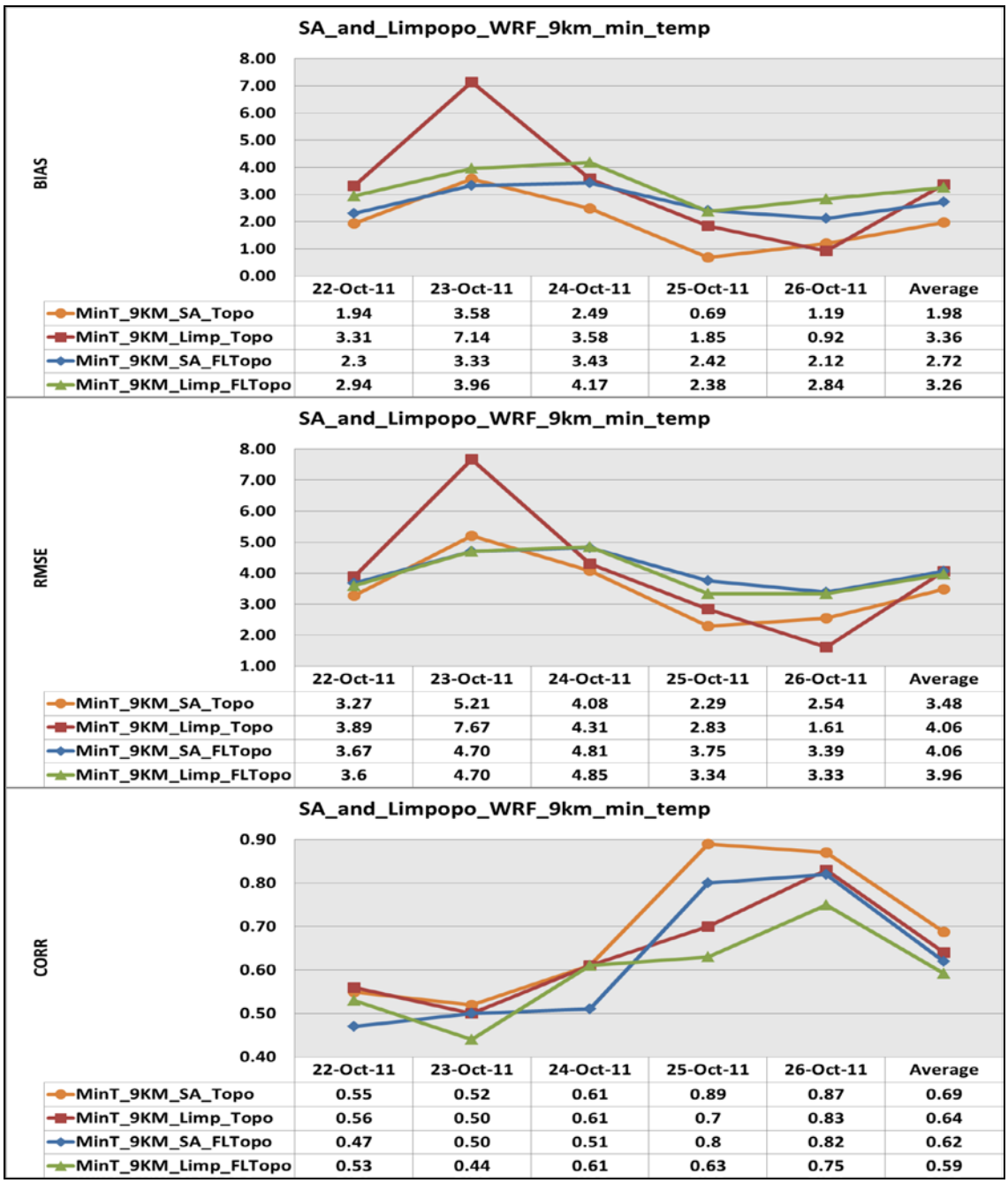

Figure 4.8: WRF 9 km topography versus flat topography simulated minimum temperature (in degree Celsius) with statistics over SA and Limpopo region for the period 22-26 October 2011

Bias values were highest on 23 October and this affected the average values. Bias was also lowest on 25 October than for all the days. The RMSE values (middle) were double the values of bias over the country and almost similar to bias over Limpopo region. CORR values (bottom) were also positive and slightly larger over the country than over Limpopo region. These values were however lowest on 23 October and highest on 25 October. This result shows the model's improvement with time, an indication the model

simulations are reliable, accurate and show consistency. However, results on 23 October affected the scores negatively and were difficult to explain.

When topography was removed, bias values (top) and RMSE (middle) values were large over the country and less over Limpopo region. The results indicate that the model simulations lose reliability and accuracy in simulation without topography. The CORR values (bottom) were however positive and slightly lower than in simulation with topography (Figure 4.8).

For both simulations, bias values were positive and larger than the +/- 0.5^{o}C and the RMSE values were also larger than 2^{o}C, as compared to the MM5 model benchmark applied in Tesche and Tremback (2002). This result indicates that the model is over-predicting minimum temperatures and under-predicting maximum temperatures; and therefore it could not handle diurnal variations very well. The model simulations with topography show consistency and reliability in predicting minimum temperatures. However, for simulation without topography, there is less consistency and reliability, which is an indication that topography is necessary for minimum temperatures simulations.

c) Maximum wind speed

Figure 4.9 depicts winds speed statistics over the country and Limpopo region. For simulation with topography, this result show negative bias (top) over the country except for 25 October. On this day, results indicate that the model simulation of wind speed was very close to observation. Bias was also negative and large over Limpopo region than over the country. The RMSE values (middle) confirm that bias values were almost similar over the country and Limpopo region. The CORR values (bottom) were positive and show a slight weak relationship between the WRF model and observations over the country and Limpopo region. This result also shows that simulations were accurate and reliable and has small variations and that the model simulation with topography was able to reproduce wind speed over any region of the country.

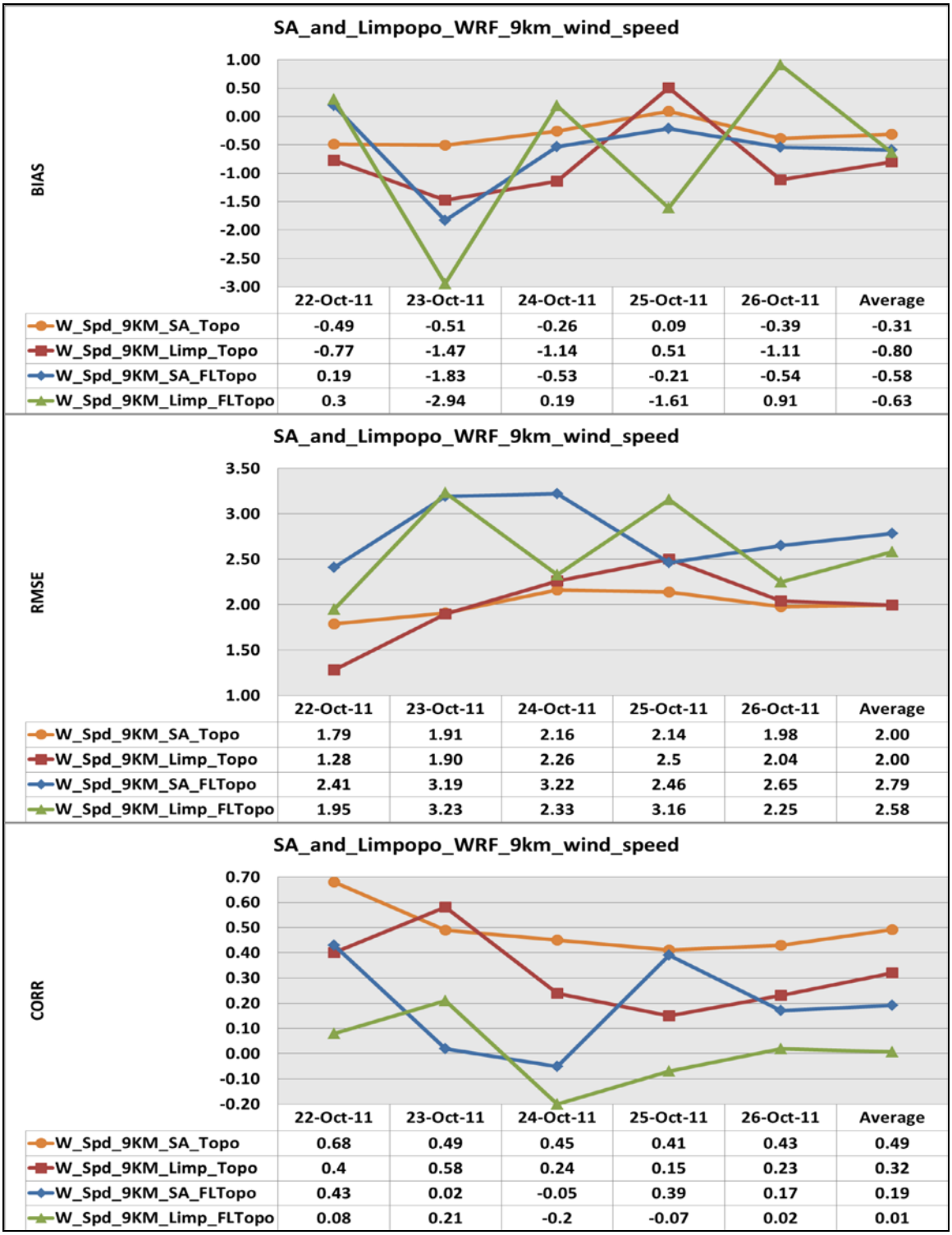

Figure 4.9: WRF 9 km topography versus flat topography simulated wind speed (in ms^{-1}) with statistics over SA and Limpopo region for the period 22-26 October 2011

When the model topography was removed, bias values (top) increased for most of the days over the country and slightly reduced over Limpopo region. The RMSE values

(middle) show similar pattern as bias, they increased for all the days over the country and Limpopo region and also show large variations. The CORR values (bottom) were reduced by more than half over the country and Limpopo region and also show large variations. This result has shown that simulation without topography failed to reproduce observed wind speed and was unreliable and less accurate; and also shows that topography is important for winds simulation.

From both simulations (with and without topography), bias values were slightly closer to +/- 0.5 m/s, the RMSE values were also close to 2 m/s benchmark values used by Tesche and Tremback (2002) for the MM5 model. This result also confirms that that the model simulation with topography can reproduce observed wind speed and that topography has an influence on wind speed and direction.

d) Maximum relative humidity

Statistics for relative humidity simulation over SA and Limpopo region is depicted in Figure 4.10. Simulation with topography shows low negative bias values (top) for all the days over the country and as well as Limpopo region. Such bias was on average less than 10%. An unusually high negative bias over Limpopo region on 23 October (-24.41) resulted in poor average score, but for the rest of the days, results were consistent.

However, on the 25 October, bias was very much less over the country and Limpopo region; an indication that the model simulations were close to observation. The average RMSE value (middle) was also high over the country, but slightly lower over Limpopo region, with some inconsistencies between days. On the 25 October, the RMSE values were lower than for the rest of the days. The CORR values (bottom) were also higher over the entire country than over Limpopo region. An inconsistent value on 23 October was however difficult to explain. This result indicates that the WRF model prediction has some inconsistency which is difficult to explain.

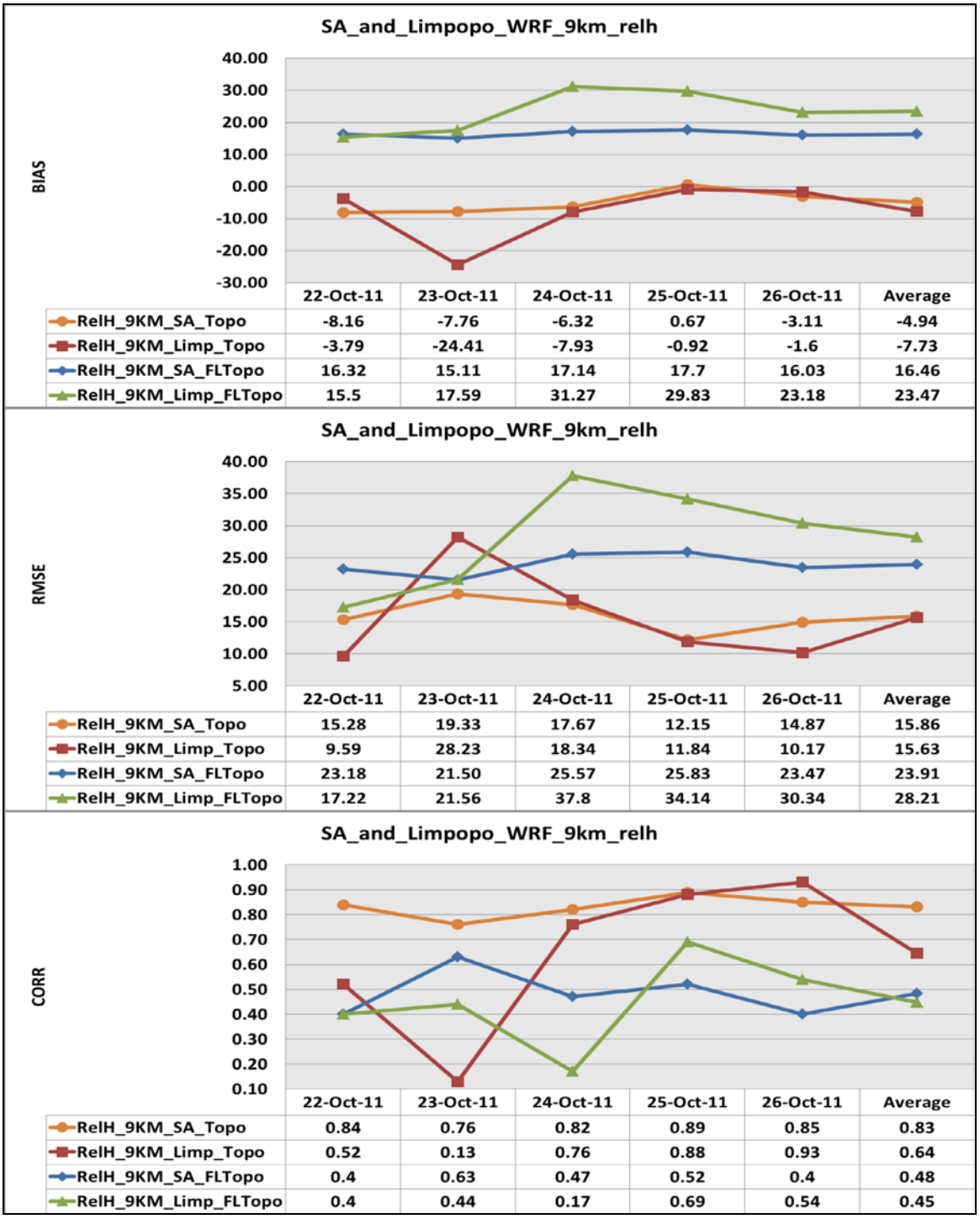

	22-Oct-11	23-Oct-11	24-Oct-11	25-Oct-11	26-Oct-11	Average
RelH_9KM_SA_Topo	-8.16	-7.76	-6.32	0.67	-3.11	-4.94
RelH_9KM_Limp_Topo	-3.79	-24.41	-7.93	-0.92	-1.6	-7.73
RelH_9KM_SA_FLTopo	16.32	15.11	17.14	17.7	16.03	16.46
RelH_9KM_Limp_FLTopo	15.5	17.59	31.27	29.83	23.18	23.47

	22-Oct-11	23-Oct-11	24-Oct-11	25-Oct-11	26-Oct-11	Average
RelH_9KM_SA_Topo	15.28	19.33	17.67	12.15	14.87	15.86
RelH_9KM_Limp_Topo	9.59	28.23	18.34	11.84	10.17	15.63
RelH_9KM_SA_FLTopo	23.18	21.50	25.57	25.83	23.47	23.91
RelH_9KM_Limp_FLTopo	17.22	21.56	37.8	34.14	30.34	28.21

	22-Oct-11	23-Oct-11	24-Oct-11	25-Oct-11	26-Oct-11	Average
RelH_9KM_SA_Topo	0.84	0.76	0.82	0.89	0.85	0.83
RelH_9KM_Limp_Topo	0.52	0.13	0.76	0.88	0.93	0.64
RelH_9KM_SA_FLTopo	0.4	0.63	0.47	0.52	0.4	0.48
RelH_9KM_Limp_FLTopo	0.4	0.44	0.17	0.69	0.54	0.45

Figure 4.10: WRF 9 km topography versus flat topography simulated relative humidity (%) with statistics over SA and Limpopo region for the period 22-26 October 2011

When the model topography was removed, bias (top) and RMSE values (middle) were at least doubled over the entire country and also Limpopo region. The CORR values (bottom) were reduced over the country and also Limpopo region. This result indicates that WRF simulation with topography was more accurate and reliable than simulation

without topography. The removal of topography completely deteriorated all the scores and it could be said that topography has an influence on the simulations.

4.2 Heavy precipitation (16-18 January 2012) and heat wave event (15-18 January 2012)

4.2.1 Synoptic description with topography

(a) Mean sea level pressure and winds

Figure 4.11 shows the SAWS daily weather bulletin map (SAWS, 2012) for the period 15 to 18 January 2012 at 12h00 UTC; whereas Figure 4.12 shows the WRF model synoptic MSL map for the same period. The daily weather bulletin showed a tropical depression Dando that resulted in heavy precipitation and flooding over the north-eastern parts of SA. Dando developed over the Indian Ocean and intensified as it moved over Mozambique Channel. It should be noted that as in the previous section, the resolution of SAWS synoptic map is lower that the model resolution which is at a resolution of 9 km. The WRF model simulated the first surface low pressure system over the Mozambique Channel with a strong trough line extending towards the higher escarpment area over Limpopo region of SA and parts of Mozambique. It has a steep pressure gradient which resulted in strong onshore winds to the south of the low pressure system. The WRF model simulation was in agreement with SAWS observations. Both the model simulated and observed low pressure system has a central pressure of 1000 hPa although it was reported that Dando has the central pressure of 994 hPa. The observed maximum average wind speed was at least 17.5 m/s whereas WRF simulated winds speed were at least 15 m/s.

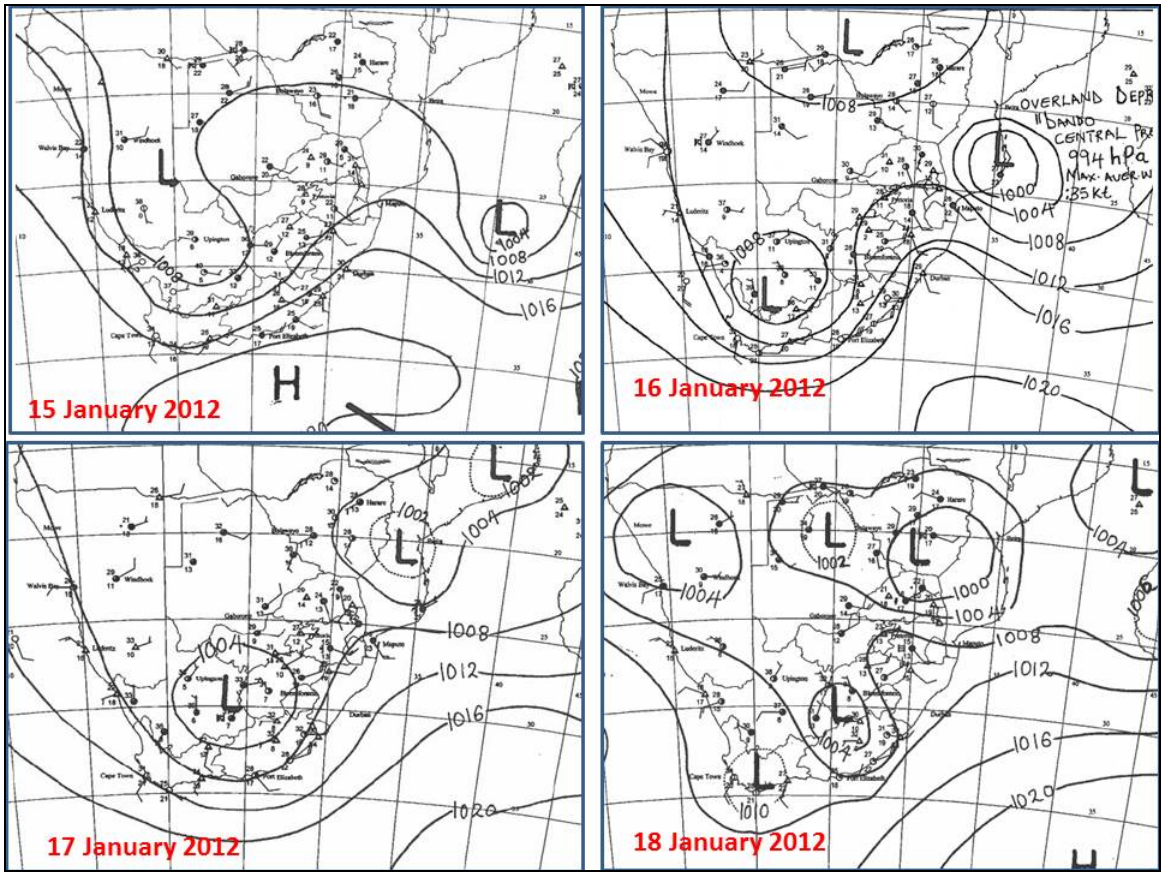

Figure 4.11: SAWS synoptic map as at 12h00 UTC (adapted from SAWS, 2012) with 1000 hPa level pressure (contour) and surface wind in knots (barbs) for the period 15-18 January 2012. Figure is labelled as follows: top left (15 January); top right (16 January), bottom left (17 January) and bottom right (18 January).

As a result of the low pressure system, there was abundance of moisture transport from the Indian Ocean towards the escarpment region of SA which enhanced convergence over the region. The WRF model simulated winds speed and direction over the Indian Ocean region also show a very close agreement with SAWS observations. The WRF model simulated a second low pressure system over the tropics with a 1008 hPa isobar over Zimbabwe. This was also in agreement with SAWS observations as SAWS synoptic map shows the 1008 hPa isobar over Zimbabwe. This low pressure system resulted in northerly winds and moisture transport from tropics towards the northeastern parts of the country including Limpopo region. The WRF model also simulated a high pressure system over the south coast of the country with a ridge line towards the high escarpment area of SA (from Figure 4.11 and Figure 4.12, only the ridge line is indicated in both maps). This simulation was also in close agreement with SAWS observations as both

WRF and SAWS show the 1016 hPa isobar located very close to (33°S and 40°E). The anti-cyclonic motion from the high pressure system and the cyclonic motion from the low pressure system enhanced the moisture transport from the Indian Ocean towards the high escarpment region over the eastern half of the country.

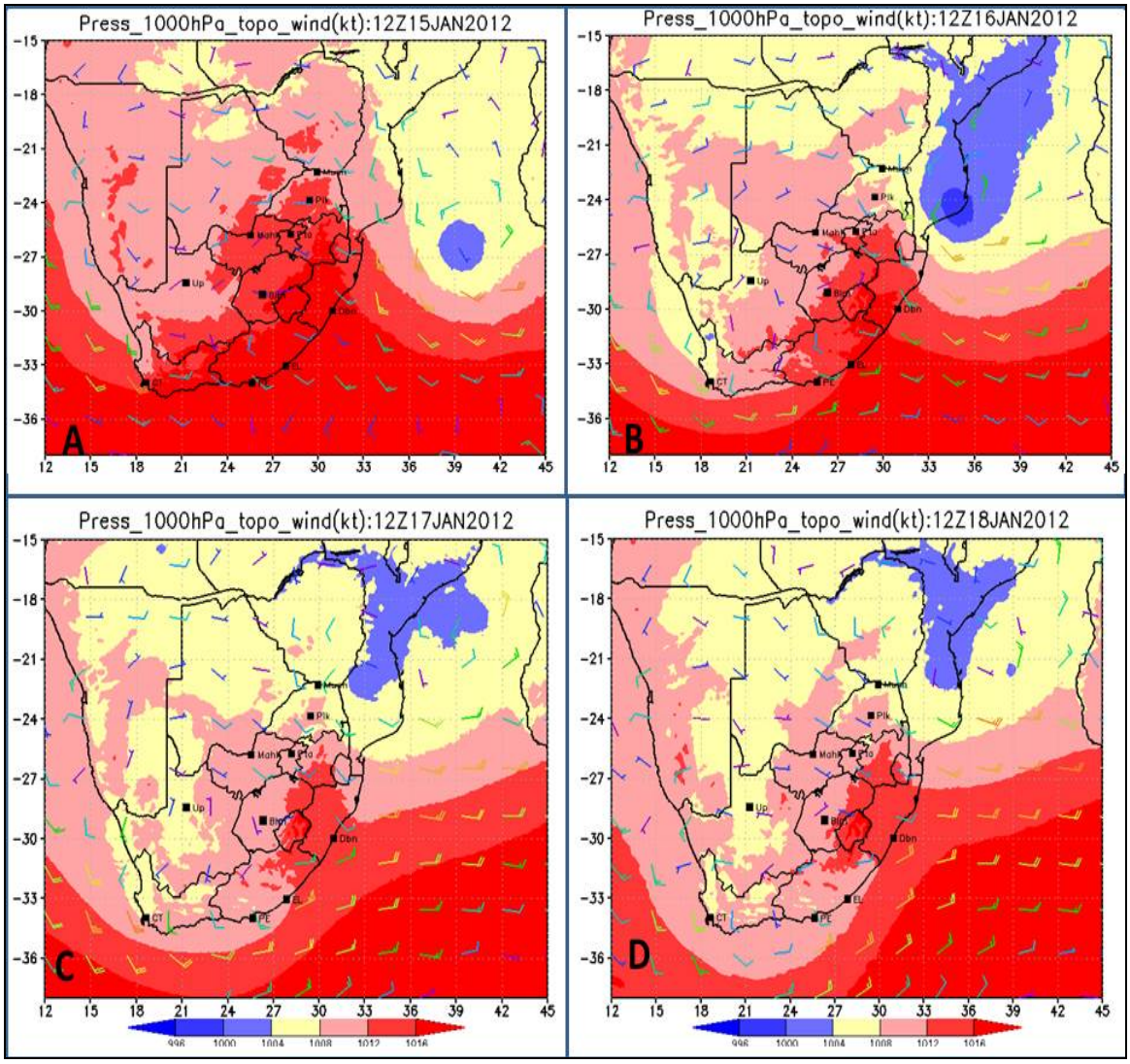

Figure 4.12: WRF 9 km simulated synoptic map at 12h00 UTC with 1000 hPa level pressure (contour), and surface winds (barbs in kt) for the period 15-18 January 2012. Figure is labelled as follows: top left (15 January); top right (16 January), bottom left (17 January) and bottom right (18 January).

A third low pressure system was situated over the interior of SA with a trough over the eastern parts of the country. This low pressure system has a central pressure of 1008 hPa and was also well captured by the WRF model simulation. The combination of the low

pressure system over the interior of the country, the high pressure system over the east coast and the low pressure system over the Mozambique enhanced moisture convergence over the higher escarpment areas of the country, to the east of the surface trough over the country. This combination also enhanced the moisture uplift (see Figure 4.13a and 4.14a) leading to cloud formation and rainfall over KZN province and Limpopo region of SA (see Figure 4.15).

During the same period of the depression over the Mozambique Channel (see Figure 4.11), a heat wave was experienced over the Cape region. The WRF model also indicates the presence of the high pressure system ridging into the west coast of the country towards Western Cape Province (from Figure 4.12 only the ridge line is indicated by the 1012 hPa isobar over Western Cape Province). This was also in good agreement with SAWS observations. However, due to its location, it has less influence on synoptic circulation over the land. The low pressure system over the interior resulted in offshore flow leading to advection of warm and dry air towards the west coast from the interior over Cape region. This resulted in very high temperatures above 40^{o}C over Cape region. Table 4.3 indicates the maximum vertical velocity at different heights over the country, with highest maximum updrafts at 700 hPa level. Table 4.4 lists all the stations that registered maximum temperatures above 38^{o}C together with the WRF model simulations for the period 15-18 January 2012.

(b) Moisture fluxes at different levels and vertical velocity

Figure 4.13 depicts areas of moisture flux convergence and divergence whereas Figure 4.14 shows the WRF model simulation of vertical velocity over the subcontinent from 1000 hPa to 500 hPa over a 24 hours period on 16 January 2012. At 1000 hPa, the WRF model simulated a combination of strong moisture convergence and strong updraft over the Mozambique Channel resulting in enhanced rainfall over Limpopo region. The WRF model also simulated a combination of strong moisture flux divergence (Figure 4.13a) and downdrafts (Figure 4.14a) over the west coast, just behind the surface trough over Western Cape.

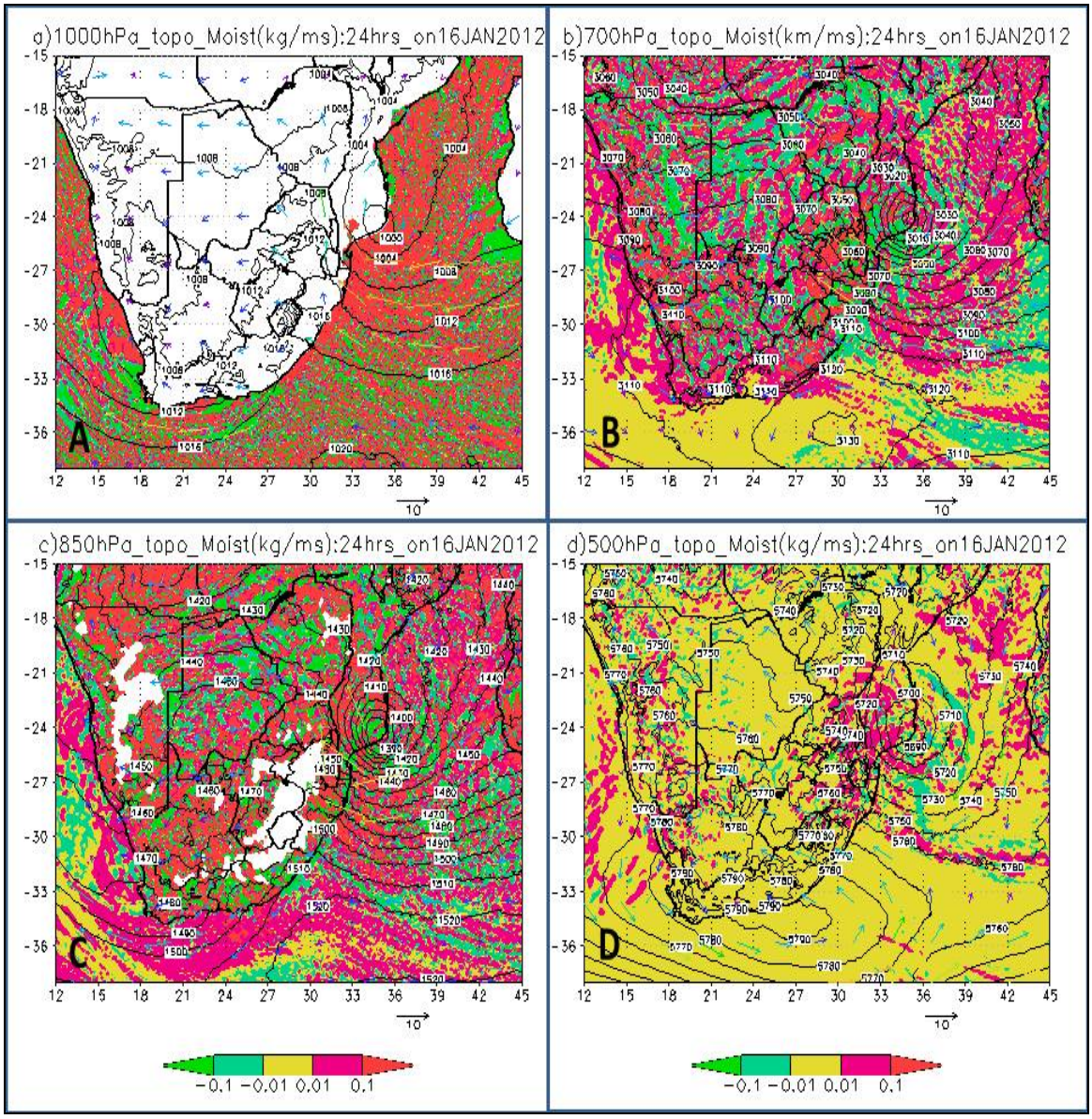

Figure 4.13: The WRF model simulation of 1000 hPa (top left), 850 hPa (bottom left), 700 hPa (top right) and 500 hPa (bottom right) geopotential height levels (contoured), moisture flux (kgm^{-1}s^{-1}) is shaded and horizontal winds (vectors ms^{-1}) on 16 January 2012. The yellow colour on the image, interval (-00.1to 0.01) indicates transition area, whereas white colour indicates that topography is higher than the plotted geopotential heights.

At 850 hPa level, the WRF model simulations with topography show a low pressure system over the Mozambique Channel. It resulted in strong easterly winds on the southern side of the low pressure system. Such winds have an average wind speed of 60m/s, which was twice the strength of the simulated winds at 1000 hPa. This could attribute to the fact that near the surface, there are more obstacles which increases friction and therefore result in lower wind speed.

The cyclonic motion from the low pressure system result in both enhanced moisture flux convergence (Figure 4.13c) and increased updrafts (Figure 4.14c) over the north-eastern parts of the country. The eastern parts of the escarpment area have topography higher than 850 hPa and therefore neither moisture fluxes nor vertical velocity were indicated in the WRF model simulation. The ridging high over the western parts of the country started pushing the surface trough over the western interior of the country eastwards. The winds were southerly due to anti-cyclonic motion of a ridging high pressure system (Figure 4.12c). The combination of the ridging high pressure system and the low pressure system over the interior resulted in enhanced moisture flux divergence (Figure 4.13c) and very strong downdrafts over the west coast of the country (Figure 4.14c).

At 700 hPa the WRF model simulations with topography show similar moisture flux pattern (Figure 4.13b) and vertical velocity (Figure 4.14b) pattern when compared to simulation at 850 hPa, but both were slightly less intense than at 850 hPa.

At 500 hPa, the low pressure system over the Mozambique Channel started weakening, resulting in an area of weakened moisture flux convergence (Figure 4.13d) and weakened updrafts over Limpopo region (Figure 4.14d). Over the Cape region, a high pressure system was ridging over the south coast (Figure 4.13d). This resulted in less moisture flux divergence and weak downdrafts over Westrn Cape coast and also moisture flux convergence and weak updrafts over the Northern Cape (Figure 4.13d).

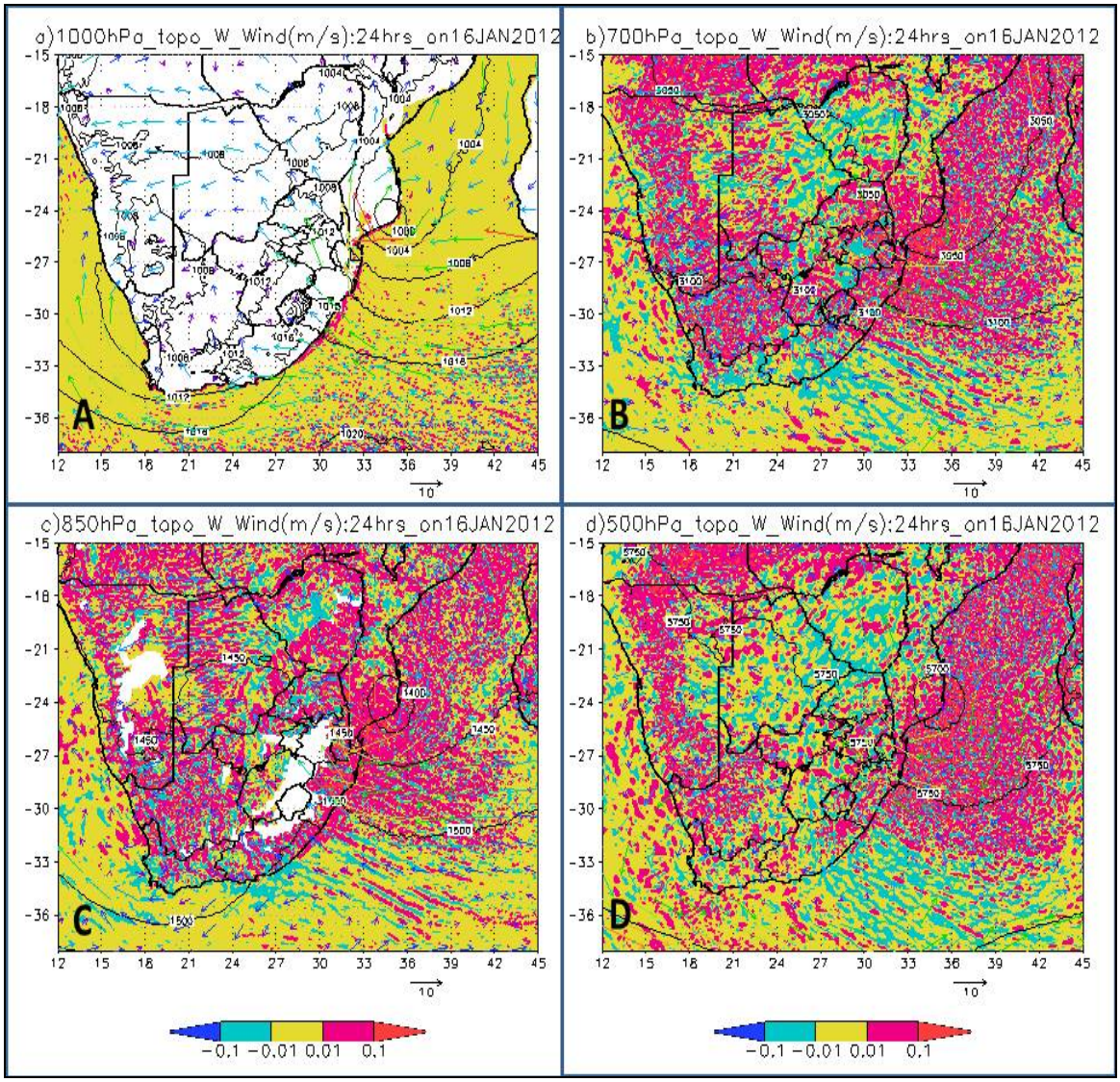

Figure 4.14: The WRF model simulation of 1000 hPa (top left), 850 hPa (bottom left), 700 hPa (top right) and 500 hPa (bottom right) geopotential height levels (contoured), vertical velocity (shaded in ms^{-1}) and horizontal winds (vectors in ms^{-1}) simulation as on 16 January 2012. The yellow colour on the image, interval (-00.1to 0.01) indicates transition area, whereas white colour indicates that topography is higher than the plotted geopotential heights.

Table 4.3 indicates the maximum vertical velocity at different heights over the country, with highest maximum updrafts at 700 hPa level. It is also evident that the WRF model simulated highest vertical velocity on the 16 January when the depression Dando was most dominant.

Table 4.3: The WRF 9 km topography versus flat topography simulated maximum vertical velocity (m/s) during heavy precipitation event over Limpopo region for the period 16-18 January 2012

	WRF 9 km maximum vertical velocity (m/s)					
	16-Jan-12		17-Jan-12		18-Jan-12	
	WRF9_topo	WRF9_fltopo	WRF9_topo	WRF9_fltopo	WRF9_top	WRF9_fltopo
850 hPa	0.60	0.35	1.00	1.20	0.50	0.70
700 hPa	0.80	0.14	1.20	2.70	0.70	1.10
500 hPa	0.45	0.18	0.55	5.00	1.00	1.60
average	0.62	0.22	0.92	2.97	0.73	1.13
maximum	0.80	0.22	1.20	5.00	1.00	1.60

(c) Rainfall simulation

As a result of the above discussed synoptic scale circulation over the north-eastern parts of the country, the WRF model simulated rainfall bands oriented in a north-west to south-east direction over the central parts of the country from the Northwest province towards KZN Province (from the 16-18 January). This rain-band was similar in orientation to the ITCZ as simulated in a study by Cretat *et al*., (2012). On the16th January, the WRF model simulation with topography (Figure 4.15a) simulated localized rainfall maximum above 200 mm over the east coast of SA. This area includes some parts of Eastern Cape, KZN provinces, Limpopo region and Mozambique.

On the 17 and 18th January, the WRF model simulations with topography simulated more rainfall over eastern parts of Limpopo region, the east coast of KZN province and Mozambique, with rainfall maximum up to 350 mm. Over a period of 48 hours, all the simulations show that heavy rainfall occurred just to the windward side of the escarpment, including Mozambique. The WRF model simulation also shows some rainfall over the western interior of the country including the Western and Northern Cape provinces. However, very low rainfall was simulated over the central parts of the country, including Gauteng, Free State, Northwest and Eastern Cape provinces (Figure 4.15 c and e).

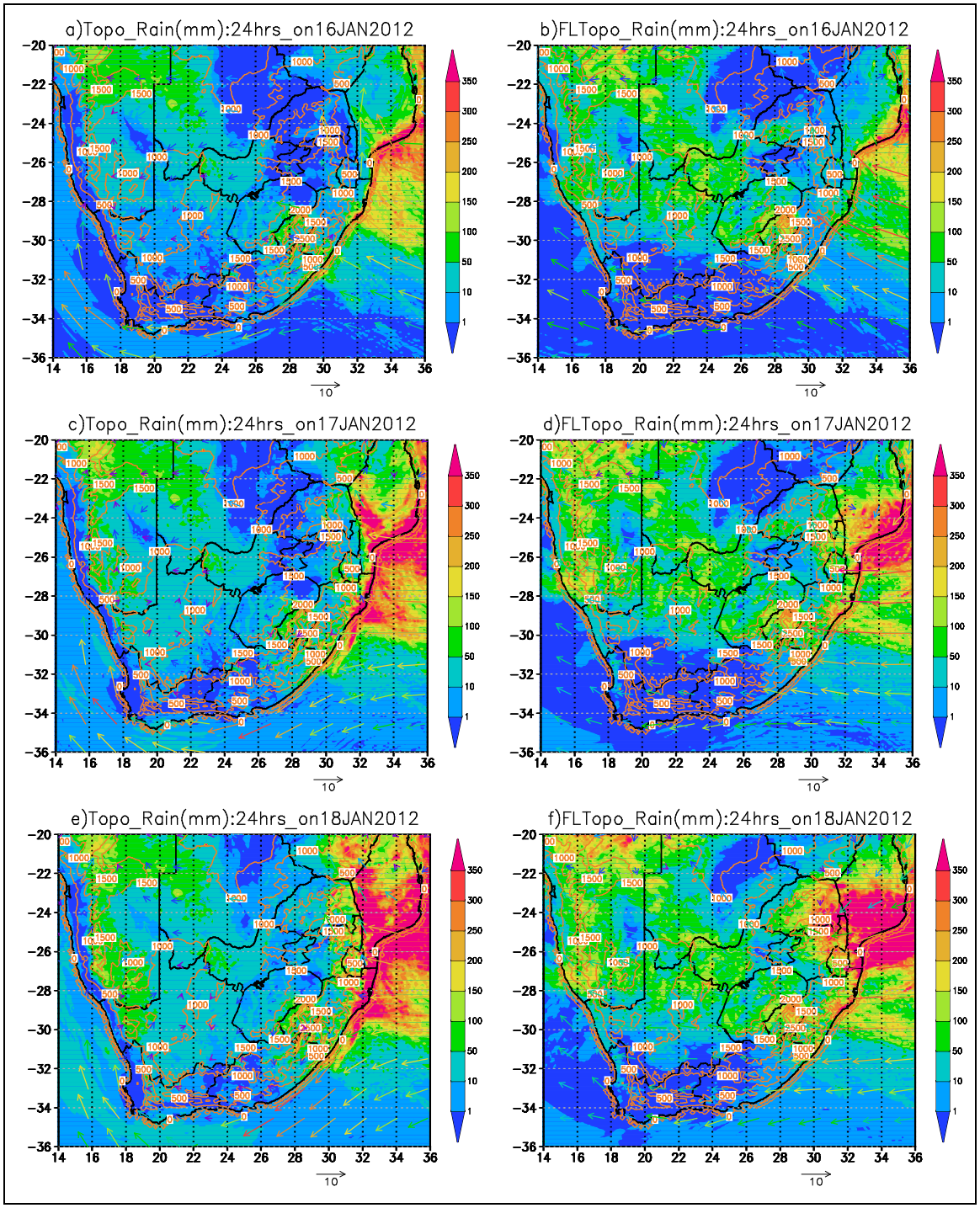

Figure 4.15: WRF 9 km rainfall simulation with topography (left) and without topography (right) for the period 16-18 January 2012. Rainfall (mm/day) is shaded and topography (m) is plotted as contours, whereas horizontal winds (vectors in ms^{-1}). A24 hour's rainfall is calculated as a total accumulated rainfall over the station from 06h00 UTC on the day of simulation to 06h00 UTC the following day. The image is labelled as follows: top left (16 January, with topography); top right (16 January, without topography); middle left (17 January, with topography); middle right (17 January, without topography); bottom left (18 January, with topography) and bottom right (18 January, without topography).

From these simulations, it could be deduced that easterly winds were responsible for the advection of warm moist air from the tropical Indian Ocean and the Agulhas current region towards the east coast of South Africa. As a result of topography over the eastern escarpment, both moisture flux convergence and vertical velocity were enhanced resulting in cloud formation and therefore rainfall. It can be deduced that topographic heights and orientation enhanced rainfall.

(d) Maximum temperature simulation

Figure 4.16 shows the WRF model simulation of maximum temperatures for the period 15-18 January 2012. This simulation indicates that maximum temperature changes with height. These simulations show a west to east temperature isotherm gradients over the Cape region. Lower temperatures were simulated over the eastern side over higher topography areas along the escarpment. Higher temperatures were simulated over lower topography areas over Cape region, where the altitude is less than 500 metres. Very high temperatures above 40^{o}C were simulated over the border between Northern and Western Cape where the altitude is between 0 and 500 m. As topography rises to 1000 m over Cape region, these temperatures were reduced to values below 40^{o}C.

The winds were easterly over the central interior of the country towards the Cape region. As these winds flow across the country towards the west coast, the speed increases as they descend down topography and experienced surface warming and turbulent mixing. By the time they reached the west coast, they were hot and dry. At the same time subsidence due to upper air high pressure system resulted in dynamic warming due to adiabatic heating (adiabatic heating of berg winds). Subsidence and advection resulted in very high temperatures over the west coast. This type of synoptic circulation has been confirmed in a study by Lengoasa (1988) and also Mason and Jury, (1997). The southerly winds were also simulated over Atlantic Ocean. From this analysis, it is shown that if onshore flow by southerly were responsible for the advection cold and dry air from the Atlantic Ocean into the west coast, very high temperatures would have not been experienced. Therefore this analysis confirms that the berg winds together with subsidence were the most dominant factors that intensified the heat wave event over Cape region. From this simulation it could also be deduced that the WRF model simulations slightly under-predicts very high temperatures above 44^{o}C (Figure 4.16).

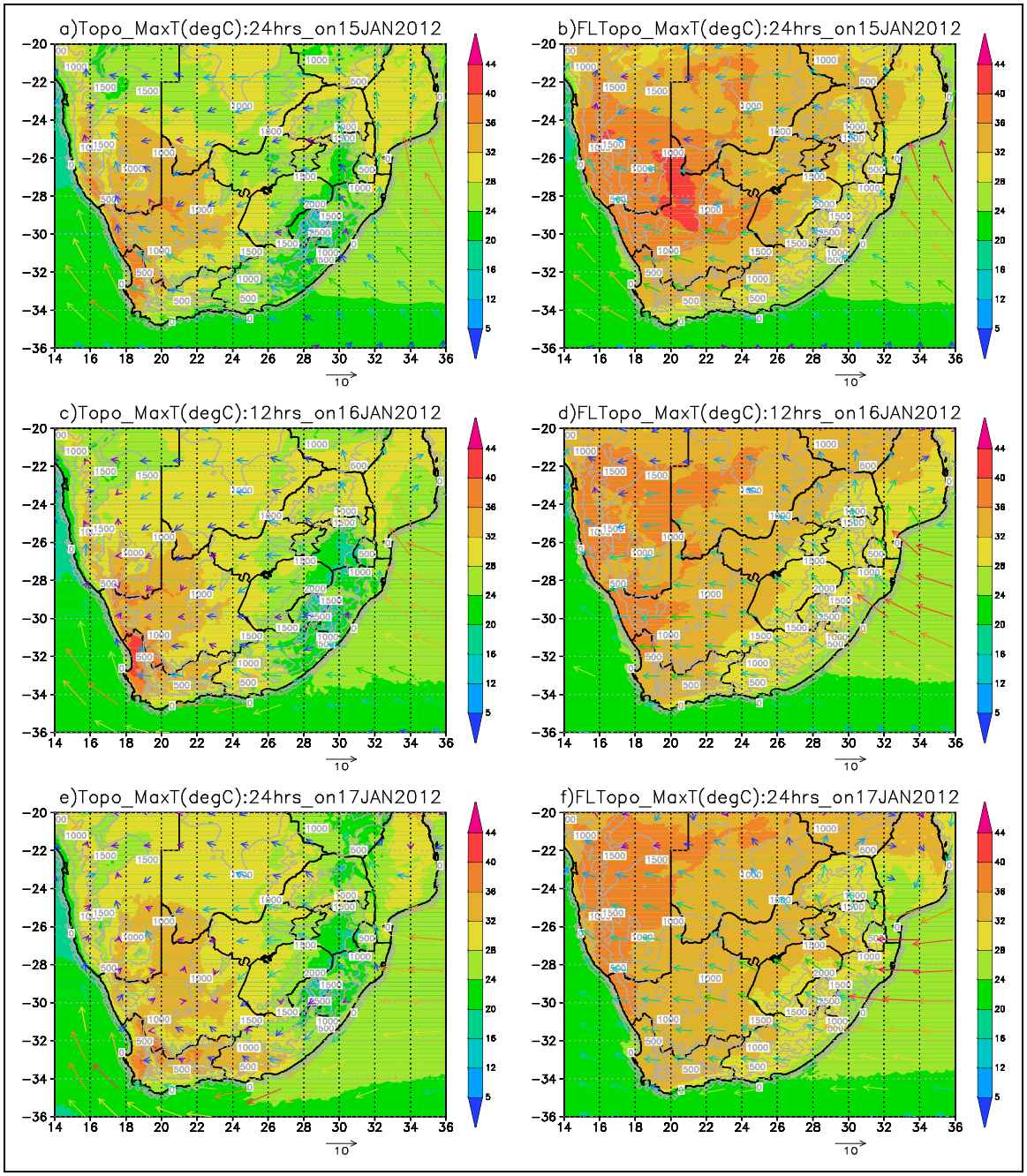

Figure 4.16: WRF maximum temperature (degree Celsius) simulation for the period 15-17January 2012. Maximum temperatures are shaded and topography (m) is contoured, whereas horizontal winds vectors are in (ms^{-1}). A 24 hours temperature is calculated as the recorded maximum temperatures at the station from 00h00 UTC on the day of simulation to 00h00 UTC the following day. The image is labelled as follows: top left (15 January, simulation with topography); top right (15 January, simulation without topography); middle left (16 January, simulation with topography); middle right (16 January, simulation without topography); bottom left (17January, simulation with topography) and bottom right (17 January, simulation without topography).

4.2.2 Synoptic description without topography

(a) Mean sea level pressure and winds

At sea level (1000 hPa); the low pressure system over the Indian Ocean covers large area and moves inland faster than in simulation with topography. This could be due to that topography over the eastern escarpment blocked this low pressure system in simulation with topography. The low pressure system over the tropics also covers larger areas. The high pressure system over the east coast weakened and disintegrated quickly as compared to simulation with topography. As a result of the removed topography, easterly winds were able to move inland and reach the central interior of the country. The low pressure system over the western interior of the country weakened and covered larger area. The ridging high pressure system over the west coast also weakened and moved inland quicker than in the model simulation with topography (Figure A.4).

(b) Moisture fluxes and vertical velocity at different vertical levels

Simulation without topography indicates that there were moisture fluxes and a combination of updrafts and downdrafts over the entire domain including the land. Simulation with topography only indicates moisture fluxes and vertical motions only over the surrounding oceans. This was due to that the topography of SA is located above 1000 hPa level. However, over the west coast, there was intensified moisture flux divergence (Figure A.5) and downdrafts as compared to convergence and updrafts along the east and northeast coast (Figure A.6).

At 850 hPa, the low pressure system over the Mozambique Channel started weakening and the high pressure system over the south coast intensified and covered a larger area. Over the land, the ridging high pressure system to the east coast of the country became weaker and resulted in weak divergence and downdrafts over the eastern parts of the escarpment and Limpopo region. The low pressure system over the central interior of the country pushes further north towards Namibia. The easterlies moved over the higher topography areas along the escarpment and reached the interior of the country. There was a reduction of moisture flux divergence and weakened downdrafts over the western interior of SA and the entire domain (Figure A.6).

At 700 hPa the WRF model shows that the low pressure system started weakening over the Mozambique Channel. The wind speed started decreasing to an average of 40 m/s. Almost the entire interior of the country was convered by a ridge as a result of a high pressure system located further south of the country. This high pressure system was also weakening and ridging in over larger areas including south coast (not shown). The low pressure system over the tropics moved further north of 15^{o}S. There was less moisture flux convergence and weakened updrafts at this level than at 850 hPa, with more flux convergence and updrafts around a low pressure system over the north-eastern parts of the country and the Indian Ocean (Figure A.5). The entire western half of the country convered by a high pressure system located further south of the country. This high pressure system was strengthening and ridging in over larger areas including Eastern, Western and Northern Cape provinces (Figure A.4). It resulted in weaker moisture flux divegence and downdrafts over Cape region. However, there was still moisture convergence and updrafts on the border between Northern Cape and Namibia due a low pressure system covering most of Namibia (Figure A.6).

At 500 hPa, the low pressure system over the Mozambique Channel was slightly weaker than in simulation with topography. It resulted in weaker moisture flux convergence and updratfs. The high pressure system over the southern coast was stronger and covered larger area than for simulation with topography (Figure A.4). Likewise the high pressure over the south coast was strengthened. It resulted in stronger divergence and downdrsfts than in simulation with topography over the Cape region. The entire interior of the country was dominated by a ridging high pressure system over the south coast leading to more divergence and subsidence (Figure A.6).

(c) Rainfall simulation

The WRF model simulation without topography has simulated almost similar rainfall pattern as in simulation with topography over the east coast. However the rainfall maximum was lower than in simulation with topography and was also widespread over the domain. This model run has simulated rainfall over almost the entire Limpopo region (Figure 4.15 b, d and f). The WRF model simulations without topography show less rainfall over the east coast, but more rainfall was spread over the central to western interior of SA. The WRF model simulation with topography did not show the rainfall

over the central to western interior of the country (Figure 4.15b). Therefore it can be deduced that topographic heights and orientation enhanced rainfall, and when topography is removed, the WRF model simulated rainfall over almost the entire domain.

(d) Maximum temperature simulation

The WRF model simulation without topography shows that higher temperatures were reduced and lower temperatures increased over the entire country. This simulation could not capture the spatial distribution of lower temperatures over the higher topography areas along the escarpment. Over western interior, this simulation shows that the Cape region experienced temperatures lower than 40^{o}C. This could be attributed to that the easterlies remain constant during advection towards the west coast. The removal of topography might have resulted in constant surface heating and turbulent mixing. However, there was subsidence due to dynamic warming as a result of adiabatic heating. This resulted in the WRF model simulating only mild temperatures as compared to simulation with topography (Figure 4.16). However, these simulated temperatures were lower than the observed temperatures shown in table 4.4.

4.2.3 Statistical analysis: simulation with and without topography (heavy precipitation 16-18 January 2012)

In this section the WRF model output for rainfall, maximum and minimum temperatures, wind speed as well as relative humidity over Limpopo region of SA are discussed. The statistical values are compared for both the model simulations at 9 km with and without topography. For rainfall, the statistics include bias, probability of detection (POD) and Pearson correlation coefficient (CORR). For temperatures, wind speed and relative humidity, statistical values include bias, root mean square error (RMSE), and Pearson correlation coefficient (CORR).

a) Rainfall

Figure 4.17 shows the WRF model rainfall simulation over Limpopo region on 17 January 2012 together with verification statistics. It is shown that most rainfall was recorded over parts of Limpopo region during the period of two days (17 and 18 January). The model simulation with topography over-predicted rainfall over the north-

eastern parts of Limpopo province and under-predicted rainfall over Mpumalanga province. However, the model captured a no-rain event on the western parts of the Limpopo region (Figure 4.17a).

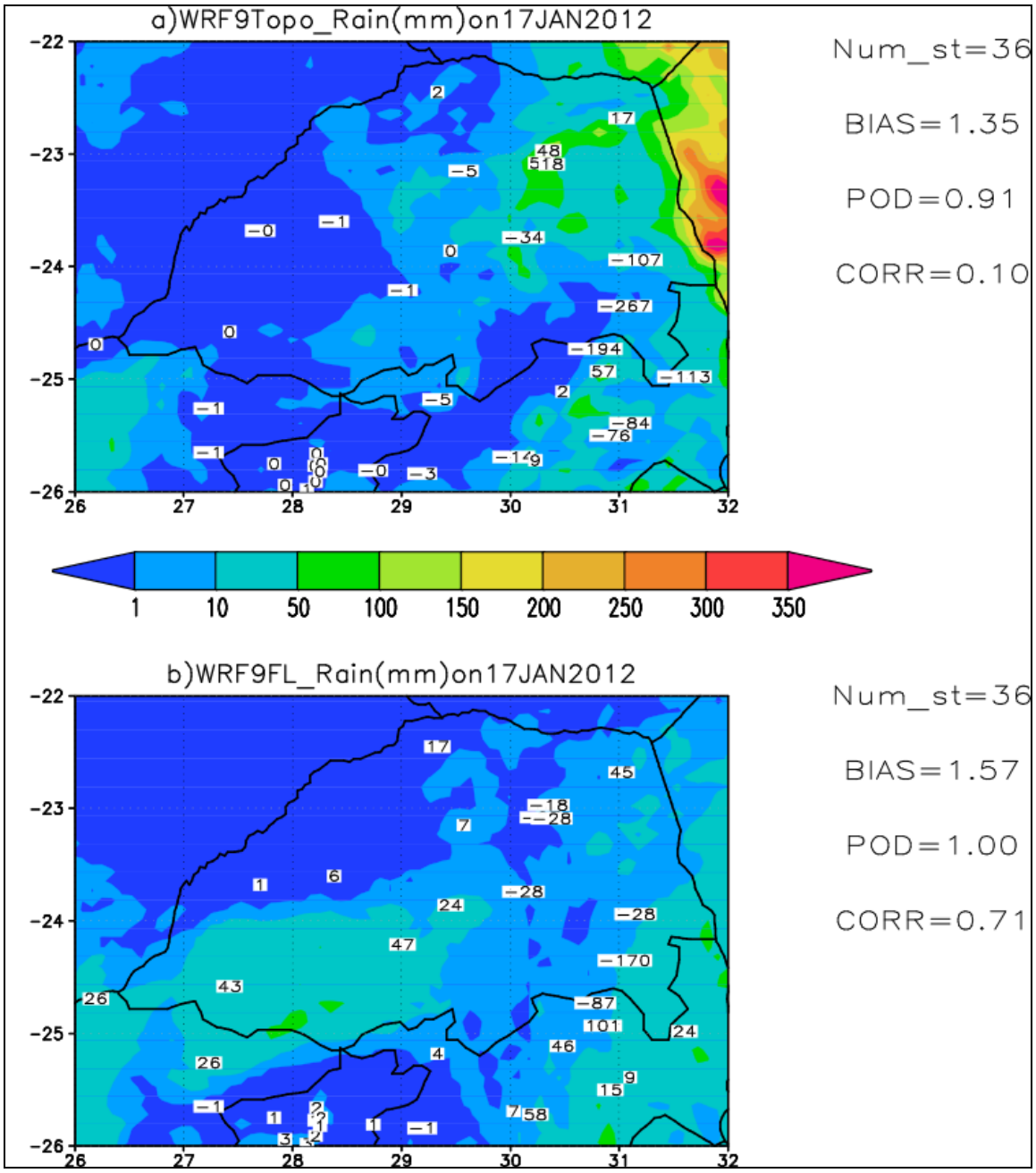

Figure 4.17: WRF 9 km topography versus flat topography simulated rainfall (mm/day) with statistics over Limpopo region on 17 January 2012. Bias values at each observation station are indicated as numbers.

When the model topography was removed, the model simulated rainfall over almost the entire Limpopo region. The rainfall maximum was less than in WRF simulation with topography over the Limpopo region. The model also under-predicted rainfall over most stations over western parts of Limpopo province and over-predicted rainfall for stations over Mpumalanga provinces.

The WRF model simulations also displaced some rainfall from the north-eastern border to the western border of the Limpopo region (Figure 4.17b). From these two simulations it can be deduced that simulation with topography was able to reproduce observed rainfall and simulation without topography produce unreliable results.

Figure 4.18 shows rainfall bias values for the 0.1, 10 and 20 mm rainfall thresholds respectively. The average bias increases with rainfall threshold, with average bias at 0.1 mm being less than the bias at both 10 and 20 mm thresholds respectively over the country. Over Limpopo region, simulation with topography shows that bias was less than over the country. The average bias was reduced with time at 0.1 mm, but increase with time for both 10 and 20 mm thresholds respectively. When topography was removed over the country, bias was slightly reduced at 0.1 mm, increased at 10 and 20 mm respectively. However, over Limpopo region bias increased with time for all rainfall thresholds respectively (Figure 4.18).

From these two simulations, it could be deduced that rainfall simulation with topography has less bias for all rainfall thresholds, and more bias for simulation without topography. This result also confirms that the presence of topography enhanced moisture flux convergence, leading to enhanced rainfall whereas the removal of topography reduced moisture fluxes, leading to reduced rainfall. Therefore this result proved that topography enhanced rainfall and that simulation with topography yields reliable results.

Figure 4.19 shows the POD values for rainfall thresholds 0.1, 10 and 20 mm respectively. The average POD values reduces as rainfall thresholds increases over the country and also Limpopo region in simulation with topography. At 0.1 mm threshold, an average POD value was higher than at both 10 mm and 20 mm threshold respectively. This model simulation indicates good results for low rainfall thresholds than at higher rainfall

thresholds. The average POD values were increased as topography was removed, for all the thresholds over the country and also Limpopo region (Figure 4.19). This result assumes more than 80% detection when topography is removed, and such the results are unrealistic.

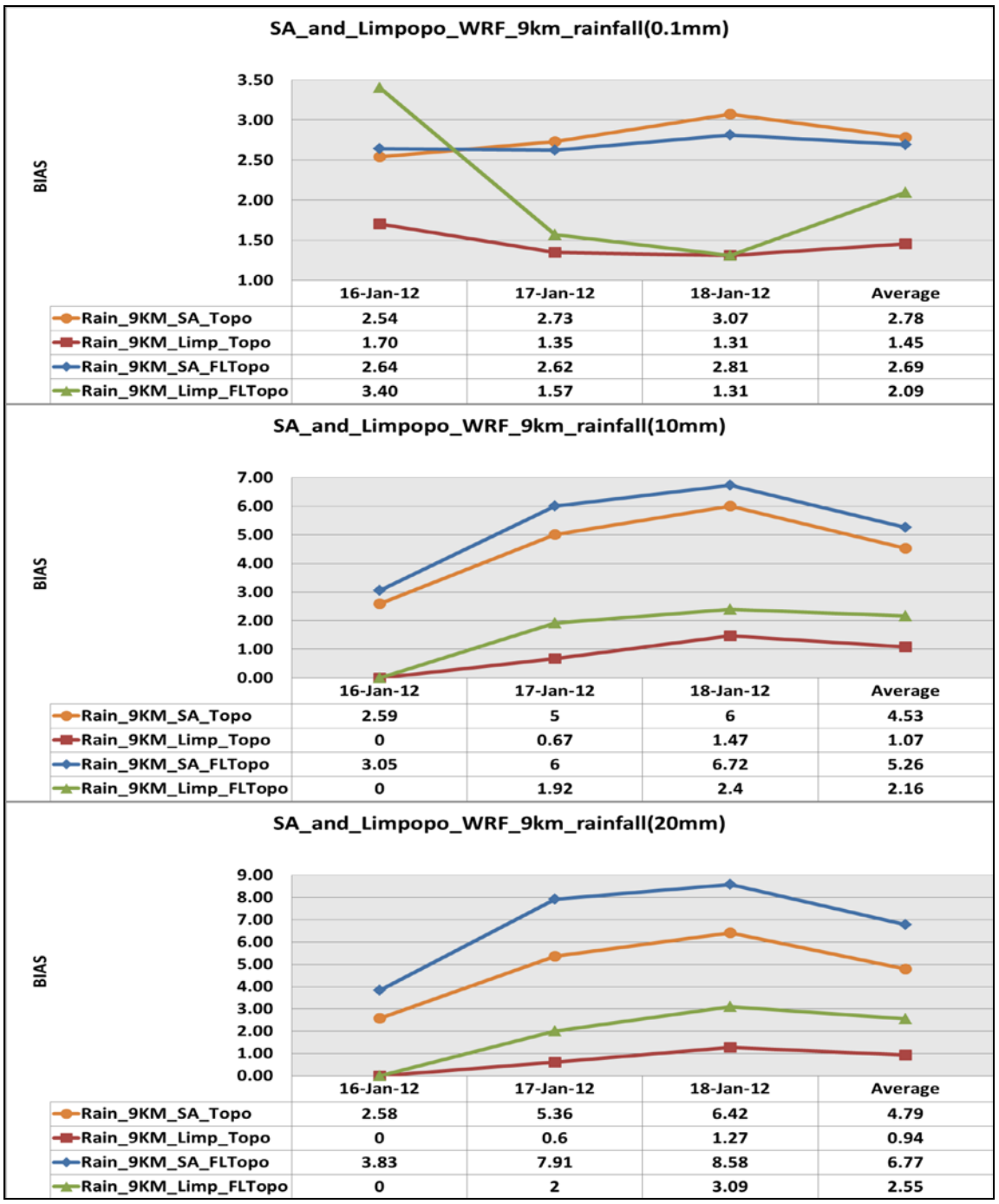

Figure 4.18: WRF 9 km topography versus flat topography rainfall(mm/day) bias for the 10.mm, 10 mm and 20 mm threshold over SA and Limpopo region for the period 16-18 January 2012

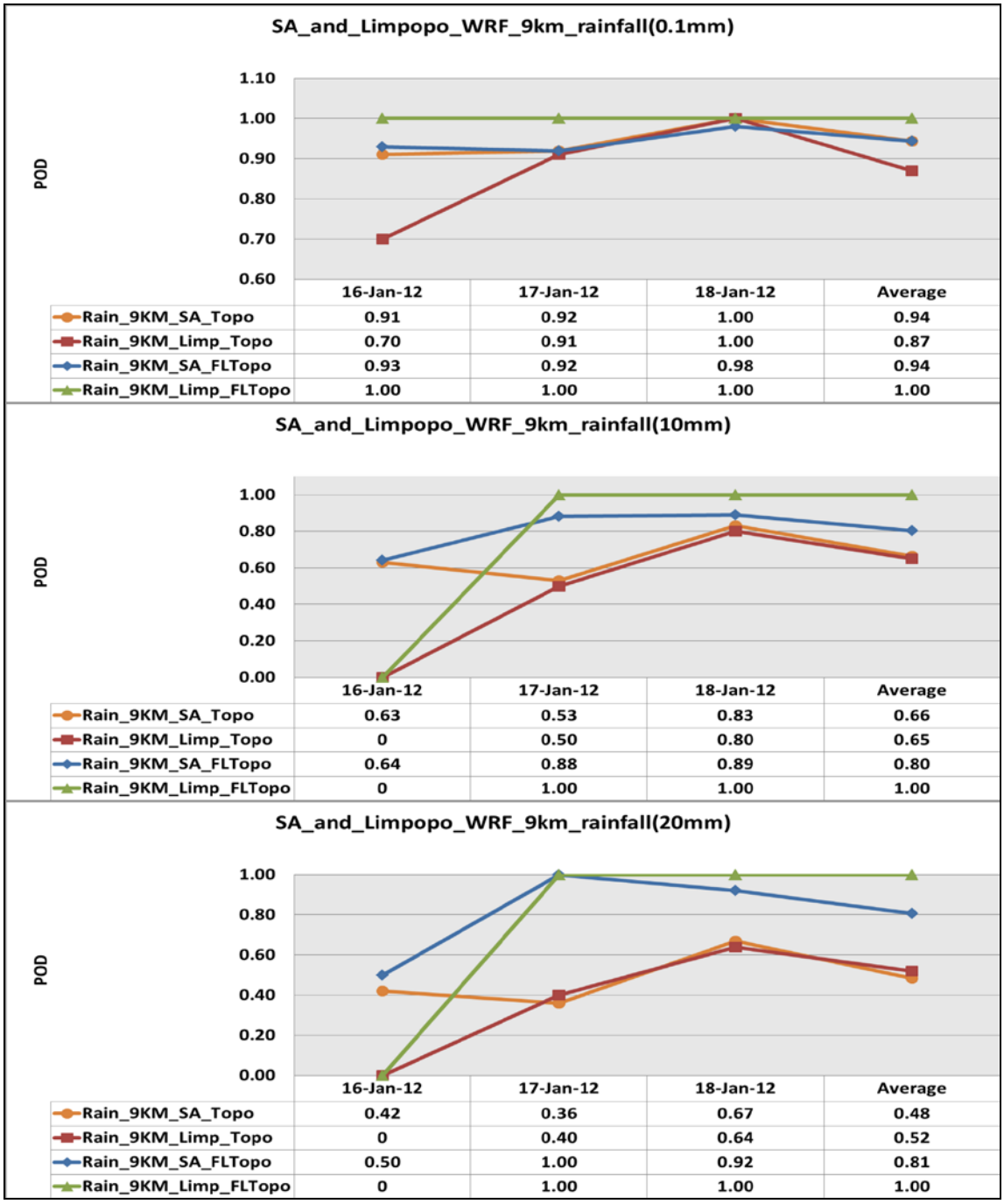

Figure 4.19: WRF 9 topography versus flat topography rainfall (mm/day) POD for the threshold 0.1 mm, 10 mm, and 20 mm over SA and Limpopo region for the period 16-18 January 2012

Figure 4.20 show the rainfall CORR values for the 0.1, 10 and 20 mm rainfall thresholds respectively over the country and Limpopo region. The CORR values show mixed results over SA for simulation with topography and for all the thresholds. On average, the CORR values were weak but positive over the country and Limpopo region. The average CORR values increased with rainfall thresholds, with average at 0.1 mm lower than at both 10

and 20 mm thresholds over the country and Limpopo region. However, the averages at both 10 and 20 mm thresholds were similar over the country and Limpopo region.

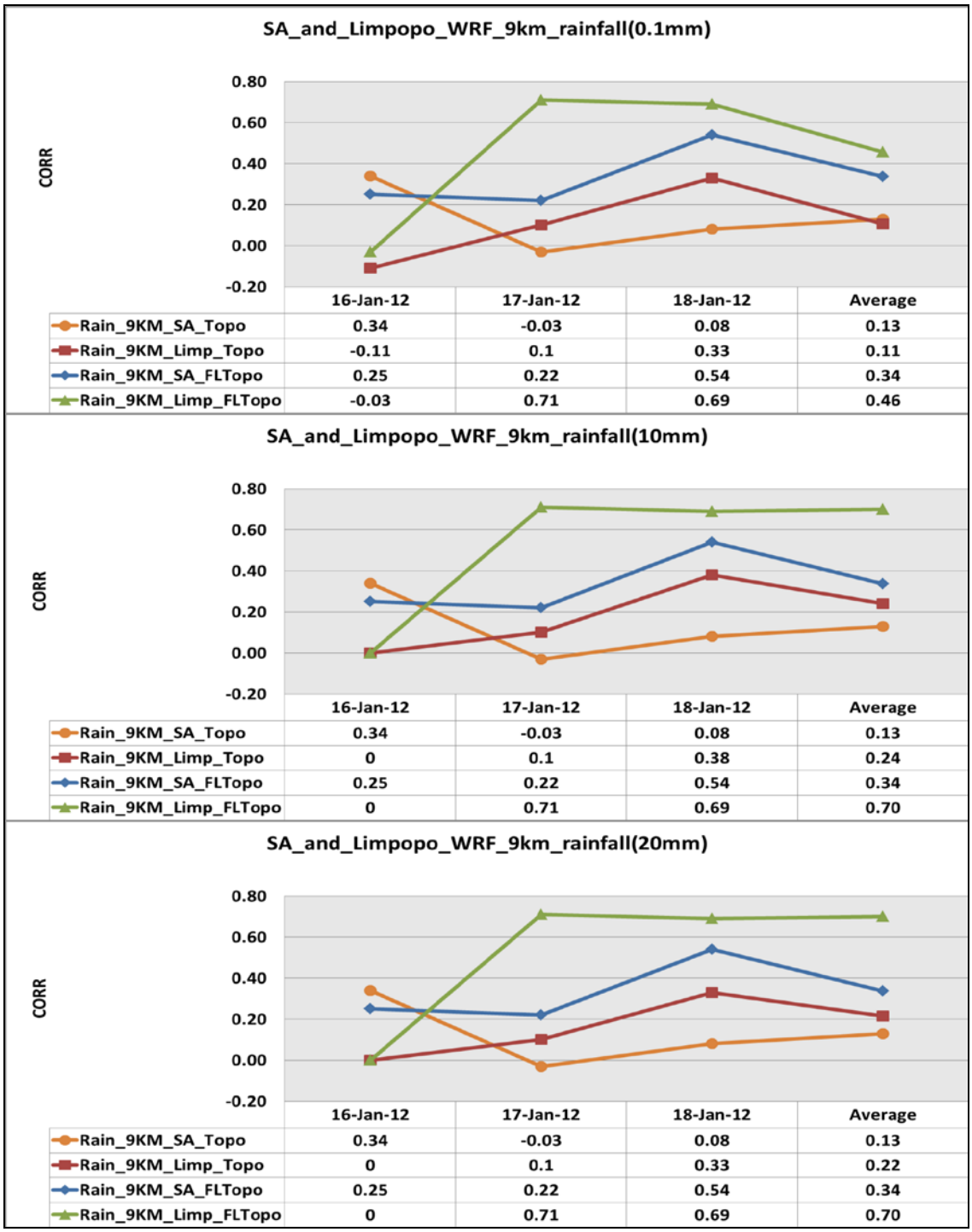

Figure 4.20: WRF 9 km topography versus flat topography rainfall (mm/day) CORR for the threshold 0.1 mm, 10 mm, and 20 mm over SA and Limpopo region for the period 16-18 January 2012

When topography was removed over the country, the average CORR values were more than doubled at 0.1 mm and tripled at both 10 and 20 mm rainfall thresholds respectively. Simulations over Limpopo region shows that on average the CORR value was lower at 0.1 mm threshold, doubled at both 10 mm and 20 mm thresholds respectively (Figure 4.20). All this scores give an indication that statistically, simulation with topography yield acceptable results and when topography is removed, simulations results are unreliable and that model simulation with topography is capable of reproducing observed rainfall over the country.

Table 4.4: Station observed versus WRF simulated rainfall (mm) over Limpopo and Mpumalanga provinces for the period 16-18 January 2012.

	Station observed vs WRF 9 km rainfall_16-18 January 2012				
			Total rainfall		
	Station name	stid	observed	wrf9_topo	wrf9_fltopo
1	Hoedspruit (lat:-24.35; lon: 31.05)	68291	378.20	21.65	514.73
2	Kruger Airport(lat:-25.39; lon:31.1)	68290	215.20	199.68	405.05
3	Levubu(lat:-23.08; lon: 30.28)	68182	85.00	438.21	218.97
4	Mara(lat:-23.09; lon:30.38)	68176	51.40	12.83	160.08
5	Marken (lat:-23.6; lon: 28.38)	68163	35.20	11.79	73.63
6	Nelspruit (lat:-25.5; lon:30.92)	68289	144.20	71.01	380.06
7	Phalaborwa(lat:-23.94; lon:31.15)	68191	145.80	103.39	452.89
8	Punda Maria(lat:-22.68; lon: 31.02)	68196	33.40	118.17	287.47
9	Skukuza(lat:-24.98; lon:31.6)	68296	278.60	107.91	474.10
10	Thohoyandou (lat:-23.09; lon: 30.38)	68183	70.00	289.04	214.64
11	Tshivhase Tea Est (lat:-22.97; lon: 30.35)	68184	149.80	348.86	209.65
12	Tzaneen (lat:-23.74; lon: 30.12)	68188	120.00	173.96	263.14
13	Vaalhoek(lat:-24.73; lon:30.78)	68282	318.00	7.43	527.77
		Maximun	378.20	438.21	527.77
		Minimum	33.40	7.43	73.63
		Average	137.22	156.86	305.62
		Median	144.20	107.91	287.47
		BIAS		19.64	168.40

Table 4.4 shows the number of stations that recorded rainfall as well as the WRF model simulation for the period 16-18 January 2012 over the north-eastern parts of the country (named Limpopo region). The station observed average rainfall is higher than the median of the monthly rainfall as tabulated in Schulze (1997) climate record for January (see Figure A.7). From this table, it is shown that the model has either under-predict and over-predict high rainfall for some stations. In most stations, the removal of topography resulted in model results with double Figures as compared to observed rainfall, whereas

in others, the model simulated rainfall very well. Such results also confirm that rainfall was enhanced by topography.

In table 4.5 it is shown statistically that over the entire country, both WRF simulation with topography (panel-a) and without topography (panel-b) shows significant difference between the WRF simulation and observation. It is also noticeable that the t-test values are lower in simulation with topography than in simulation without topography. This resulted in the rejection of null hypothesis. However, over Limpopo region (panel-c) shows an agreement between WRF simulations with topography and observation for the first two rainfall days and also the average results. This resulted in the acceptance of null hypothesis. It was only on the 18th January that statistic indicates significant difference between WRF simulation and observations, resulting in the rejection of the null hypothesis. This statistical result was almost similar in WRF simulation without topography (panel-d), except that for the average results, the null hypothesis was rejected.

Table 4.5: Students t-test for rainfall at 9 km grid resolution over SA and Limpopo region for the period 16-18 January 2012 for both simulation with topography (a and c), and also for simulations without topography (b and d). A 95% confidence level was applied, and "TRUE" indicates that there is significant difference between the mean of observation and the mean for the WRF simulation, whereas "FALSE" indicate that there was no significant difference between the mean of observation and the mean for the WRF simulation.

a) Rain_9KM_SA_Topo				
Date	16-Jan-12	17-Jan-12	18-Jan-12	Average
T_test	4.0500	3.8800	5.2400	4.3900
df	404.00	406.00	406.00	405.33
T_crit95%	1.9600	1.9600	1.9600	1.9600
significant difference	TRUE	TRUE	TRUE	TRUE
b) Rain_9KM_SA_FLTopo				
Date	16-Jan-12	17-Jan-12	18-Jan-12	Average
T_test	5.7600	6.5700	8.5400	6.9567
df	404.00	406.00	406.00	405.33
T_crit95%	1.9600	1.9600	1.9600	1.9600
significant difference	TRUE	TRUE	TRUE	TRUE
c) Rain_9KM_Limp_Topo				
Date	16-Jan-12	17-Jan-12	18-Jan-12	Average
T_test	-0.7800	-1.7300	2.1800	-0.1100
df	72.00	70.00	74.00	72.00
T_crit95%	1.9935	1.9940	1.9920	1.9932
significant difference	FALSE	FALSE	TRUE	FALSE
d) Rain_9KM_Limp_FLTopo				
Date	16-Jan-12	17-Jan-12	18-Jan-12	Average
T_test	0.9300	0.3100	5.3700	2.2033
df	72.00	70.00	74.00	72.00
T_crit95%	1.9935	1.9940	1.9920	1.9932
significant difference	FALSE	FALSE	TRUE	TRUE

b) Maximum temperature

In Figure 4.21, maximum temperature statistics for simulation with and without topography over the country and Limpopo region is depicted. Simulations with topography show high negative bias (top) over the country than over Limpopo region. The RMSE values (middle) were also slightly higher over the country than over Limpopo region. The CORR values (bottom) were likewise also very high over the country, and

slightly lower over Limpopo region. This result also shows that that the scores deteriorate with times and that the WRF model is capable of simulating temperature over the country.

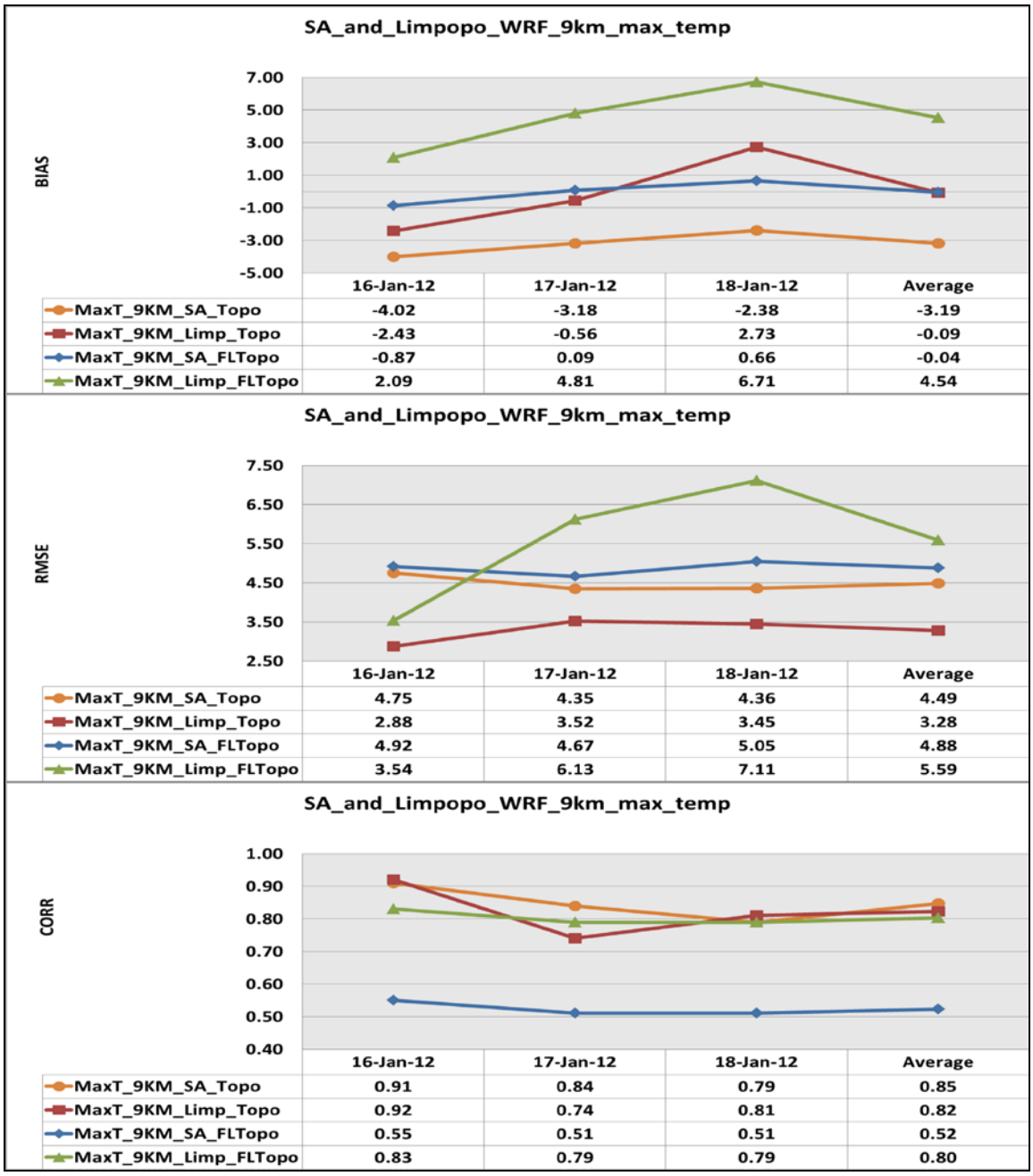

Figure 4.21: WRF 9 km topography versus flat topography maximum temperatures (degree Celsius) statistics over SA and Limpopo region for the period 16-18 January 2012

When the model topography was removed, bias values (top) were reduced over the country. However, over Limpopo region, there was an increase in bias, with a sign

change from a low negative to very high positive values. The RMSE values (middle) were also increased over the country and also Limpopo region. These RMSE values were lower over the country than over Limpopo region. The CORR values (bottom) were reduced over the country and Limpopo region. This result indicates that the WRF model did not reproduce observed maximum temperatures when topography is removed from the model during simulations (Figure 4.21).

The results show that simulation with topography over Limpopo region and simulation without topography over the country achieved bias within +/- 0.5^{o}C used by Tesche and Tremback (2002) for the MM5 model benchmark. However, for all simulations the RMSE values were larger than 2^{o}C benchmark. Form this analysis, it can be deduced simulation with topography was necessary, although the model did not capture observed temperatures very well.

c) Minimum temperature

Figure 4.22 shows minimum temperature statistics over the country and Limpopo region. Simulation with topography shows that bias values (top) were reasonably low and positive over the entire simulation period over the country and Limpopo region. Over Limpopo region, bias values were lower than over the entire country. It is also shown that over Limpopo region, the RMSE values (middle) were also lower than over the country, with RMSE values over Limpopo region almost half of the RMSE values over the entire country. The CORR values (bottom) were also positive and relatively high over the country and over Limpopo region. The CORR values for minimum temperatures were lower than the CORR values for maximum temperatures. This result confirms that the WRF model was more capable of simulating minimum temperature than maximum temperatures.

When the model topography was removed, bias values (top) increased at least four times over the country and also remained positive. However over Limpopo region, bias values increased at least more than seven times. The RMSE values (middle) increased at least three times over the country and almost eight times over Limpopo region. The CORR values (bottom) were reduced almost three times over the country, whereas over Limpopo region, these CORR values were reduced by more than half. This result

indicates the importance of topography, an indication that with topography, the WRF model is more capable of simulating minimum temperatures over the country.

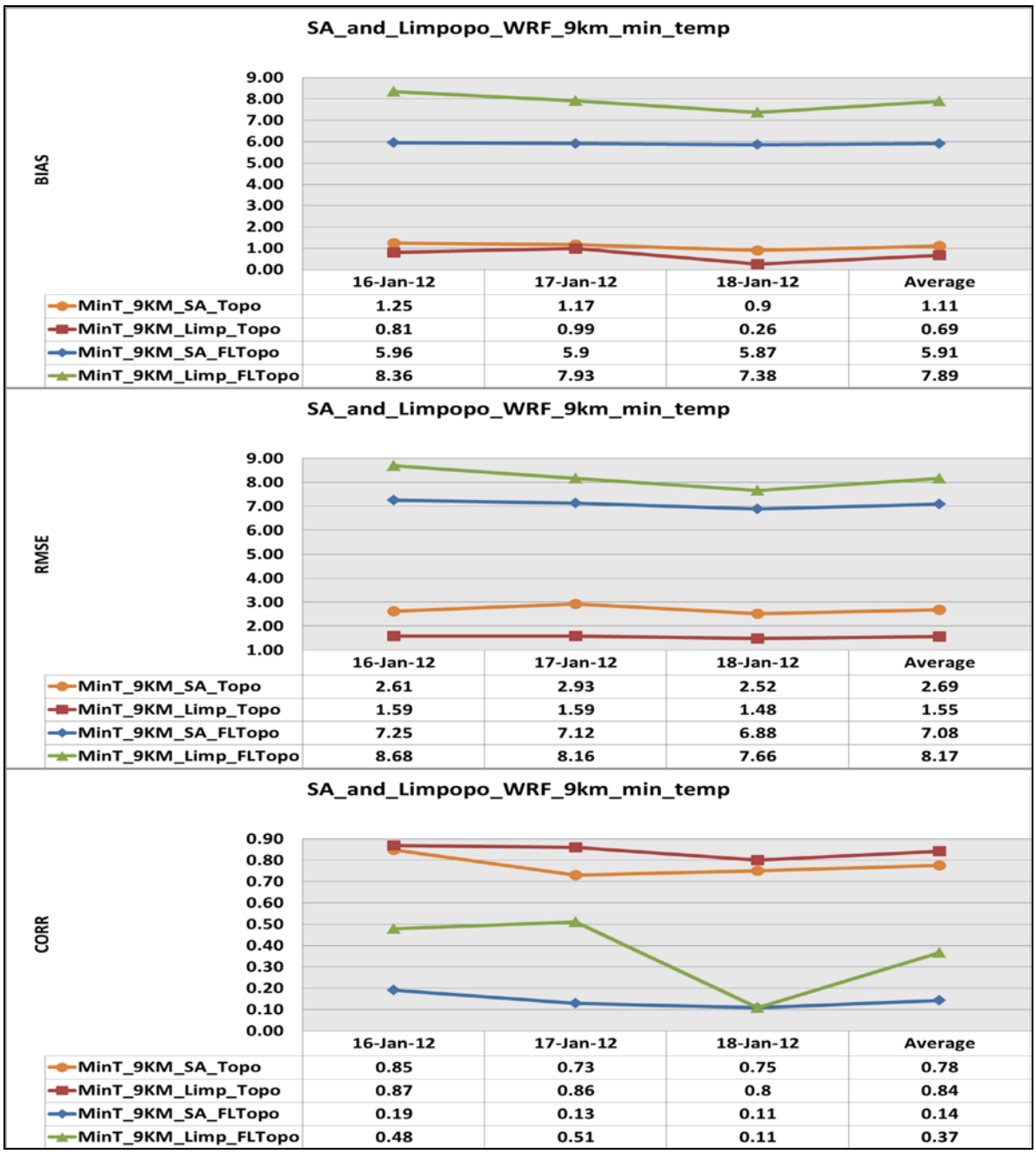

Figure 4.22: WRF 9 km topography versus flat topography minimum temperatures (degree Celsius) statistics over SA and Limpopo region for the period 16-18 January 2012

For both simulations with and without topography, bias values were positive and slightly larger than the +/- 0.5^{o}C benchmark applied in Tesche and Tremback (2002). The RMSE values were also larger than 2^{o}C, except over Limpopo region in simulation with

topography when compared to the MM5 model benchmark values. It can be deduced that although the results were not within the selected benchmark, the model is capable of simulating temperatures and that topography is important in temperature simulation.

c) Maximum wind speed

Figure 4.23 shows wind speed statistics over the country and also Limpopo region for both simulations with and without topography. The model simulation with topography shows negative bias values (top) over the country. However, over Limpopo region, bias values were low and mostly negative, but a positive value on 16 January resulted in the average value lower than over the country. It is also shown that bias values shows that the scores deteriorate as prediction time progresses. The RMSE values (middle) were inconsistent and high over the country, and lower over Limpopo region. The CORR values were very low over the country and slightly higher over Limpopo region. These values also show inconsistency with prediction time step. This result indicates that although the WRF model is capable of simulating wind speed, the scores deteriorate as simulations time progresses.

When the model topography over the country was removed, bias (top) changed sign from negative to positive values and were lower over the country. However, bias values were slightly improved over Limpopo region although they were negative, and higher than over the country. The RMSE values (middle) were also reduced over the country. However, the RMSE values were reduced by almost half over Limpopo region. The CORR values (bottom) were reduced over the country, whereas over Limpopo region, the CORR values were increased. Therefore simulation without topography resulted in inconsistent results and therefore this simulation shows that topography is important to yield realistic simulation of wind speed.

From this results, bias values were on average negative and slightly larger than the +/- 0.5 m/s and the RMSE values were at times close to 2 m/s benchmark values used by Tesche and Tremback (2002) for the MM5 model for both simulations with and without topography. As a concluding remark, topography plays an important role in for realistic wind speed simulation.

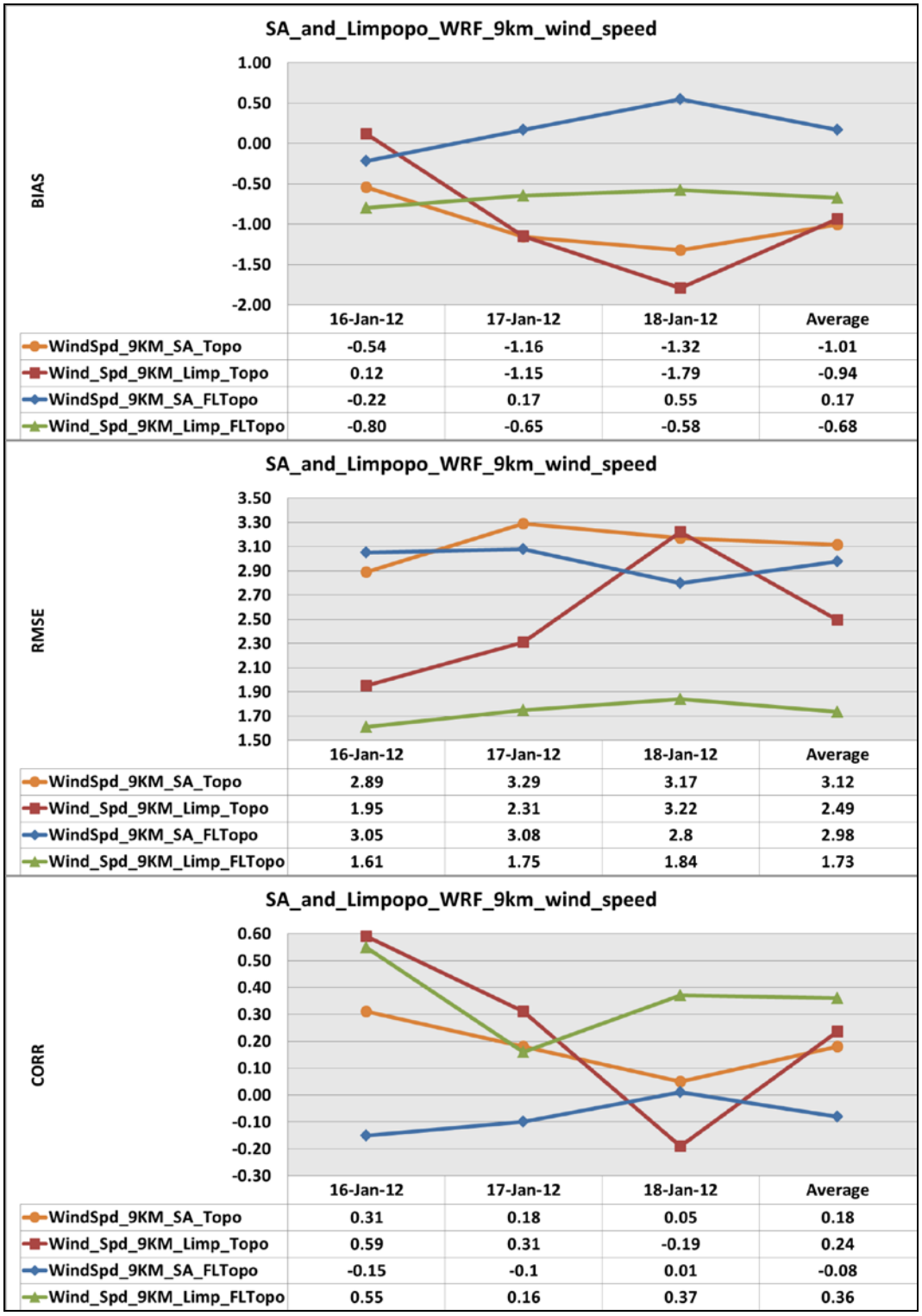

	16-Jan-12	17-Jan-12	18-Jan-12	Average
WindSpd_9KM_SA_Topo	-0.54	-1.16	-1.32	-1.01
Wind_Spd_9KM_Limp_Topo	0.12	-1.15	-1.79	-0.94
WindSpd_9KM_SA_FLTopo	-0.22	0.17	0.55	0.17
Wind_Spd_9KM_Limp_FLTopo	-0.80	-0.65	-0.58	-0.68

	16-Jan-12	17-Jan-12	18-Jan-12	Average
WindSpd_9KM_SA_Topo	2.89	3.29	3.17	3.12
Wind_Spd_9KM_Limp_Topo	1.95	2.31	3.22	2.49
WindSpd_9KM_SA_FLTopo	3.05	3.08	2.8	2.98
Wind_Spd_9KM_Limp_FLTopo	1.61	1.75	1.84	1.73

	16-Jan-12	17-Jan-12	18-Jan-12	Average
WindSpd_9KM_SA_Topo	0.31	0.18	0.05	0.18
Wind_Spd_9KM_Limp_Topo	0.59	0.31	-0.19	0.24
WindSpd_9KM_SA_FLTopo	-0.15	-0.1	0.01	-0.08
Wind_Spd_9KM_Limp_FLTopo	0.55	0.16	0.37	0.36

Figure 4.23: WRF 9 km topography versus flat topography wind speed (ms^{-1}) statistics over SA and Limpopo region for the period 16-18 January 2012

d) Maximum relative humidity

Figure 4.24 shows relative humidity statistics over the country and Limpopo region for both simulations with and without topography. These simulations show low negative bias values (top) over the entire country and also for the entire simulation period of simulation.

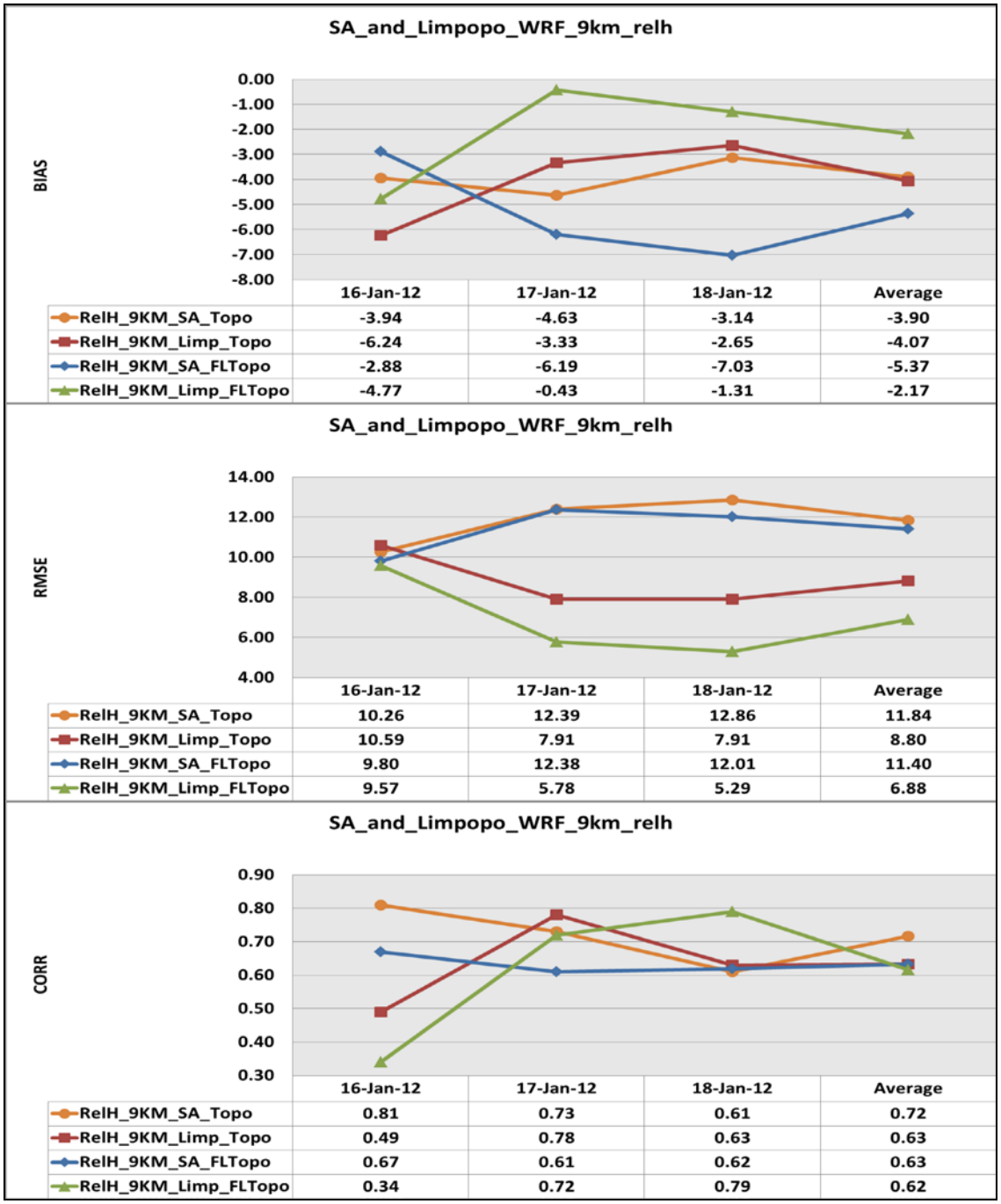

Figure 4.24: WRF 9 km topography versus flat topography relative humidity (%) statistics over SA and Limpopo region for the period 16-18 January 2012

However, over Limpopo region, bias values were twice higher than over the country although these values improved with time. The RMSE values (middle) show opposite behaviour over the country and Limpopo region. These values increased with time over the country and a decrease with time over Limpopo region for the entire simulation period. The CORR values (bottom) were positive and initially high over the country and low over Limpopo region. These values were almost similar towards the end of simulation time period, whereby values over Limpopo region were lower than over the country. Similarly, these scores indicate that the WRF model is capable of simulating relative humidity when topography is included in the model.

When the model topography was removed, bias (top) remained negative and increased over the country. However over Limpopo region, the values improved with time and were reduced by almost half. The RMSE values (middle) were slightly increased over the country and reduced over Limpopo region. The CORR values (bottom) were positive and also reduced over the country and Limpopo region. From these simulations, it can be deduced that the model simulation with topography yield acceptable and realistic results than in simulation without topography.

4.2.4 Statistical analysis: simulation with and without topography (heat wave 15-18 January 2012)

In this section the WRF model output for maximum and minimum temperatures, wind speed as well as relative humidity over Cape region is discussed. The statistical values are compared for both the model simulations at 9 km with and without topography. For the above-mentioned variables; statistics include bias, root mean square error (RMSE), and Pearson correlation coefficient (CORR).

a) Maximum temperature

Figure 4.25 shows the WRF model simulated maximum temperatures with statistics over the Cape region. In stations along the west coast, the model simulation captured maximum temperatures distribution very well. However, for stations over the interior of the Cape region, the WRF model simulation with topography under-predicted maximum

temperature (Figure 4.25a). The WRF model simulation without topography simulated higher temperatures over the entire region. Very few stations show good agreement between the model simulation and observations (Figure 4.25c).

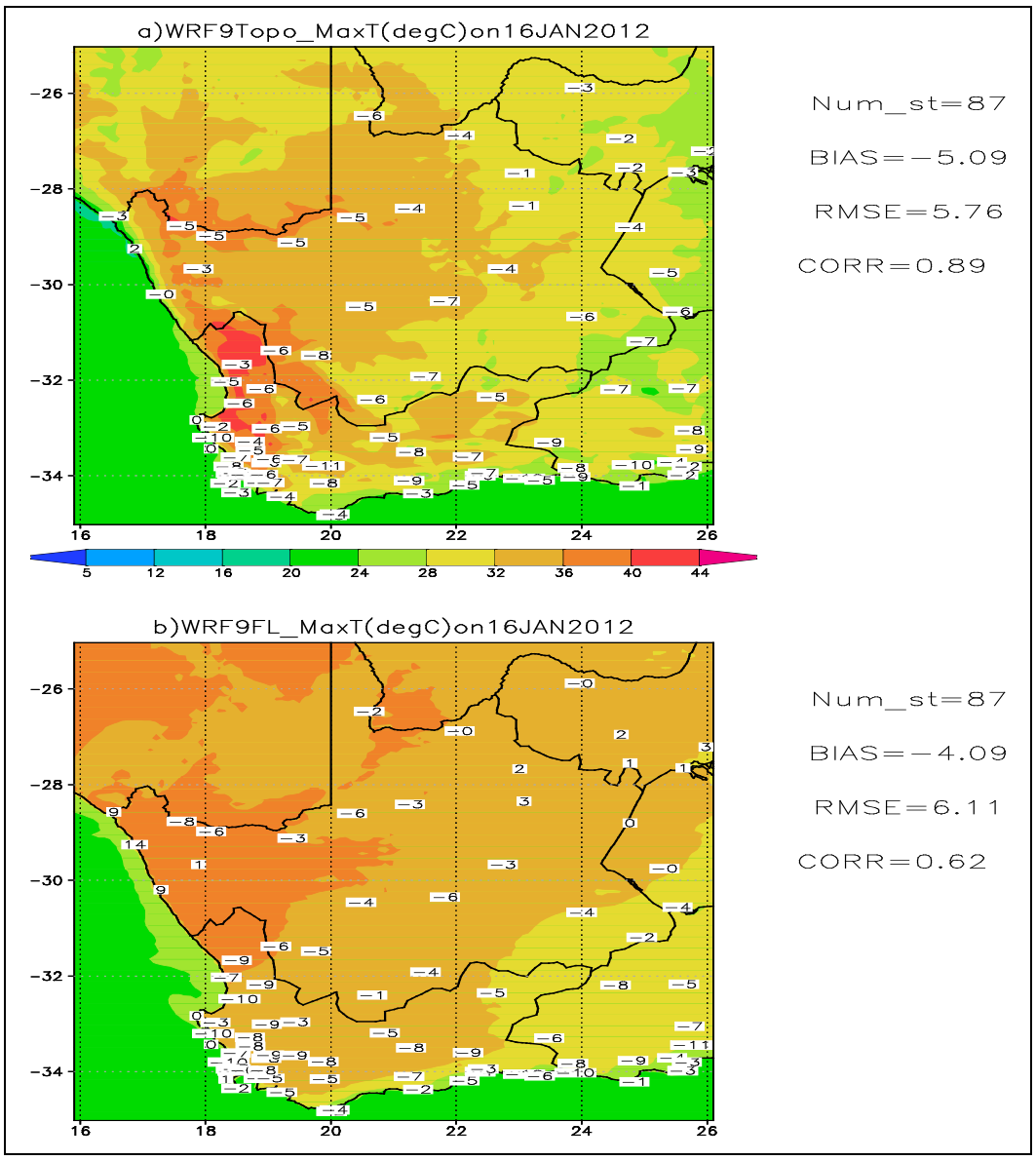

Figure 4.25: WRF 9 km topography versus flat topography simulated maximum temperatures (degree Celsius) with statistics over Cape region on 16 January 2012. Bias values at each observation station are indicated as numbers.

The maximum temperature statistics over the country and Cape region is depicted in Figure 4.25 and Figure 4.27. Simulation shows large negative bias values (top) over the country and over the Cape region, this was consistent, reliable and shows improvement

with time. The RMSE values (middle) were also high over the country, but lower than over Cape region. The CORR values (bottom) were positive and higher over the country and Cape region respectively. The high CORR values were an indication that the WRF model simulations have a good agreement with observations. This result gives an indication that WRF model is capable of simulating maximum temperatures over the country as it has simulated maximum temperature over the Cape region accurately, reliably and consistently.

When the model topography was removed, bias values (top) were reduced over the country and improved, with sign change from negative to positive. However, over Cape region, bias values were also slightly improved, but remained negative. There was an increase in RMSE values (middle) over the country and a decrease over Cape region. The RMSE values in simulation without topography over Cape region were slightly better than for simulations with topography. The CORR values (bottom) were also consistently reduced over the country as well as over the Cape region. The WRF model simulation of maximum temperature without topography over Cape region shows improved bias, but both RMSE and CORR were negatively affected. This result indicates that simulation with topography yield accurate and reliable results than simulation without topography.

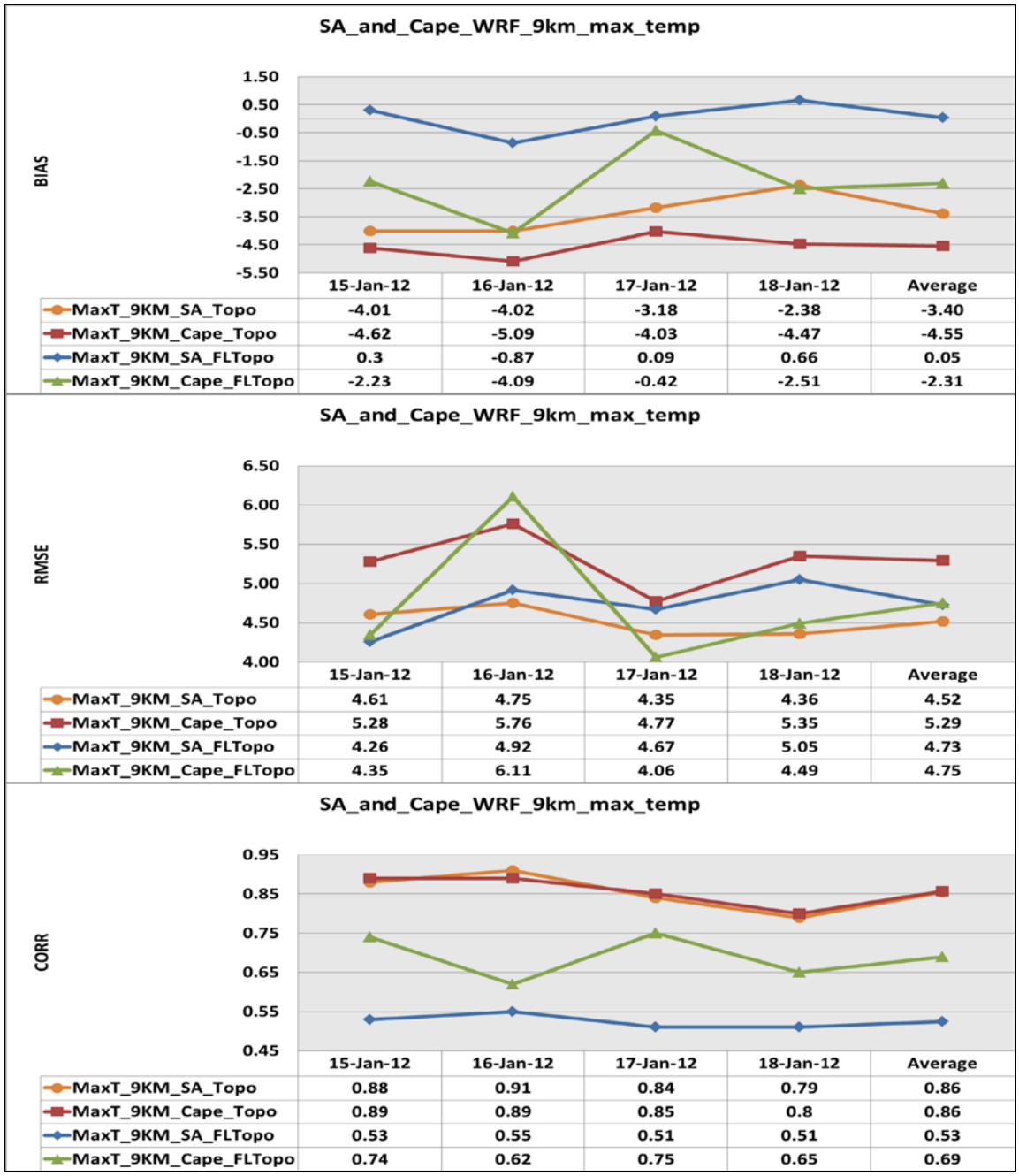

Figure 4.26: WRF 9 km topography versus flat topography maximum temperatures statistics over Cape region for the period 15-18 January 2012

From these simulations, the results indicates that simulation without topography over the country has bias within +/- 0.5^{o}C as applied by Tesche and Tremback (2002) for the MM5 model benchmark. The rest of the simulations have bias larger than +/- 0.5^{o}C. Likewise the RMSE values were also larger than 2^{o}C benchmark value for all the simulations. This result indicates that the topography over Cape region influenced the intensity of the heat wave event.

Table 4.6: Station observed versus the WRF model simulated high maximum temperatures (degree Celsius) over the Cape region of SA during heat wave for the period 15-18 January 2012

Maximum temperatures (> 38 degree celsius) 9 km topography versus flat topography														
		on 15 January 2012				on 16 January 2012			on 17 January 2012			on 18 January 2012		
no	Station name	stid	Obs	wrf_topo	wrf_fltopo	Obs	wrf_topo	wrf_fltopo	Obs	wrf_topo	wrf_fltopo	Obs	wrf_topo	wrf_fltopo
1	Calvinia WO(lat:-31.48; lon: 19.76)	68618	38.60	31.00	35.81	40.10	32.27	35.22	40.80	36.05	35.45	40.20	34.07	35.71
2	Langgewens(lat:-33.28; lon:18.71)	68716	39.50	35.26	33.12	42.90	38.64	34.87	40.10	37.81	35.28	39.00	35.21	35.01
3	Malmesbury(lat:-33.47; lon: 18.72)	68715	40.20	34.97	32.72	43.10	37.86	34.61	41.70	36.51	35.07	40.10	35.15	34.76
4	Paarl (lat:-33.72; lon: 18.97)	68713	38.80	33.18	32.14	42.30	36.46	33.97	40.60	35.58	34.92	40.50	34.76	34.34
5	Porterville (lat:-33.01; lon:18.98)	68717	40.00	35.71	33.94	43.60	37.90	35.00	40.70	37.12	35.43	40.50	34.03	35.34
6	Redelindshuys (lat: -32.48; lon: 18.54)	68710	43.70	36.63	34.63	46.00	40.40	35.68	41.10	33.19	35.65	39.30	29.00	35.61
7	Vanwyksvlei(lat:-30.35; lon:21.82)	68524	41.00	33.95	37.02	40.30	33.37	34.74	39.00	34.34	34.04	n/a	n/a	n/a
8	Vioolsdrif (lat:-28.70; lon:17.60)	68411	45.50	38.60	38.90	45.00	40.35	37.23	40.20	36.62	36.09	39.60	35.35	35.83
9	Vredendal (lat:-31.67; lon: 18.5)	68614	43.40	38.54	25.67	45.30	41.99	36.38	43.10	32.24	35.48	39.50	30.83	35.88
10	Wellington (lat:-33.65; lon: 19.01)	68810	39.30	33.40	32.29	43.30	37.10	34.05	42.00	36.77	34.91	40.80	35.49	34.40
11	Worcester AWS(lat:-33.66; lon:19.42)	68821	n/a	n/a	n/a	42.40	35.54	33.82	38.80	33.64	34.12	40.90	36.54	34.14
		Average	41.00	35.12	33.62	43.12	37.44	35.05	40.74	35.44	35.13	40.04	34.04	35.10
		BIAS		-5.88	-7.38		-5.67	-8.07		-5.29	-5.61		-6.00	-4.94

Table 4.6 show the number of stations that registered very high temperatures over the Cape regions. The station observed maximum temperatures are also much higher than the average daily maximum temperatures as tabulated in Schulze (1997) climate record for January. The table also show the model simulated maximum temperature at 9 km with and without topography. The results show that although the model simulations with topography were lower than observations by at least 4^{o}C, the removal of topography reduced bias.

Table 4.7: Students t-test for maximum temperatures at 9 km grid resolution over SA and Cape region for the period 15-18 January 2012 for both simulation with topography (a and c), and also for simulations without topography (b and d). A 95% confidence level was applied, and "TRUE" indicates that there is significant difference between the mean of observation and the mean for the WRF simulation, whereas "FALSE" indicate that there was no significant difference between the mean of observation and the mean for the WRF simulation.

	a) MaxT_9KM_SA_Topo				
Date	**15-Jan-12**	**16-Jan-12**	**17-Jan-12**	**18-Jan-12**	**Average**
T_test	**-9.0956**	**-7.6933**	**-6.7401**	**-4.8431**	**-7.0930**
df	**400.00**	**404.00**	**406.00**	**406.00**	**404.00**
T_crit95%	**1.9659**	**1.9659**	**1.9658**	**1.9658**	**1.9659**
significant difference	**TRUE**	**TRUE**	**TRUE**	**TRUE**	**TRUE**
	b) MaxT_9KM_SA_FLTopo				
Date	**15-Jan-12**	**16-Jan-12**	**17-Jan-12**	**18-Jan-12**	**Average**
T_test	**0.7180**	**-1.8330**	**0.2198**	**1.4814**	**0.1465**
df	**400.00**	**404.00**	**406.00**	**406.00**	**404.00**
T_crit95%	**1.9659**	**1.9659**	**1.9658**	**1.9658**	**1.9659**
significant difference	**FALSE**	**FALSE**	**FALSE**	**FALSE**	**FALSE**
	c) MaxT_9KM_Cape_Topo				
Date	**15-Jan-12**	**16-Jan-12**	**17-Jan-12**	**18-Jan-12**	**Average**
T_test	**-0.7092**	**-6.3895**	**-5.8827**	**-6.5168**	**-4.8745**
df	**170.00**	**170.00**	**172.00**	**172.00**	**171.00**
T_crit95%	**1.9740**	**1.9740**	**1.9739**	**1.9739**	**1.9739**
significant difference	**FALSE**	**TRUE**	**TRUE**	**TRUE**	**TRUE**
	d) MaxT_9KM_Cape_FLTopo				
Date	**15-Jan-12**	**16-Jan-12**	**17-Jan-12**	**18-Jan-12**	**Average**
T_test	**-2.8207**	**-5.4122**	**-3.6305**	**-3.8472**	**-3.9276**
df	**170.00**	**170.00**	**172.00**	**172.00**	**171.00**
T_crit95%	**1.9740**	**1.9740**	**1.9739**	**1.9739**	**1.9739**
significant difference	**TRUE**	**TRUE**	**TRUE**	**TRUE**	**TRUE**

From table 4.7, statistical significance testing indicates that there was a significant difference between WRF simulation with topography over the country (panel-a) and observation and also over the Cape region (panel-c). It resulted in the rejection of the null hypothesis. This result also applies to significance test over Cape region in simulation without topography. However, the test indicates that there was no significant difference

between WRF simulation without topography over the country (panel-c) and observations. As a result, the null hypothesis was accepted.

b) Minimum temperature

Figure 4.27 shows minimum temperature statistics over the country and the Cape region. Simulation with topography shows low and positive bias values (top) over the country. However, over the Cape region bias values were positive and higher than over the entire country. The RMSE values (middle) values were high over the country and were almost double over the Cape region. The CORR values (bottom) were positive and higher over the country than over Cape region. These CORR values indicate good agreement between the WRF model simulations and observed minimum temperatures over the country and Cape region. This result also indicates that the WRF model is consistent and reliable and captured the minimum temperature distribution very well as compared to maximum temperatures.

When the model topography was removed, bias values (top) remained positive and high for all days over the country, but lower over the Cape region. The RMSE values (middle) were increased and double over the country, and also lower over the Cape region. The CORR values (bottom) were reduced at least three times over the country. Likewise, over the Cape region, the CORR values were slightly lower than over the entire county. This simulation shows that the scores deteriorated in simulation without topography, an indication that without topography, the WRF model simulation loses consistency and reliability.

For both simulations, bias values were positive and slightly larger than the +/- 0.5^{o}C and the RMSE values were also larger than 2^{o}C, as compared to the MM5 model benchmark applied in Tesche and Tremback (2002). It can be deduced that for all the scores displayed, the WRF model simulations were consistent and reliable and therefore the WRF model is capable of simulating minimum temperatures over the country.

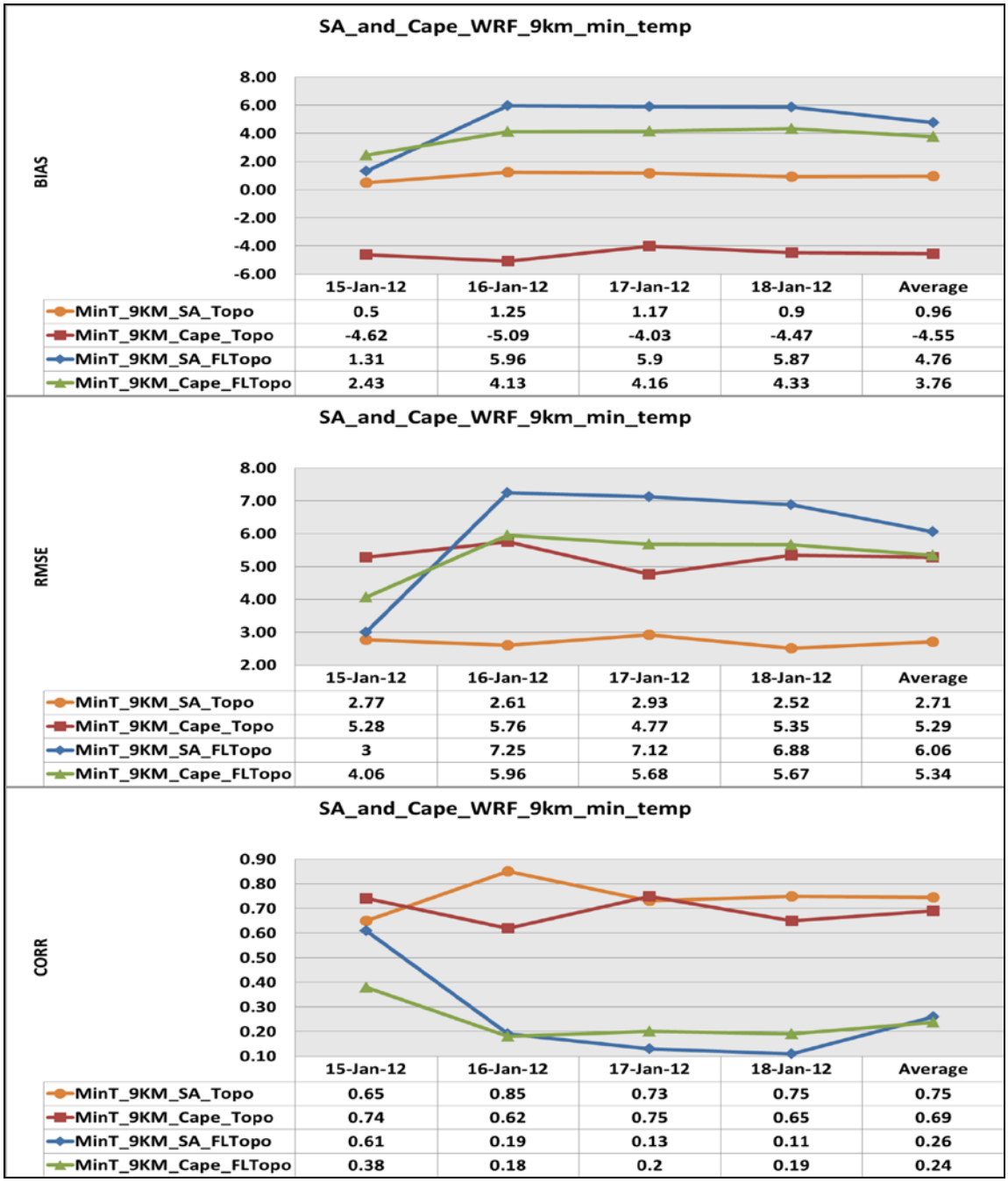

Figure 4.27: WRF 9 km topography versus flat topography minimum temperatures (degree Celsius) statistics over Cape region for the period 15-18 January 2012

c) Maximum wind speed

The WRF model statistics over the country and Cape region for simulations with and without topography is depicted in Figure 4.28. Bias values (top) were negative over the country and also the Cape region. Bias values shows opposite behaviour on 16 January, with bias over the country much less than over the Cape region, resulting in high negative bias over Cape region. The RMSE values (middle) were also high for all the days over

the entire country, but lower than over the Cape region. The CORR values (bottom) were positive and weak over the country than over the Cape region. This result gives an indication that the WRF model reproduces the observed wind speed pattern over the country and Cape region.

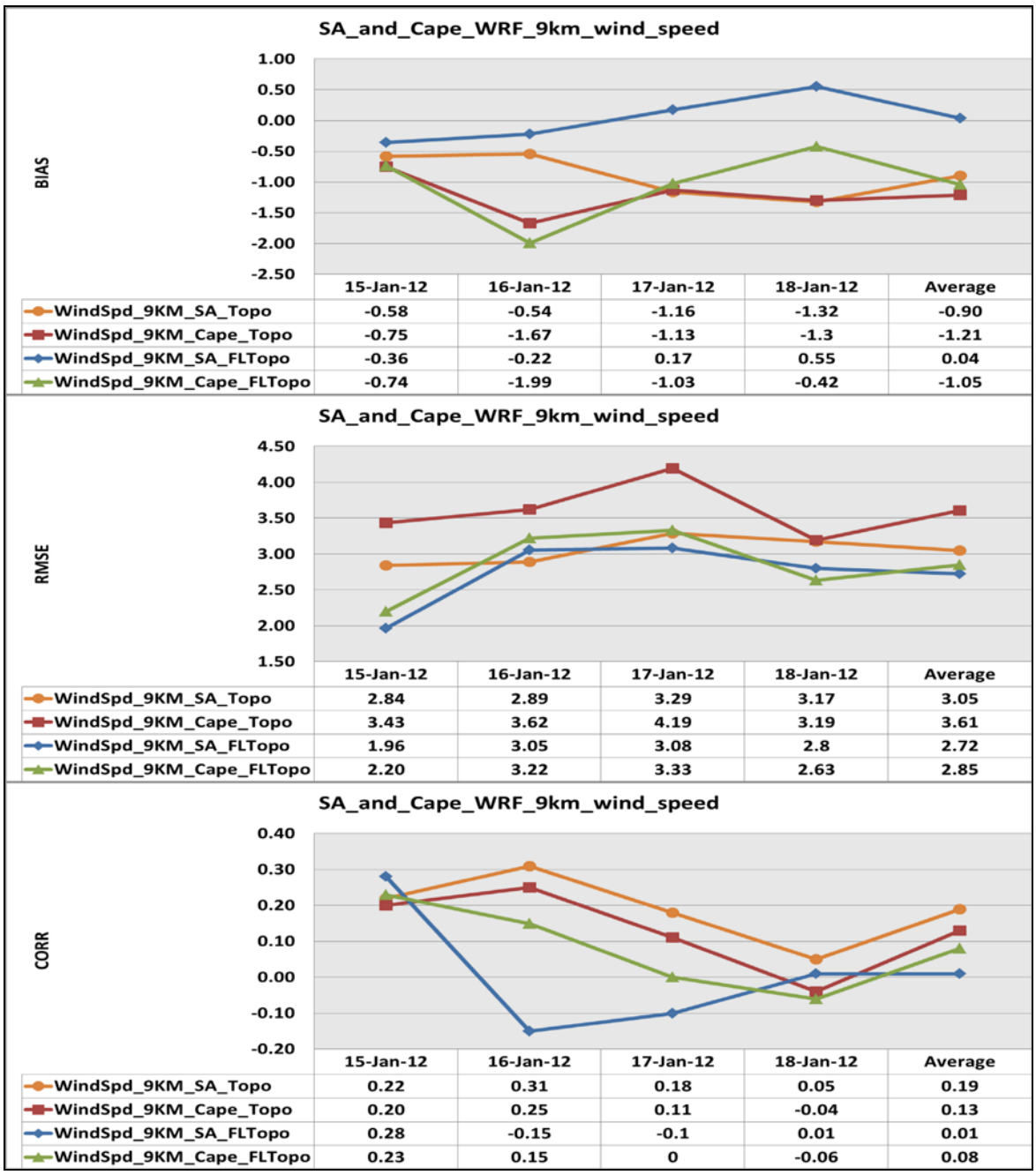

	15-Jan-12	16-Jan-12	17-Jan-12	18-Jan-12	Average
WindSpd_9KM_SA_Topo	-0.58	-0.54	-1.16	-1.32	-0.90
WindSpd_9KM_Cape_Topo	-0.75	-1.67	-1.13	-1.3	-1.21
WindSpd_9KM_SA_FLTopo	-0.36	-0.22	0.17	0.55	0.04
WindSpd_9KM_Cape_FLTopo	-0.74	-1.99	-1.03	-0.42	-1.05

	15-Jan-12	16-Jan-12	17-Jan-12	18-Jan-12	Average
WindSpd_9KM_SA_Topo	2.84	2.89	3.29	3.17	3.05
WindSpd_9KM_Cape_Topo	3.43	3.62	4.19	3.19	3.61
WindSpd_9KM_SA_FLTopo	1.96	3.05	3.08	2.8	2.72
WindSpd_9KM_Cape_FLTopo	2.20	3.22	3.33	2.63	2.85

	15-Jan-12	16-Jan-12	17-Jan-12	18-Jan-12	Average
WindSpd_9KM_SA_Topo	0.22	0.31	0.18	0.05	0.19
WindSpd_9KM_Cape_Topo	0.20	0.25	0.11	-0.04	0.13
WindSpd_9KM_SA_FLTopo	0.28	-0.15	-0.1	0.01	0.01
WindSpd_9KM_Cape_FLTopo	0.23	0.15	0	-0.06	0.08

Figure 4.28: WRF 9 km topography versus flat topography wind speed (ms^{-1}) statistics over Cape region for the period 15-18 January 2012

When the model topography was removed, bias values (top) were reduced and there was also a change of sign from negative to positive over the country for the last two days. However, over Cape region, bias remained negative for all the days, but higher than over the country. The RMSE values (middle) were also high over the country and also over Cape region. However, these values were also reduced as compared to WRF simulation with topography. The CORR values (bottom) were positive and were reduced to values close to zero over the country and also the Cape region. Both bias and RMSE scores indicates that wind speed was better simulated when topography is removed although the CORR values prove that topography was essential during the model simulation.

Bias values were on average negative and slightly larger than the +/- 0.5 m/s and the RMSE values were at times close to 2 m/s used by Tesche and Tremback (2002) for the MM5 model benchmark for both simulations with and without topography. From this simulation, it can also be deduced that simulation with topography yield realistic results although some of the scores were improved in simulation without topography.

d) Maximum relative humidity

Figure 4.29 shows relative humidity statistics over the country and Cape region. Bias values (top) were negative over the country and almost doubled over the Cape region. The RMSE values (middle) were also very high, and values over the Cape region were higher than over the entire country. The CORR values (bottom) were positive and high over the country and slightly lower over the Cape region. This result indicates that the model simulations with topography shows good were accuracy and reliability as compared to WRF simulation without topography and also indicates that WRF simulation with topography is capable of reproducing relative humidity over the country and Cape region.

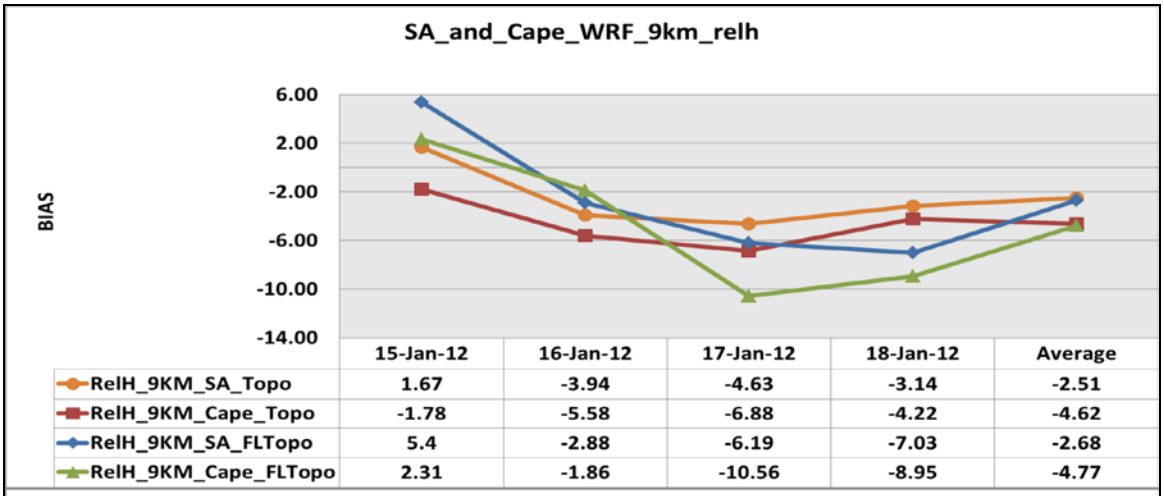

	15-Jan-12	16-Jan-12	17-Jan-12	18-Jan-12	Average
RelH_9KM_SA_Topo	1.67	-3.94	-4.63	-3.14	-2.51
RelH_9KM_Cape_Topo	-1.78	-5.58	-6.88	-4.22	-4.62
RelH_9KM_SA_FLTopo	5.4	-2.88	-6.19	-7.03	-2.68
RelH_9KM_Cape_FLTopo	2.31	-1.86	-10.56	-8.95	-4.77

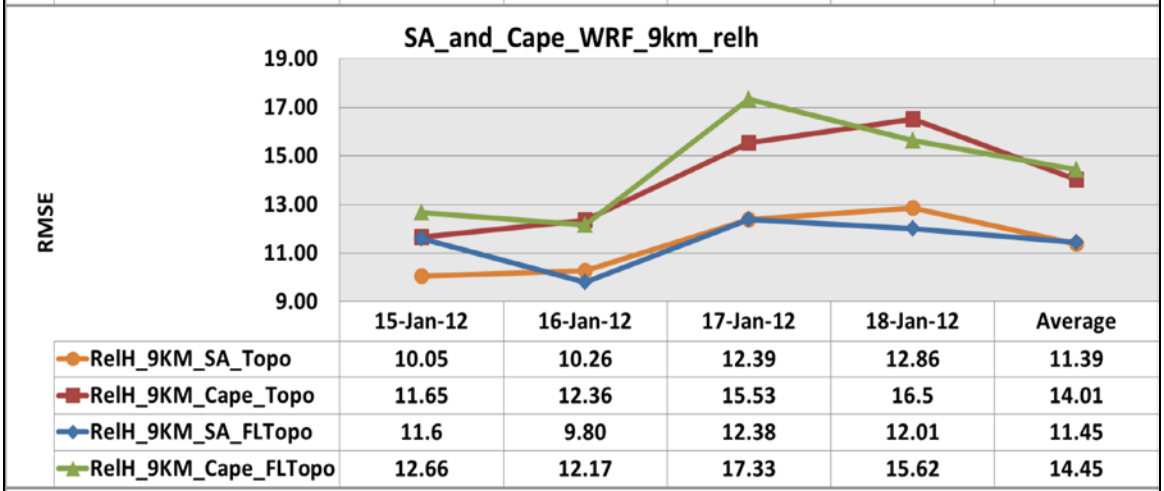

	15-Jan-12	16-Jan-12	17-Jan-12	18-Jan-12	Average
RelH_9KM_SA_Topo	10.05	10.26	12.39	12.86	11.39
RelH_9KM_Cape_Topo	11.65	12.36	15.53	16.5	14.01
RelH_9KM_SA_FLTopo	11.6	9.80	12.38	12.01	11.45
RelH_9KM_Cape_FLTopo	12.66	12.17	17.33	15.62	14.45

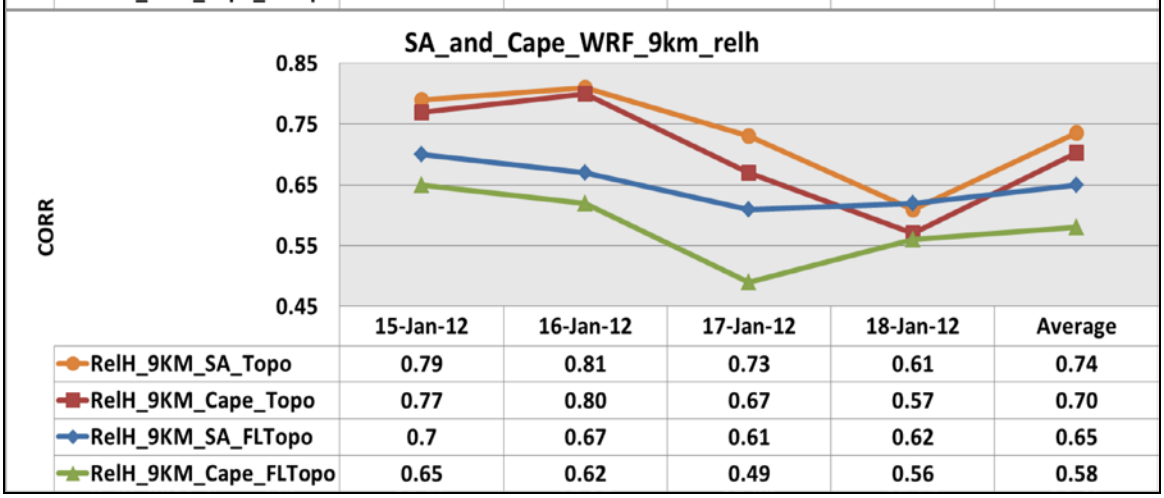

	15-Jan-12	16-Jan-12	17-Jan-12	18-Jan-12	Average
RelH_9KM_SA_Topo	0.79	0.81	0.73	0.61	0.74
RelH_9KM_Cape_Topo	0.77	0.80	0.67	0.57	0.70
RelH_9KM_SA_FLTopo	0.7	0.67	0.61	0.62	0.65
RelH_9KM_Cape_FLTopo	0.65	0.62	0.49	0.56	0.58

Figure 4.29: WRF 9 km topography versus flat topography relative humidity (%) statistics over Cape region for the period 15-18 January 2012

When the model topography was removed, bias (top) increased slightly over the country and the Cape region, with values over the Cape region higher than over the country. The RMSE values (middle) were also increased over the country, but lower than values over

the Cape region. The CORR values (bottom) were reduced over the country and also over the Cape region. All the scores show that the WRF model started losing accuracy and reliability as time progresses. The results also gives an indication that there was not much difference in relative humidity simulation with and without topography although the scores where reduced in simulation without topography. However, it could be deduced that simulation with topography was realistic as compared to flat topography runs.

4.3 Discussion and summary of results

The WRF model simulations have shown that topography of SA influenced both heat waves and precipitation events. For all the case studies, it was found that simulation with topography shows either an over-prediction or under-prediction of the variables analysed. When the model topography is removed, results becomes unreliable in most instance, and in few cases, the scores were improved.

Previous research studies including Persson (2003) and Libonati *et al*., (2008) has shown that NWP models are subjected to systematic error. The model systematic bias have been found to persists when models forecasts near-surface variables like temperatures (Cheng and Steenburgh, 2007) and wind speed (Mass *et al*., 2002; Jimenez and Dudhia, 2011). The model errors were also found to be due to either inaccuracies in initialization data (Cheng and Steenburgh, 2007; Schulze, 2007), errors within the model formulations including physics and dynamics (Galanis and Anadranistakis, 2002; Cheng and Steenburgh, 2007; Libonati *et al*., 2008; Blamey and Reason, 2009).

a) Heat wave events over Limpopo and Cape regions of South Africa

A deviation in the mean atmospheric flow pattern has been found to result in a variety of weather patterns including heat wave conditions. These extreme weather events have been found to be either localized or extended over large areas (Harrison, 1988; Potgieter, 2006; Landman, (2012). According to Cassou *et al*., (2005) heat wave events are caused by large scale synoptic pressure system, with an upper air high pressure system covering most parts of the country and suppressing convective instabilities resulting in light winds with dry and clear sky and therefore warming. It enhances subsidence, solar heating and warm air advection. The WRF model simulations were able to reproduce such synoptic

scale events and were consistent with a study by Cassou *et al*., (2005) and also Barriopedro *et al*., (2011). According to Kruger and Shongwe (2004); and also Lyon (2009), the DJF season has experienced an upward trend of temperatures that result in an increase in heat wave frequency over the recent decades. From the current studies, the heat wave over Limpopo region occurred towards the end of spring season (October) and could be an indication of climate change (IPCC, 2007). However, the occurrence of the heat wave over Cape region occurred during January falls under DJF season and therefore agrees with the findings by Kruger and Shongwe (2004); and also Lyon (2009).

During the two heat wave events, the WRF model simulations have shown that the temperature of SA is influenced by topography and also latitudes as discussed in previous findings by authors including Giorgi (1990); Smith (2004) and Jimenez and Dudhia (2011). From the current studies it was also found that temperatures decreases as latitudes increases towards the poles, with higher temperatures towards the tropics, as has also been shown in Schulze (1997). The WRF model has simulated maximum temperatures higher than 38^{o}C for at least two successive days (see tables 4.1 and 4.4). These simulations agree with the study of heat wave by Robinson (2000). The WRF model simulated lower temperatures over higher topography areas and higher temperatures over lower altitudes areas, confirming a study by Schulze (1997) and also Libonati *et al*., (2008). Changes in altitudes were found to affect solar radiation and temperature distribution (Esau *et al*., 2012).

During October heat wave, the WRF model simulations show the north to south temperatures isotherms. Lower temperatures were simulated over the higher topography areas to the southern parts of the region and higher temperatures were simulated over the lower topography areas on the northern parts of the region. These simulations also show that higher temperatures migrated south from the tropical regions towards the northern parts of the country including Limpopo region (see Figure 4.4). When topography was removed, higher temperatures were reduced over the entire country. This result indicates that topography influenced maximum temperatures. It could also be said that the removal of topography has removed the influence of northerly wind from the tropics, resulting in subtropical winds from the south reducing very high temperatures into mild temperatures.

During the January heat wave over Cape region, higher temperatures were located over the west coast, to the west of higher topography areas along the escarpment, and confirm the findings of Van Schalkwyk (2011). When topography was removed, higher temperatures penetrated further east into the interior, where topography rises to altitude higher than 1500 m. This result indicates that topography influenced maximum temperatures. It could also be said that without topography, the influence of berg winds flow from inland towards the west coast was reduced, leaving subsidence to be the dominant factor in the heat wave occurrence.

However, for both heat wave events, the synoptic scale events were similar; there was a surface low pressure system with dry air advection behind the surface low pressure system and a high pressure system in upper atmosphere resulting in subsidence. Topography also played a role in the intensity of heat wave. Over Limpopo region, the removal of topography led to reduction of higher temperatures whereas over the Cape region it led to increased temperatures. This could be attributed to model topographic heights over Cape region, which is different from topography over Limpopo region.

These extreme weather case studies were also in agreement with Cretat *et al*., (2012) findings for the WRF model simulations on a regional scale, where they found a negative bias on average -3K especially over the coasts. These simulations have shown that the WRF model under-predicted maximum temperatures and over-predicted minimum temperatures. This could be attributed to a chosen PBL schemes that have been found to affect temperature and moisture profiles in lower troposphere. According to Cretat *et al*., (2012), the cumulus schemes exert strongest influence on vertical profiles of temperature by modifying the latent heat release. Caldwell *et al*., (2009) also found that temperature bias depends on RCM models used and that the WRF model data mirrors the observations, whereby along the coast, both minimum and maximum temperatures were warmer in the WRF model simulations. This was however attributed to a +2 K in SST bias near the coast inherited from the GCM data.

Table 4.1 and 4.6 show the number of stations that registered very high temperatures over the Limpopo and Cape regions respectively. The tables also show the model simulated maximum temperature at 9 km with and without topography. These results show that even though the model simulations with topography were lower than observations by at

least 4^{o}C, the removal of topography increased bias (for Limpopo region). Likewise table 4.2 and table 4.7 indicates the t-test statistics results for the maximum temperatures during the October 2011 and January 2012 heat waves respectively. During the October heat wave event, the null hypothesis was rejected for both simulations with and without topography. During the January heat wave event, the results were almost similar to the October results, except that the null hypothesis was accepted for the WRF 9 km simulation without topography over SA.

b) Heavy precipitation event that resulted in floods over Limpopo region of South Africa

The WRF model simulations have shown that rainfall over SA is influenced by topography. The higher topography over the eastern escarpment of SA forces moist air to rise as a result of topographic lifting and this resulted in enhanced rainfall (Tennant and Van Heerden, 1994; Bruyere, 1997; Schulze, 1997; Tyson and Preston-Whyte, 2000; Riphagen *et al*., 2001; Singleton and Reason, 2005; Potgieter, 2006; Blamey and Reason, 2009; Galewsky, 2009; Kruger *et al*., 2010). Most of the rainfall occurred on the windward side of the slopes.

High altitudes over the escarpment areas are associated with steep topographic gradients and have been found to result in storm development and increased thunderstorms activities (Bruyere, 1997; Schulze, 1997). The WRF model simulation shows an abundance of moisture at low levels, a lot of this moisture was generated from the tropics including Angola. Some of this moisture was from the both tropical Atlantic and Indian Ocean respectively. Due to cyclonic motion of a low pressure system over the Mozambique Channel and a high pressure system over the east coast of the country, moisture was advected towards the east coast of the country. This simulation confirms the findings of Hargraves and Jury (1997); Potgieter (2006); Singleton and Reason (2005); Blamey and Reason (2009) and also Boulard *et al*., (2012). According to a study by Riphagen *et al*., (2001), the presence of surface trough during convection results in an increase in moisture to the east of the trough. A low pressure system over the interior of the country resulted in strong uplift which enhanced rainfall over the eastern parts of the country.

The removal of topography results in the model simulating precipitation over almost the entire domain. It also resulted in the model simulation displacing rainfall maximum further west into the interior of the country whereas rainfall occurred over the eastern parts of the country. These WRF model simulations confirm the findings by Singleton and Reason (2005) which shows that the removal of topography has large effect on the large scale flow and the location of precipitation maximum. It displaces precipitation maximum further west of the domain.

The WRF model is a mesoscale model and due to its higher grid resolution can be adequately used for simulating convective activities. However, simulation have also shown that at the chosen grid resolution, the model over-estimate rainfall (Galanis *et al*., 2006; Reason *et al.,* 2006; Libonati *et al*., 2008; Mbedzi, 2010). The prediction of summer convective activities and rainfall is determined by the chosen cumulus parameterization scheme (Reason *et al.*, 2006; Gilliland and Rowe, 2009; Cretat *et al*., 2012; Landman, 2012; Ratna *et al*., 2013). For the current study, it was found that the GDE scheme (Grell and Devenyi, 2002) applied in the WRF model has been able to reproduce rainfall over SA during the study period. The GDE scheme effectively simulates the atmospheric instability, vertical motions and the vertical distribution of moisture in the atmosphere that produce rainfall (Ratna *et al*., 2013). From the January's heavy precipitation event, the WRF model triggered convection very early, leading to over-estimation of rainfall such that the simulated rainfall covered larger area than observations. However, the model applied scheme was able to represent the spatial distribution and the intensity of precipitation. This results also agree with the findings of Gilliland and Rowe (2009); Cretat and Pohl (2011) and also Cretat *et al*., (2011, 2012).

The present study found the correlation between WRF interpolated values and SAWS station data over Limpopo region very low as it varies between 0.22 (with topography) and 0.7 (without topography). However, a study by Cretat and Pohl (2011); Cretat *et al*., (2011) found the correlation between WRF grids and rain gauges over SA to vary between 0.7 and 0.8, but such results were achieved on a seasonal time scale. Likewise Boulard *et al*., (2012) found a rainfall spatial correlation between WRF and observed rainfall gauges between 0.38 and 0.86 during a study on inter-annual rainfall variability studies. Ratna *et al*., (2013) found a rainfall spatial correlation between WRF GDE scheme and SA observed rainfall gauges to be 0.87, for a simulation over DJF season for

a period of 20 years (from 1991 to 2011). Their correlation scores were higher than the scores achieved in the present study. It was found that when the PBL scheme interacts with cumulus parameterization scheme, they influence precipitation (Cretat *et al*., 2012).

Caldwell *et al*., (2009) found that RCM models over-predict precipitation in mountainous area. Extreme events were also found to be localised and strongly influenced by topography. Their studies also found that WRF was able to capture regional scale rainfall variability, although the model simulations over-predicts rainfall in regions of higher topography and under-predicts rainfall in rain shadow. The WRF model simulations during precipitation event over eastern parts of SA agree with such studies as the model simulations have positive bias. Caldwell *et al*., (2009) also mentioned that parameterization schemes used for sub-grid scales may perhaps not be needed when model grid resolution is less than 10 km. Model simulation bias or under-prediction may be attributed to poor representation of topography at low resolution grid spacing.

A study by Ratna *et al.,* (2013) has indicated that when the model simulated enhanced low level moisture convergence due to a highly unstable atmosphere, it result in widespread rainfall which result in positive bias. However; when moisture and vertical velocity are reduced due to a stable atmosphere, it result in negative rainfall bias. Ratna *et al.,* (2013) also found that the GDE scheme over-estimate convective rainfall and under-estimate stratiform rainfall. Therefore from the current result, WRF simulation show positive rainfall bias for all the applied rainfall categories, of which it may be deduced that positive bias was caused by enhanced moisture which led to wide spread rainfall over Limpopo region. The results from the t-test (table 4.5) indicate that WRF simulation with topography and also without topography over Limpopo regions shows no significant difference between the model simulation and observations. This resulted in the acceptance of the null hypothesis.

c) Testing for the nonhydrostatic approximation

From the three case studies investigated, it was important to review some mesoscale systems scaling analysis. The hydrostatic models make use of equation 1.2 (see chapter 1, section 1.1.2) and ignores the vertical motion dw/dt as insignificant. However, nonhydrostatic models include vertical acceleration term dw/dt (see equation 1.1) since

vertical motion is of significance during updrafts and thunderstorm formations (Holton, 2004; Markowski and Richardson, 2010). The application of scaling analysis of vertical velocity has shown that in general it has an order of $O(w) \approx 10ms^{-1}$ and cannot be ignored (Holton, 2004 and also Markowski and Richardson, 2010). From the simulations performed, especially during the precipitation event, both simulations with and without topography have achieved vertical velocity of an order of $O(w) \approx 10ms^{-1}$ and therefore dw/dt cannot be ignored in nonhydrostatic approximation. However, simulations without topography were unreliable and inconsistent.

d) Testing for the temperature advection equation

The application of temperature advection equation $\partial T / \partial T = -u\partial T / \partial x - v\partial T / \partial y$ as in equation 1.3 gives an indication of temperature gradients. According to Lengoasa (1988), the location of either the high and low pressure system determines wind speed and direction. Therefore wind movement also determine areas of very high and low temperatures.

During the October heat wave, there was an advection of hot air from the tropics (dominant winds were northerly) towards the northern parts of the country including Limpopo region. These winds were subjected to surface heating and turbulent mixing as they descend from higher topography areas towards Limpopo valley, resulting in very high temperatures along the Limpopo valley. However, when topography was removed, the winds (dominant winds were southerly) remained constant, and there was uniform surface heating and turbulent mixing resulting in mild temperatures over Limpopo valley.

Similarly, for the January heat wave case study, there was an advection of warm and dry air from the central interior (dominant winds were easterly) towards the west coast of the country. These winds were subjected to surface heating and turbulent mixing as they descend from higher topography areas towards the west coast (berg winds), resulting in high temperatures over the Cape region. When topography was removed, there was a weaker temperature advection, with easterlies still dominant. However, the winds were constant, with uniform surface heating and turbulent mixing. This also results in a region of uniform mild temperatures over the western interior of the country.

CHAPTER 5

HIGH GRID RESOLUTION WRF MODEL SIMULATION OF EXTREME WEATHER EVENTS

This chapter is aimed at evaluating the influence of different grid resolutions in the WRF model simulations of extreme weather events. This is considered the third objective of this study. The performance of the 3 km nested grid resolution WRF model simulations is compared to the performance of 9 km grid which has been discussed in the previous chapter. As in the previous chapter, rainfall, temperatures, maximum wind speed and maximum relative humidity are analysed. The areas of focus include Limpopo and Cape regions respectively. The case studies include (i) heat wave over the Limpopo region of SA from 22 to 26 October 2011 and (ii) heavy rainfall associated with tropical depression Dando from 16 to 18 January 2012 over the north-eastern parts of SA and (iii) the heat wave over the Cape region from 15 to 18 January 2012.

5.1 Heat wave episode 22-26 October 2011

a) Maximum temperature

The WRF model simulated maximum temperature at both 9 and 3 km grid resolution over Limpopo region is depicted in Figures 5.1 and 5.2. It is shown that increasing the model grid resolution to 3 km over Limpopo region has improved spatial distribution of the maximum temperatures simulations and also the verification statistics. The two figures indicate that there is an improved agreement between the WRF model simulations and observations as compared to simulation at 9 km grid resolution. For some stations there was no error at 9 km grid resolution and such an increase in resolution did not yield any improvements. The results in Figure 5.2 show that when the model grid resolution is increased to 3 km, bias values (top) remained negative, but consistently reduced for all the days, with lowest bias achieved on 25 October. It should be mentioned that on this day, the high temperatures were well simulated by the model (see also table 5.1). The RMSE values (middle) were similarly reduced as compared to 9 km grid resolution result. The CORR values (bottom) also shows improvement for all the days, except for 25 October when the scores remained similar to a 9 km simulation and lower than for all the days. From this analysis, there are very high CORR values on 23 October and very low values on 25 October which are very difficult to draw conclusions from. These results

also indicate that model results are improved as model grid resolution is increased. However, for both resolutions, bias values were negative and larger than the +/- 0.5^{o}C and likewise the RMSE values were also larger than 2^{o}C, as compared to the MM5 model benchmark applied in Tesche and Tremback (2002). This result indicates that although there was improvement in statistics, the model did not perform very well.

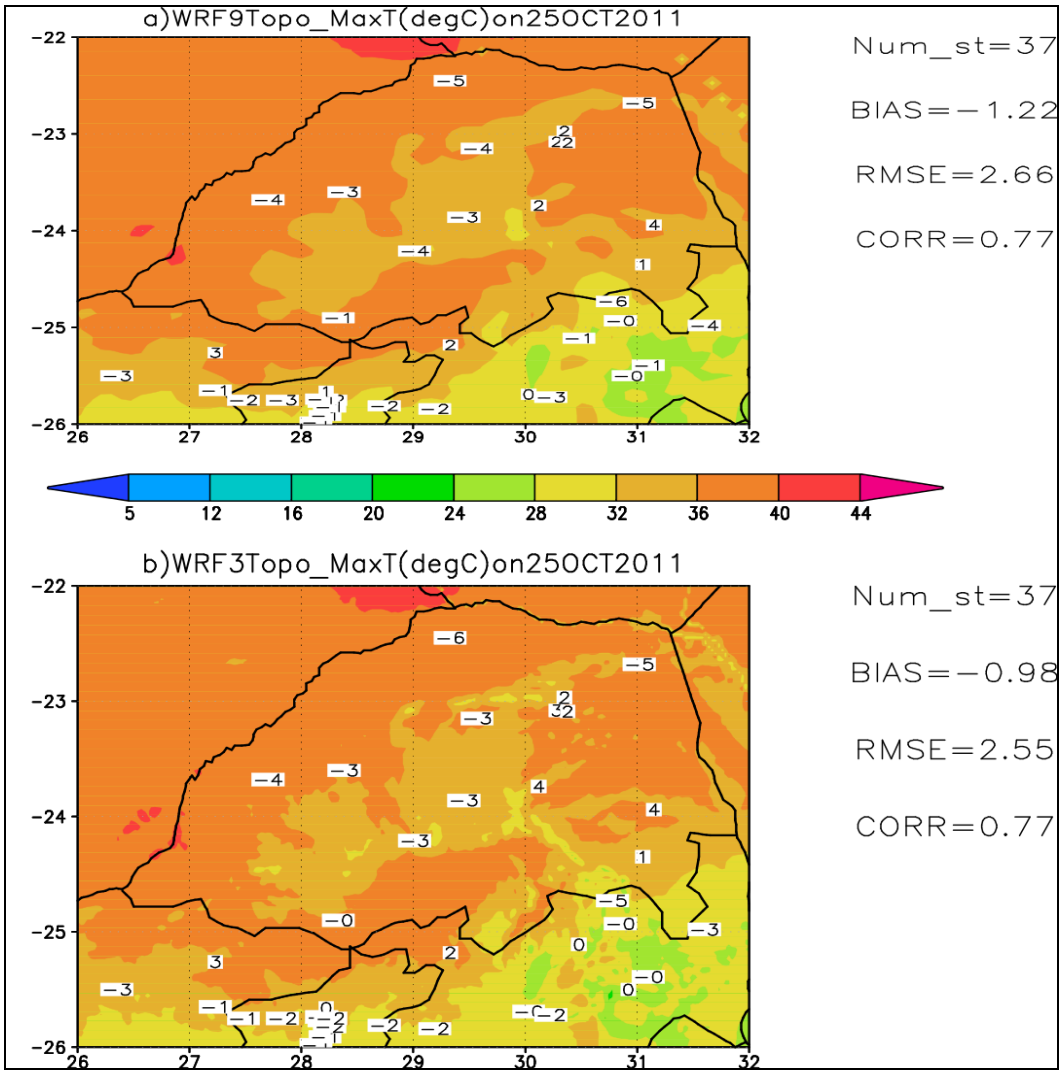

Figure 5.1: WRF 9 km (a) versus 3 km (b) simulated maximum temperature with statistics over Limpopo region on 25 October 2011. Bias values at each observation station are indicated as numbers.

In Table 5.2, it is depicted statistically that there was a significant difference between the mean of the WRF model simulation and observations even when the model grid resolution was increased from 9 km to 3 km. The t-statistic also shows different results

over Limpopo region on 25 October, which indicated agreement between the model simulation and observations. It is also noticeable that there was a slight improvement in t-test statistic as the model grid resolution was increased. However, this did not change the decision rule as the null hypothesis was still rejected at both 9 and 3 km grid resolution.

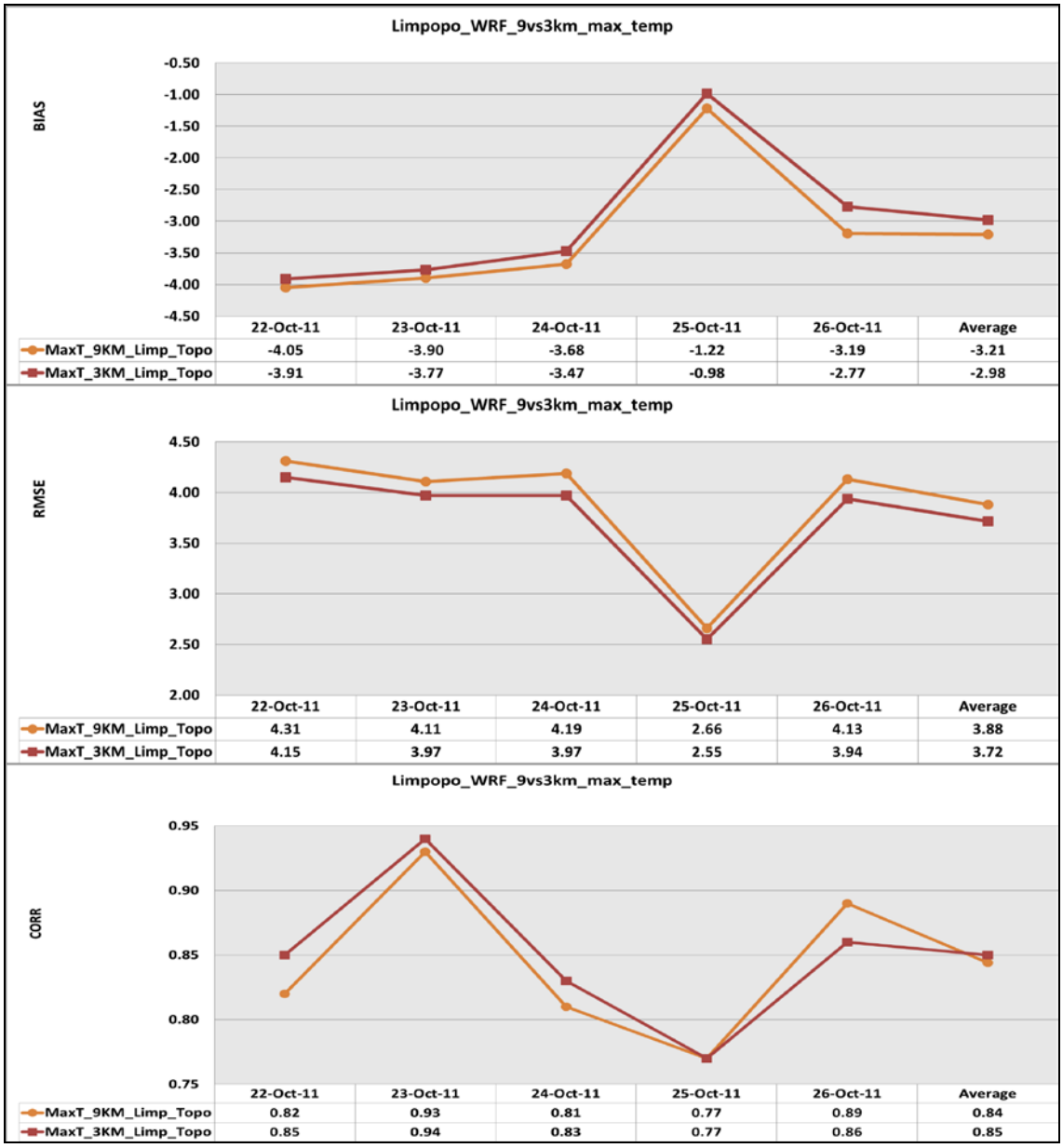

Figure 5.2: WRF 9 km versus 3 km maximum temperature statistics over Limpopo region for the period 22-26 October 2011.

Table 5.1: Station observed versus the WRF (9 and 3 km) model simulated maximum temperatures over northern parts of the country during heat wave for the period 23-25 October 2011.

Maximum temperatures(> 38 degree celsius) 9 km versus 3 km with topograph											
			on 23 October 2011			on 24 October 2011			on 25October 2011		
no	Station name	stid	Obs	wrf9_topo	wrf3_topo	Obs	wrf9_topo	wrf3_topo	Obs	wrf9_topo	wrf3_topo
1	Lephalale(lat:-23.68; lon:27.7)	68155	40.00	35.31	35.25	41.50	36.80	36.72	42.60	39.00	38.95
2	Mara(lat:-23.15; lon: 29.57)	68176	38.20	33.10	33.27	38.20	33.51	33.86	39.90	36.21	36.47
3	Marico(lat:-25.5; lon: 26.35)	68248	39.40	34.41	34.31	41.30	35.70	35.85	38.20	34.74	35.03
4	Venetia (lat:-22.45; lon:29.33)	68172	40.20	34.99	34.57	38.60	34.13	33.97	42.70	37.54	37.10
		Averag	39.45	34.45	34.35	39.90	35.04	35.10	40.85	36.87	36.89
		BIAS		-5.00	-5.10		-4.86	-4.80		-3.98	-3.96

Table 5.2: Students t-test for maximum temperatures over Limpopo region at both 9 km (a) and 3 km (b) grid resolution for the period 22-26 October 2011. A 95% confidence level was applied, and "TRUE" indicates that there is significant difference between the mean of observation and the mean for the WRF simulation, whereas "FALSE" indicate that there was no significant difference between the mean of observation and the mean for the WRF simulation.

	a) MaxT_9KM_Limp_Topo					
Date	22_Oct_2011	23_Oct_2011	24_Oct_2011	25_Oct_2011	26_Oct_2011	Average
T_test	-7.6762	-5.8578	-5.2454	-1.4095	-3.0339	-4.6446
df	70.00	68.00	70.00	70.00	70.00	69.60
T_crit95%	1.9944	1.9955	1.9944	1.9944	1.9944	1.9946
significant difference	TRUE	TRUE	TRUE	FALSE	TRUE	TRUE
	b) MaxT_3KM_Limp_Topo					
Date	22_Oct_2011	23_Oct_2011	24_Oct_2011	25_Oct_2011	26_Oct_2011	Average
T_test	-7.42	-5.67	-4.79	-1.12	-2.59	-4.3184
df	70.00	68.00	70.00	70.00	70.00	69.60
T_crit95%	1.9944	1.9955	1.9944	1.9944	1.9944	1.9946
significant difference	TRUE	TRUE	TRUE	FALSE	TRUE	TRUE

b) Minimum temperature, maximum wind speed and maximum relative humidity

The above mentioned findings also applies to minimum temperature (Figure 5.3), maximum wind speed (Figure 5.4) and also maximum relative humidity (Figure 5.5). However, it can be said that increasing the grid resolution did not yield much

improvement in minimum temperature simulations. For maximum wind speed (Figure 5.4) it can be deduced that an increase in grid resolution to 3 km was perhaps not enough and that maybe a much higher grid resolution (less than 1 km) would have produced better results. For maximum relative humidity (Figure 5.5), there was no noticeable improvement in all the scores as grid resolution was increased grid.

Figure 5.3: WRF 9 km versus 3 km minimum temperature statistics over Limpopo region for the period 22-26 October 2011.

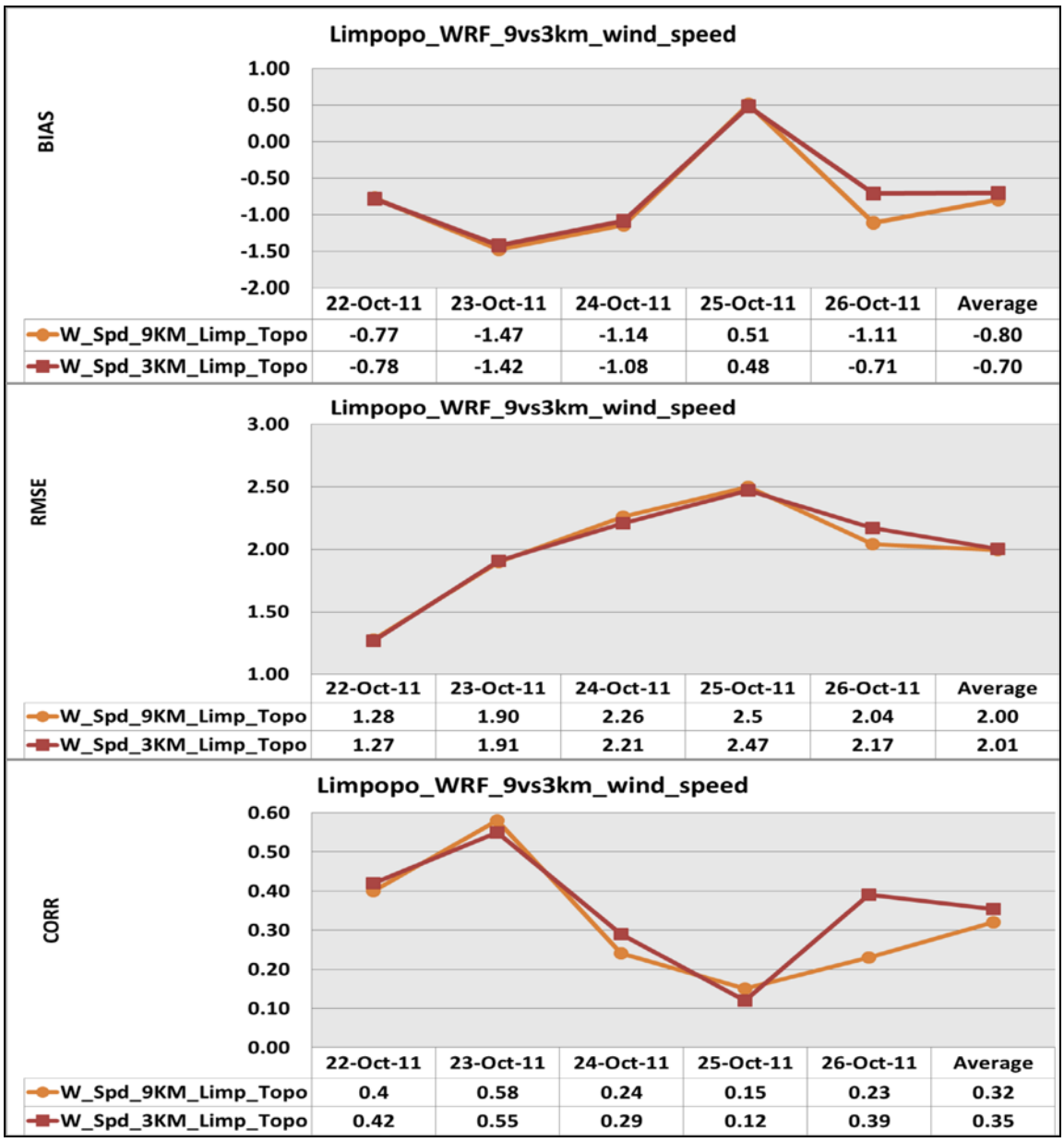

Figure 5.4: WRF 9 km versus 3 km wind speed statistics over Limpopo region for the period 22-26 October 2011.

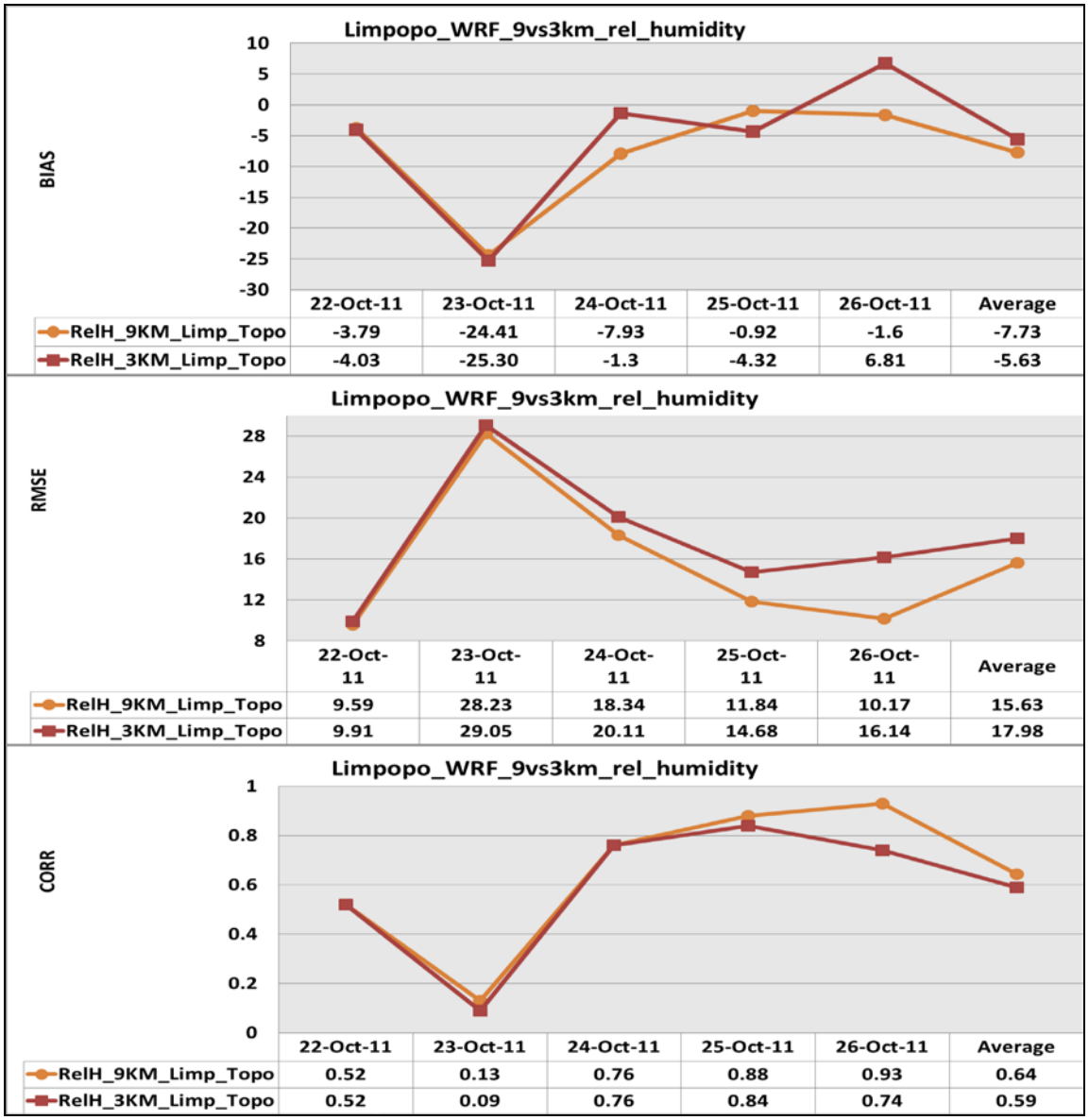

Figure 5.5: WRF 9 km versus 3 km relative humidity statistics over Limpopo region for the period 22-26 October 2011.

5.2 Heavy precipitation event 16-18 January 2012

5.2.1 The role of model grid resolution on vertical velocity

In Figure 5.6 the WRF model simulated vertical velocity at both 9 and 3 km grid resolution is depicted. It is shown that at both 850 (Figure 5.6b) and 700 hPa (Figure 5.6d), an increase in model grid resolution enhanced vertical velocity. There were increased updrafts over the eastern parts of the Limpopo region as compared to the rest of the region and also the 9 km grid resolution.

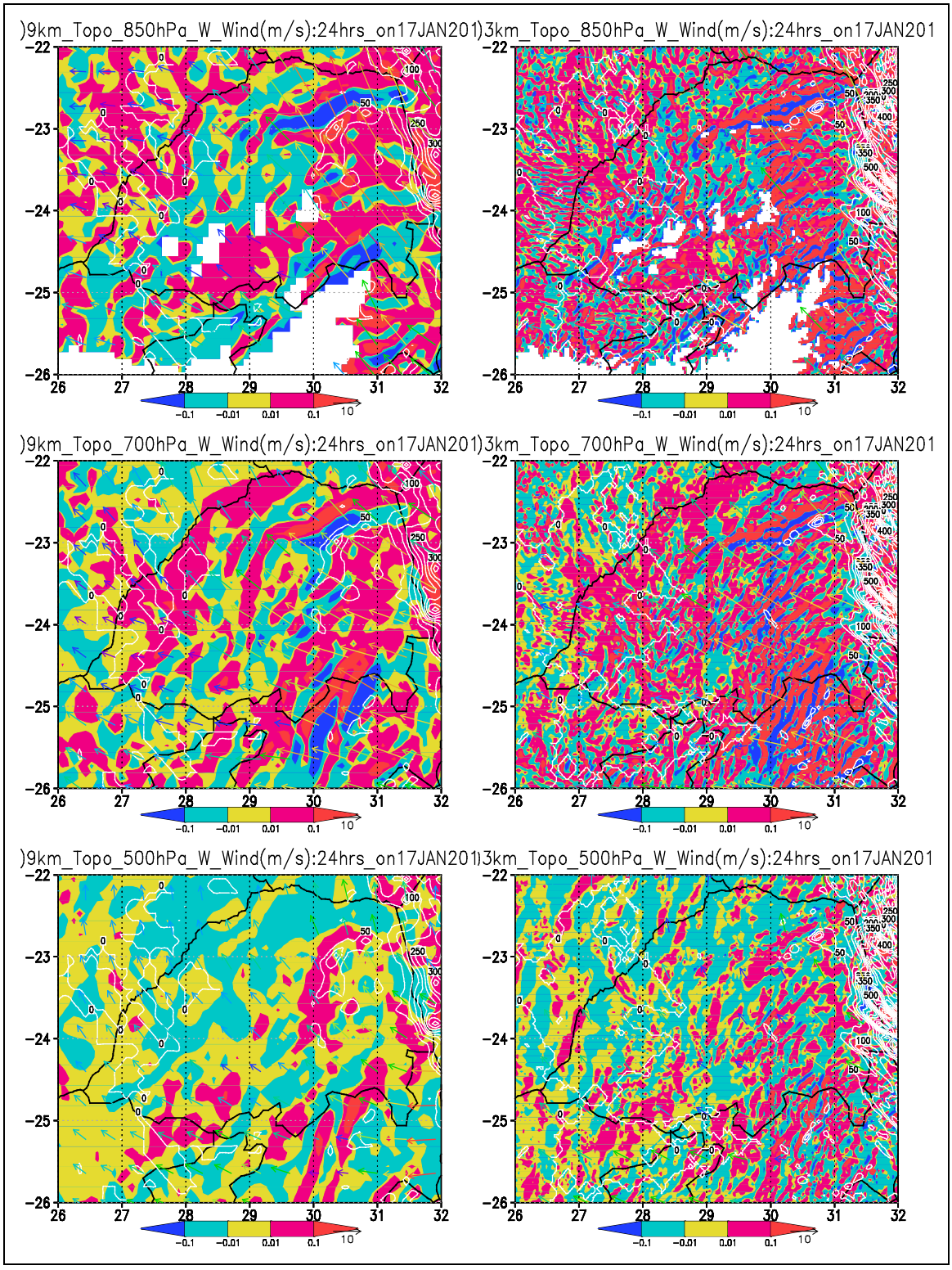

Figure 5.6: WRF 9 km versus 3 km simulated vertical velocities (m/s) at 850, 700 and 500 hPa heights over Limpopo region on 17 January 2012.Areas of rainfall (mm) are depicted in white colours, whereas wind speed and directions are shown as vectors.

The eastern parts of the region were also an area of enhanced rainfall. The western parts of the region show weak updrafts and therefore received less or no rain. At 500 hPa, both updrafts and downdrafts were reduced over the entire region (Figure 5.6f). At all levels, horizontal winds were dominantly easterlies and were stronger in areas of updrafts. Most rainfall was confined to areas of updrafts and over the eastern parts of the region.

Table 5.2 compares the WRF model simulated vertical velocity at both 9 and 3 km grid resolution over South Africa for the period 16-18 January 2012. An increase in grid resolution improved result in increased updrafts. The maximum updrafts velocity of 12 m/s was simulated at 500 hPa on 18 January 2012. Such large values of updrafts coincide with maximum rainfall recorded.

Table 5.3: The WRF 9 km versus 3 km simulated maximum vertical velocity (m/s) during heavy precipitation event that resulted in floods over Limpopo region of South Africa for the period 16-18 January 2012

				WRF 9 versus 3 km maximum vertical velocity (m/s)				
	16-Jan-12			17-Jan-12			18-Jan-12	
	WRF9_topo	WRF3_topo		WRF9_topo	WRF3_topo		WRF9_topo	WRF3_topo
850 hPa	0.60	2.50		1.00	2.50		0.50	2.50
700 hPa	0.80	4.50		1.20	5.00		0.70	6.00
500 hPa	0.45	2.70		0.55	9.00		1.00	12.00
average	0.62	3.23		0.92	5.50		0.73	6.83
maximum	0.80	4.50		1.20	9.00		1.00	12.00

5.2.2 Statistical simulations at high model grid resolution

a) Rainfall

The WRF 3 km simulated rainfall together with statistics over Limpopo region is displayed in Figures 5.7, 5.8,5.9 and 5.10. It is shown that an increase in model grid resolution from 9 to 3 km has resulted in improved spatial distribution of rainfall as compared to 9 km grid resolution and also statistics. At 3 km grid resolution, rainfall was intensified over the border between Limpopo region and Mozambique as compared to a 9 km simulation. This simulation also over-predicted rainfall over most stations in

Limpopo region (see also table 5.3). However, the simulation captured a no-rain event over the western parts of the Limpopo region.

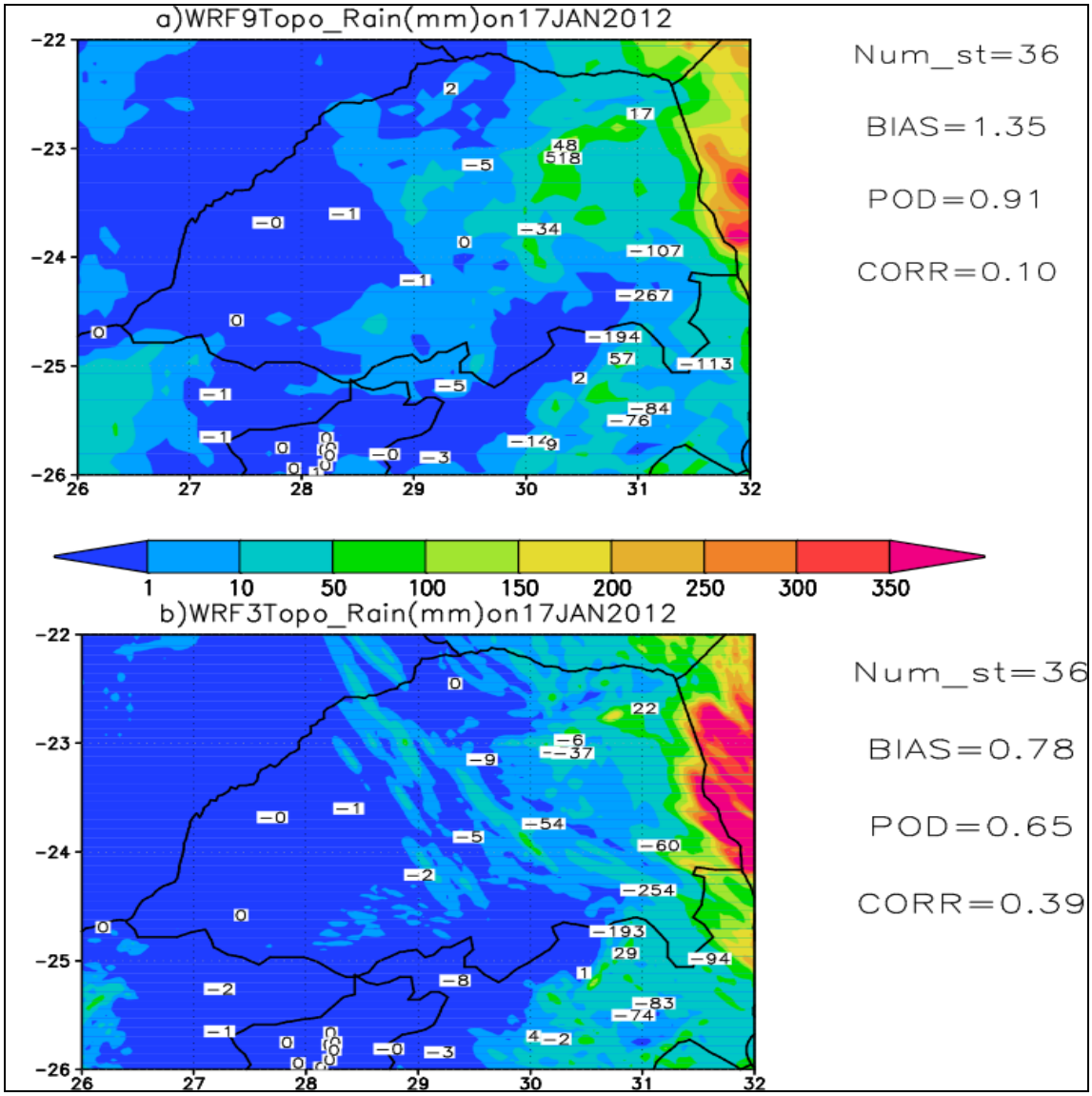

Figure 5.7: WRF 3 km simulated rainfall with statistics for the 0.1 mm category over Limpopo region on 17 January 2012. Bias values at each observation station are indicated as numbers.

An increase in grid resolution has reduced bias for a 0.1 mm threshold for almost all the days (Figure 5.8). There was a consistent and slight increase in bias at both 10 mm and 20 mm thresholds respectively. This result also shows less bias at both 10 and 20 mm threshold and high bias at 0.1 mm threshold. This result indicates that only for a low rainfall threshold (0.1 mm) bias was improved as grid resolution was increased whereas it increases with rainfall the other two thresholds.

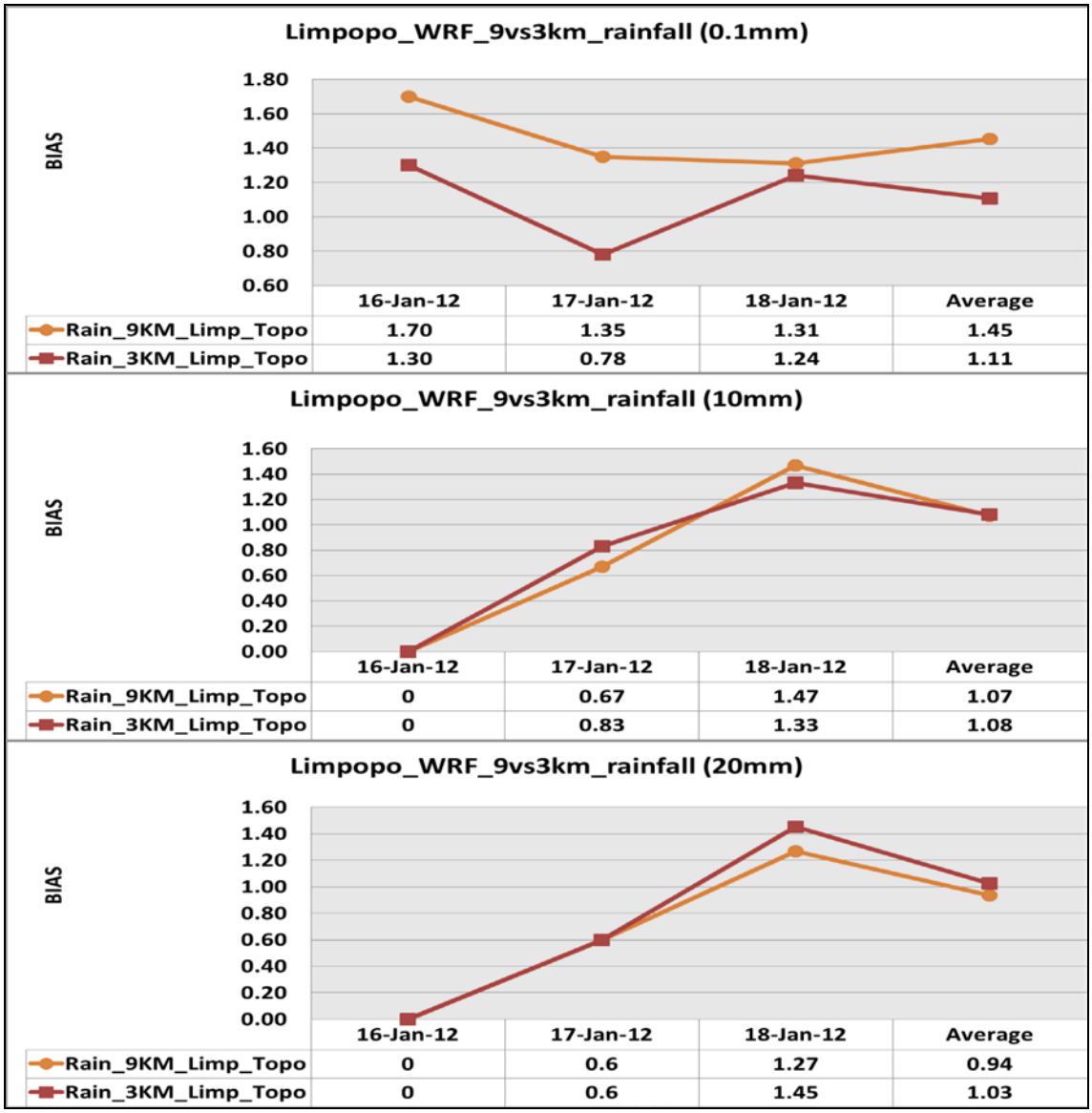

Figure 5.8: WRF 9 km versus 3 km rainfall bias for the 10.mm, 10 mm and 20 mm threshold over Limpopo region for the period 16-18 January 2012.

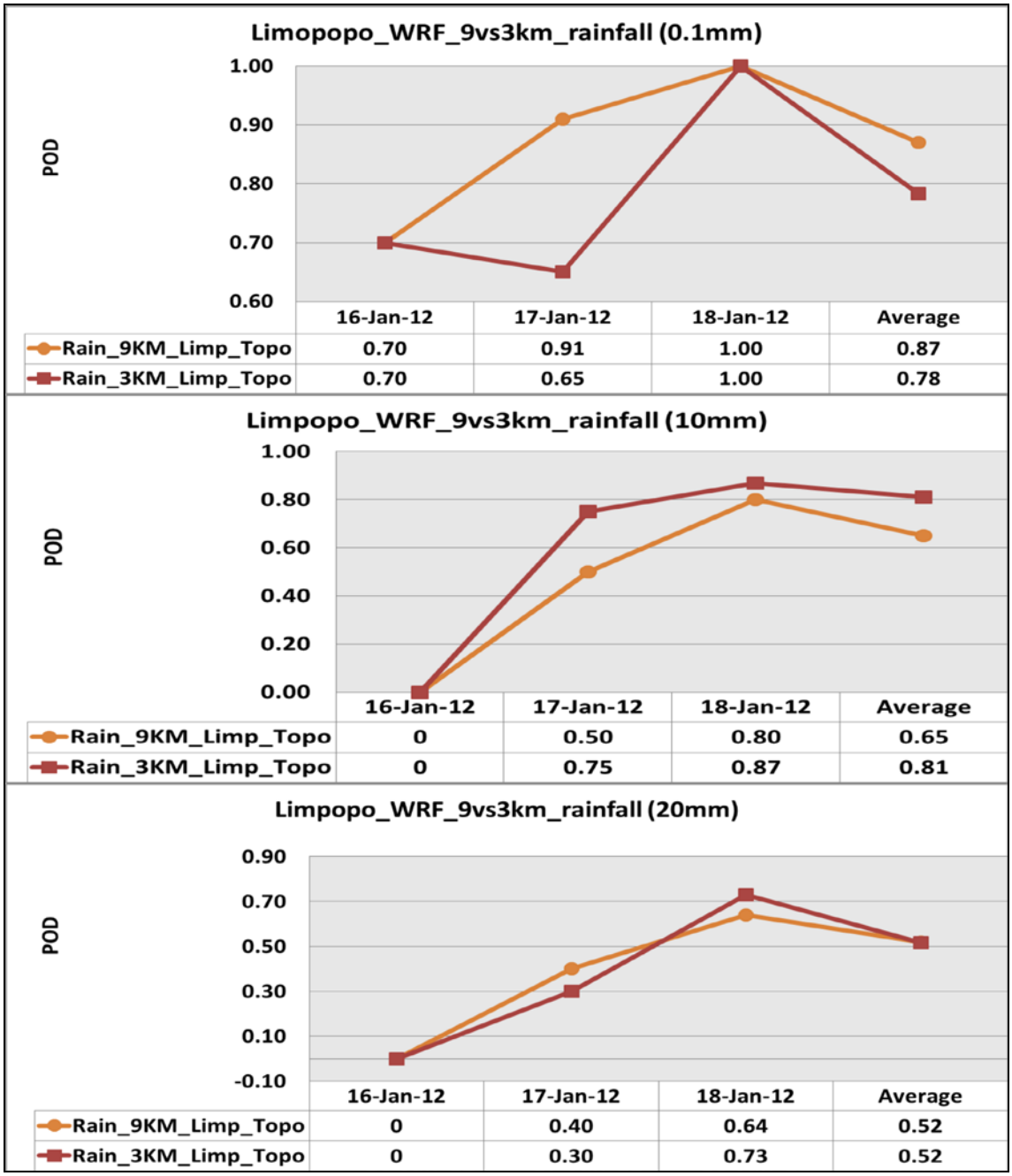

Figure 5.9: WRF 9 km versus 3 km rainfall POD for the threshold 0.1 mm, 10 mm, and 20 mm over Limpopo region for the period 16-18 January2012.

The POD scores at 0.1 mm, 10 mm and 20 mm rainfall thresholds are depicted in Figure 5.9. The *POD* values were reduced for the 0.1 mm threshold, improved at 10 mm threshold and remain the same for the 20 mm threshold as resolution was increased to 3 km. These values indicate that an increase in grid resolution did not yield much improvement for both 0.1 and 20 mm, with the exception of the 10 mm rainfall threshold.

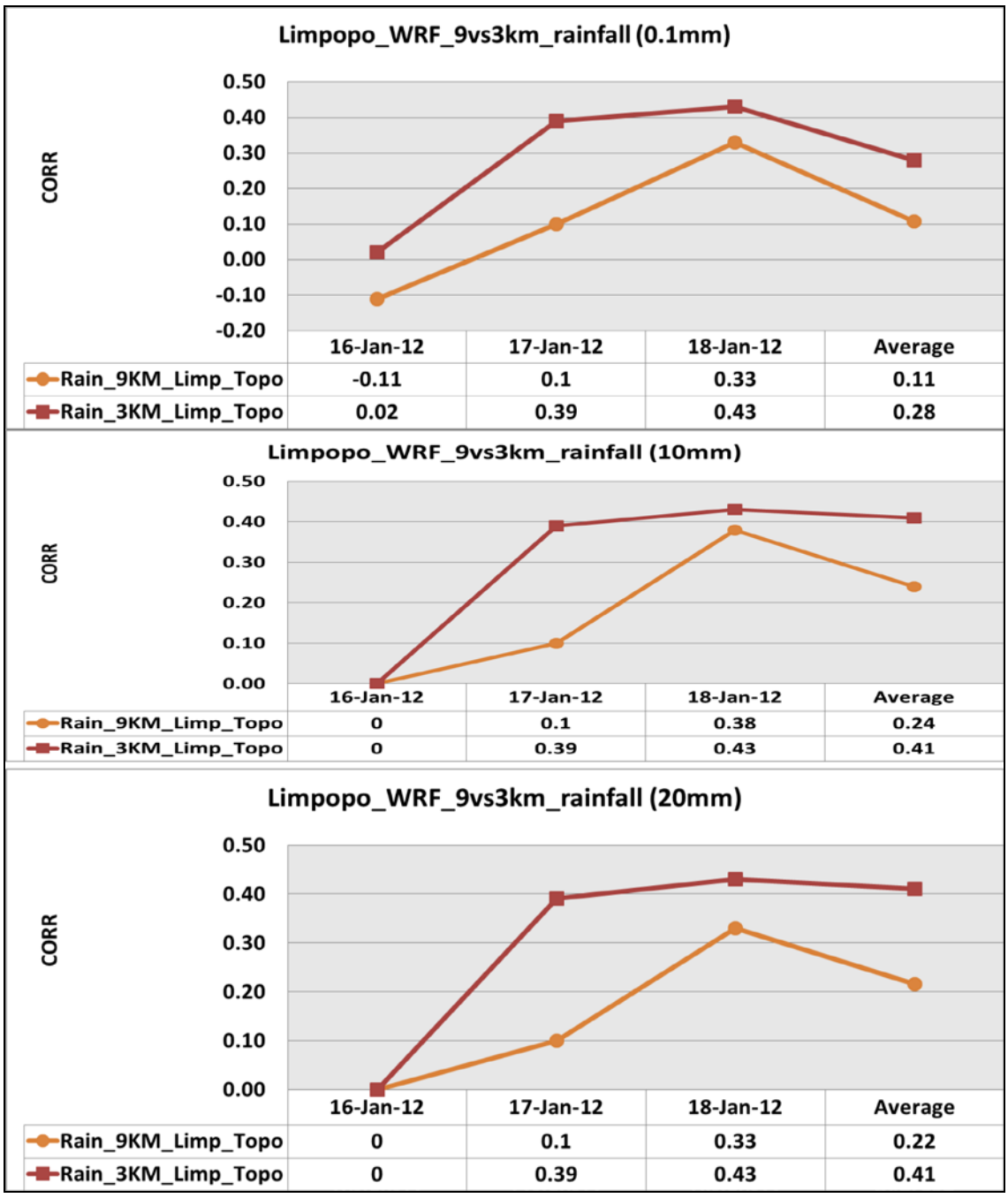

Figure 5.10: WRF 9 km versus 3 km rainfall CORR for the threshold 0.1 mm, 10 mm, and 20 mm over SA and Limpopo region for the period 16-18 January 2012.

There was also a slight improvement of CORR values as grid resolution was increase to 3 km and the average values were almost doubled for all rainfall thresholds. These averages were mostly improved at both 10 and 20 mm rainfall thresholds. However, the CORR values were still lower for the 0.1 mm threshold (Figure 5.10). It should be noted that rainfall over Limpopo region was first recorded from the 16 January and therefore the

zero values for bias, *POD* and CORR on 16 January at 10 and 20 mm thresholds indicates that the model did not simulate any rainfall greater than 10 mm for that day. This result has also shown convincingly that an increase in grid resolution improved WRF model ability to simulate heavy rainfall.

Table 5.3 shows the number of stations that recorded rainfall as well as the WRF model simulated rainfall at both 9 and 3 km for the period 16-18 January 2012 over the north-eastern parts of the country (named Limpopo region). From this table, it is shown that the model has either under-predict and over-predict heavy rainfall for some stations. An increase in model horizontal grid resolution shows similar rainfall distribution pattern as at 9 km grid resolution. This table indicates the complexity to simulate rainfall at specific stations.

Table 5.4: Total station observed versus WRF 9 and 3 km simulated rainfall over region for the period 16-18 January 2012

	Station observed vs WRF 9 and 3 km rainfall_16-18 January 2012				
			Total rainfall		
	Station name	stid	observed	wrf9_topo	wrf3_topo
1	Hoedspruit (lat:-24.35; lon: 31.05)	68291	378.20	21.65	97.05
2	Kruger Airport(lat:-25.39; lon:31.1)	68290	215.20	199.68	163.02
3	Levubu(lat:-23.08; lon: 30.28)	68182	85.00	438.21	164.49
4	Mara(lat:-23.09; lon:30.38)	68176	51.40	12.83	16.58
5	Marken (lat:-23.6; lon: 28.38)	68163	35.20	11.79	39.75
6	Nelspruit (lat:-25.5; lon:30.92)	68289	144.20	71.01	19.11
7	Phalaborwa(lat:-23.94; lon:31.15)	68191	145.80	103.39	150.37
8	Punda Maria(lat:-22.68; lon: 31.02)	68196	33.40	118.17	136.18
9	Skukuza(lat:-24.98; lon:31.6)	68296	278.60	107.91	134.76
10	Thohoyandou (lat:-23.09; lon: 30.38)	68183	70.00	289.04	207.20
11	Tshivhase Tea Est (lat:-22.97; lon: 30.35)	68184	149.80	348.86	196.89
12	Tzaneen (lat:-23.74; lon: 30.12)	68188	120.00	173.96	132.45
13	Vaalhoek(lat:-24.73; lon:30.78)	68282	318.00	7.43	11.78
		Maximum	378.20	438.21	207.20
		Minimum	33.40	7.43	11.78
		Average	137.22	156.86	114.38
		Median	144.20	107.91	134.76
		BIAS		19.64	-22.84

In table 5.5 it is shown statistically that there was no significant difference between the WRF model simulation and the observations on the 16 January, but there was also a significant difference on the next two consecutive days (17 and 18 January). The averages also show no significant difference. This resulted in the acceptance of the null hypothesis on the16 January and a rejection of the null hypothesis on the 17 and 18 January. It should also be mentioned that there was a slight improvement in t-statistic value as the model grid resolution was increased to 3 km. This results were however not conclusive.

Table 5.5: Students t-test for rainfall at both 9 km (a) and 3 km (b) grid resolution over Limpopo region for the period 16-18 January 2012. A 95% confidence level was applied, and "TRUE" indicates that there is significant difference between the mean of observation and the mean for the WRF simulation, whereas "FALSE" indicate that there was no significant difference between the mean of observation and the mean for the WRF simulation.

	a) Rain_9KM_Limp_Topo			
Date	**16-Jan-12**	**17-Jan-12**	**18-Jan-12**	**Average**
T_test	**-0.7800**	**-1.7300**	**2.1800**	**-0.1100**
df	**72.00**	**70.00**	**74.00**	**72.00**
T_crit95%	**1.9935**	**1.9940**	**1.9920**	**1.9932**
significant difference	**FALSE**	**FALSE**	**TRUE**	**FALSE**
	b) Rain_3KM_Limp_Topo			
Date	**16-Jan-12**	**17-Jan-12**	**18-Jan-12**	**Average**
T_test	**-1.7300**	**-2.3200**	**2.0200**	**-0.6767**
df	**72.00**	**70.00**	**74.00**	**72.00**
T_crit95%	**1.9935**	**1.9940**	**1.9920**	**1.9932**
significant difference	**FALSE**	**TRUE**	**TRUE**	**FALSE**

b) Maximum temperature, minimum temperature, maximum wind speed and maximum relative humidity

Statistics for maximum temperature (Figure 5.11), minimum temperature (Figure 5.12), maximum wind speed (Figure 5.13) and maximum relative humidity (Figure 5.14) as simulated by WRF model at both 9 and 3 km grid resolution over Limpopo region are depicted. For maximum temperature (Figure 5.11), an increase in grid resolution has

reduced bias (top), RMSE (middle) and improved CORR (bottom) values over Limpopo region.

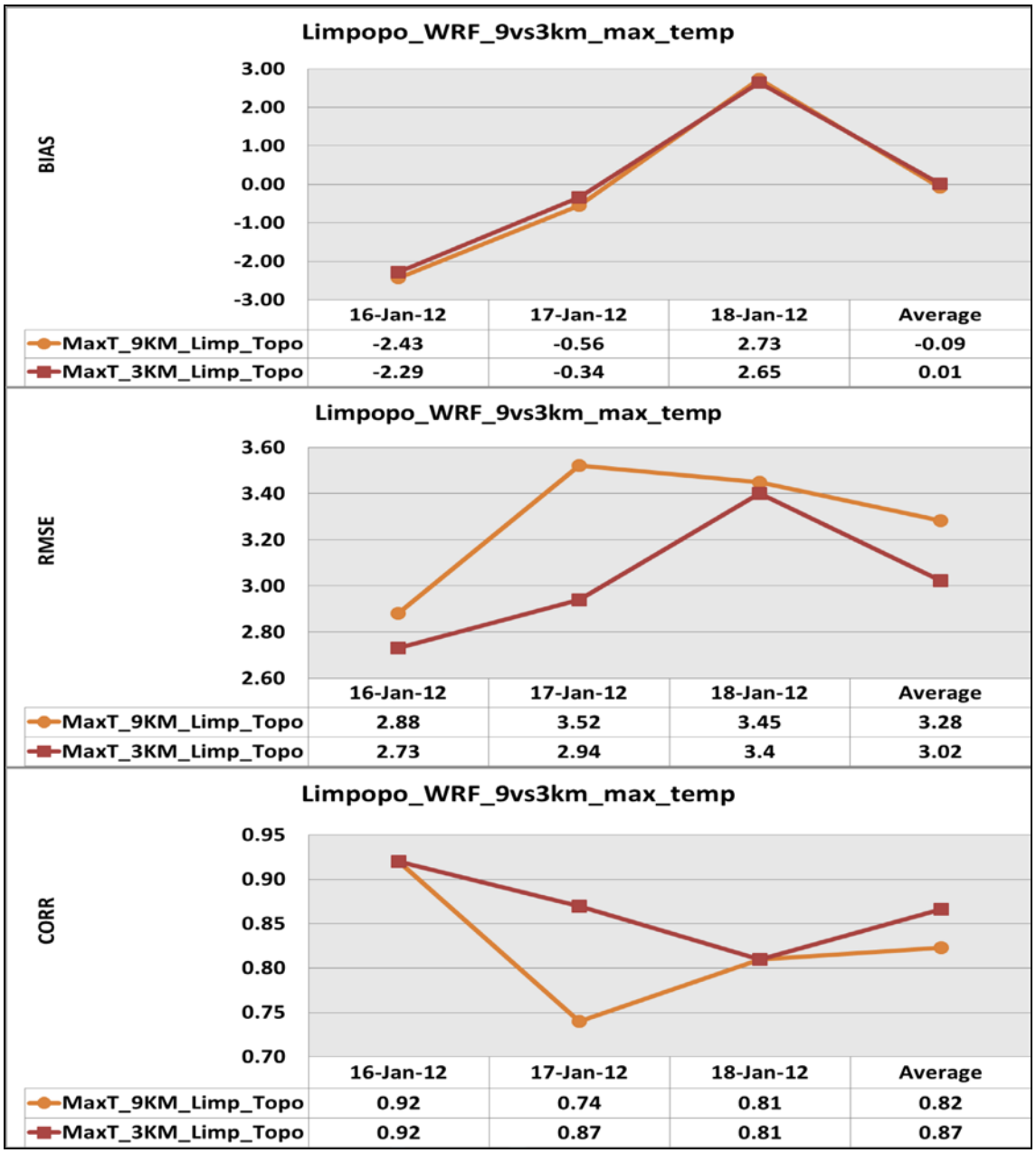

Figure 5.11: WRF 9 km versus 3 km maximum temperatures statistics over Limpopo region for the period 16-18 January 2012.

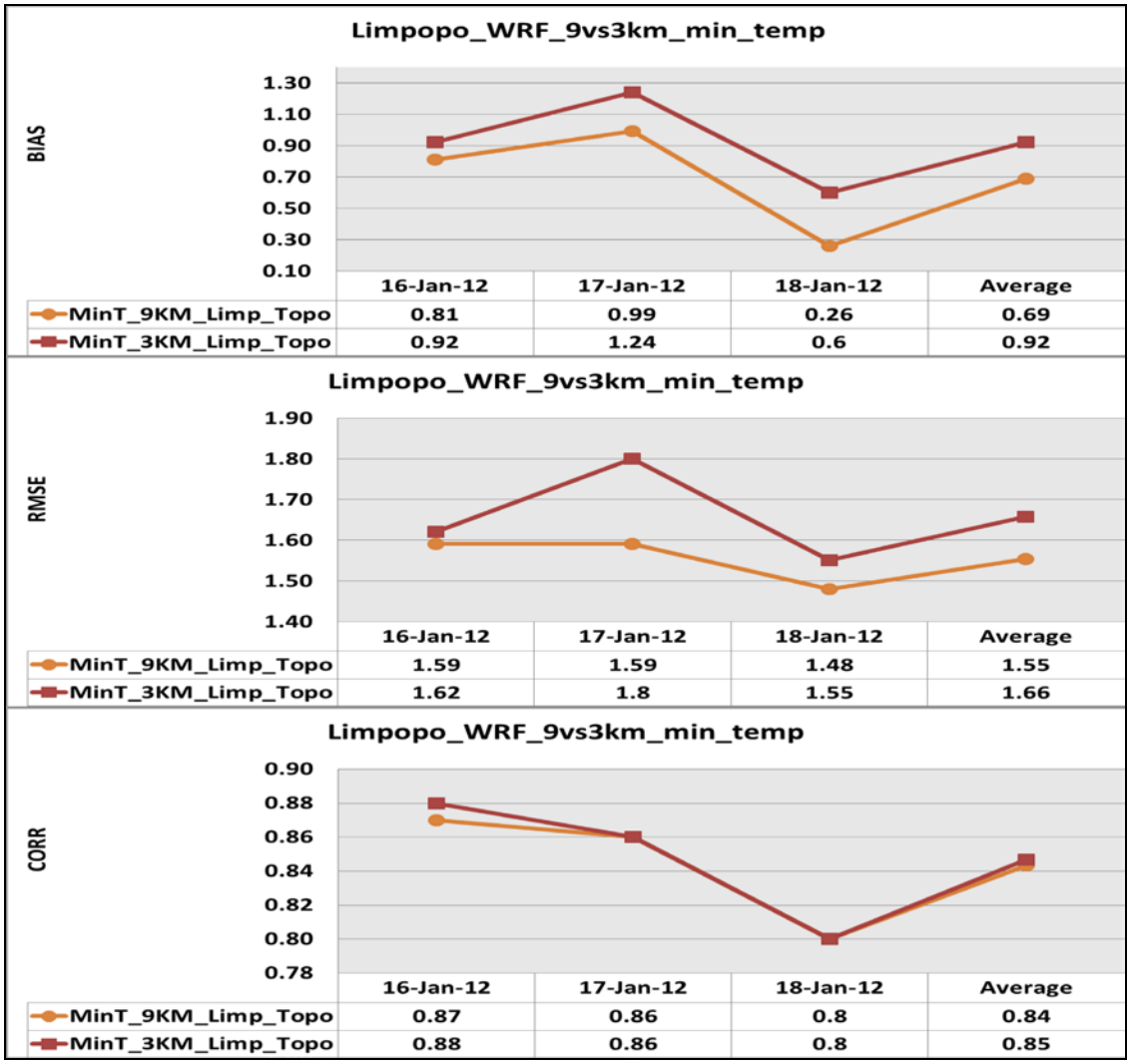

Figure 5.12: WRF 9 versus 3 km minimum temperatures statistics over Limpopo region for the period 16-18 January 2012.

For minimum temperatures (Figure 5.12), there has been an increased bias values (top) and also the RMSE values (middle). However, it did not have any impact on the CORR values (bottom), as values remained similar to 9 km grid results. Such results indicate that the model was simulating minimum temperature very well.

Simulation of maximum wind speed (Figure 5.13) shows that an increase in model grid resolution slightly improved bias (top) and RMSE values (middle). The CORR values (bottom) were on average similar for both WRF 9 and 3 km resolution, but with a slight improvement.

Verification statistics for relative humidity simulation (Figure 5.14) indicates that bias values (top) remained negative and slightly increased at 3 km grid resolution. The RMSE (middle) and the CORR values (bottom) were however slightly improved. Therefore it is difficult to say that an increase in grid resolution has improved relative humidity simulations.

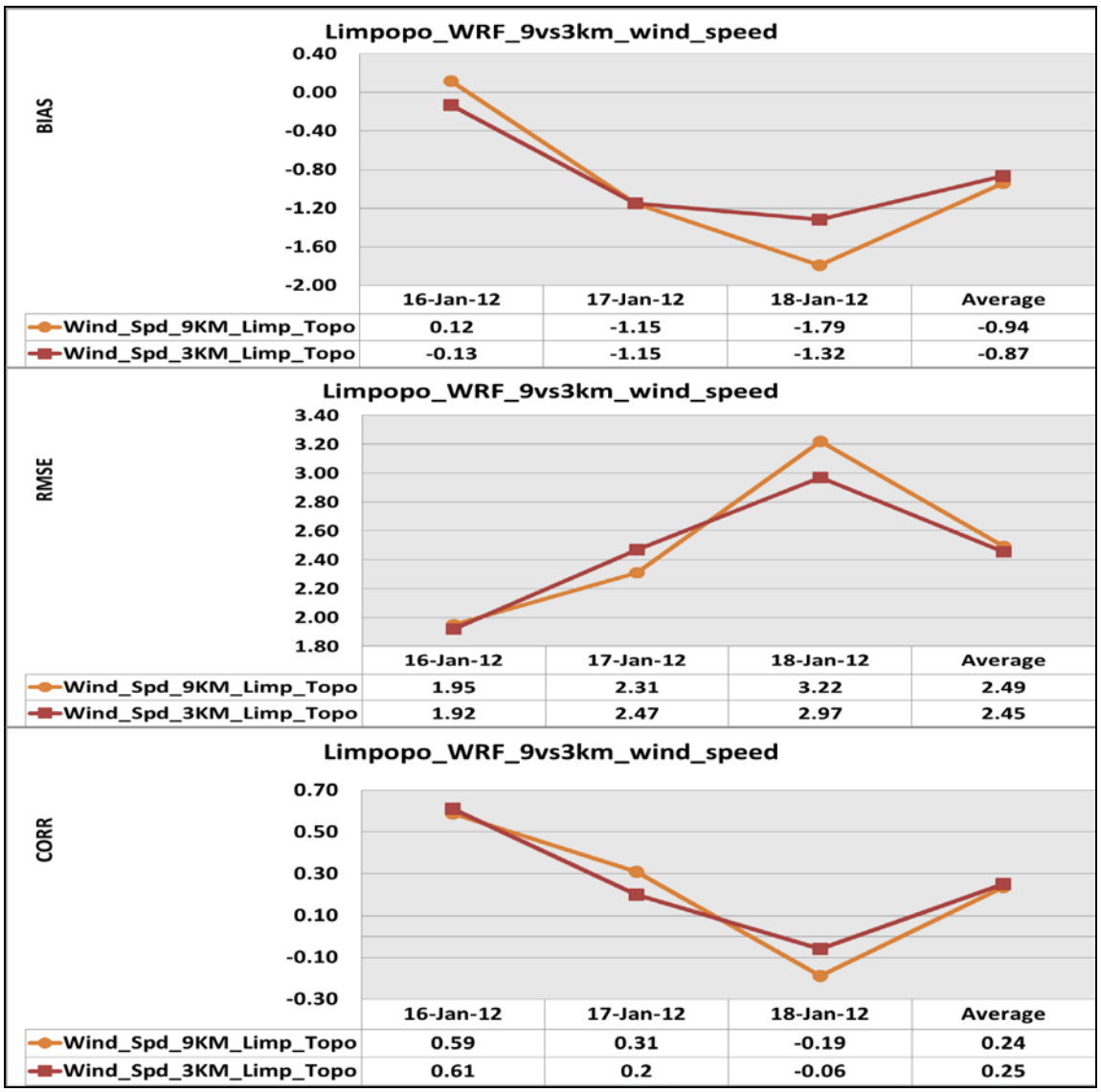

Figure 5.13: WRF 9 versus 3 km wind speed statistics over Limpopo region for the period 16-18 January 2012.

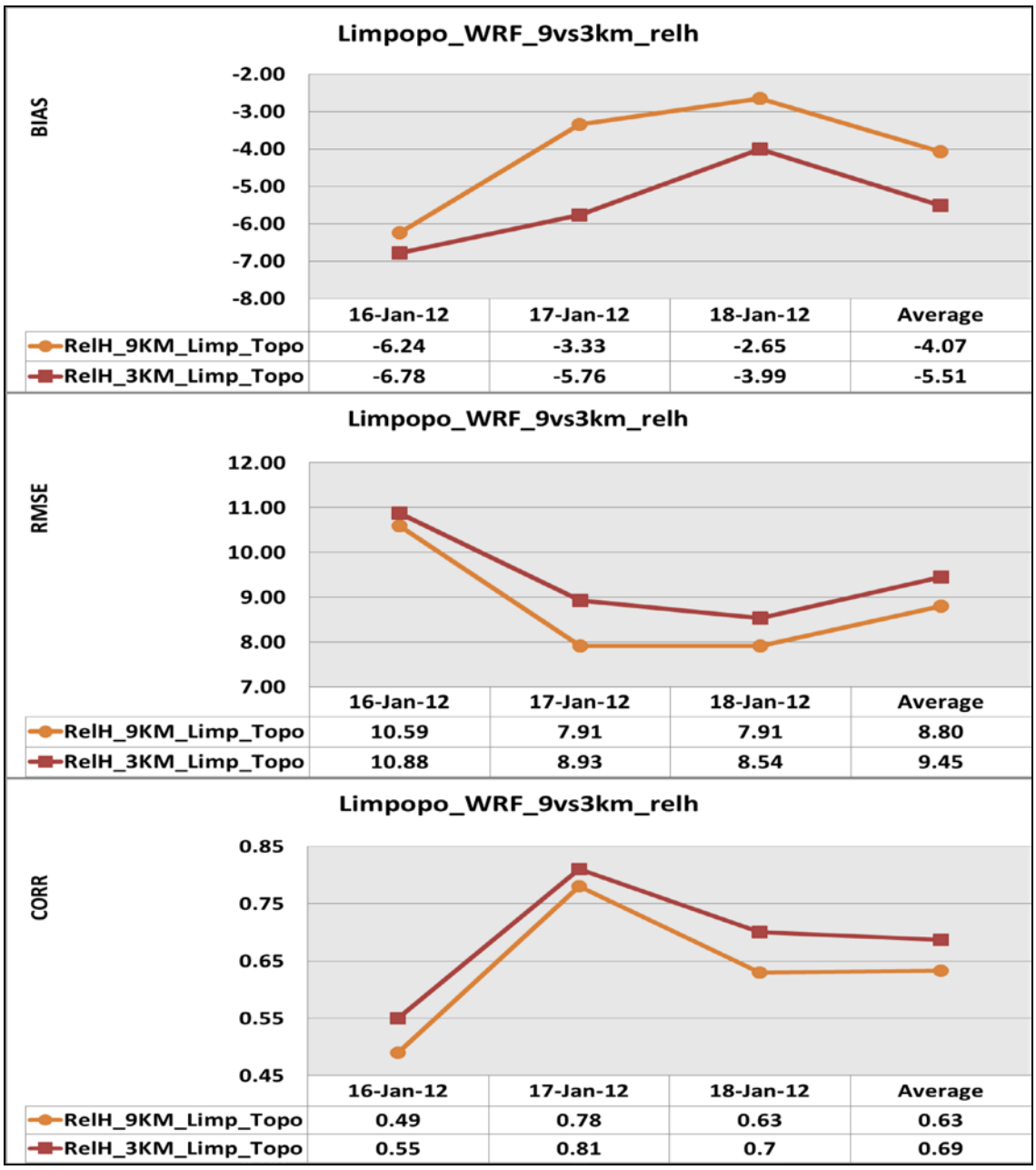

Figure 5.14: WRF 9 versus 3 km relative humidity statistics over Limpopo region for the period 16-18 January 2012.

5.3 Heat wave episode 15-18 January 2012

a) Maximum temperature

The WRF model simulation of maximum temperature at both 9 and 3 km grid resolution together with statistics over the Cape region is depicted in Figures 5.15 and 5.16. An increase in grid resolution improved details as well as statistics when compared to a 9 km

grid simulation. However, the model simulation still under-predicted maximum temperature as compared to WRF 9 km runs.

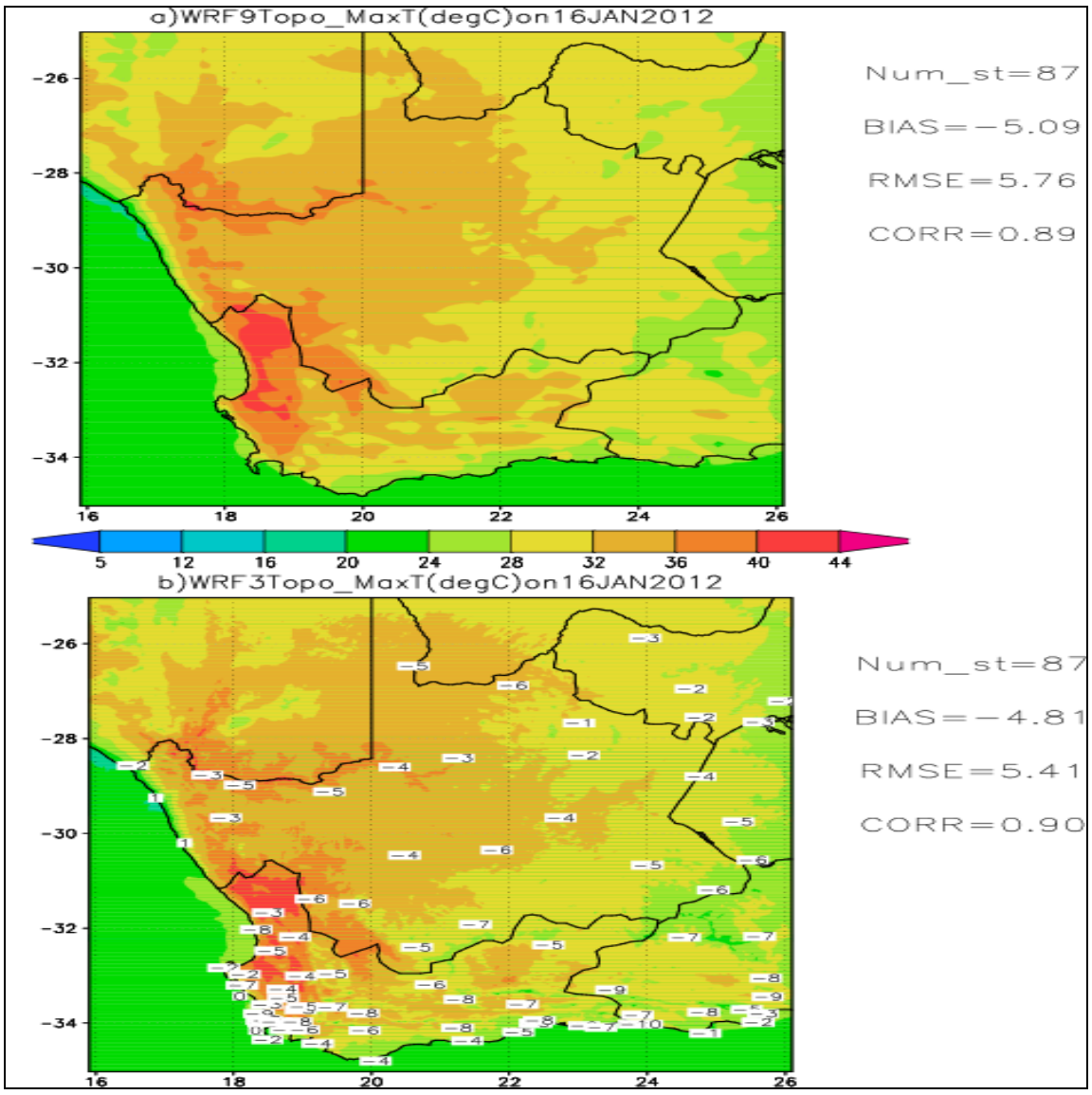

Figure 5.15: WRF 9 km (a) versus 3 km (b) simulated maximum temperatures with statistics over Cape region on 16 January 2012. Bias values at each observation station are indicated as numbers.

An increase in grid resolution has slightly reduced bias values (top) and the RMSE values (middle) when compared to 9 km grid resolution. The CORR (bottom) values were increased. However, all these results did not indicate any consistency. The very low bias and RMSE values on 17 January could be any indication that the model was able to

reproduce the heat wave event very well as compared to other days. For both resolutions, bias values were negative and larger than the +/- 0.5°C and likewise the RMSE values were also larger than 2°C, as compared to the MM5 model benchmark applied in Tesche and Tremback (2002). This result indicates that the model did not simulate maximum temperatures very well, although on overall an increase in grid resolution was justified.

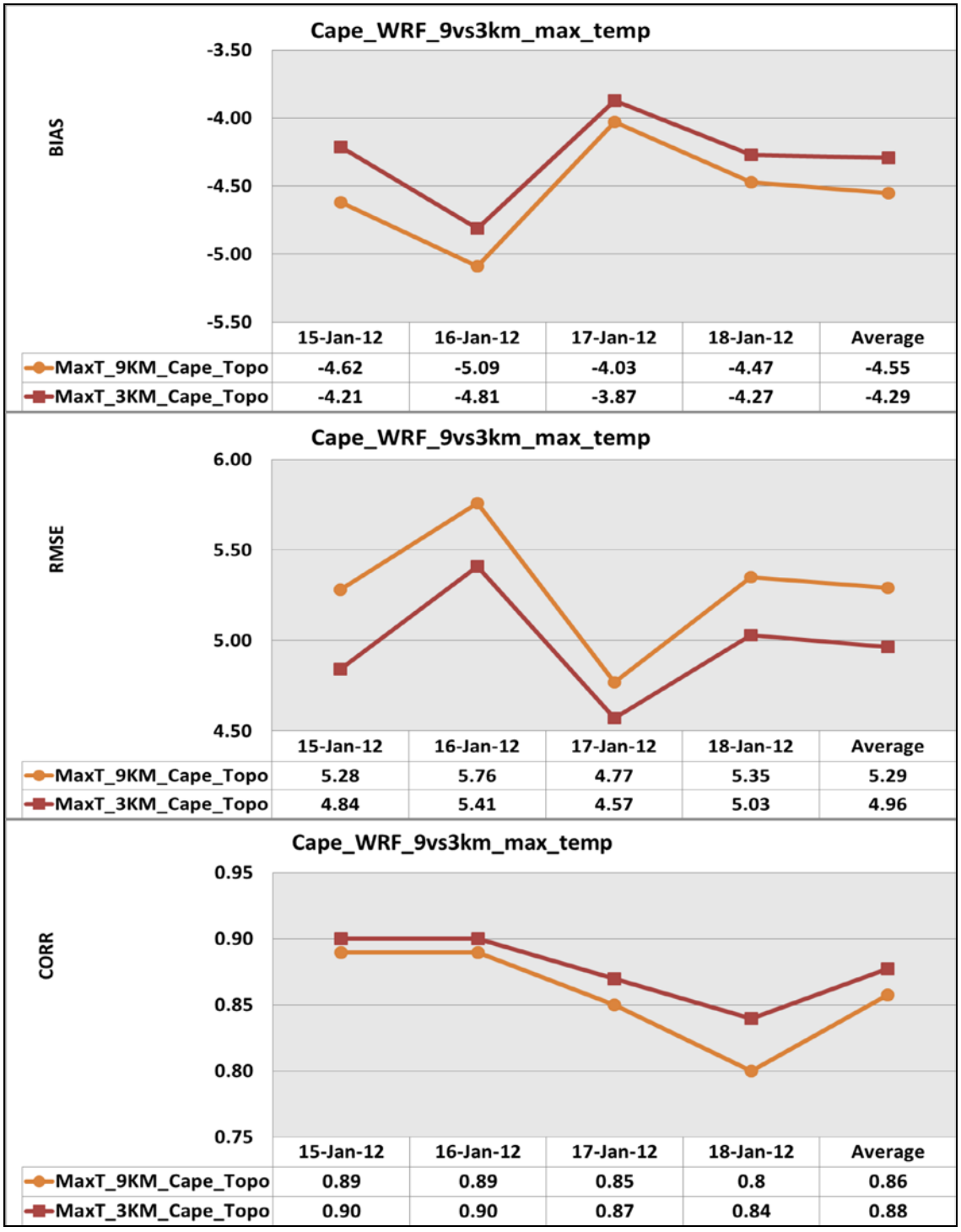

Figure 5.16: WRF 9 versus 3 km maximum temperatures statistics over Cape region for the period 15-18 January 2012.

In table 5.6, the total number of stations that recorded very high temperatures for a period of at least two days over the Cape regions is depicted. The table also show the model simulated maximum temperature at 9 km and also 3 km grid resolution respectively. This result gives an indication that although there was large bias, an increase in grid resolution to 3 km has slightly improved the maximum temperature simulations over Cape region and was considered necessary.

Table 5.6: Station observed vs. the WRF (9 and 3 km) model simulated maximum temperatures over northern parts of the country during heat wave for the 15-18 January 2012. Where either the observed or WRF model simulated temperature is less than 38^{o}C, the column is marked not applicable (n/a).

	Maximum temperatures (> 38 degree celsius) 9 km versus3 km with topography													
			on 15 January 2012			on 16 January 2012				on 17 January 2012			on 18 January 2012	
	Station name	stid	Obs	wrf9_topo	wrf3_topo	Obs	wrf9_topo	wrf3_topo	Obs	wrf9_top	wrf3_topo	Obs	wrf9_topo	wrf3_topo
1	Calvinia WO(lat:-31.48; lon: 19.76)	68618	38.60	31.00	31.96	40.10	32.27	33.80	40.80	36.05	36.49	40.20	34.07	37.34
2	Langgewens(lat:-33.28; lon:18.71)	68716	39.50	35.26	35.76	42.90	38.64	38.69	40.10	37.81	37.15	39.00	35.21	36.07
3	Malmesbury(lat:-33.47; lon: 18.72)	68715	40.20	34.97	35.83	43.10	37.86	38.52	41.70	36.51	36.08	40.10	35.15	34.93
4	Paarl (lat:-33.72; lon: 18.97)	68713	38.80	33.18	33.88	42.30	36.46	37.14	40.60	35.58	35.96	40.50	34.76	35.50
5	Porterville (lat:-33.01; lon:18.98)	68717	40.00	35.71	37.44	43.60	37.90	39.84	40.70	37.12	37.58	40.50	34.03	36.97
6	Redelindshuys (lat: -32.48; lon: 18.54)	68710	43.70	36.63	37.70	46.00	40.40	40.77	41.10	33.19	32.53	39.30	29.00	30.80
7	Vanwyksvlei(lat:-30.35; lon:21.82)	68524	41.00	33.95	33.87	40.30	33.37	34.09	39.00	34.34	34.61	n/a	n/a	n/a
8	Vioolsdrif (lat:-28.70; lon:17.60)	68411	45.50	38.60	40.49	45.00	40.35	41.66	40.20	36.62	38.55	39.60	35.35	37.14
9	Vredendal (lat:-31.67; lon: 18.5)	68614	43.40	38.54	39.02	45.30	41.99	41.88	43.10	32.24	32.95	39.50	30.83	33.99
10	Wellington (lat:-33.65; lon: 19.01)	68810	39.30	33.40	34.84	43.30	37.10	38.22	42.00	36.77	37.83	40.80	35.49	37.02
11	Worcester AWS(lat:-33.66; lon:19.42)	68821	n/a	n/a	n/a	42.40	35.54	35.89	38.80	33.64	35.28	40.90	36.54	36.71
		Average	41.00	35.12	36.08	43.12	37.44	38.23	40.74	35.44	35.91	40.04	34.04	35.65
		BIAS		-5.88	-4.92		-5.67	-4.89		-5.29	-4.83		-6.00	-4.39

From table 5.7, it was proved statistically that there was a significant difference between the WRF model simulation and observation at both 9 and 3 km grid resolution over the Cape region. However, an increase in grid resolution did not yield any improvement in the t-statistic values. Therefore the null hypothesis was rejected.

Table 5.7: Students t-test for maximum temperatures at both 9 km (a) and 3 km (b) grid resolution over SA and Cape region for the period 15-18 January 2012. A 95% confidence level was applied, and "TRUE" indicates that there is significant difference between the mean of observation and the mean for the WRF simulation, whereas "FALSE" indicate that there was no significant difference between the mean of observation and the mean for the WRF simulation.

	a) MaxT_9KM_Cape_Topo				
Date	**15-Jan-12**	**16-Jan-12**	**17-Jan-12**	**18-Jan-12**	**Average**
T_test	**-0.7092**	**-6.3895**	**-5.8827**	**-6.5168**	**-4.8745**
df	**170.00**	**170.00**	**172.00**	**172.00**	**171.00**
T_crit95%	**1.9740**	**1.9740**	**1.9739**	**1.9739**	**1.9739**
significant difference	**FALSE**	**TRUE**	**TRUE**	**TRUE**	**TRUE**
	b) MaxT_3KM_Cape_Topo				
Date	**15-Jan-12**	**16-Jan-12**	**17-Jan-12**	**18-Jan-12**	**Average**
T_test	**-5.3714**	**-5.9053**	**-5.4554**	**-6.0021**	**-5.6835**
df	**170.00**	**170.00**	**172.00**	**172.00**	**171.00**
T_crit95%	**1.9740**	**1.9740**	**1.9739**	**1.9739**	**1.9739**
significant difference	**TRUE**	**TRUE**	**TRUE**	**TRUE**	**TRUE**

b) Minimum temperature, maximum wind speed and maximum relative humidity

The above discussed findings also applies to minimum temperature (Figure 5.17), maximum wind speed (Figure 5.18) and maximum relative humidity (Figure 5.19).

Simulation of minimum temperature (Figure 5.17), an increase in grid resolution consistently increased the bias values (top). However, bias was very high on the 16 January and was difficult to determine the cause. This value shows improvement after the 16 January for the last three days. There was no impact on RMSE values (middle) as these values remained similar to a 9 km simulation. There was also a slight increase of CORR values (bottom). The very high CORR values on the 16 January was also difficult to explain as bias was also very high on the day. This result could not be used to draw conclusions of WRF performance.

For maximum wind speed (Figure 5.18), such an increases in grid resolution resulted in increased bias (top). However, the RMSE values (middle) were reduced. The lowest values of RMSE were recorded on 18 January and are not easy to understand.

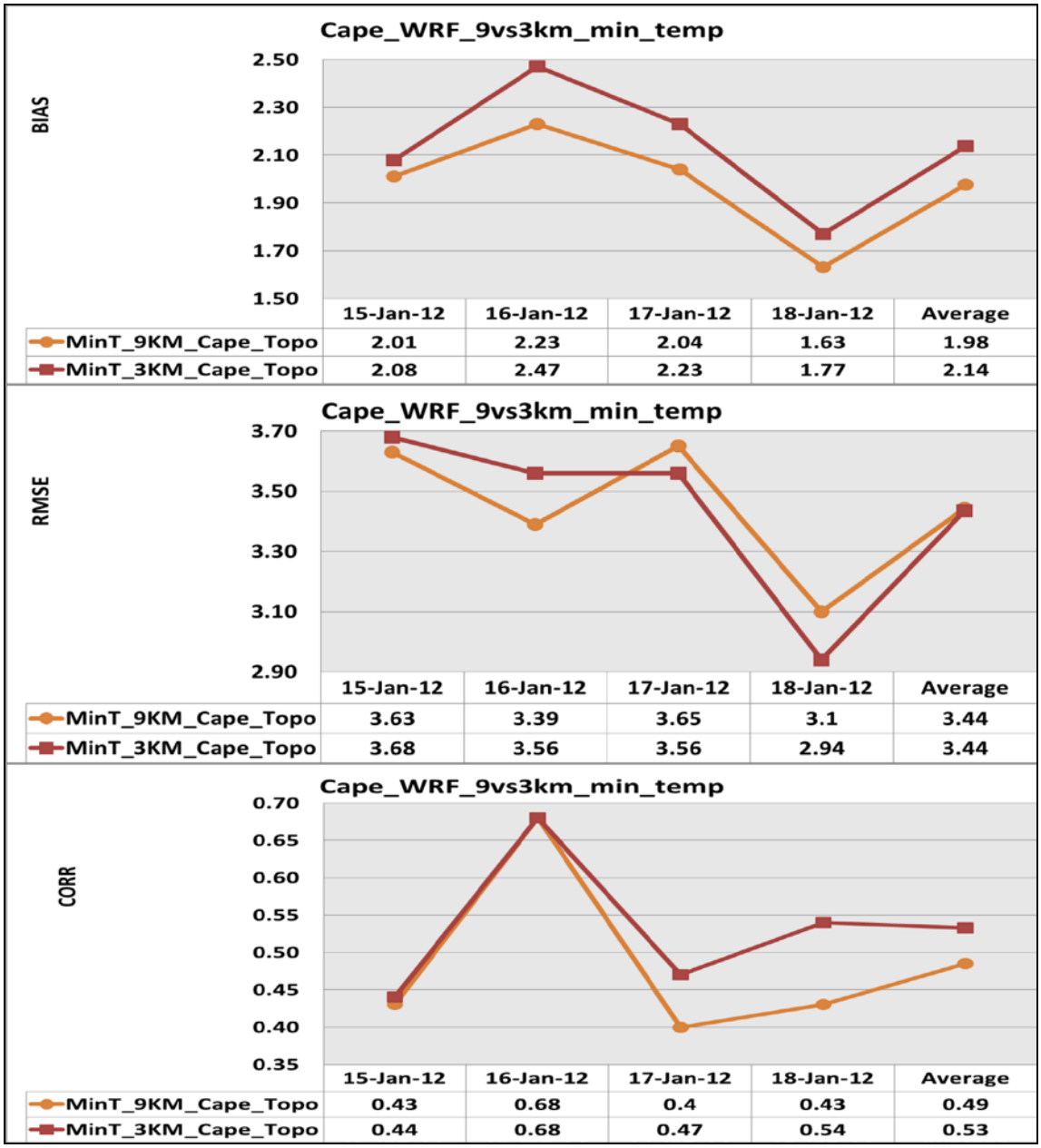

Figure 5.17: WRF 9 versus 3 km minimum temperatures statistics over Cape region for the period 15-18 January 2012.

The CORR values (bottom) were however increased. The very low CORR values on the 18 January could be an indication that the model started losing its accuracy and reliability as prediction time progresses, but since the RMSE values were also low, this makes it difficult to understand.

Likewise for maximum relative humidity (Figure 5.19), an increase in grid resolution increased bias (top). Both the RMSE values (middle) and the CORR values (bottom)

were also increased. However, the CORR values decreases with time during the simulation. Therefore since both bias and RMSE increased and only CORR values were improved, this result does not clearly indicate the WRF model performance in simulating relative humidity over the region.

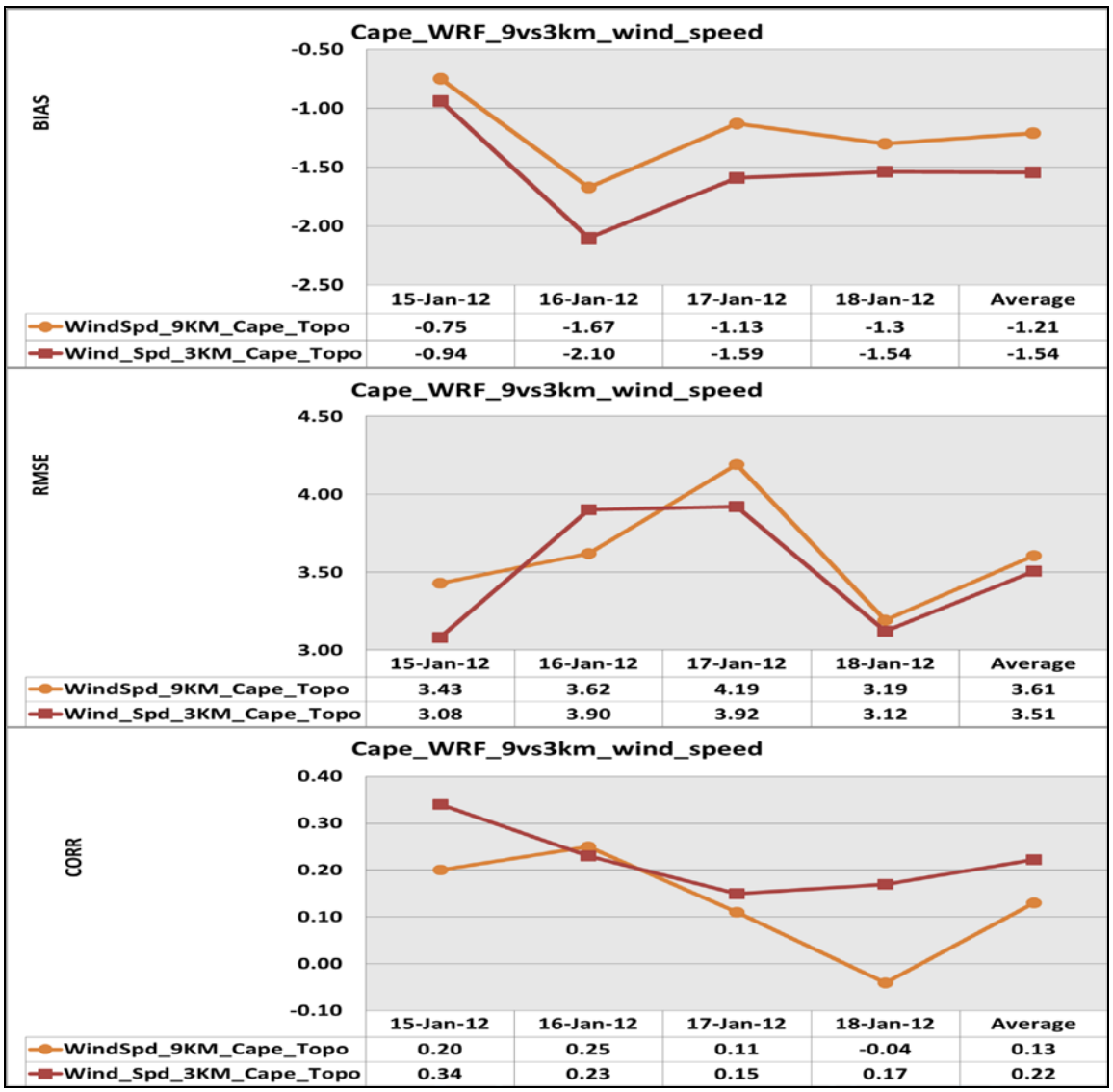

Figure 5.18: WRF 9 versus 3 km wind speed statistics over Cape region for the period 15-18 January 2012.

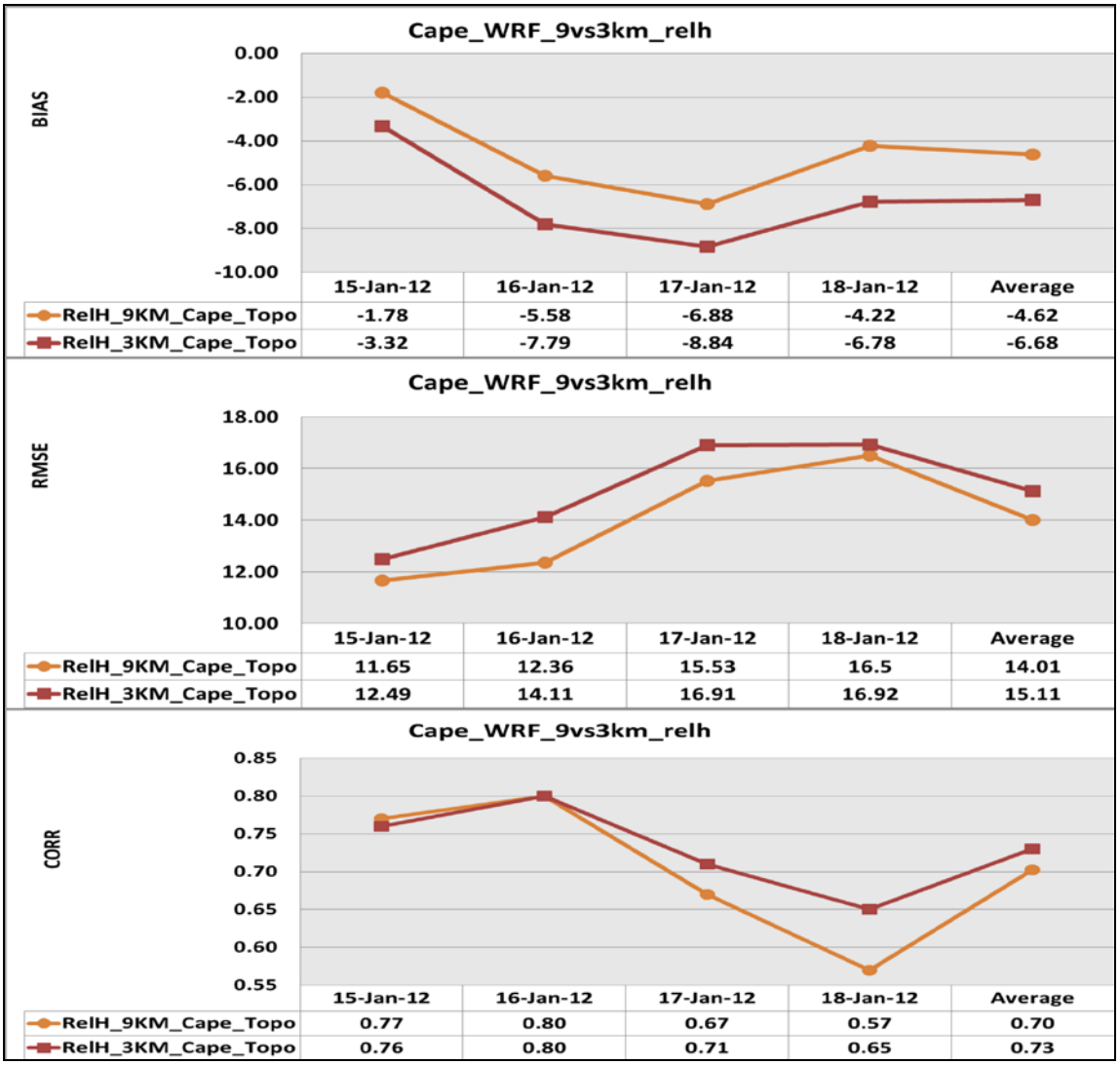

Figure 5.19: WRF 9 versus 3 km relative humidity statistics over Cape region for the period 15-18 January 2012.

5.4 Discussion and summary of results

The WRF model simulations at increased grid resolution for the three case studies are summarized. Previous studies have shown that an increase in model grid resolution was motivated by the fact that only high grid resolution model runs produce detailed forecasts with superior quality (Mass *et al*., 2002; Schulze, 2007; Bonnardot and Cautenet, 2009; Landman, 2012) and improves the representation of both the model physics and dynamics (Riphagen *et al*., 2001).

Therefore in this study, an increase in grid resolution also improves the model output and a slight improvement in statistics for both heat wave and rainfall event. This could be attributed to the increased grid resolution from 9 to 3 km (for each 3 km grid, there are at least 9 grid points). This is also due to an increase in geographical input data from 2 arc-minutes to 30 arc-seconds which shows improved spatial resolution. Although all model physics were included at both 9 and 3 km grid resolution and was similar, only cumulus parameterization scheme was not included at 3 km grid resolution. It should also be noted that the only time step specified was 54 seconds for the 9 km grid resolution and it was unnecessary to specify the time step for the nested run (18 seconds). It is therefore speculated that an increase of grid resolution of less than 3 km could have improved the results.

a) Heat wave events over Limpopo and Cape regions of South Africa

During both heat waves period (22-26 October 2011) and (15-18 January 2012), the model simulations shows that when the grid resolution was increased, the model simulations under-predicted maximum temperature, wind speed and relative humidity, and over-predicted minimum temperature. Table 5.1 and 5.4 show the number of stations that registered very high temperatures over the Limpopo and Cape regions respectively. These tables also confirm that the model under-predicted maximum temperatures during heat waves, with a slight improvement in simulations details when model grid resolution was increased. As a result, the verification statistics were only slightly improved in both study cases. Therefore it is deduced that in general, at an increased resolution, model simulations and also statistics are improved and it was necessary run the WRF model at higher grid resolution.

b) Heavy precipitation event that resulted in floods over Limpopo region of South Africa

During the precipitation event from 16 to 18 January 2012, the WRF model verification scores indicate that the model simulations at 3 km grid resolution over-predicted rainfall, and minimum temperature. The WRF model simulations also under-predicted maximum temperature, wind speed and relative humidity. All these results also show that at an increased grid resolution, the WRF model simulations are comparable to observations.

However, when simulations at 9 km grid resolution are closer to observation, it might not be necessary to run the model at higher grid resolution. The simulations at 3 km grid resolution were able to reproduce the spatial distribution of maximum rainfall, and also reduced bias. These results also confirm the study by Mass *et al.*, (2002) and also Gilliland and Rowe, (2009) where they found that high grid resolution modeling is able to resolve convection explicitly. An increase in model grid resolution assists in understanding the contributing effects of topography on weather and also climatic implication of the area. Therefore according to previous studies, an increase in model grid resolution results in a more detailed representation of terrain (Schulze, 2007), and greater potential for deep valleys (Riphagen *et al*., 2001; Bonnardot and Cautenet, 2009; Vigaud *et al*., 2012).

CHAPTER 6

SUMMARY AND RECOMMENDATIONS

This chapter summarises the results of the WRF model simulations. These simulations were performed at both 9 and 3 km horizontal grid resolution over the SA domain for the two sets of model runs, *i.e.*, one with topography and also another without topography. The chapter lists how the aims and objectives were achieved and also assesses the contribution of the nonhydrostatic approach to NWP modelling and how these findings contribute to science. The chapter ends by drawing conclusions and some recommendations.

6.1 Summary

The role of the topography and grid size resolution in the weather simulation was studied using the research options incorporated in the WRF model setup. From this study, the following three objectives were achieved:

a) *To evaluate the capability of the WRF model as a NWP model to predict extreme weather events including heavy precipitation and heat wave events over SA*

With the first aim the WRF model was run at 9 km horizontal grid resolution with topography to predict both heat waves and heavy precipitation that lead to floods over SA and the output were verified against SAWS station observations. From these simulations it was found that:

Rainfall: the model simulations were able to capture the spatial distribution of rainfall over the country and Limpopo region during January 2012. The model initiated rainfall a day earlier over Limpopo region, which resulted in over-prediction for all rainfall thresholds. There was a positive CORR values between the WRF model and observed rainfall which varies between 0.22 (with topography) and 0.7 (without topography). It was expected that CORR values should be greater than 0.77 as achieved in previous studies including Cretat and Pohl (2011); Cretat *et al*., (2011) who found the correlation between WRF grids and rain gauges over SA to vary between 0.7 and 0.8 (on a seasonal time scale); Boulard *et al*., (2012); and also Ratna *et al*., (2013). Maximum temperature: the model simulations captured the spatial distribution very well over the country during both heat wave events although the model under-predicted maximum temperatures by at least 4^{o}C during all the heat wave events. The CORR values were on average greater than

0.84 during both October and January heat waves, an indication of strong positive linear relationship between model simulations and SAWS observations. Minimum temperature was simulated better than maximum temperature for all the experiments. For wind speed, the model simulations also show a very good agreement with observations. However, for relative humidity simulations, the spatial distribution was similar to maximum temperatures.

The results indicate that the physical parameterization scheme applied resulted in the WRF model under-predicting maximum temperatures and therefore the intensity of the heat wave events. However, the same parameterization scheme including the GDE cumulus parameterization scheme resulted in over-prediction of heavy precipitation event that lead to floods. These results proved statistically the complexity of NWP model's capability of simulating weather over South Africa, including both heavy rainfall and heat waves.

b) To evaluate the influence of topography on extreme weather events over SA

For the second aim, the WRF model runs at 9 km with and without topography during heavy precipitation event that lead to floods and both heat wave events were compared with observations to determine which model run achieved better results. From simulation with topography (objective one), it was found that the WRF model was capable of simulating both heat waves events and heavy precipitation event that lead to floods. It was found from the WRF simulation without topography that:

Rainfall: the model simulation with and without topography over-predicted rainfall, however simulation without topography scattered the rainfall over almost the entire domain. Simulation with topography show less bias as compared to simulation without topography except for the 0.1 mm threshold. Simulation with topography show low CORR values and these values were doubled in simulation without topography. Therefore simulation with topography has proved that topographic heights and steepness over the eastern parts of the country contribute to enhanced rainfall. Results from simulation with topography were more accurate, reliable and realistic than in simulation without topography. Maximum temperature: both the model simulations with and without topography under-predicted maximum temperatures. Very high values were well captured in simulation with topography. However, high values were reduced and low values increased in simulation without topography. Simulation with topography yield

realistic, accurate and reliable results than simulation without topography which deteriorates the model reliability. This was shown by bias which remained negative and increased over Limpopo (October simulation) and Cape (January simulation) regions. There was a change in bias sign from negative to positive over Limpopo region (January simulation). The CORR values were reduced for all heat wave events. Therefore by comparing the two simulations, simulation with topography shows that topography intensified the heat wave, whereas the removal of topography reduced the intensity of the heat wave and therefore it can be deduced that topography has an influence on the two heat wave events. For minimum temperature, wind speed and relative humidity, the model simulation with topography shows both high and low values whereas simulation without topography removed very low and high values.

This result indicates the importance of topography and it can be deduced that for reliable simulations, topography must be considered in numerical weather prediction purpose. When winds ascends towards steep topography, it enhanced moisture and increase rainfall, whereas when winds flow downslope, wind speed increases, and enhances surface warming resulting in very high temperatures. From this extreme weather events simulation, it can be concluded that topography has enhanced both heat wave events and heavy precipitation event that lead to floods and therefore has an impact on weather over South Africa.

c) To evaluate the influence of grid resolution on simulations of extreme weather events over SA

For the last aim, the model's 3 km grid nested output over Limpopo and Cape regions were compared with SAWS observations and 9 km grid runs to determine if increasing the model grid resolution has an effect on the model output. From these simulations it was also found that:

Rainfall: the model simulation at 3 km grid resolution show an improved spatial distribution over the domain, and statistics shows that the results at 3 km grid were slightly improved when compared to results at 9 km grid results. The WRF model simulations were able to capture a no-rain event over the western part of Limpopo region.

Maximum temperature: an increased model grid resolution improved the spatial and temporal distribution of maximum temperatures. Similarly, statistics were also improved during both heat waves events respectively. For minimum temperature, wind speed and

relative humidity, an increased model grid resolution also improved the spatial and temporal distribution of these variables. An increased model grid resolution also resulted in a slight improvement in statistics for all the case studies. However, it could also be mentioned that minimum temperature simulations were already good at 9 km grid resolution and an increase in resolution could not have a large impact on the simulations. From these results, it could be accepted that an increase in grid resolution is very important in numerical weather modelling as it improves details of the weather simulations.

From this study, it is concluded that the WRF model is capable of simulating the extreme weather events including heavy precipitation event that lead to floods and heat wave events over the country. The topography of SA, specifically in this instance, the topography over the eastern parts of the country including the escarpment enhanced rainfall formation that resulted in floods. The topography over the country also enhanced the heat wave event that resulted in very high temperatures. An increase in model grid resolution from 9 to 3 km improved the spatial distribution and slightly improved statistics for all the simulated variables during heavy precipitation event that lead to floods and both heat wave events.

Therefore the WRF model could be used as mesoscale model for NWP purpose over SA since its application at higher grid resolution adequately captured some important mesoscale features and represent local sub-grid scale features very well. Such mesoscale features includes, cumulus clouds, tornadoes, dust devils and turbulence (Markowski and Richardson, 2010). This finding supports previous research findings by Giorgi (1990); Mass *et al.*, (2002); Reason *et al.*, (2006); Caldwell *et al*., (2009); Mbedzi (2010); Ratnam *et al*., (2011) and Cretat *et al*., (2012). The nonhydrostatic modelling approach was found to appropriately simulate both the mesoscale events when topography was included in model integration as described in Holton (2004) and Markowski and Richardson (2010).

6.2 Assessing the scientific contribution of this study

It was found in this study that the WRF model together with all the physical and dynamical schemes including the GDE cumulus parameterization scheme, topography

data and the input data simulated all the variables over SA during extreme weather events with sufficient accuracy. Therefore the WRF model is appropriate for simulating the daily SA weather and could be used with confidence.

1. Vertical velocity: in simulation with topography, vertical velocities (updrafts) were well simulated and show realistic spatial distribution, whereas in simulation without topography, the updrafts were less and more wide spread over the entire domain. When dynamical scaling was applied, it shows that vertical velocity could not be ignored in simulation with topography, as applied in nonhydrostatic modelling, but could be ignored in simulation without topography as in the hydrostatic approach. This is due to the fact that in simulation with topography, vertical velocity gives an indication of the correct area of precipitation whereas in simulation without topography, vertical velocity is spread over the domain which also results in rainfall spreading over almost the entire domain.

2. Topographic variations:

2.1 This study has found that topography over the north-eastern parts of the country including Limpopo region contributed to rainfall and heat wave. These findings were proved by removing the topography over the area as both intense rainfall and heat wave were reduced. Simulation with topography has shown that the steepness of topography result in wind speed increase with height and enhanced moisture fluxes resulting in increased rainfall. Topography also result in wind speed increase down the steep slope, enhanced temperature advection and warming, resulting in higher temperatures in low lying areas.

2.2 The topographic heights over Cape region also influenced the intensity of heat wave over the area. As compared to simulation over Limpopo region, very high temperatures were simulated over isolated areas towards the west coast. However, when topography was removed, the intensity of maximum temperatures was reduced and areas of higher temperatures spread towards the western interior of the country. In this areas, there was a wind speed increase as winds flow down the steep topography, which enhanced temperature advection and warming, resulting in higher temperatures over the west coast of South Africa.

3. Topographic resolution. From all the simulations performed, it was shown that when model grid point resolution is increased, the model topographic resolution was also increased. Such an increase in grid and topographic resolutions also improved the spatial distribution of the analysed variables and also the statistics.

6.3 Recommendations

From the studies conducted, it was found that the WRF model settings used were capable of simulating both extreme weather events (heavy precipitation and heat waves), and that topography influenced extreme weather events and that the increased grid resolution also improves the simulations. It is recommended that:

1. Numerical weather prediction modellers can benefit by applying NWP models at a higher model grid resolution (including high grid resolution topography). However, such high resolution model simulations are subject to bias which can be corrected by applying the kalman filtering system as has been mentioned by authors including Homleid, (1995); Galanis and Anadranistakis, (2002); Galanis *et al.*, (2006), Cheng and Steenburgh, (2007); Libonati *et al.*, (2008) and also Louka *et al.*, (2008).

2. In this study, one way nesting approach was applied just to see how the model performs at 3 km grid resolution. It is understood that two way nesting could be used, but this was not done since it was speculated that it would change the results and therefore affect the objective of the study. However, for future studies, it is recommended that two way nesting could be applied in order to see how the results differ.

3. Although it is not completely true that by increasing the number of processors will result in fast processing of the result, it will be advisable to do cost versus benefits analysis during model integration. During this study and also operational runs, it was found that when 16 processors are applied over a grid of with 451 grid points in the east-west and 337 grid points in south-north, it takes approximately seven hours to produce simulations for 72 hours with six hourly outputs. However, an increase in the number of processors limit users from executing other jobs as most of the memory is

allocated to the model runs. This limitation also depends on the capacity of the computer applied.

4. Statistical analysis (Wilks, 2011) has shown that model temperatures are subjected to multiplicity which requires re-sampling in order to draw conclusion from significance testing; this study did not focus on re-sampling when performing interpolation from model grids to station. This was due to that it was understood that since the model grids were at least 9 km it was assumed (i) to be unnecessary since the observations stations over the country are placed very far from each other and (ii) that weighted averages will solve the issue. However, in future studies, the re-sampling technique may be applied.

5. Although in this study the remote sensing data was not used to initialise the model runs, its incorporation in NWP models could benefit users. The availability of satellite dataset can improve the model accuracy over the southern hemisphere, especially over the oceans where there is a scarcity of observation network data to initialize NWP models (Potgieter, 2006; Mbedzi, 2010). Such tools could be used to study wind systems, their variability, secular variations, climatology and variations of SSTs (Reason *et al.*, 2006).

APPENDIX A

In appendix A, all the images described in both section 4.1.2 and 4.2.2 are tabulated in order to enhance the readability of the dissertation. The images include WRF synoptic map for the periods (23-26 October 2011) and (15-18 January 2012) reactively. Also included are the moisture fluxes and vertical velocity for the above mentioned periods.

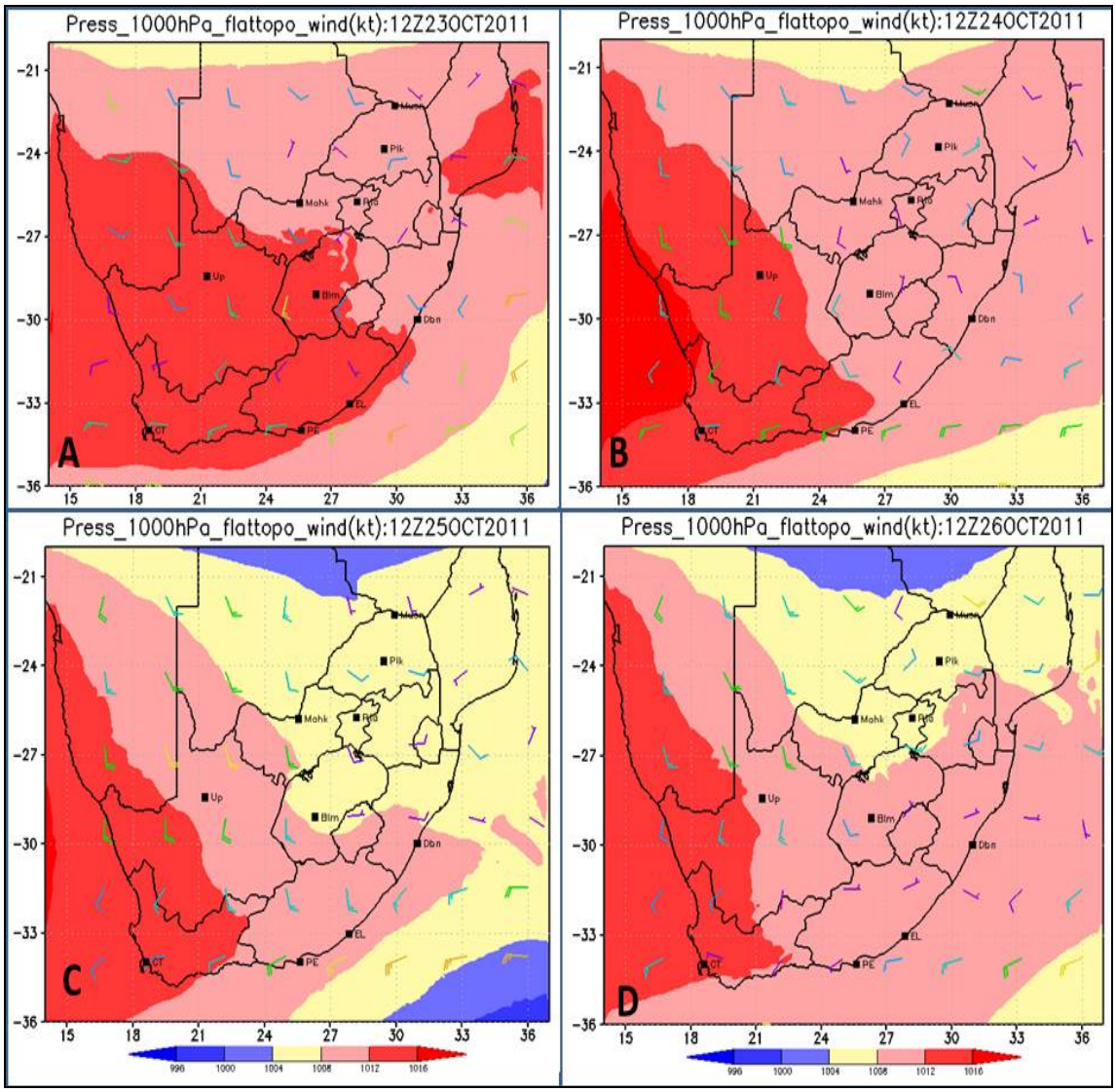

Figure A.1: WRF 9 km simulated synoptic map at 12h00 UTC with mean sea level pressure in hPa (contours), and surface winds (barbs in knots) simulation for the period 23-26 October 2011. Figure is labelled as follows: top left (23 October); top right (24 October), bottom left (25 October) and bottom right (26 October).

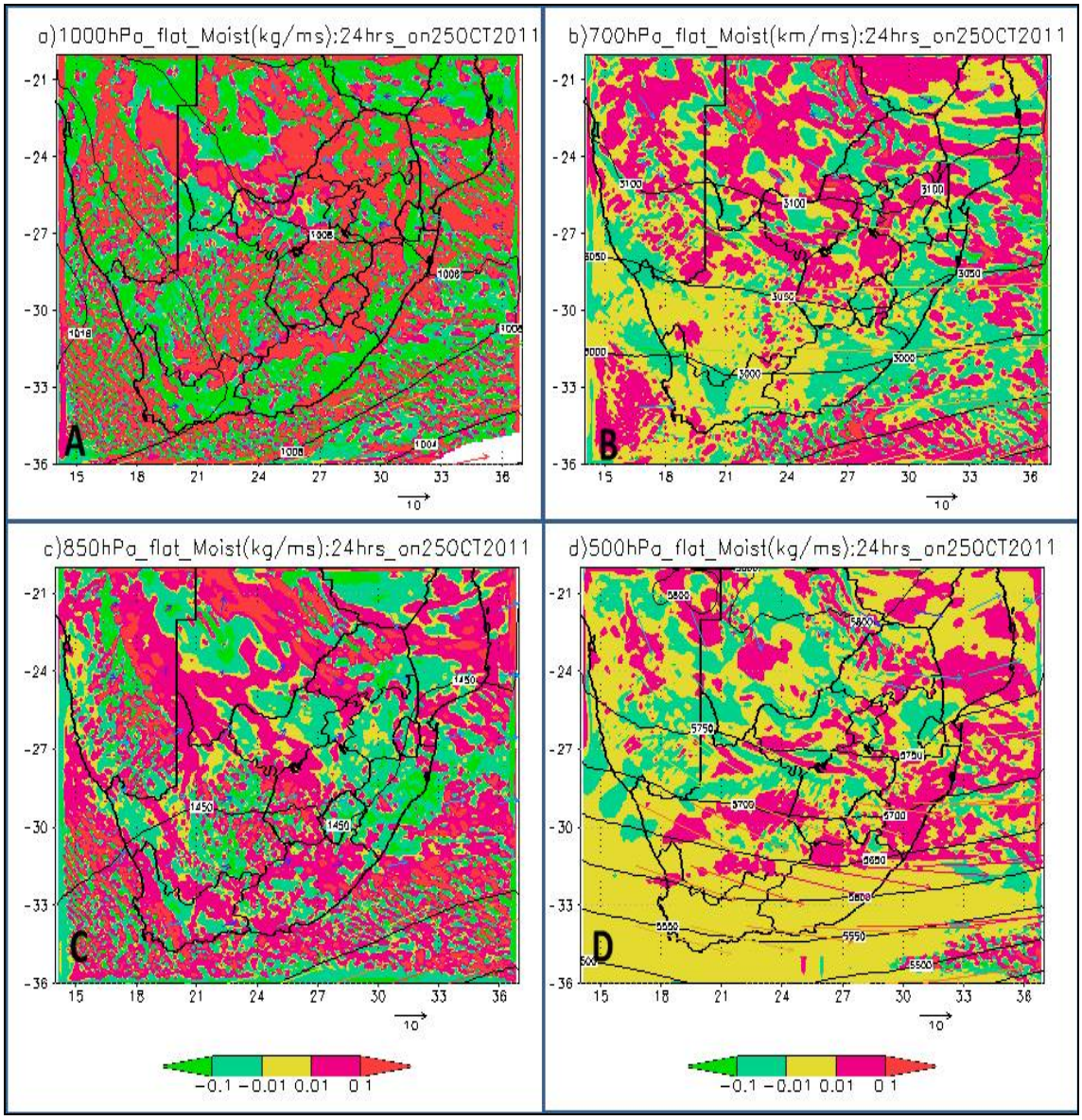

Figure A.2: The WRF model simulation of 1000 hPa (top left), 850 hPa (bottom left), 700 hPa (top right) and 500 hPa (bottom right) geopotential height levels (isobars in contour), moisture flux in $kgm^{-1}s^{-1}$(shadings) and horizontal winds (vector on ms^{-1}) simulation as on 25 October 2011. The yellow colour on the image, interval (-00.1to 0.01) indicates transition area, whereas white colour indicates that topography is higher than the plotted geopotential heights.

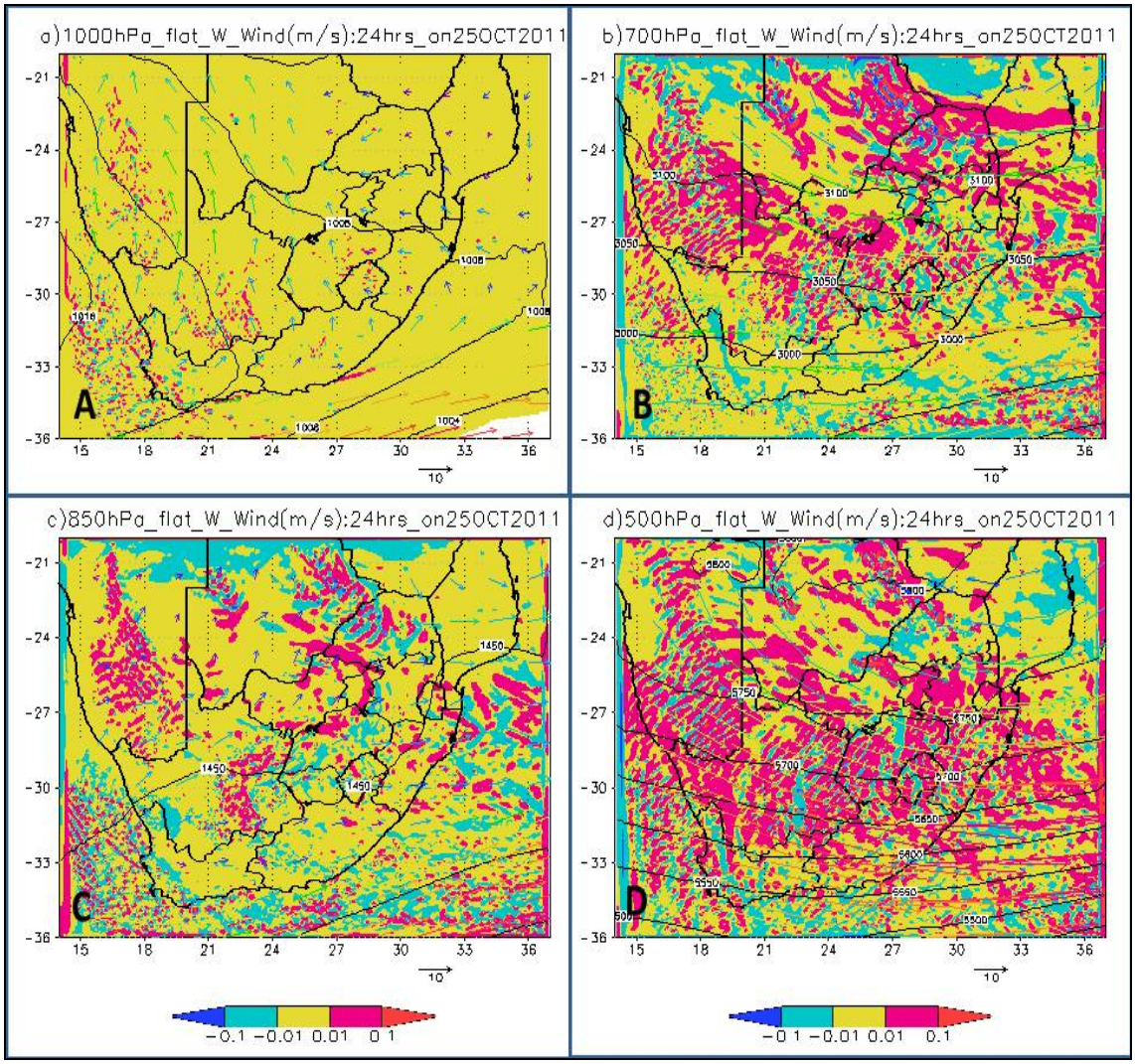

Figure A.3: The WRF model simulation of 1000 hPa (top left), 850 hPa (bottom left), 700 hPa (top right) and 500 hPa (bottom right) geopotential height levels (isobars are in contours), vertical velocity in ms^{-1} (shaded) and horizontal winds (vector in ms^{-1}) simulation as on 25 October 2011. The yellow colour on the image, interval (-00.1to 0.01) indicates transition area, whereas white colour indicates that topography is higher than the plotted geopotential heights.

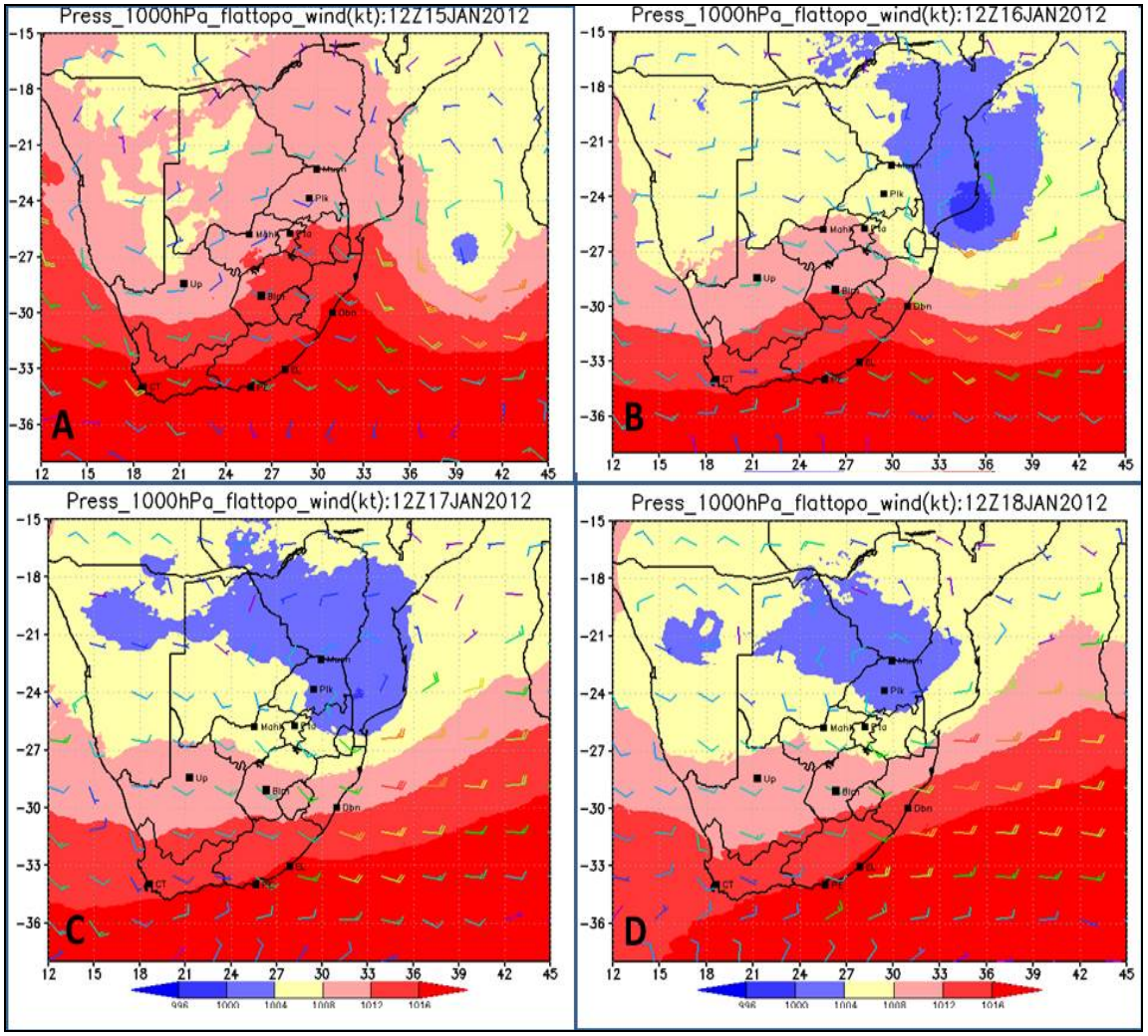

Figure A.4: WRF 9 km simulated synoptic map at 12h00 UTC with mean sea level pressure in hPa (contours), and surface winds (barbs in knots) simulation for the period 15-18 January 2012. Figure is labelled as follows: top left (15 January); top right (16 January), bottom left (17 January) and bottom right (18 January).

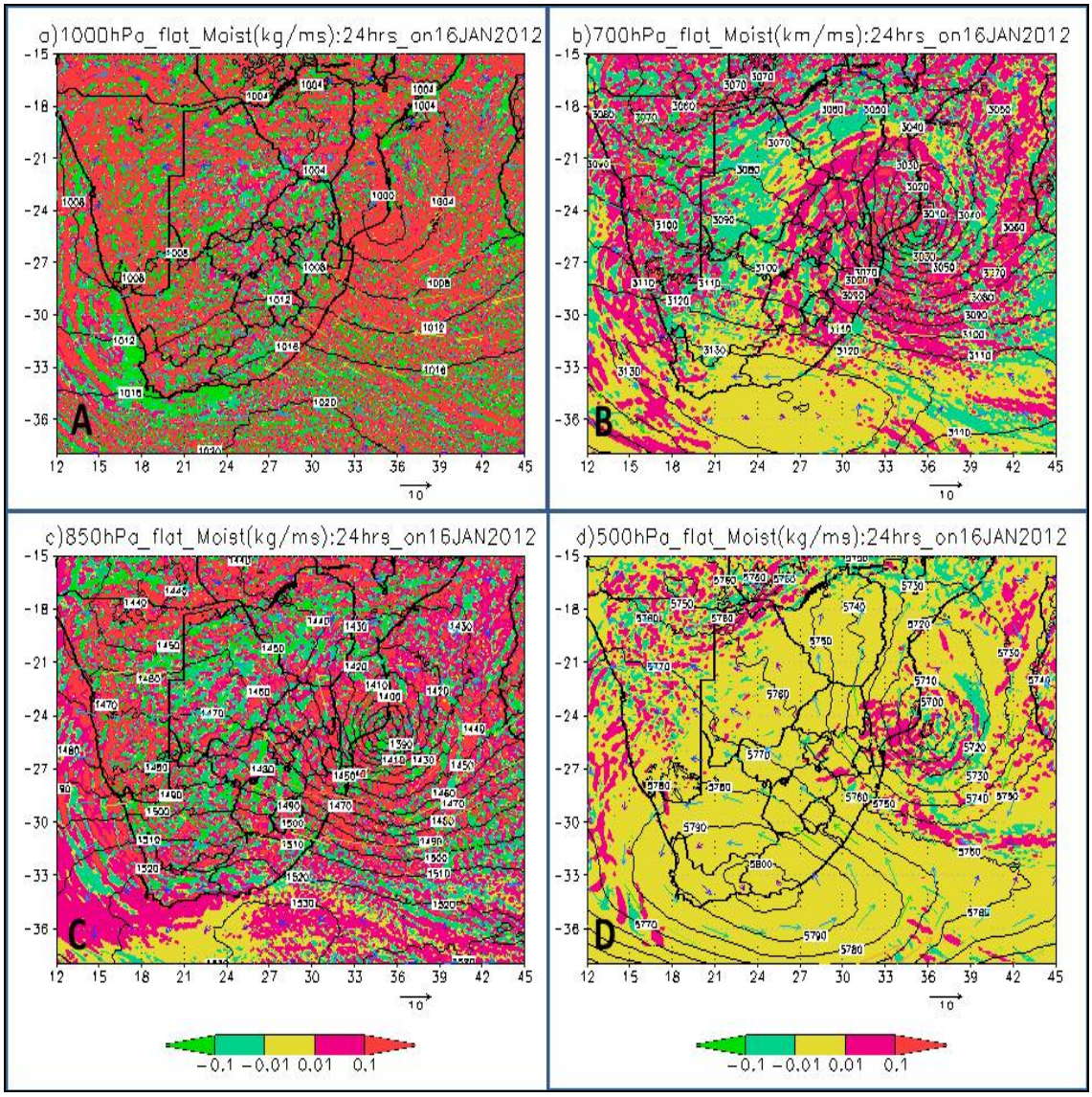

Figure A.5: The WRF model simulation of 1000 hPa (top left), 850 hPa (bottom left), 700 hPa (top right) and 500 hPa (bottom right) geopotential height levels (isobars in contour), moisture flux in $kgm^{-1}s^{-1}$(shadings) and horizontal winds (vector on ms^{-1}) simulation as on 16 January 2012. The yellow colour on the image, interval (-00.1to 0.01) indicates transition area, whereas white colour indicates that topography is higher than the plotted geopotential heights.

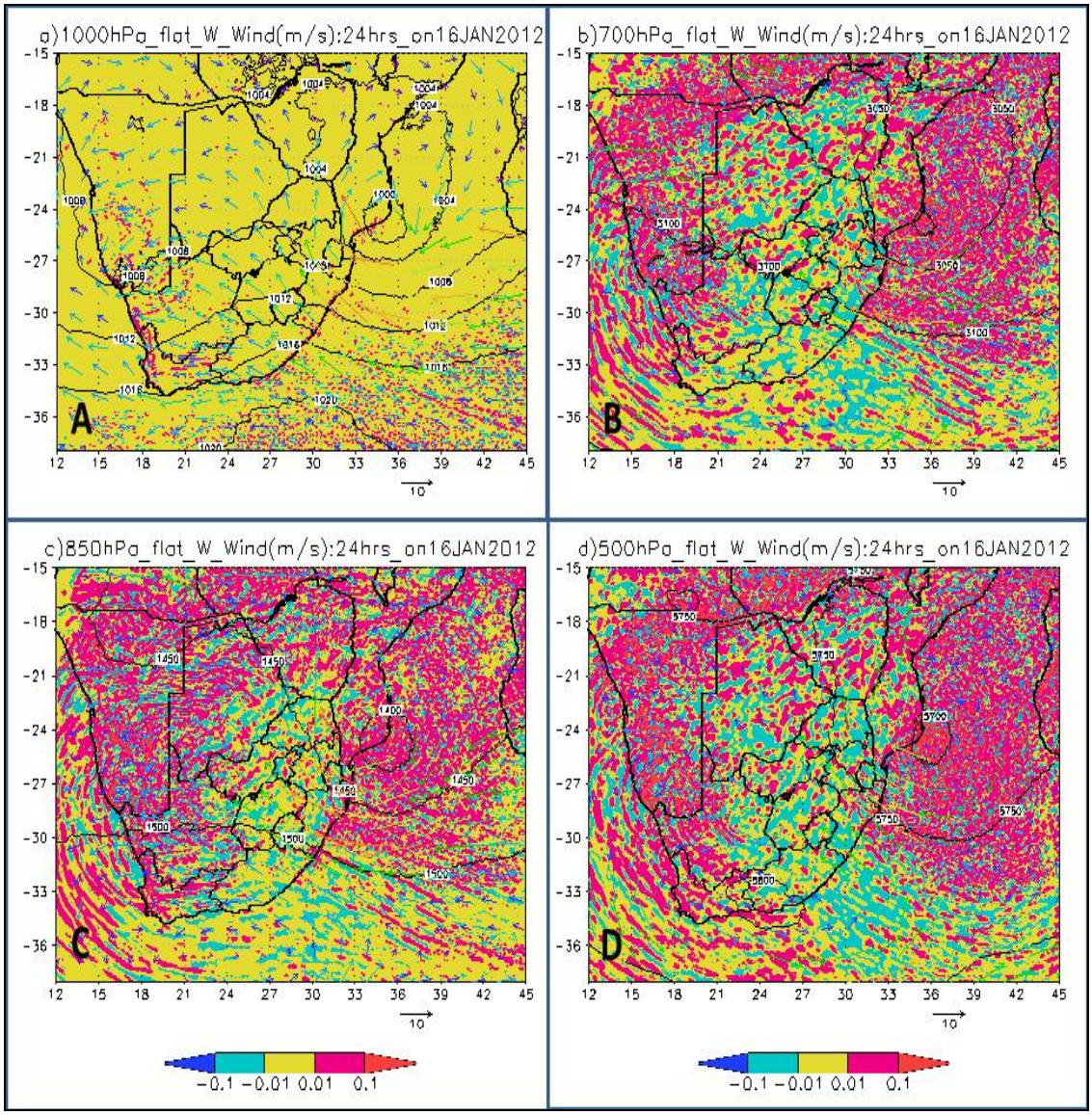

Figure A.6: The WRF model simulation of 1000 hPa (top left), 850 hPa (bottom left), 700 hPa (top right) and 500 hPa (bottom right) geopotential height levels (isobars are in contours), vertical velocity in ms^{-1} (shaded) and horizontal winds (vector in ms^{-1}) simulation as on 16 January 2012. The yellow colour on the image, interval (-00.1to 0.01) indicates transition area, whereas white colour indicates that topography is higher than the plotted geopotential heights.

Median monthly precipitation (rainfall), January							
Province	Mean value	CV(%)	Maximum value	Minimum value	Exceedence probabililty		
					20%	50%	80%
Limopopo	89	29	323	21	106	86	69
Mpumalanga	117	24	323	51	134	114	97
North-west	74	30	136	26	98	75	50
Northern Cape	13	112	73	0	23	8	0
Gauteng	110	6	160	81	115	110	104
Free State	74	34	266	18	100	73	50
Kwazulu-Natal	121	26	336	54	143	117	95
Eastern Cape	57	66	209	2	94	44	24
Western Cape	9	118	98	0	14	6	1

Figure A.7: The distribution of median monthly rainfall during January for some of the provinces of SA (named Limpopo region). It should be noted that the formerly Northern province has been renamed Limpopo province (adapted from Schulze, 1997)

REFERENCES

Barriopedro, D., Fischer, E. M., Luterbacher, J., Trigo, R., and Garcia-Herrera, R., 2010: The hot summer of 2010: Redrawing the temperature record map of Europe. *Science*, **332**, 220(2011), Doi:10.1126/science.1201224, 220-224

Blamey, R.C., and Reason, C.J.C., 2009: Numerical simulation of a mesoscale convective system over the east coast of South Africa, *Tellus 61A*, doi: 10.1111/j.1600-0870.2008.00366.x, 17-34

Bonnardot, V., and Cautenet, S., 2009: Mesoscale atmospheric modelling using a high horizontal grid resolution over a complex coastal terrain and a wine region of South Africa. *Journal of applied Meteorology and Climatology*, **48**, 330-348

Boulard, D., Pohl, B Cretat, J., Vigaud, N., and Pham-Xuam, T., 2012: Downscaling large-scale climate variability using a regional climate model: the case of ENSO over Southern Africa, *Climate Dynamics*, doi: 10.1007/s00382-012-1400-6

Bruyere, C.L., 1997: Numerical Modelling of severe thunderstorms over the South African Highveld with the aid of the Clark cloud model. MSc Dissertation, University of Pretoria, South Africa, 140 pp.

Caldwell, P., Chin, H. S., Bader, D. C., and Bala, G., 2009: Evaluation of a WRF dynamical downscaling simulation over California, *Climatic Change*, **95**, doi: 10.1007/s10584-009-9583-5, 499-521

Cassou, C., Terray, L., and Phillips, A.S., 2005: Tropical Atlantic influence on European heat waves. *Journal of Climate*, **18**, 2805-2811

Cheng, W. Y. Y., and Steenburgh, W.J., 2007: Strength and weaknesses of MOS, running-mean bias removal, and Kalman filter techniques for improving model forecasts over the western United States, *Weather and Forecasting*, **22**, 1304-1318

Cretat, J., Macron, C., Pohl, B., and Richard, Y., 2011: Quantifying internal variability in a regional climate model: a case study for Southern Africa. *Climate Dynamics*, **37**, doi: 10.1007/s00382-011-1021-5; 1335-1356

Cretat, J., and Pohl, B., 2011: How physical parameterizations can modulate internal variability in a regional climate model, *Journal of the atmospheric Sciences*, **69**, doi: 10.1175/JAS-D-11-0109.1, 714-724

Cretat, J., Pohl, B., Richard, Y., and Drobinski, P., 2012: Uncertainty in simulating regional climate of Southern Africa: sensitivity to physical parameterizations using WRF, *Climate Dynamics*, **38,** doi: 10.1007/s00382-011-1055-8,613-634

Dyson, L.L., 2008: A Meteorological Community Project in South Africa. *American Meteorological Society*, DOI: 10.1175/BAMS-89-2-163; 163-167

Emmanouil, G., Galanis, G. and Kallos, G., 2006: Statistical methods for the prediction of night-time cooling and minimum temperature; *Meteorol. Appl.*, **13**, 1-13

Engelbrecht, F.A., McGregor, J.L., and Rautenbach, C.J. DeW, 2007: on the development of a new nonhydrostatic atmospheric model in South Africa, S.*A. J. Sci*., **103**, 127-134

Esau, I., Luhunga, P., Djolov, G., Rautenbach, C.J. deW and Zilitinkevich, S., 2012: Links between observed micro-meteorological variability and land-use patterns in the Highveld priority area of South Africa. *Meteorol. Atmos. Phys*. DOI 10.1007/s00703-012-0218-4

Galanis, G., and Anadranistakis, M., 2002: A one dimensional Kalman Filter for the correction of near surface temperature forecasts. *Meteorol. Applic*. **9**, (437-441)

Galanis, G., Louka, P., Katsafados, P., Pytharoulis, I., and Kallos, G., 2006: Applications of kalman filters based on non-linear functions to numerical weather predictions, *Ann. Geophy*, **24**, 2451-2460

Galewsky, J., 2009: Rain shadow development during the growth of mountain ranges: An atmospheric dynamics perspective, *J. of Geophy. Res*.,**114**,doi:10.1029/2008JF001085

Gilliland E. K. and Rowe, C. M. 2007: A comparison of cumulus parameterization scheme in the WRF model," in Proceedings of the 87th AMS Annual Meeting& 21th Conference on Hydrology, p. 2.16, San Antonio, Tex, USA, 2007.

Giorgi, F., 1990: Simulation of regional climate using a regional model nested in a general circulation model, *American Meteorological Society*, 941-963

Giorgi, F., and Bi, X., 2000: A study of internal variability of a regional climate model, *Journal of Geophysical research*, **105**, D24, 29503-29521

Gordon, N., and Shaykewich, J., 2000: Guidelines on performance assessment of public weather services, World Meteorological Organisation, WMO/TD No.**1023**, 32 pp.

Grell, A.G., and Devenyi, D., 2002: A generalized approach to parameterizing convection combining ensemble and data assimilation techniques, *Geophysical Research Letters*, **29 (14)**, 1693, DOI: 10.1029/2002GL015311, 2002

Gross, G., Vogel, H., and Wippermann, F., 1987: Dispersion over and around a steep obstacle for varying thermal stratification-numerical simulations. *Atmospheric Environment*, **21 (3)**; 483-490

Hargraves, R., and Jury, M., 1997: Composite meteorological structure of flood events over the eastern mountains of South Africa. *Water SA*, **23, 4**, 357-364

Harrison, M.S.J, 1988: A generalized classification of South African summer rain-bearing synoptic systems, *Journal of Climate*, **4**,547-660

Holton, J.R., 2004: An Introduction to Dynamic Meteorology, Fourth Edition, Elsevier Academic Press, 539 pp.

Homleid, M., 1995: Diurnal corrections of short-term surface temperature forecasts using Kalman filter, *Weather and forecasting*, **10**, 689-707

IPCC, 2007: Summary of Policymakers. In: *Climate Change 2007*: The Physical Science Basis. Contribution of Work Group I to the Fourth Assessment Report of the Intergovernmental Panel on Climate Change [Solomon, S., D. Qin, M. Manning, Z. Chen, M. Marquis, K.B. Averyt, M. Tignor and H.L. Miller (eds.)]. Cambridge University Press, Cambridge, United Kingdom and New York, NY, USA, 18 pp.

Jandieri, G., Surmava, A., and Gvelesiani, A., 2011: On the wind and turbulence in the lower atmosphere above complex terrain, *International Journal of Geoscience*, 2011 (**2**); 13-28

Jimenez, P. A., and Dudhia, J., 2011: Improving the representation of resolved and unresolved topographic effects on surface wind in the WRF model, *Journal of Appl. Meteor. and Climatol.* **51**, 300-316, DOI:10.1175/JAMC-D-11-084.1

Kgatuke, M. M., Landman, W.A., Beraki, A. and Mbedzi, M.P., 2008: The internal variability of the RegCM3 over South Africa, *Int. J. Climatol*, **and 28,505**-520

Klemp, J.B., and Skamarock, W.C., 2004: Model numeric for convective-storm simulation. In: Fedorovich, E., Rotunno, R., and Stevens, B., (eds.) Atmospheric turbulence and Mesoscale Meteorology. Cambridge University Press; 117-137

Kruger, A.C., and Shongwe S., 2004: Temperature trends in South Africa: 1960-2003, *Int. J. Climatol*, **24**, 1929-1945

Kruger, A.C., Goliger, A. M., Retief, J.V., and Sekele S., 2010: Strong wind climatic zones in South Africa; *Wind and Structures*, **13(1)**; 37-55

Landman, S., 2012: A multi-model ensemble system for short-range weather prediction in South Africa, MSc Dissertation, University of Pretoria, South Africa, 132 pp.

Lengoasa, J. R., 1988: A note on atmospheric circulation and surface temperature fields over South Africa, *The South African Geophysical Journal*, **70 (2)**, 1988, 127-134

Libonati, R., Trigo, I., and DaCamara, C., 2008: Correction of 2 m-temperature forecasts using Kalman filtering technique, *Atmospheric Research*, **87**, 2008, 183-197

Louka, P., Galanis, G., Siebert, N., Kariniotakis, G., Katsafados, P., Pytharoulis, I., and Kallos, G., 2008: Improvements in wind speed forecasts for wind power prediction purpose using Kalman filtering, *Journal of Wind engineering and industrial Aerodynamics*, **96**, 2348-2362

Lyon, B., 2009: Southern African Summer Drought and Heat Waves: Observations and Coupled Model Behaviour; *Journal of climate*, Doi:10.1175/2009JCLI3101.1, 6033-6046

Lutgens, F.K., and Tarbuck, J.T., 2010: The Atmosphere: An introduction to Meteorology, Eleventh Edition, Prentice Hall (Pearson) Printers, 508 pp.

Marengo, J., Cornejo, A., Saatyamurty, P., and Nobre, C., 1997: Cold surges in tropical and extratropical South America: The strong event in June 1994: *Monthly Weather Review*, **125**, 2759-2786

Markowski, P., and Richardson, Y., 2010: Mesoscale Meteorology in Midlatitudes: Advancing Weather and Climate Science, Wiley-Blackwell Publications, 407 pp.

Mason, S. J., 1996: Climatic change over the lowveld of South Africa. *Climatic Change*, **32**, 35-54

Mason, S. J., and Jury, M.R., 1997: Climatic variability and change over southern Africa. *Progress in Physical Geography*, **21**, 23-50

Mass, C.F., Ovens, D., Westrick, K., and Colle, B.A., 2002: Does increasing horizontal resolution produce more skilful forecast? The results of two years of real time numerical weather prediction over the Pacific North-west. *American Meteorological Society*, 407-430

Mbedzi, M. P., 2010: Simulation of tropical cyclone-like vortices over the southwest Indian Ocean, MSc Dissertation, University of Pretoria, South Africa, 115 pp

McPherson, R.A., 2007: A review of vegetation-atmosphere interactions and their influences on mesoscale phenomena; *Progress in Physical Geography*; **31(3)** 261-285

McQueen, J. T., Draxler, R. R., and Rolph, G. D., 1995: Influence of grid size and terrain resolution on wind field predictions from an operational mesoscale model, *Journal of Applied Meteorology*, **34**, 2166-2181

Muller, G.V. and Berri, G.J., 2007: Atmospheric circulation associated with persistent generalized frosts in Central-Southern South America, *Monthly Weather Review*, **135**, 1268-1289

National Centers for Environmental Prediction/National Weather Service/NOAA/U.S. Department of Commerce. 2000, updated daily. NCEP FNL Operational Model Global Tropospheric Analyses, continuing from July 1999. Research Data Archive at the National Center for Atmospheric Research, Computational and Information Systems Laboratory. http://dx.doi.org/10.5065/D6M043C6. Accessed 22 Oct 2011.

Olivier, J., and Rautenbach, C. J.de., 2002: The implementation of fog water collection systems in South Africa, *Atmospheric Research*, **64**, 227-2389

Persson, A., 2003: User Guide to ECMWF forecast products, Meteorological Bulletin M3.2, 123 pp.

Pezza, A. B., and Ambrizzi, T, 2005: Dynamical conditions and synoptic tracks associated with different types of cold surge over tropical South America, Int. J. Climatol., **25**, 215-241

Pielke Sr. R.A., 2002: Mesoscale Meteorological Modeling, Second Edition, Academic Press; 676 pp.

Potgieter, C.J., 2006: Accuracy and skill of the Conformal-Cubic Atmospheric Model in short-range weather forecasting over southern Africa; an MSc dissertation, University of Pretoria, 172 pp.

Ratna S. B., Ratnam, J.V., Behera, S. K., Rautenbach, C.J. deW., Ndarana, T., Takahashi, K., and Yamagata, T., 2013: Performance assessment of three convective parameterization schemes in WRF for downscaling summer rainfall over South Africa, *Climate Dynamics*, doi: 10.1007/s00382-013-1918-2

Ratnam, J.V., Behera, S. K., Masumoto, Y., Takahashi, K, and Yamagata, T., 2011: A simple regional coupled model experiment for summer-time climate simulation over southern Africa, *Climate Dynamics*, doi: 10.1007/s00382-011-1190-2

Reason, C.J.C., Engelbrecht, F., Landman, W.A., Lutjeharms, Piketh, S. Rautenbach, C.J. deW and Hewitson, B.C., 2006: A review of South African research in atmospheric science and physical oceanography during 2000-2005, *South African J. of Science*,**102**, 35-43

Riphagen, H.A., Bruyere, C.L., Jordaan, W., Poolman, E.R., and Gertenbach, J.D., 2001: Experiments with NCEP Regional Eta Model at the South African Weather Bureau, with Emphasis on terrain Representation and its effect on precipitation Predictions, *Monthly Weather Review*, 1246-1263

Robinson, P.J., 2000: On the definition of a heat wave, *Journal of applied Meteorology*, 762-775

SAWS, 2011: South African Weather Service, Daily Weather Bulletin, October 2011: ISSN 0011-5517

SAWS, 2012: South African Weather Service, Daily Weather Bulletin, January 2012: ISSN 0011-5517

Schulze, R.E., 1997: South African Atlas of Agrohydrology and -Climatology, Water Research Commission, Pretoria, Report, TT82/96

Schulze, G. C., 2007: Atmospheric observations and numerical weather prediction. *S.A. Journ. Sci*, **103**, 318-323

Singleton A.T., and Reason, C.J.C., 2005: Numerical simulations of severe rainfall event over the Eastern Cape coast of South Africa: Sensitivity to sea surface temperature and topography, *Tellus* **581A** (2006), doi: 10.1111/j.1600-0870.2006.00180.x, 355-367

Skamarock, W. C., and Klemp, J.B., 2008: A time-split nonhydrostatic atmospheric model for weather research and forecasting applications, *Journal of Computational Physics*, **227**, 3465-3485

Smith, R.B., 2004: Mountain meteorology and regional climates. In: Fedorovich, E., Rotunno, R., and Stevens, B., (eds.) Atmospheric turbulence and Mesoscale Meteorology. Cambridge University Press; 117-137

Stull, R. B., 1988: An Introduction to Boundary Layer Meteorology, Kluwer Academic Publishers, 666 pp.

Taljaard, J.J., 1994: Atmospheric Circulation Systems, Synoptic Climatology and Weather Phenomena of South Africa; Part 1: Controls of the weather and climate of South Africa; Technical Paper no **27**; Weather Bureau, ISSN: 0379-6736

Taljaard, J.J., 1995: Atmospheric Circulation Systems, Synoptic Climatology and Weather Phenomena of South Africa; Part 3: The synoptic climatology of South Africa in January and July; Technical Paper no **29**; Weather Bureau, ISSN: 0379-6736

Taljaard, J.J., 1996: Atmospheric Circulation Systems, Synoptic Climatology and Weather Phenomena of South Africa; Part 5: Temperature Phenomena in South Africa; Technical Paper no **31**; Weather Bureau, ISSN: 0379-6376

Tennant, W.J., and Van Heerden, J., 1994: The influence of orography and local sea-surface temperature anomalies on the development of the 1987 Natal floods: a general circulation model study, *S.A. Journal of Science*, **90**, 45-49

Tesche, T.W. and Tremback, C., 2002: Operational evaluation of MM5 meteorological model over the continental United States: Protocol for annual and episodic evaluation, Task order 4TCG-68027015, AG-TS-90/158

Tyson, P.D., and Preston-Whyte, R.A., 2000: The Weather and Climate of Southern Africa; Oxford University Press; 396 pp.

Van Schalkwyk, L., 2011: Fog forecasting at Cape Town International Airport: A climatological approach, MSc Dissertation, University of Pretoria, South Africa, 152 pp.

Vigaud, N., Pohl, B., and Cretat, J., 2012: Tropical-temperate interactions over Southern Africa simulated by regional climate model, *Climate Dynamics*, doi: 10.1007/s00382-012-1314-3

Wang, W., Bruyere, C., Duda, M., Dudhia, J., Gill, D., Lin, H., Michalakes, J., Rizvi, S., and Zhang, X., 2010: Weather Research and Forecasting, ARW Version 3 Modeling System User's Guide, http://www.mmm.ucar.edu/WRF/users/docs/user_guide_V3/contents.html

Watterson, I.G., 1993: Global Climate Modelling, in Modelling Environmental Systems, Edited by Jakeman, A.J., Beck , M.B., and McAleer, M.J., *John Wiley and Sons Ltd*, 343-364

Wilks, D. S., 2011: Statistical Methods in the Atmospheric Sciences, 3rd Edition; 704 pp